TECHNISCHE UNIVERSITÄT MÜNCHEN

Lehrstuhl für Technische Chemie II

Structural requirements and reaction pathways of hydrogenolytic C−C bond cleavage in naphthenes over supported platinum and iridium domains

Hui Shi

Vollständiger Abdruck der von der Fakultät für Chemie der Technischen Universität München zur Erlangung des akademischen Grades eines

Doktors der Naturwissenschaften (Dr. rer. nat.)
genehmigten Dissertation.

Vorsitzender: Univ.-Prof. Dr. Ing. Kai-Olaf Hinrichsen

Prüfer der Dissertation:

1. Univ.-Prof. Dr. Johannes A. Lercher
2. Univ.-Prof. Dr. Klaus Köhler
3. Univ.-Prof. Dr. Moniek Tromp (nur schriftliche Beurteilung)
   Univ.-Prof. Dr. Tom Nilges (nur mündliche Prüfung)

Die Dissertation wurde am 08.10.2012 bei der Technischen Universität München eingereicht und durch die Fakultät für Chemie am 04.12.2012 angenommen.

“There are things we do not know we don’t know.”

Donald Rumsfeld (1932-)

Acknowledgements

There is no doubt that I could not have completed this work without the invaluable advice and support, technically and intellectually, from my friends and colleagues in this group.

First of all, I want to thank Johannes (Prof. Dr. J. A. Lercher) for offering me the opportunity to work in his group. Being not a ‘fast’ student, I managed eventually to present you a decent piece of thesis work, owing to the enlightenment and freedom you’ve granted. I am convinced that your school of thoughts has left a remarkable trail on my career path yet to develop.

I am full of gratitude to my supervisor Dr. Oliver Y. Gutiérrez for the discussions we had, and for the encouragement you gave me. Oliver, your ‘simple’ yet ‘pictorial’ mind has been an important additive to my way of thinking. Now, I’ve fully appreciated the value of transforming dull words into vivid illustrations, which I learnt from you, and would like to keep it routine in my toolbox.

I am most grateful to my lab mate, Xianyong Sun, for his companion in the past three years and his unfailing assistance in a variety of ways. More often than not, our conversation triggers not only joy but inspiration. For me, it is simply impossible to count how many times I have been amazed by his profound knowledge and experience in reactor technologies. If I were you, Xianyong, I must have been more complacent and proud than you are. In you, I witness ‘humility is virtue’. You are blessed to blaze a glorious path, ahead of your forthcoming graduation.

My first year here in this group were made a lot easier with the help of Dr. Xuebing Li, who has found his most pleasant location to stay, and Dr. Herui Dou, who is still pursuing a place to his heart’s content. Their technical advice saved me a lot of trouble in my early days here, without which I would have been a lonely fighter against all odds.

I could have excused myself for not being an active visitor to the birthday celebrations and coffee breaks held in our kitchen, but for now, do allow me to express my sincere regrets that I did not often make it to appear to share those happy moments with my colleagues. Life here would have been a less comfortable one, had the German natives and Bavarian locals been not as helpful and candid.

Our technical staff has been a strong support to all students in this group. I am thankful to all of them: Xaver Hecht for building the new (and current) parallel reactor system and carrying out the BET and chemisorption measurements; Martin Neukamm for conducting the AAS measurement and giving suggestions on the handling and disposal of chemicals; Andreas Marx for tackling problems of electronics and computers and for saving my USB stick (and my ass!). Our former and current secretaries, Stefanie Maier, Helen Lemmermöhle, Katharina Thies, Bettina Federmann and Karen Schulz, deserve particular thanks for their help in administrative matters that keeps the whole group functioning.

Particularly, it has been a great pleasure and unforgettable experience to work with Prof. Gary L. Haller during the final stage of my work.

Last but not least, I am deeply indebted to my family, relatives and friends from whom I've been receiving endless support.

Hui Shi
July. 2012

Abstract

The structural requirements and reaction pathways of C−C bond cleavage in cyclic hydrocarbons have been explored over Pt and Ir catalysts devoid of Brønsted acidity. The C−C bond cleavage rates monotonically increase with increasing Pt particle size, while the hydrogenolysis rates first decrease and then increase with Ir particle size. For Ir-catalyzed hydrogenolysis of six-membered naphthenes, low-coordination atoms and high H*-coverage favor single endocyclic C−C bond cleavage over multiple and exocyclic C−C bond cleavage, whereas the low-index planes and high temperature do the opposite. The endocyclic C−C bond hydrogenolysis proceeds via a rate-limiting C−C bond rupture of partly dehydrogenated intermediates. H-deficiencies of the catalytic intermediates determine the product selectivities along different reaction pathways. The presented in-depth analysis of hydrogenolysis on metal surfaces allows identifying parameters as guidelines for designing active and selective catalysts for fuel upgrading.

Die strukturellen Anforderungen und Reaktionswege der C−C-Bindungsspaltung in zyklischen Kohlenwasserstoffen wurden über Pt und Ir-Katalysatoren frei von Brønsted-Acidität untersucht. Die Raten der C−C-Bindungsspaltung steigen mit zunehmender Pt-Partikelgröße monoton an, während die Raten der Hydrogenolyse zuerst abnahmen und dann mit der Ir Partikelgröße zunahmen. Für die Ir-katalysierte Hydrogenolyse von Naphthenen begünstigen niedrig koordinierte Atome und eine hohe H*-Bedeckung die einfache endocyclische C−C-Bindungsspaltung gegenüber mehrfacher und exocyclischer C−C-Bindungsspaltung, wohingegen niedrig indizierte Metalloberflächen und hohe Temperaturen das Gegenteil bewirken. Die Hydrogenolyse endocyclischer C−C-Bindungen verläuft über einen geschwindigkeitsbestimmenden C−C-Bindungsbruch von teilweise dehydrierten Zwischenprodukten. Der Wasserstoff-Mangel der Zwischenprodukte bestimmt die Produktselektivitäten in verschiedenen Reaktionspfaden. Diese detailreiche Analyse der Katalytischen Kreislaufs der Hydrogenolyse an Metalloberflächen sollte es ermöglichen, aktivere und selektivere Katalysatoren zu entwickeln.

Table of contents

Acknowledgements ……………………………………………..………i

Abstract…………………………………………………..……..…iii

Table of contents ……………………………………..…..…….iv

Chapter 1

Introduction…………………………………………………….. 1

1.1. General background 2
1.2. Ring opening on acidic catalysts 6
1.3. Ring opening via bifunctional catalysis 6
  1.3.1. Ring opening of bicyclic and monocyclic hydrocarbons on bifunctional catalysts 7
  1.3.2. Fundamental considerations 8
1.4. Hydrogenolysis of alkanes and cycloalkanes on noble metals 13
  1.4.1. Ring opening of five-membered naphthenes on monofunctional metal catalysts 14
  1.4.2. Ring opening of six-membered naphthenes on monofunctional metal catalysts and model surfaces 16
1.5. Scope of this thesis 18
1.6. References 21

Chapter 2

Catalytic consequences of particle size and electronic properties of supported Pt clusters in the ring opening of cyclopentane on Pt/Al_2O_3 ………………………………………………… ………… … 24

2.1. Introduction 25

2.2. Experimental 26
  2.2.1. Catalyst preparation 26
  2.2.2. Catalyst characterization 27
  2.2.3. Kinetic measurements 28
2.3. Results and discussions 30
  2.3.1. Particle size and dispersion measurements 30
  2.3.2. Catalytic activity in the ring opening of cyclopentane 35
  2.3.3. Understanding the effect of Pt precursor on ring opening activity by probing the electronic states of small Pt clusters 44
  2.3.4. Effect of Cl: on the activation barrier or on the reactant coverage? 49
  2.3.5. Origin(s) of the antipathetic structure sensitivity 52
  2.3.6. Resolving the discrepancies in the observed structure sensitivity between the literature and this work 55
2.4. Conclusions 56
2.5. Acknowledgements 57
2.6. Appendix 58
2.7. References 61

Chapter 3

On the active sites and reactive intermediates in the hydrogenolytic cleavage of C–C bonds in cyclohexane over supported iridium clusters 64

3.1. Introduction 65
3.2. Experimental 67
  3.2.1. Catalyst preparation 67
  3.2.2. Catalyst characterization 68
  3.2.3. Steady state kinetic measurements 70
3.3. Results 71

3.3.1. Catalyst characterization 71
3.3.2. Thermodynamics and kinetics of minor reaction channels in CH conversion 77
3.3.3. Structure sensitivity of CH hydrogenolysis: rates and selectvities 81
3.3.4. H_2 pressure dependences of rates and selectivities 88
3.3.5. Temperature dependences of rates and selectivities over Ir clusters of different sizes 97
3.4. Discussion 99
3.4.1. Cleavage patterns of cyclohexane in primary and secondary pathways . 100
3.4.2. Implications of H_2 pressure effects on product formation rates and apparent activation energies in cyclohexane hydrogenolysis 102
3.4.3. Mechanistic considerations based on a classical microscopic model for alkane hydrogenolysis 105
3.4.4. Structure sensitivity of cyclohexane hydrogenolysis: the sympathetic branch 111
3.4.5. Structure sensitivity of cyclohexane hydrogenolysis: the antipathetic branch 114
3.4.6. H-deficiency of reactive intermediates as the selectivity mediator for single scission and terminal/internal multiple scissions 117
3.5. Conclusions 120
3.6. Acknowledgments 121
3.7. Appendix 121
3.8. References 125

Chapter 4

Structure sensitivities of hydrogenolytic cleavage of endocyclic and exocyclic C–C bonds in methylcyclohexane over supported iridium clusters ……. ……………………………………………… ………… .. 128

4.1. Introduction 129

4.2. Experimental 130

4.2.1. Catalyst preparation 130

4.2.2. Catalyst characterization 131

4.2.3. Steady-state kinetic measurements 132

4.3. Results 133

4.3.1. Characterization of the supported iridium catalysts 133

4.3.2. Minor reaction channels in methylcyclohexane conversion 134

4.3.3. Structure sensitivity of methylcyclohexane hydrogenolysis: rates of turnovers via endo- and exocyclic C−C bond cleavages 135

4.3.4. Product selectivities as a function of conversion and Ir dispersion 137

4.3.5. H_2 pressure dependences of rates and selectivities over Ir clusters of different sizes 148

4.3.6. Temperature dependences of rates and selectivities over Ir clusters of different sizes 157

4.3.7. Kinetic simulation based on a classical mechanistic model 161

4.4. Discussion 165

4.4.1. Selectivities of C−C bond cleavages in methylcyclohexane along primary and secondary pathways 165

4.4.2. Apparent and intrinsic structure sensitivities of endocyclic and exocyclic C−C bond cleavage 170

4.4.3. Microscopic implications of H_2 pressure effects on product formation rates 172

4.4.4. Apparent and intrinsic energetics of endocyclic C−C bond activation... 175

4.5. Conclusions 177

4.6. Acknowledgements 179

4.7. Appendix 179

4.8. References 181

Chapter 5

Mechanistic implications from deuterium isotope effects…………… 183

5.1. Introduction 184

5.2. Theoretical background 185

5.2.1. H/D isotope effects 185

5.2.2. Statistical thermodynamics approach: evaluation of partition functions 189

5.3. Experimental 190

5.3.1. Catalyst preparation and characterization 190

5.3.2. Switch experiments between MCH-d_0–H_2 and MCH-d_{14}–D_2 mixtures . 190

5.4. Results and discussion 191

5.4.1. Measurements of isotope effects on conversion rates 191

5.4.2. Some postulated mechanisms and relevant IE predictions 196

5.5. Conclusions 201

5.6. Appendix 202

5.7. References 206

Chapter 6

Summary and conclusions…………………………………………….. 207

Curriculum vitae ……..……………………………..…………………210

List of publications……………………………….………………….211

List of presentations………………………………...………………..213

Chapter 1

Introduction

1.1. General background

Stringent environmental regulations and legislations associated with clean fuels have prompted intensive research on the quality improvement of gasoline and diesel [1−3]. These quality standards call for mitigation of sulfur levels, polynuclear aromatics, volatility and density, to name a few in relation to diesel fuels. Higher cetane numbers (CNs) are also aimed at for upgraded diesel fuels [4,5]. Particularly, multi-ring aromatics greatly decrease the CN, increase the amount of particulates in the exhaust gases, and worsen the overall quality (e.g., density and viscosity) of the diesel [6]. Moreover, light cycle oil (LCO) has been increasingly added as a blending component to the diesel pool to meet the surging demand for diesel fuel in the United States [7]. However, LCO also contains high concentrations of aromatics, which require further upgrading.

Commercially demonstrated upgrading technologies of the diesel-range fuels include aromatics saturation (ASAT) and hydrocracking [2,7,8], despite their inherent limitations. While preserving the molecular backbones in diesel range and reducing the density of middistillate fuels, ASAT alone cannot enhance the CN to a level that will fully meet future demands. Hydrocracking, in contrast, concentrates minimally branched, high-CN alkanes in the diesel range, whereas it suffers from excessive reduction of the molecular weight and, as a result, lower yields in the diesel range [6].

According to McVicker et al., a potential route to a low-aromatics, density-reduced, high-cetane-index diesel fuel is ASAT of a low-sulfur middistillate stream followed by selective ring opening (SRO) of naphthenic rings to chain alkanes [9−11]. Contrary to unselective cracking, ring opening (RO) could result in a high CN product without loss of reactant molecular weight. As illustrated in Scheme 1-1 for some relevant C_{10} compounds, the CN greatly increases when a molecule such as decalin with two naphthenic rings is converted into a normal paraffin. However, one must keep in mind that not every ring-opening product (ROP) exhibits a CN higher than that of the naphthenic compound from which it originated [12].

Scheme 1-2 outlines the transformations likely to occur during the hydroconversion of polynuclear aromatics to alkanes [9]. Although RO can be catalyzed merely by Brönsted acid sites as shown by Kubička et al. [13], this type of catalysis has only been subjected to a few studies [3,6,13], either because of the much higher temperatures to induce acid catalysis at reasonably high rates, or due to the significant skeletal isomerizations occuring at all temperatures. Regardless, severe deactivation caused by the inevitable use of high temperatures and stronger acidities seems to be the gravest problem when one explores the ring opening reactions on such monofunctional acid catalysts. We only briefly describe the acid-catalyzed RO reactions in the next section.

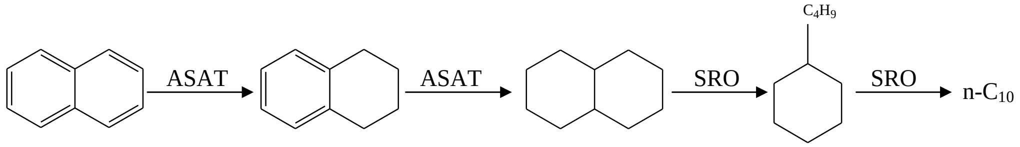
C4H9
ASAT
ASAT
SRO
SRO
n-C10

Density	1.025	0.973	0.896	0.799	0.730
CN	10−20	15−20	35−38	58−62	72−76

Scheme 1-1. Aromatic saturation (ASAT) of polynuclear aromatics followed by selective ring opening (SRO) provides density and cetane number benefits (after ref [9]).

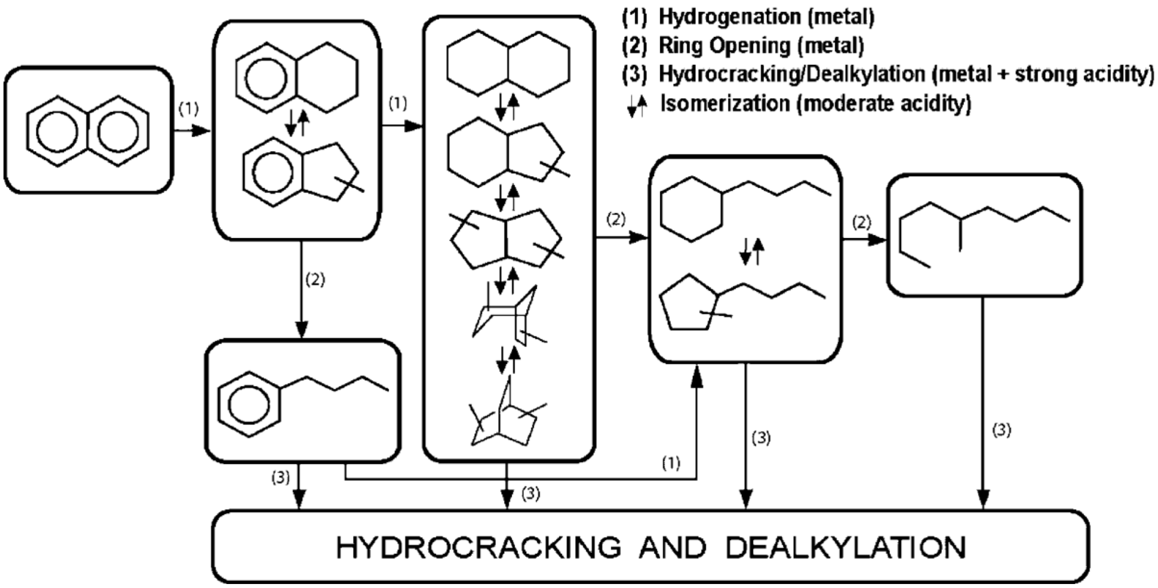
(1) Hydrogenation (metal)
(2) Ring Opening (metal)
(3) Hydrocracking/Dealkylation (metal + strong acidity)
Isomerization (moderate acidity)
(1)
(1)
(2)
(2)
(2)
(1)
(3)
(3)
(3)
(3)
HYDROCRACKING AND DEALKYLATION

Scheme 1−2. Key reactions during the conversion of multiring aromatics to paraffins [9].

Most studies applied saturated molecules (e.g., decalin [3,6,13−18], cyclohexanes [19−21]) as the starting feed, because intially abundant multi-ring aromatics and naphtheneoaromatics are readily hydrogenated to naphthenes under typical RO conditions [22]. Tetralin, indan and naphthlene were also used in a number of reports, where RO reactions were always accompanied by hydrogenation of the unsaturated ring [6,23−25]. Following deep hydrogenation of the unsaturated ring(s), SRO of the resultant naphthenic rings is the essential reaction [9]. To achieve acceptable RO rates, acid functions are often present to facilitate the ring contraction (RC) from six-membered naphthenes to five-membered naphthenes. The RO selectivies will also be remarkably affected by the acid-mediated RC step, since the effect of substituents associated with the ring backbone changes with the size of the ring. Metal- and acid-catalyzed hydrocracking and dealkylation reactions must be suppressed to avoid losses in middistillate yield. Secondary isomerization of product alkanes must also be minimized, as increased branchiness greatly reduces cetane values [6]. In Section 1.3, naphthenics ring opening with bifunctional catatlytic systems is to be discussed.

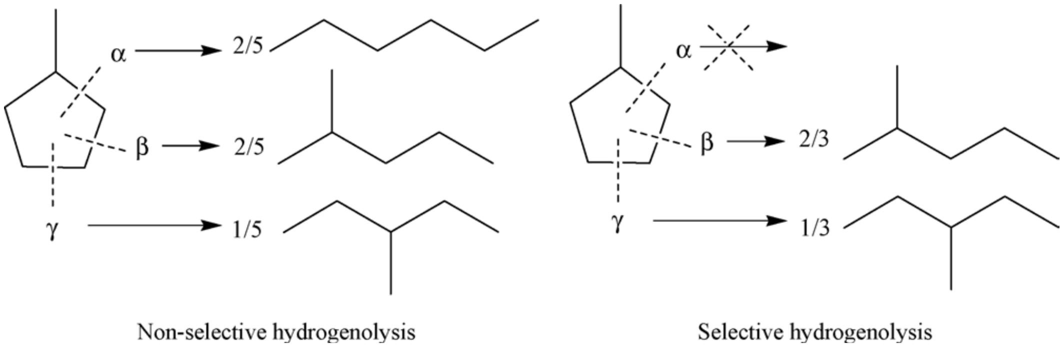

Figure 1−1. Non-selective and selective hydrogenolysis of methylcyclopentane (after ref [35]).

To this date, most investigations into the purely metal-catalyzed RO reactions have dealt with methylcyclopentane (MCP), i.e., a methyl-substituted five-member-ring, as the probe molecule [26−36]. Significant amount of knowledge has accumulated on this probe molecule, most of which concerns the effect of metal specificity and particle size on the ring opening product (ROP) distribution [37]. Over supported Pt catalysts with small particle sizes, the rupture of endocyclic C–C bonds is statistical (non-selective), producing 2-methylpentane (2MP), 3-methylpentane (3MP) and n-hexane (nHx) in a ratio of 2MP:3MP:nHx = 2:1:2, corresponding to the number of bond types in the molecule (Figure 1-1). On the other hand, the ring opening of MCP on large metal particles and metal surfaces with low Miller index planes produces selectively 2MP and 3MP, but little nHx. In some cases, MCP ring opening does not follow the ‘selective’ or ‘non-selective’ mechanism, instead producing unusually high amount of nHx or 3MP relative to its statistical ratio. This ‘partially selective’ mechanism competes with the ‘non-selective’ and ‘selective’ mechanism, occurring, for instance, on high loaded 10% Pt/Al_2O_3 at high-temperature [26]. Different surface structures and intermediates are believed to be responsible for the different mechanisms to operate, but their identities and origins remain unresolved.

In contrast to results on Pt catalysts or model surfaces, the ring opening of MCP on Ir [26,35] and Rh [36] is much less sensitive to the metal particle size. To be specific, these metals exhibit higher activity and selectivity to open the C_5 ring in bisecondary positions [9,26]. Less active Pd particles tend to catalyze preferentially exocyclic C−C bond cleavage, leading to demethylation. Other metal catalysts, such as Co, Ni, Ru and Os, show extensive hydrogenolysis, producing significant amounts of lower alkanes [36]. The proposed mechanisms and the origins of the particle size effect on the ROP distribution have been summarized in a recent review [37].

Compared to the extensively studied MCP ring opening, surprisingly few have looked into the RO of six-membered naphthenes over monofunctional metal catalysts [17,19,38]. The reason for this low research activity could be understood by the much lower rates and lower selectivities in the direct RO of a cyclohexyl ring, in contrast to the cyclopentyl ring [9]. In a practical context, however, the relevance of the RO of (fused) six-membered naphthenes is higher than that of five-membered naphthenes. A detailed evaluation of the reaction kinetics by widely varying the process conditions is key to the successful elucidation of the ring opening chemistry on a mechanistic and molecular level. The whole body of Section 1.4 deals with the state-of-the-art of the hydrogenolytic cleavage of (endocyclic) C−C bonds catalyzed exclusively by metal particles.

1.2. Ring opening on acidic catalysts

Under reaction conditions often applied, RO on acidic catalysts proceeds in an indirect way, that is, isomerization occurs prior to endocyclic C−C bond cleavage. Kubička et al. [13] studied the activity of H-Beta-25, H-Beta-75, H-Y-12, H-Mordenite-20, and H-MCM-41 in the RO of decalin at 498–573 K in the presence of hydrogen (a total pressure of 2 MPa). Skeletal isomerization, stereoisomerization, ring opening, and cracking were the prevalent reaction types. It was found that decalin must first be isomerized to alkyl-substituted bicyclononanes and bicyclooctanes to make possible its ring opening. Methylbicyclo[4.3.0]nonanes, dimethylbicyclo[3.2.1]octanes, and dimethylbicyclo[3.3.0]octanes formed by decalin skeletal isomerization were the most abundant isomers, which were subsequently converted into ROPs. The presence of Brønsted acid sites proves essential for both isomerization and RO, that is, a higher Brønsted acidity results in a higher initial activity. The acidity together with the pore structure influences catalyst deactivation. As observed by these authors and earlier by Corma et al. [3], 12 MR zeolites (USY or even better Beta zeolite) based catalysts are superior to small to medium pore zeolites, in terms of RO selectivity and extent of deactivation. As a general rule, the density of acid sites needs to be adjusted to an optimum, high enough to achieve conversion, but not too high that would result in fast deactivation [6]. As expected, the selectivities of ROPs attainable on acid zeolites seemed to be smaller than on their bifunctional counterparts [14] (see more in the next section), and the same typical cracked products were reported with a preponderance of isobutane and MCP.

1.3. Ring opening via bifunctional catalysis

In this section, we would like to first provide a selection of highlights from recent studies on bifunctionally catalyzed ring opening, and then raise a number of important concerns that have not been particularly addressed in previous contributions. Although the RO of naphthenes on bifunctional catalysts is not within the scope of the thesis (Section 1.5), the fundamental questions into these systems, after being fully addressed, are believed to resolve the discrepancies in the observations and to shed light on the mechanism(s) of such bifunctional RO catalysis.

1.3.1. Ring opening of bicyclic and monocyclic hydrocarbons on bifunctional catalysts

Bifunctional catalysts employed in the RO of decalin and tetralin are mostly based on zeolites. As a general observation, the attainable selectivities of ROPs in the presence of metal components (high hydrogen pressures) are higher than on their monofunctional zeolite counterparts.

Resasco and coworkers have shown that the two products of the hydrogenation of tetralin, i.e., *cis*- and *trans*-decalin have different reactivity in the subsequent RC and RO reactions [6]. Specifically, to maximize the CN, one would require a high fraction of *cis*-decalin in the feed for the RO step. After conducting a comparative study of tetralin hydroconversion on Ni, Pt and Pd catalysts, the authors reached the conclusion that the intrinsic selectivity for each isomer is about the same on Ni and Pt, while the *trans*-form is favored on Pd [23]. In all cases, the intrinsic *trans*/*cis* ratio was much lower than the equilibrium. At high tetralin conversions, the *trans*/*cis*-decalin ratio continuously increased with conversion over Ni and Pt catalysts due to increasing *cis*-to-*trans* isomerization. In contrast, over Pd catalyst the ratio remains unchanged over the entire tetralin conversion range, due to the low isomerization activity of Pd compared to those of Ni and Pt [23].

As a result of the many potential hydroconversion routes (ring opening, isomerization and hydrocracking) with different activation barriers, all catalyzed by Brönsted acidity, reaction temperature plays a crucial role in modifying the product distribution [24]. Regardless, modest yields of ROPs still containing one naphthenic ring were reported in most of the previous studies [14,16−18]. Yields of open-chain decanes were rarely reported, most probably due to analytical limitations. Very recently, Weitkamp and coworkers reported on remarkable yields (30−40%) of open-chain decanes in the hydroconversion of decalin over Ir- and Pt-containing La-X or Na,H-Y catalysts [15,38]. The delicate balance in the concentration (or ratio) and the close proximity of the acidic and metallic sites are critical for the optimal catalytic performance [39]. These authors failed to address the ring opening pathways in detail, and admitted that RO is the least well understood reaction involved in the complex network of decalin hydroconversion on bifunctional catalysts.

Despite a few successful demonstrations of applying advanced analytic techniques (e.g., two dimensional GC) to these reactions [15,25,38,39], widely spanning GC spectra and complicated analysis of reaction products by general means prevent the majority of researchers from obtaining accurate information on the detailed reaction pathways and microscopic mechanisms, in the RO of bicyclic hydrocarbons.

In comparison, cyclohexane and its alkyl derivatives represent interesting, albeit less studied than decalin and tetralin, probe molecules for exploring the fundamentals in RO of six-membered naphthenes over bifunctional or monofunctional metal catalysts. In a systematic study on methylcyclohexane (MCH) conversion over bifunctional Ir catalysts supported on W-doped ZrO_2-SiO_2, the influence of W and Ir loading was investigated [20]. It was found that the best RO yields were obtained with the 1.2%Ir/WO_x/ZrO_2-SiO_2 (1.5 W-atoms/nm^2). It was concluded for these bifunctional catalysts that MCH isomerization to alkylcyclopentanes occurs before RO, suggested by the initial selectivity to ring contraction products (RCPs) and ROPs at zero contact time. According to McVicker et al., the acidic Pt/USY catalyst by itself is not active for MCH RO but effectively catalyzes RC of MCH (98% selectivity); addition of two parts by weight of the Pt/USY ring-contraction catalyst to one part of Ir/Al_2O_3 doubled the RO yield and halved the cracking yield of the Ir-only catalyst [9]. Similarly, bicyclohexane (BCH) conversion over an admixed catalyst system comprised of one part Pt/USY(Si/Al = 37) and five parts Ir/Al_2O_3 increased the RO yield from 14 to 30%. Increasing the amount of Pt/USY threefold, however, resulted in a decrease in ROP yield from 14 to 10% relative to that with the Ir/Al_2O_3 catalyst. The large ROPs yield and selectivity differences exhibited by the 5:1 and 5:3 metal-to-acid admixtures clearly illustrates the important role metal/acid site balance plays in SRO chemistry [9].

1.3.2. Fundamental considerations

It is important to note that two different categories of bifunctional catalysis may take place in the context of RO on metal/acid catalysts. These two types mainly differ in the nature of the active sites, acidic or metallic, that are involved in the rate determining step of the C−C bond cleavage (Figure 1-2).

(a) Dehydrogenation equilibrium on metal and protonation on Brönsted acid sites

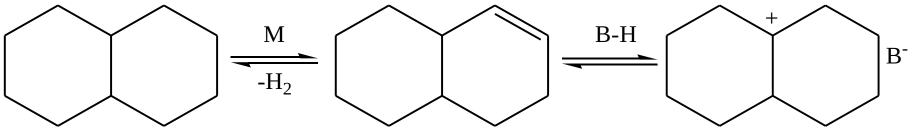

(b-1) Direct C−C bond cleavage on Brönsted acid sites and hydrogenation on metal

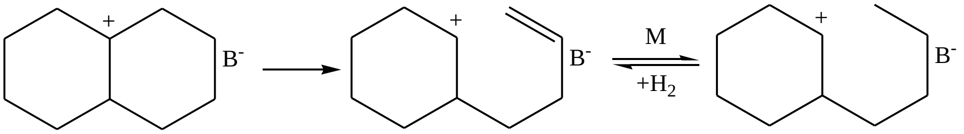

(b-2) Ring contraction (RC) and C−C bond cleavage on Brönsted acid sites and hydrogenation on metal

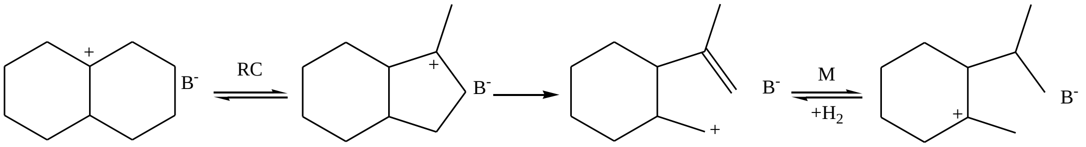

(c-1) Desorption of ring contraction products and hydrogenation at metal sites

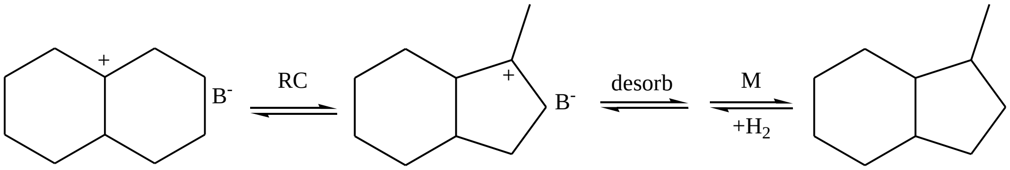

(c-2) Hydrogenolysis of the endocyclic C−C bonds in the smaller ring on metal

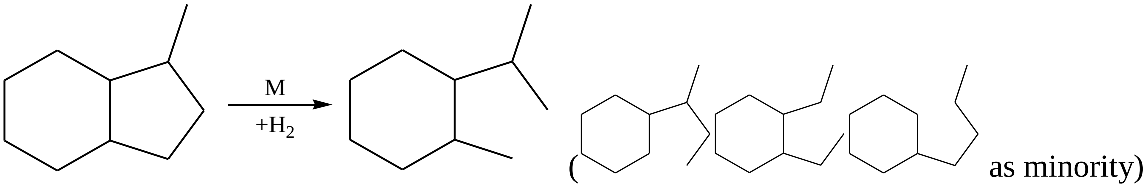

Figure 1-2. Ring opening on bifunctional catalysts: (a) Dehydrogenation equilibrium on metal and protonation on Brönsted acid sites, generally applicable on bifunctional catalysts; (b) endocyclic C−C bond cleavage on Brönsted acid sites; (c) endocyclic C−C bond cleavage in the contracted ring on metal. Final product desorption from acid sites is

not shown for (b). Hydrogenolysis of C−C bonds in the C_6-ring, which is not depicted in (c), can occur, albeit at much lower rates than that of C_5-ring opening.

Ring opening of cyclic hydrocarbons via the first type of bifunctional catalysis bears significant resemblance to that via monofunctional acid catalysis, in the sense that the acidic function, rather than the metallic one, mediates the C−C bond cleavage. In a typical scenario of hydrocracking via bifunctional (metal and acid) catalysis, it is well accepted that the metal first catalyzes the dehydrogenation of alkane to the thermodynamic endpoint; the resulting alkenes diffuse to the Brönsted acid sites, where the adsorbed carbocations can undergo β-scissions (and skeletal rearrangments); the formed products are desorbed from the Brönsted acid sites as alkenes and then shuttle back to the metallic sites for re-hydrogenation and eventual desorption into gas-phase [40]. In this kind of bifunctional catalysis, the step of β-scissions of the carbocations which occurs on the acidic sites is rate- and selectivity-determining, while the metal only serves as the dehydrogenating-hydrogenating function. Obviously, RO occurs as a mechanistically primary reaction and must show a non-zero selectivity at infinite space velocity. In cyclic hydrocarbons, the β-scissions of endocyclic C−C bonds are much slower than those in chain alkanes, caused by an unfavorable orientation of the p-orbital at the positively charged carbon atom and the β-bond to be broken [15].

In the second type of bifunctional RO catalysis, the ring-contracted primary products (either via a bifunctional pathway, or catalyzed by some metal like Pt but not Ir [38]) undergo activation at the surface metal atoms instead of acidic centers (metal/acid proximity plays a role here). If there are two rings in the ring-contracted intermediates, the endocylic C−C bonds in the smaller ring are preferably cleaved (Figure 1-2(c)). Ring opening products, in this case, are secondary in mechanistic nature. The distinction between two types of bifunctional RO catalysis can be made by studying the selectivity changes with space velocities. When the metal and acid sites are close enough to each other, however, the ROPs may still be discerned as kinetic primary products. To further differentiate these two mechanisms, a detailed quantitative evaluation of product distribution is mandatory. For instance, RO at substituted positions is not favorable on surface metal atoms as a result of steric hindrance, but is preferred on acid sites due to the greater stability of the tertiary carbenium ions.

The above two types of bifunctional RO catalysis possibly co-exist under a majority of circumstances, but their relative importance varies with the reaction temperature, the metal specificity and particle size, the acid strength, as well as the metal/acid ratio and proximity. While the metal specificity and particle size can be considered inconsequential in the first type of bifunctional RO catalysis (as long as the dehydrogenation-hydrogenation equilibria are attained), such metal characteristics are definitely important for the second type that involves a metal-catalyzed C−C bond cleavage step (Figure 1-2(c)). Since the metal- and acid-catalyzed C−C bond cleavage exhibit significantly different transition states, the temperature and local surface structure (e.g., particle size of the metal, solvation environment of carbocation intermediates) dictate the activity and selectivity of the overall RO catalysis on bifunctional catalysts.

In the case of six-membered naphthenes, the reactant upon dehydrogenation (mainly on metal, though protolytic dehydrogenation is also possible) can experience both ring contraction and protolytic C−C bond cleavage on the Brönsted acid sites, depending on the reaction temperature and the acid strength. Ring contraction is easier to occur, in terms of the requirement of temperature and acid strength. And most noble metals effect the opening of the five-membered ring with considerably lower activation energies and higher rates than do the Bronsted acid sites. If the reaction temperature is such (relatively lower temperatures) that favors the RC, the RO is thought to proceed via secondary reactions of the RCPs. If the temperature and acid strength is high enough to induce acid-catalyzed cleavage of endocyclic C−C bonds, then the RO can be catalyzed by the acidic sites. But keep in mind that the high temperature and strong acidity would also induce significant hydrocracking of the alkyls, to a greater extent than the cyclics. Therefore, high temperature and strong acidity are not suited for SRO catalysis. Although Kubička et al. [14] and Rabl et al. [15] concluded that the first ring opening to one-ring C_{10} naphthenes happens simultaneously on the acid sites via carbocations and on the noble metal via hydrogenolysis, there is a high chance that only one of the two is dominant. We speculate that the metal (mainly Pt, Ir) not only serves as the dehydrogenation-hydrogenation function, but can also be active for the endocyclic C−C bond cleavage when there is no significant Brönsted acidity. In line with this speculation, McVicker et al. reported that the most active and RO-selective mixture of Ir/Al_2O_3 and Pt/USY was only twice active and slightly more RO-selective than Ir/Al_2O_3 [9]. In addition, a most recent study revealed that less conventional bifunctional catalysts, i.e., Pt- and Ir-containing K,Cs,Rb-exchanged Y zeolites with low and weak Brönsted acidities, exhibited much higher selectitivies to direct ROPs, the same as expected from hydrogenolysis pathways on metals, than those M/zeolites (M = Pt or Ir) containing sufficiently strong Brönsted acidities [38]. Hydrogenolysis of the endocyclic C−C bonds in decalin on Pt-containing faujasites gives much more butylcyclohexane than on Ir-containing ones. In stark contrast, these authors found under the same conditions (5.2 MPa H_2, 473−528 K) that the nature of the noble metal (M = Pt or Ir, differing very much in their hydrogenolysis activities) does not have a significant impact on the activities or selectivities of the bifunctional M/La-X catalysts in decalin hydroconversion [15].

The question arises, as to why the conclusions about the role of the metal could entirely change from one bifunctional system to another. To provide a plausible interpretation, one needs to consider that the activation of the cyclic hydrocarbon and dihydrogen may occur on different sites in a classical bifunctional scenario. The effect of metal specificity is small in this case, because, whenever there are sufficiently strong Brönsted acidities, the hydrocarbon coverage on the metal would be much lower compared to that on the acid sites. At the present stage, the above question is still left open. What has been made certain, however, is that this type of bifunctional catalysis is responsible for the formation of RCPs and C−C bond ruptures in the exocyclic alkyl substituents, the latter leading eventually to hydrocracked products.

From a mechanistic point of view, the hydrogen pressure dictates the concentration of olefinic species by virtue of the dehydrogenation pre-equilibrium, but it does not, in principle, affect the intrinsic activation barrier or entropy changes because of the kinetic irrelevance of any H-derived species (gas phase H_2, weakly held hydrogen, or H-adatoms) in the rate-determining step of ring opening in a classical bifunctional catalysis (the 1st type as defined above). Kubička et al. found that the initial activity of bifunctional Pt catalysts in decalin conversion remained practically unaltered when the hydrogen pressure was increased from 0.7 to 3.7 MPa, suggesting that the ring opening reaction of decalin is zero-order reaction with respect to hydrogen [14]. However, the high conversion levels (> 80%) and ubiquitous deactivation could have shadowed the reliability of this observation. Surprisingly, the choices of reaction conditions in the literature seem to be rather arbituary, H_2-pressure dependences of rates and selectivities remaining unexplored.

To fully elucidate the RO reactions on bifunctional catalysts, all the above concerns await to be addressed by rigorous kinetics studies combined with tools such as modeling and theoretical treatments, which have been rarely applied in these reactions. Considering the severely entangled interaction between the metallic and acidic sites, in any of the above scenarios, almost no straightforward relationship could be expected between the surface structure and the catalytic performance in such bifunctional catalytic systems. A separation of the metal catalysis from the acid catalysis is, therefore, of obvious necessity.

1.4. Hydrogenolysis of alkanes and cycloalkanes on noble metals

In the context of alkanes, hydrogenolysis is the breaking of C−C bonds by the action of hydrogen, leading to alkanes of lower molar mass [41]. For a collective description of the kinetics studies in hydrogenolysis and the general theories behind, the interested readers are referred to chapters 13 and 14 in a book written by G.C. Bond [41]. Hydrogenolysis of hydrocarbons with up to seven carbon atoms was extensively studied in the 1960s and 1970s by Gault and coworkers, mainly by the ^{13}C tracer technique. The large body of experimental results has been reported in an excellent review [26].

Typical catalysts for hydrogenolysis are noble metals on non-acidic or weakly-acidic supports. Base metals like Ni and Co have been also studied. The reactions are exothermic and possess large equilibrium constants (Table 1-1), but need temperatures that generally exceed 400 K because activation energies are high. Classical mechanisms for hydrogenolysis are assumed to involve dehydrogenative activation of the hydrocarbon and the rate-determining C–C bond rupture step, with differing details in the specific elementary steps among different proposals [41]. On a metal such as Pt, C–H bonds are activated much more readily than C–C bonds, and dehydrogenative chemisorption takes place at temperatures much lower than those required for hydrogenolysis. At sufficiently high temperatures, a certain fraction (reactive ones) of the H-depleted carbonaceous intermediates undergo C–C bond cleavage, whereupon the products are hydrogenated and desorbed. It is evident from such a mechanism that the selectivity of hydrogenolysis will be largely influenced by the nature of the metal and the mode of adsorption of the reactant hydrocarbon, unlike the classical bifunctional scenario.

Table 1-1. Thermodynamics for hydrogenolytic pathways in cyclohexane (c-C_6H_{12}) conversion (thermochemistry data for relevant compounds at reference conditions acquired from CRC Handbook of Chemistry and Physics 84th Edition)

Pathway	ΔH_{rxn}^o (kJ mol^{-1})	ΔS_{rxn}^o (J K^{-1} mol^{-1})	K_{rxn} at T	
			T = 523 K	T = 573 K
c-C_6H_{12} + H_2 = n-C_6H_{14}	-43.8	-40.2	188	78
c-C_6H_{12} + 2H_2 = n-C_5H_{12} + CH_4	-98.1	-24.4	3.3×10^{8}	4.6×10^{7}
c-C_6H_{12} + 2H_2 = n-C_4H_{10} + C_2H_6	-86.2	-20.5	3.4×10^{7}	6.1×10^{6}
c-C_6H_{12} + 2H_2 = 2C_3H_8	-84.2	-19.3	2.5×10^{7}	4.6×10^{6}

While RO and deep (multiple) hydrogenolysis both concern C–C bond cleavage, the latter needs to be avoided in the naphthene upgrading for practical reasons (e.g., value losses). The main difference between these two reactions relates to the fact that the former (RO) is cleavage of endocyclic C–C bonds and the latter is cleavage of C–C bonds in chain alkanes. Bond strengths, hybridization states and orbital overlaps (with bonding orbitals of surface metal atoms) of C–C bonds and associated C–H bonds are important for the thermodynamics and kinetics, thus influencing the activities and selectivites of these two hydrogenolytic reactions on surface domains of noble metals.

1.4.1. Ring opening of five-membered naphthenes on monofunctional metal catalysts

Ring opening of methylcyclopentane (MCP) has been extensively studied, as we have mentioned in Section 1.1. The metal specificity and dispersion, as well as the support, are found to be consequential to the ROPs distribution, particularly in the case of Pt. It has been suggested in the literature that two extremes of mechanisms, ‘selective’ or ‘non-selective’, according to the extent that the substituent shields the adjacent C–C bonds [26]. A ‘partially selective’ mechanism has also been proposed to account for the observations on acidic oxide (unexpectedly high selectivities to nHx and 2MP but not 3MP) or zeolite (significantly higher selectivity to 3MP) supported noble metal catalysts, but it is not guaranteed that these peculiar selectivities are not due to bifunctionality or shape-selective features. It is probably safer to believe that the condition of the surface and the nature of the sites (geometric and electronic effects included) available determine the extent to which the methyl group interferes with the process of chemisorption or the stability the adsorbed state, so that a gradual transition between the two limits might be envisaged [41].

Besides MCP, the effect of the side chain length was explicitly studied by McVicker et al. [9]. Extension of the side-chain to pentyl lowered the ring-opening selectivity, but it remained above 70% for Pt/Al_2O_3, Rh/Al_2O_3 and even Ru/Al_2O_3, while for Ir/Al_2O_3 it was still 92% [9]. The number of alkyl substituent on the five-membered ring has also a remarkable effect on the ring opening selectivity and activity. McVicker et al. showed that on Ir/Al_2O_3, ring-opening selectivity depended on the number of CH_2–CH_2 bonds, which argues for the dicarbene mechanism [9]. The chemisorbed state of cyclopentene was reported to be more or less perpendicular to the Ir(111) surface by a NEXAFS study, in support of this mechanism.

The relation between the prevalent surface structure and the catalytic activity in RO reactions of five-membered naphthenes, however, has only been subjected to a few studies. On Pt/Al_2O_3, the turnover rate of cyclopentane (CP) RO was shown to decrease with decreasing particle size [42], similar to that observed on Rh/Al_2O_3 [43]. In contrast, CP RO on Ir/Al_2O_3 was found to be insensitive to particle size [42]. Some possible explanations for the particle size effect on the activity include electronic effects, morphology, and support effects [26,44]. However, some of the observations were suspected to be confounded by unintended artifacts, such as self-poisoning carbon deposition or adventitious impurities [45,46]. Moreover, the structure sensitivity was only explored at a single set of conditions, without knowledge of its extendibility to other conditions, e.g., different H_2 pressures. Although monofunctional Pt catalysts are always less active, than Ir and Rh catalysts, in the RO of five-membered naphthenes, they remain important catalysts of choice owing to the higher cleavage selectivities towards substituted endocyclic C−C bonds. Bimetallic Pt-Ir and Pt-Rh catalysts, with optimized compositions and structures of the bimetallic clusters, also exhibit superior activities and selectivities to their monometallic Ir and Rh counterparts [34].

1.4.2. Ring opening of six-membered naphthenes on monofunctional metal catalysts and model surfaces

Ample experimental evidence exists that six-membered naphthenes are (much) less reactive than five-membered naphthenes towards RO, a fact generally believed to originate from the substantially lower ring strain (6–7 kcal mol^{-1}) than that (1 kcal mol^{-1}) in five-membered naphthenes [9]. This interpretation would imply that the intrinsic activation barrier is higher in the RO of six-membered naphthenes than of five-membered naphthenes on the same catalyst, as long as the C-C bond does not break from so early on in the transition state that the activation barrier becomes irrelevant to the ring strain. Early transition states might be involved in RO reactions catalysed by Ru catalysts, which showed low activation barriers (e.g., 60 kJ mol^{-1} in hydrogenolysis of n-butane on Ru/Al_2O_3 [47]) and much higher catalytic activities in alkane hydrogenolysis.

Unlike in the RO of five-membered naphthenes, where promising features (mainly in selectivity terms) are shown for monofunctional Pt catalysts, such Pt catalysts, in the absence of appropriate acidity, require much higher reaction temperatures than monofunctional Ir and Rh catalysts in the conversion of six-membered naphthenes [9]. Moreover, SiO_2- and Al_2O_3-supported Pt catalysts, which opened MCP with 97-98% selectivity to C_6-alkanes, displayed only 4–5% selectivity for ring opening MCH to C_7-alkanes [9]. Instead, dehydroaromatization occurs as the dominant reaction pathway at all practical temperatures on monofunctional Pt catalysts. Ni- and Ru- catalysts, on the other hand, prefer deep hydrogenolysis [9]. As a result, Ir catalysts hold promise among the monofunctional catalysts for achieving SRO of C_6-carbocycles in a single, direct scission.

Thus far, only a few studies have dealt with direct ring opening of (fused) C_6-carbocycles on monofunctional Ir catalysts. Houalla's group has been investigating MCH ring opening over Ir catalysts on different supports (ZrO_2-SiO_2, Al_2O_3 and their W-doped forms), some of them containing catalytically unimportant amounts of Brönsted acidity [17,20]. Ring opening was found to occur predominantly at unsubstituted C−C bonds, typical of a so-called 'dicarbene mechanism'. For Ir/ZrO_2-SiO_2 catalysts, the Ir content had no significant affect on the activation energy calculated for direct ring opening of MCH (about 138 kJ/mol). Since the Ir dispersions were very similar (13%) in these catalysts, independent of the Ir content [20], the monofunctional catalysts would naturally be expected to behave similarly. For Ir/Al_2O_3 catalysts, again, the Ir loading had no remarkable impact on the product selectivity, consistent with the fact that an increase in the Ir loading (0.6 to 1.8%) only led to a slight decrease in the Ir dispersion (56 to 40%). The apparent activation energy decreased monotonically from 150 to 142 kJ mol^{-1} with increasing Ir loading from 0.6 to 1.8% [17]. Although these authors did not focus on these observations, we find in our catalytic systems similar phenomena and good ways of interpreting those findings (Chapters 3 and 4).

In a recent study by Resasco and coworkers, the RO reactions of 1,2- and 1,3-dimethylcyclohexane (1,2- and 1,3-DMCH) were investigated over Ir catalysts supported on Al_2O_3, SiO_2, and TiO_2 [19]. This study nicely disclosed the versatility of Ir-catalyzed ring opening processes, aiming at the improvement of either cetane or octane numbers, by changing the support characteristics. Ir/Al_2O_3 was demonstrated to be the most selective toward RO at substituted positions. This preferred path on alumina-supported catalysts appears to be related to a support effect rather than to an effect of metal dispersion, because catalysts of different metal dispersions on Al_2O_3 display a comparable selectivity much higher than that obtained on any of the SiO_2-supported catalysts [19]. The authors pointed out that only a specific conformer (*cis*- or *trans*-) of the DMCHs, the preponderance of which in turn depend on the type of support, favor the formation of such intermediates that lead to SRO of substituted C−C bonds and hence to CN improvement [19]. Although the mechanisms for C−C bond cleavage at substituted positions have been postulated to involve metallocyclobutane-like or adsorbed olefin species, these proposals lack unambiguous evidence for such surface species. Furthermore, we note that in none of these previous studies were there any attempts to establish structure-activity relations with respect to the metal [17,19,20].

In addition to the above-mentioned studies, there have also been emerging ones on the RO of multi-ring naphthenes such as decalin [17,38]. An exciting message has been conveyed from the most recent seminal work by Weitkamp and coworkers that monofunctional Ir catalysts on non-acidic zeolite supports (e.g., Cs-neutralized Y zeolite) entail very promising catalytic properties, compared to bifunctional catalysts with well-tuned metal-acid balance [15,38,39]. We suspect, however, that these studies (some conducted at high conversions) do not shed further light on the mechanistic picture, as a result of the complicated product analysis and simplifying grouping procedures. More in-depth investigations into the reaction kinetics (pressure dependence, activation energies) are required to reveal the locus of reactant activation (e.g., solvation of hydrocarbon in the zeolite cage) and the nature of active surface structures in the rate-determining step.

As a final note on this area, it is worth mentioning the surface science studies of cyclohexane (CH) conversion on model Pt surfaces by Somorjai and coworkers [48-50]. Not only the C–C bond breaking processes, but also the dehydrogenation and isomerization pathways were studied. The results led these authors to draw contradictory conclusions about the nature of the active sites at different reactant pressures. While the terraces of Pt(111) without steps and kinks were the most active for C–C bond breaking of cyclohexane in 100 Torr H_2 [48], kinks in the steps appeared the most active at very low cyclohexane (5×10^{-6} Pa) and H_2 (10^{-4} Pa) pressures [49,50]. Thus, the influence of reaction conditions, particularly the H_2 pressure, on the observations and interpretations is clearly illustrated by the comparison of these divergent findings from the same group.

1.5. Scope of this thesis

The success of metal-catalyzed ring opening of hydrocarbons for fuel upgrading depends on suppressing exocyclic dealkylation and multiple hydrogenolysis reactions, both of which result in value losses of fuel streams. While bifunctional ring-opening catalysis, after the metal-acid balance fine-tuned, demonstrates to be the most efficient and selective approach so far, the establishment of fundamental thermodynamic and kinetic relations represents a daunting task in such systems, due partly to the complex interaction between the metallic and acidic sites and to the multiple potential natures of the catalytic sites.

In this context, we have focused on the simpler monofunctional metal catalysts in ring opening reactions of five- and six-membered naphthenes, which are better suited for mechanistic studies. We aim to explore and understand the catalytic consequences of metal cluster size in these reactions, both in reactivity and selectivity terms. Moreover, the effects of reaction temperature and H_2 pressure on the turnover rates and selectivities, which have not been addressed in previous studies, are examined in this thesis, in order to optimize the selective ring opening (SRO) process by metal catalysis. The ultimate goal of this research is towards a rational catalyst design, by taking advantage of the fundamental insights into the structure-performance relationship.

In the second chapter of this thesis, we explored the structure-activity relation in the ring opening reaction of the simplest five-membered naphthene, i.e., cyclopentane, over supported Pt nanoparticles on alumina and silica. Unlike methylcyclopentane, this probe molecule has received limited interest, but is actually worth studying in view of its structural simplicity: essentially no selectivity issues need to be concerned. In addition to the cluster size effect, the effect of catalyst precursor, more specifically the chlorine effect, was also studied on the RO rates of cyclopentane. This chapter differs remarkably from previous work, in the sense that this reaction was conducted at sub-atmospheric pressures in foregoing studies while at above-atmospheric pressure in the current one.

In the third and fourth chapters, the effects of particle size and catalyst precursor were investigated in the ring opening of cyclohexane (CH) and methylcyclohexane (MCH) over monofunctional Ir catalysts. In the latter case (MCH), detailed discussions were presented in relation to different sorts of C−C bond cleavage selectivities, e.g., endocyclic vs. exocyclic, single vs. multiple, substituted vs. unsubstituted, and so forth. With a wide range of reaction conditions studied, kinetic modelling is shown to be a powerful tool to elucidate the reaction mechanism and the structural origins governing RO catalysis in a general context.

In the fifth chapter, deuterium isotope effects were employed as a tool for elucidating the elementary steps of CH and MCH ring opening. The measured isotope effects reflect complex origins, both thermodynamics and kinetics in nature, of the effect of isotope identity on the kinetically significant surface steps. A detailed evaluation furnished valuable information on the reaction mechanism of hydrogenolysis of six-membered naphthenes.

The final chapter concludes the whole body of research and generalizes some guiding principles for designing selective and active RO catalysts based on monofunctional metal systems.

1.6. References

1. M. Absi-Halabi, A. Stanislaus, H. Qabazard, Hydrocarb. Process 76 (1997) 45.
2. A. Stanislaus, B.H. Cooper, Catal. Rev. Sci. Eng. 36 (1994) 75.
3. A. Corma, V. Gonzalez-Alfaro, A.V. Orchilles, J. Catal. 200 (2001) 34.
4. B.I. Bertelsen, Top. Catal. 16/17 (2001) 15.
5. A. Roj, K. Karlsson, Fuels Reformulation 46 (1998).
6. M. Santikunaporn, J.E. Herrera, S. Jongpatiwut, D.E. Resasco, W.E. Alvarez, E.L. Sughrue, J. Catal. 228 (2004) 100.
7. B.H. Cooper, B.B.L. Donnis, Appl. Catal. A 137 (1996) 203.
8. B.H. Winquist, B.D. Murray, S.N. Milam, R.C. Ryan, T.W. Hastings, U.S. Patent 5,391,291 (1995).
9. G.B. McVicker, M. Daage, M.S. Touvelle, C.W. Hudson, D.P. Klein, W.C. Baird Jr., B.R. Cook, J.G. Chen, S. Hantzer, D.E.W. Vaughan, E.S. Ellis, O.C. Feeley, J. Catal. 210 (2002) 137.
10. G.B. McVicker, M.S. Touvelle, C.W. Hudson, D.E.W. Vaughan, M. Daage, S. Hantzer, D.P. Klein, E.S. Ellis, B.R. Cook, O.C. Feeley, J.E. Baumgartner, U.S. Patent 5,763,731 (1998).
11. G.B. McVicker, J.J. Schorfheide, W.C. Baird Jr., M.S. Touvelle, M. Daage, D.P. Klein, E.S. Ellis, D.E.W. Vaughan, J. Chen, S. Hantzer, U.S. Patent 6,103,106 (2000).
12. R.C. Santana, P.T. Do, W.E. Alvarez, J.D. Taylor, E.L. Sughrue, D.E. Resasco, Fuel 85 (2006) 643.
13. D. Kubička, N. Kumar, P. Mäki-Arvela, M. Tiitta, V. Niemi, T. Salmi, D.Y. Murzin, J. Catal. 222 (2004) 65.
14. D. Kubička, N. Kumar, P. Mäki-Arvela, M. Tiitta, V. Niemi, H. Karhu, T. Salmi, D.Y. Murzin, J. Catal. 227 (2004) 313.
15. S. Rabl, A. Haas, D. Santi, C. Flego, M. Ferrari, V. Calemma, J. Weitkamp, Appl. Catal. A 400 (2011) 131.
16. K.C. Mouli, V. Sundaramurthy, A.K. Dalai, Z. Ring, Appl. Catal. A 321 (2001) 17.

17. R. Moraes, K. Thomas, S. Thomas, S. van Donk, G. Grasso, J.P. Gilson, M. Houalla, J. Catal. 286 (2012) 62.
18. D. Kubička, M. Kangas, N. Kumar, M.Titta, M. Lindblad, D.Y. Murzin, Top. Catal. 53 (2010) 1438.
19. P.T. Do, W.E. Alvarez, D.E. Resasco, J. Catal. 238 (2006) 477.
20. S. Lecarpentier, J. van Gestel, K. Thomas, J.P. Gilson, M. Houalla, J. Catal. 254 (2008) 49.
21. F. Locatelli, D. Uzio, G. Niccolai, J.M. Basset, J.P. Candy, Catal. Commun. 4 (2003) 189.
22. B.C. Gates, J.R. Katzer, G.C.A. Schuit, Chemistry of Catalytic Processes. McGraw–Hill, New York, 1979.
23. S. Dokjampa, T. Rirksomboon, S. Osuwan, S. Jongpatiwut, D.E. Resasco, Catal. Today 123 (2007) 218.
24. M.A. Arribas, P. Concepción, A. Martínez, Appl. Catal. A 267 (2004) 111.
25. S. Nassreddine, L. Massin, M. Aouine, C. Geantet, L. Piccolo, J. Catal. 278 (2011) 253.
26. F.G. Gault, Adv. Catal. 30 (1981) 1.
27. H. Zimmer, Z. Paal, J. Mol. Catal. 51 (1989) 261.
28. M. Chow, G.B. McVicker, J. Catal. 112 (1988) 290.
29. Y. Zhuang, A. Frennet, Appl. Catal. A 134 (1996) 37.
30. D. Teschner, K. Matusek, Z. Paál, J. Catal. 192 (2000) 335.
31. M. Vaarkamp, P. Dijkstra, J. van Grondelle, J.T. Miller, F.S. Modica, D.C. Koningsberger, R.A. van Santen, J. Catal. 151 (1995) 330.
32. W.E. Alvarez, D.E. Resasco, J. Catal. 164 (1996) 467.
33. M. Chow, S.H. Park, W.M.H. Sachtler, Appl. Catal. 19 (1985) 349.
34. P. Samoila, M. Boutzeloit, C. Especel, F. Epron, P. Marécot, J. Catal. 276 (2010) 237.
35. L.B. Galperin, J.C. Bricker, J.R. Holmgren, Appl. Catal. A 239 (2003) 297.
36. D. Teschner, L. Pirault-Roy, D. Naud, M. Guerin, Z. Paal, Appl. Catal. A 252 (2003) 421.
37. H. Du, C. Fairbridge, H. Yang, Z. Ring, Appl. Catal. A 294 (2005) 1.

38. S. Rabl, D. Santi, A. Haas, M. Ferrari, V. Calemma, G. Bellussi, J. Weitkamp, Micropor. Mesopor. Mater. 146 (2011) 190.
39. S. Rabl, Ph.D. thesis, Universität Stuttgart, 2011.
40. P.B. Weisz, Adv. Catal. 13 (1962) 137.
41. G.C. Bond, Metal-Catalysed Reactions of Hydrocarbons, Springer, Berlin, 2005.
42. J. Barbier, P. Marecot, Nouv. J. Chim. 5 (1981) 393.
43. G.A. del Angel, B. Coq, G. Ferrat, F. Figuéras, Surf. Sci. 156 (1985) 943.
44. M. Che, C.O. Bennett, Adv. Catal. 36 (1989) 55.
45. S. Fuentes, F. Figuéras, J. Chem. Soc. Faraday Trans. 174 (1978) 174.
46. U. Wild, D. Teschner, R. Schlögl, Z. Paál, Catal. Lett. 67 (2000) 93.
47. G.C. Bond, J.C. Slaa, J. Mol. Catal. A. 98 (1995) 81.
48. R.K. Herz, W.D. Gillespie, E.E. Peterson, G.A. Somorjai, J. Catal. 67 (1981) 386.
49. G.A. Somorjai, D.W. Blakely, Nature 258 (1975) 580.
50. D.W. Blakely, G.A. Somorjai, J. Catal. 42 (1976) 181.

Chapter 2

Catalytic consequences of particle size and electronic properties of supported Pt clusters in the ring opening of cyclopentane on Pt/Al_2O_3

Ring opening of cyclopentane on alumina-supported Pt particles, derived from either Cl-free or Cl-containing precursor, was studied as a function of particle size and H_2 partial pressure. In the absence of Cl intimately bound to surface Pt atoms, measured turnover rates increased continuously with increasing Pt size (1−15 nm). Higher turnover rates on large Pt particles do not stem primarily from the coverage effects; rather, they are related to the higher concentration of low-index face atoms on large particles, and also a net result of a compensation of the activation energy and entropy. On similarly small Pt clusters prepared from the Cl-free and Cl-containing precursors, the relative adsorption coefficients of toluene over benzene, extracted from the hydrogenation rates with benzene and benzene-toluene mixtures, indicate lower electron densities of the surface atoms at the 'Cl-bound' Pt clusters. This Cl-induced electron deficiency is speculated to be the major cause for the 2- to 3-time higher activity in cyclopentane ring opening, compared to those Pt clusters similar in size but devoid of intimate chlorine species.

2.1. Introduction

Cyclic C_5 molecules hold a special place in catalytic chemistry, as compelling evidence from mechanistic studies over platinum catalysts indicated them as intermediates in the skeletal isomerisation of alkanes [1,2]. Relative to its methyl-substituted derivative, namely, methylcyclopentane (MCP), cyclopentane (CP) itself is less frequently studied [3−6], in spite of its conceived simplicity (no positional selectivity issues) for establishing structure-activity relations in ring opening/hydrogenolysis reactions over metal catalysts.

It is, in the first place, important to appreciate that structure sensitivity reflects the property of the whole catalytic system, rather than simply the reaction concerned. Indeed, various fashions of structure sensitivities for cyclic C_5 (CP and MCP) ring opening were presented over different catalysts [3−9], though some were suspected to be complicated by unintended artifacts, such as self-poisoning carbon deposition or adventitious impurities [10,11]. For instance, the turnover frequency (TOF) for CP hydrogenolysis at 573 K changed by more than an order of magnitude over Pt/Al_2O_3 catalysts of 0.05 to 0.8 dispersion [4], as also found in MCP hydrogenolysis on Rh/Al_2O_3 of 0.1 to 1.0 dispersion [5]. In contrast, negligible effects of metal dispersion were observed for CP hydrogenolysis over Al_2O_3 supported Pd and Ir catalysts [4,5]. For Rh catalysts (on SiO_2), even erratic effects of metal cluster size were reported on the TOFs of CP and MCP hydrogenolysis [5,6]. The reason for structure insensitivity of hydrogenolysis reactions is by no means straightforward to perceive, in light of the ubiquitous role of surface coordination in the binding and reactivity of adsorbed intermediates. By contrast, the antipathetic structure sensitivity has been typically interpreted by a large ensemble size requirement that is better fulfilled on flat surfaces of large particles [12]. Note that these studies were performed at sub- or near-atmospheric H_2 pressures and were, therefore, often accompanied by noticeable deactivation [5]. Moreover, the structure sensitivity was only explored at a single set of conditions, without knowledge of its extendibility to other operating conditions.

Here, we report cyclopentane ring opening (multiple hydrogenolysis to $C_{<5}$ alkanes is marginal at differential conditions) turnover rates on Pt clusters with a broad range of dispersion (0.07−0.98), under reaction conditions where deactivation is suppressed to low extents by applying higher H_2 pressures (1−10 bar) and H_2-to-hydrocarbon ratios (H_2/CP = 10−150) than those in previous reports. Measured turnover rates monotonically increased with increasing Pt cluster size (1−15 nm) with concomitant changes of apparent activation barriers and reactant coverages. We also show that the choice of metal precursor for catalyst preparation has a significant impact on the catalytic activity. To gain insight into the remarkable differences in catalytic activities of catalysts prepared from chlorine-free and chlorine-containing precursors, we probe the electronic states of platinum in catalysts of similar dispersions by competitive hydrogenation of benzene and toluene. The kinetic data suggest that C−C bond hydrogenolysis is very sensitive to electronic perturbation of surface Pt atoms and that electron-deficient Pt species catalyze the CP ring opening more efficiently than the neutral Pt atoms. These findings might also underscore the indispensability of appropriate levels of Cl in the catalysts for higher hydrogenolysis activities of the C−C bonds.

2.2. Experimental

2.2.1. Catalyst preparation

$Pt(NH_3)_4(NO_3)_2$ (Aldrich, 97%) was dissolved in doubly-distilled water to an aqueous solution (0.05 M) before use. The catalysts were prepared by incipient wetness impregnation using 1.1 cm^3 of this solution per gram of support (γ-alumina, 104 m^2 g^{-1}, Evonik Degussa Alu C, ~0.4 wt% Cl, < 30 ppm S). Typically, portions of the solution were added dropwise to a beaker containing γ-Al_2O_3 while stirring with a quartz rod. The impregnated sample was first dried at 393 K overnight in synthetic air (Westfalen, 20.5 vol.% O_2 in N_2) and then treated at 673 K in flowing H_2 (Westfalen, 99.9999%) for 5 h. The resulting material was divided into five portions treated at varying temperatures (573, 673, 773, 873 and 923 K) for 5 h in dry synthetic air flow and then in H_2 at 723 K for 5 h. A temperature increment of 1 K min^{-1} was applied for all thermal treatments, whereas flow rates of 100 cm^3 min^{-1} (g-sample)$^{-1}$ were applied for all gases. Samples thus obtained are denoted as m%Pt(D)-1/Al_2O_3, where m%, D and 1 are the actual Pt loading by wt.% (AAS), the fractional Pt dispersion (H_2 chemisorption), and a denotation of the Cl-free precursor, respectively. A Pt/SiO_2 sample, starting from the same Pt precursor and applying the same treatment protocol as stated above, was named as *m*%Pt(*D*)-1/SiO_2..

$(NH_4)_2PtCl_6$ (Aldrich, 99.99%) was used in order to examine the effect of chlorine on the catalytic performance. The procedure for incipient wetness impregnation was the same as that for Cl-free catalysts except that the dissolution of this precursor salt needs to be assisted by heating the salt-water mixture (e.g., at 353 K) to form a uniform solution. The thermal treatment protocol was also the same as for the catalysts prepared from $Pt(NH_3)_4(NO_3)_2$. The resultant samples are designated as *m*%Pt(*D*)-2/Al_2O_3, where *m*%, *D* and 2 are the actual Pt loading by wt.% (AAS), the fractional Pt dispersion (H_2 chemisorption), and a denotation of the Cl-containing precursor, respectively.

2.2.2. Catalyst characterization

2.2.2.1. H_2 chemisorption and N_2 physisorption

Hydrogen uptakes were determined volumetrically on a Sorptomatic 1990 instrument. The catalyst samples were pretreated in 100 kPa of static H_2 at 723 K for 2−3 h and then evacuated at the same temperature for 0.5 h before chemisorption measurements at 307 K. An equilibrating time of 2−5 min was used for each pressure increment step in a pressure range of 0.5−13.2 kPa. After completing the first isotherm, the sample was evacuated (10^{-4} kPa, 1 h) and the second isotherm was measured. The amount of chemisorbed hydrogen was determined by extrapolating the linear part ($P > 5$ kPa) of the difference isotherm (the second isotherm subtracted from the first one) to zero pressure. Dispersions (*D*), defined as the fraction of Pt atoms exposed at surfaces, were estimated by assuming a $H_{strong}/Pt_{surface}$ stoichiometry of one [13].

The surface areas of the catalyst samples were characterized by N_2 physisorption at 77 K on the Sorptomatic 1990 instrument. Prior to measurements, all samples were outgassed at 523 K for 2 h. The specific BET surface area was calculated from the adsorption isotherms over a relative pressure range (p/p^0) of 0.03−0.10.

2.2.2.2. Transmission electron microscopy

Transmission electron micrographs were recorded with a JEM-2010 JEOL transmission electron microscope (TEM) with an accelerating voltage of 120 kV. Samples of the catalysts were ground and ultrasonically dispersed in ethanol for 2 min. Drops of the dispersions were applied on a copper grid-supported carbon film, which upon drying for at least two hours was introduced into the vacuum system and evacuated before measurement.

2.2.2.3. Atomic absorption spectroscopy (AAS)

The platinum contents in the catalysts were determined by atomic absorption spectroscopy (AAS) using a UNICAM Solaar M5 Spectrometer. Before measurement, typically 50−80 mg of the solid sample was dissolved in 0.5 cm^3 of hydrofluoric acid (10%) at its boiling point (about 383 K).

2.2.2.4. Infrared spectroscopy: CO adsorption

The infrared spectra for CO adsorption were monitored in transmission mode on a Bruker VERTEX 70 spectrometer at a resolution of 4 cm^{-1}. The samples were prepared as self-supporting wafers (10−12 mg cm^{-2}) and activated in static H_2 ($p = 15 \pm 3$ mbar) for 2 h at 673 K (heating rate = 10 K/min). After cooling to 313−318 K, the samples were exposed to successive dosages of CO ($p = 2.0 \times 10^{-6}$−1.0×10^{-1} mbar), equilibrated at each pressure (for ca. 5 min) and then outgassed ($p = 2.0$−3.5×10^{-7} mbar) for ca. 20 min. All spectra were collected at 318 ± 3 K. Infrared absorption bands in 1990−2200 cm^{-1} were fitted with combined Gaussian and Lorentz functions for quantitative deconvolution of overlapping peaks.

2.2.3. Kinetic measurements

2.2.3.1. Ring opening of cyclopentane

Ring opening of cyclopentane (CP) was studied in a multifold parallel reactor system including an array of six stainless steel tubular reactors operated with plug-flow hydrodynamics. Catalyst samples were compacted, crushed and sieved to 180−280 μm beforehand. Typically, 20 mg of the sieved catalyst was diluted with appropriate amounts of acid-washed quartz sand of identical sieve fractions. A K-type thermocouple was attached to the external surface (within the isothermal region) of the reactor to measure and control the reaction temperature. Differences below 1 K were detected when the thermocouple was brought in direct contact with the catalyst bed. Before reactions, catalysts were pretreated in a pure H_2 flow of 20 cm^3 min^{-1} (from room temperature to 623 K, 0.2 K s^{-1} increment and 2 h dwell) and then cooled to the reaction temperature (523−563 K). CP was introduced using a flow of helium (Westfalen AG, 99.996%) passing through a series of bubblers (in a thermostatted water bath) containing liquid CP (Aldrich, ≥ 99%). Upon switching of flow configurations, the helium flow carrying saturated vapor of CP at the bath temperature mixed with a flow of H_2 (Westfalen AG, 99.999%) in a co-current mode and contacted the catalyst bed to initiate the reaction at the set temperature. Flow rates of gases and total pressures (0.35−2.0 MPa) of the reactor system were modulated by electronic mass flow controllers (MFCs) and back pressure regulators. All the kinetic measurements were conducted at differential conditions (< 5%), far from equilibrium. The products were analyzed online by a Hewlett-Packard 6890 Plus GC equipped with a DB Petro column (320 μm × 100 m) and a flame ionization detector (FID). Initial rates and selectivities were reported as values derived by extrapolation of measured steady-state rates and selectivities to zero contact time. Deactivation was observed to be minimal (2−5%) during the whole run.

2.2.3.2. Competitive hydrogenation of benzene and toluene

The competitive hydrogenation of benzene and toluene was carried out at 308−333 K in a differential, packed-bed tubular reactor at atmospheric pressure. Benzene (Merck, 99.97%) was distilled from metallic potassium before use. The gas mixture was prepared by passing He through two saturators (in two thermostat water baths) containing benzene and toluene, respectively, and mixing them with a flow of H_2. H_2 (Westfalen AG, 99.999%) and He (Westfalen AG, 99.996%) were flown through separate carrier gas purifiers (Supelco). The partial pressures of the hydrocarbons were adjusted by the flow rates of helium and H_2 metered by MFCs. Conversions were kept below 10% in all cases, typically below 5%, and mass and heat transfer limitations were excluded under these conditions. Tests with pure benzene feed were performed on the same setup. Rates were reported as values obtained after 10 minutes of time-on-stream (TOS) upon introduction of reactants.

2.3. Results and discussions

2.3.1. Particle size and dispersion measurements

Representative transmission electron micrographs are shown in Figure 2-1. The corresponding particle size distributions are shown in Figure 2-2. Surface-averaged particle diameters ($d_{av} = \Sigma n_i d_i^3 / \Sigma n_i d_i^2$) were determined from the size of 140−250 Pt crystallites in TEM images for samples with 0.07−0.55 dispersion (H_2 chemisorption).

Pt dispersions estimated from TEM were compared with those obtained from H_2 chemisorption uptakes, which gave similar results only for catalysts containing primarily large (10−16 nm) particles (Table 2-1). TEM-derived dispersions are typically smaller than those from chemisorption uptakes, probably because very small clusters become undetectable at the resolution used in conventional TEM analyses. Due in part to this problem, not enough particles were collected and analyzed when imaging the very highly dispersed (D = 0.8−1.0) samples. Turnover rates reported hereafter for cyclopentane (CP) ring opening and aromatics hydrogenation are based on H_2 chemisorption uptakes, because they directly probe the number of accessible Pt atoms at cluster surfaces.

Note that samples with the lowest (573 K) and the highest (923 K) thermal treatment temperatures within each series of catalysts (i.e., Pt-1/Al_2O_3 and Pt-2/Al_2O_3) were first analyzed by atomic absorption spectroscopy, and the Pt concentrations were found to be essentially identical between each other (0.96% and 1.00% for Pt-1 series, and 1.05% and 1.10% for Pt-2 series, respectively). Therefore, it has been assumed that the Pt concentrations in the others do not differ as a function of thermal treatment temperature within each series, and the *m* values (Pt loading by wt.%) have been reasonably taken as 0.98% for Pt-1 series and 1.08% for Pt-2 series (Table 2-1).

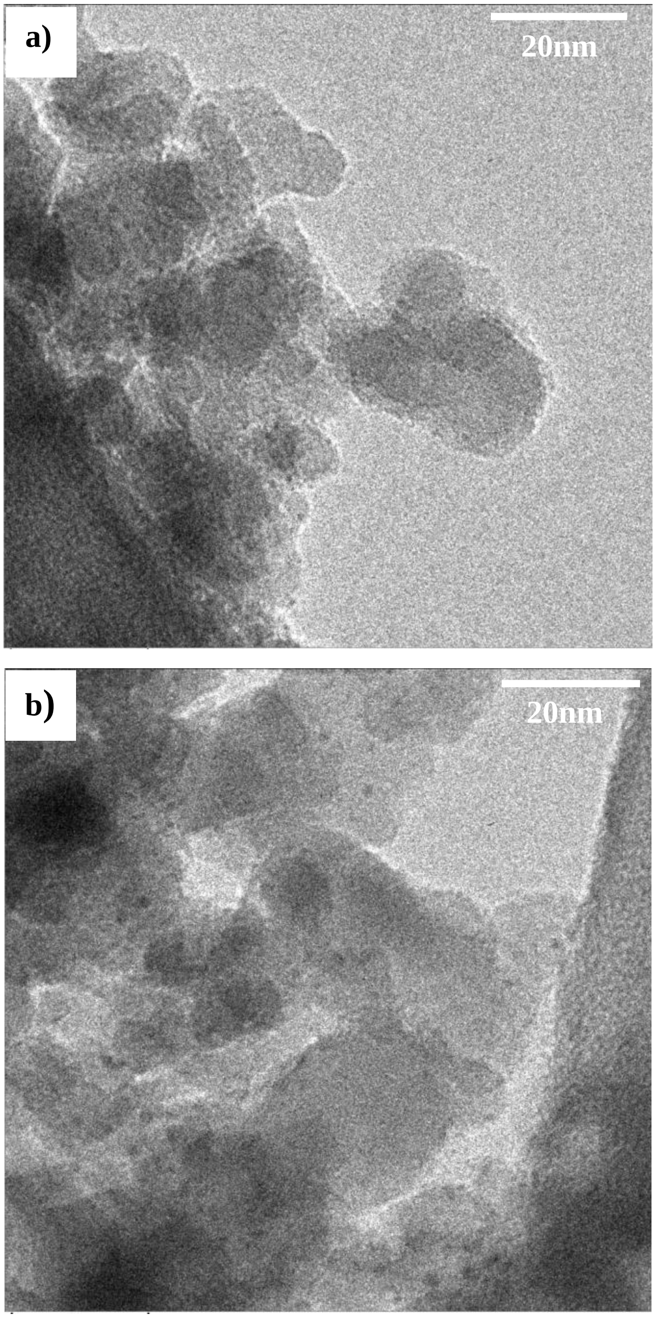

Figure 2-1. Representative transmission electron microscopy images of (a) 1.08%Pt(0.98)-2/Al_2O_3, (b) 0.98%Pt(0.81)-1/Al_2O_3, (c) 1.08%Pt(0.71)-2/Al_2O_3, (d) 0.98%Pt(0.59)-1/Al_2O_3, (e) 1.08%Pt(0.09)-2/Al_2O_3, (f) 0.98%Pt(0.07)-1/Al_2O_3, and (g) 0.41%Pt(0.55)-1/SiO_2. The corresponding TEM-derived dispersions for (d) to (g): 0.36, 0.07, 0.06 and 0.39.

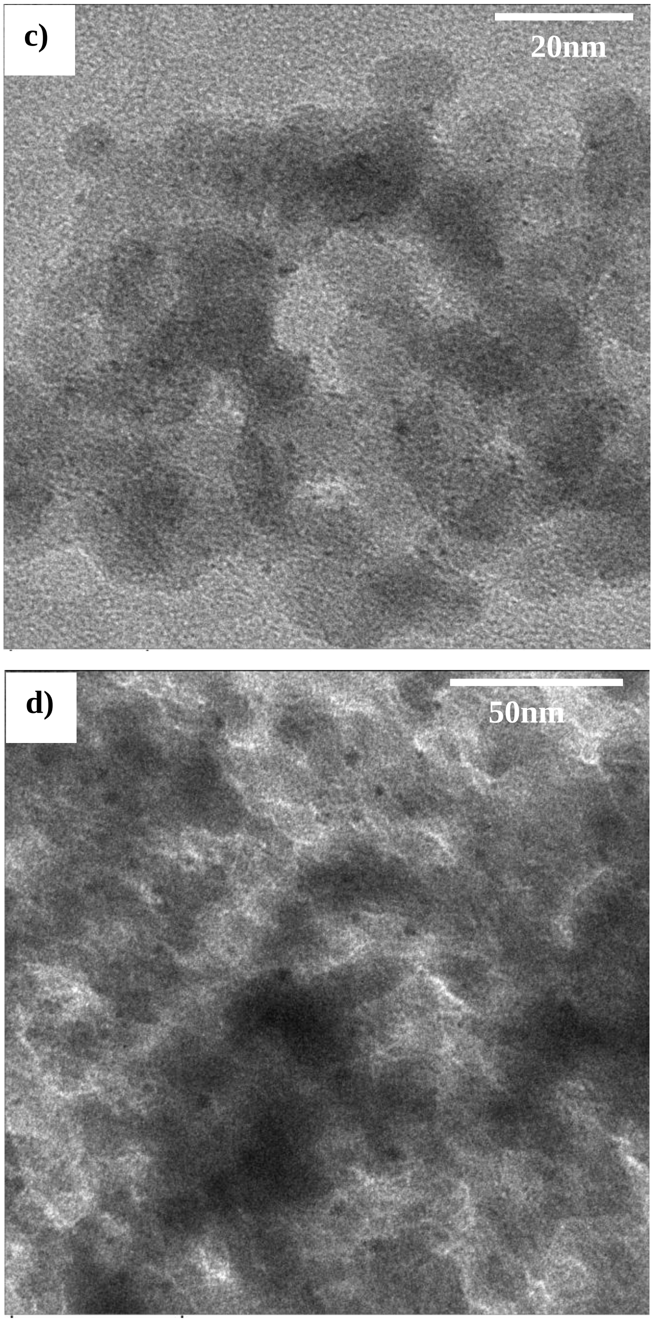
c)
20nm
d)
50nm

Figure 2-1. (continued)

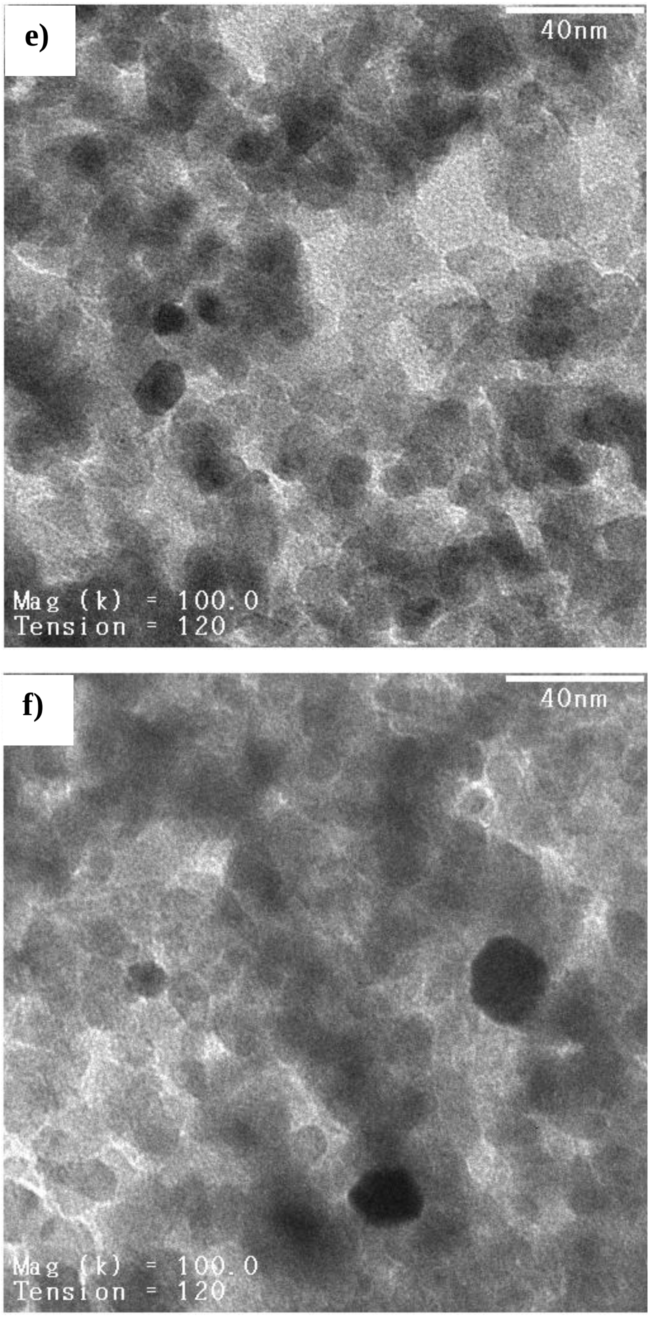
e)
40nm
Mag (k) = 100.0
Tension = 120
f)
40nm
Mag (k) = 100.0
Tension = 120

Figure 2-1. (continued)

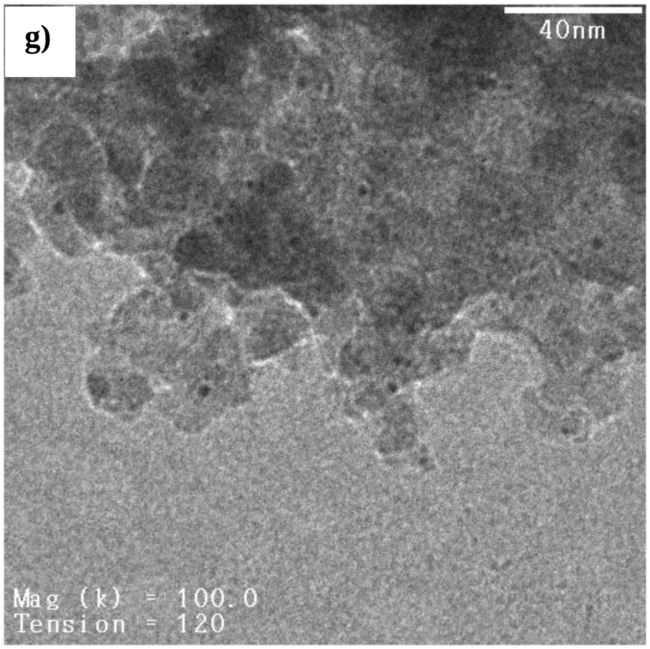

Figure 2-1. (continued)

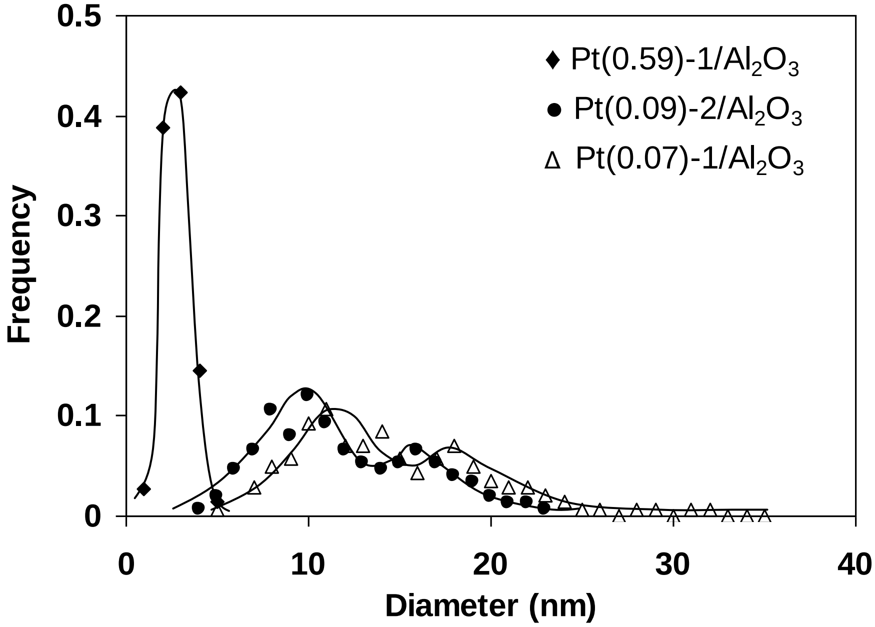

Figure 2-2. Particle size distribution as determined from an analysis of transmission electron microscopy images for (■) Pt(0.59)-1/Al_2O_3, (●) Pt(0.09)-2/Al_2O_3, (Δ) Pt(0.07)-1/Al_2O_3. Bin size is 0.5 nm, and 140−250 particles were sampled from at least six areas in every case.

Table 2-1. BET surface area, Pt concentration and dispersions (measured from H_2 chemisorption uptakes and estimated from particle sizes in transmission electron micrographs) of supported Pt catalysts.

Catalyst	BET S.A. (m^2 g^{-1})	Pt (wt%)	Pt dispersion (*D*)	
			Chemisorption	TEM[a]
Pt(0.81)-1/Al_2O_3	102	0.96	0.81	–[b]
Pt(0.59)-1/Al_2O_3	98	0.98[c]	0.59	0.36
Pt(0.51)-1/Al_2O_3	–[b]	0.98[c]	0.51	0.32
Pt(0.24)-1/Al_2O_3	97	0.98[c]	0.24	0.18
Pt(0.07)-1/Al_2O_3	93	1.00	0.07	0.06
Pt(0.98)-2/Al_2O_3	96	1.05	0.98	–[b]
Pt(0.88)-2/Al_2O_3	–[b]	1.08[c]	0.88	–[b]
Pt(0.71)-2/Al_2O_3	92	1.08[c]	0.71	–[b]
Pt(0.55)-2/Al_2O_3	95	1.08[c]	0.55	0.38
Pt(0.09)-2/Al_2O_3	91	1.10	0.09	0.07
Pt(0.55)-1/SiO_2	290	0.41	0.55	0.39

[a] Derived from the average particle diameter ($D = 1/d_{av}$).

[b] Not measured.

[c] See text.

2.3.2. Catalytic activity in the ring opening of cyclopentane

Under all conditions applied in this work, cyclopentane (CP) converts almost exclusively (> 99%) to n-pentane with negligible extents of deep hydrogenolysis and isomerization. We further note that the high selectivity (> 97%) to n-pentane is preserved even at higher temperatures (e.g., 593 K), longer contact times and higher conversion levels (e.g., > 40%). Thus, secondary reactions of re-adsorbed n-pentane product do not occur at an appreciable level on all Pt catalysts, which suggests that n-pentane does not compete with CP for the active sites in a wide range of n-pentane concentration in the gas phase. Consequently, ring opening is the only reaction pathway that needs to be evaluated.

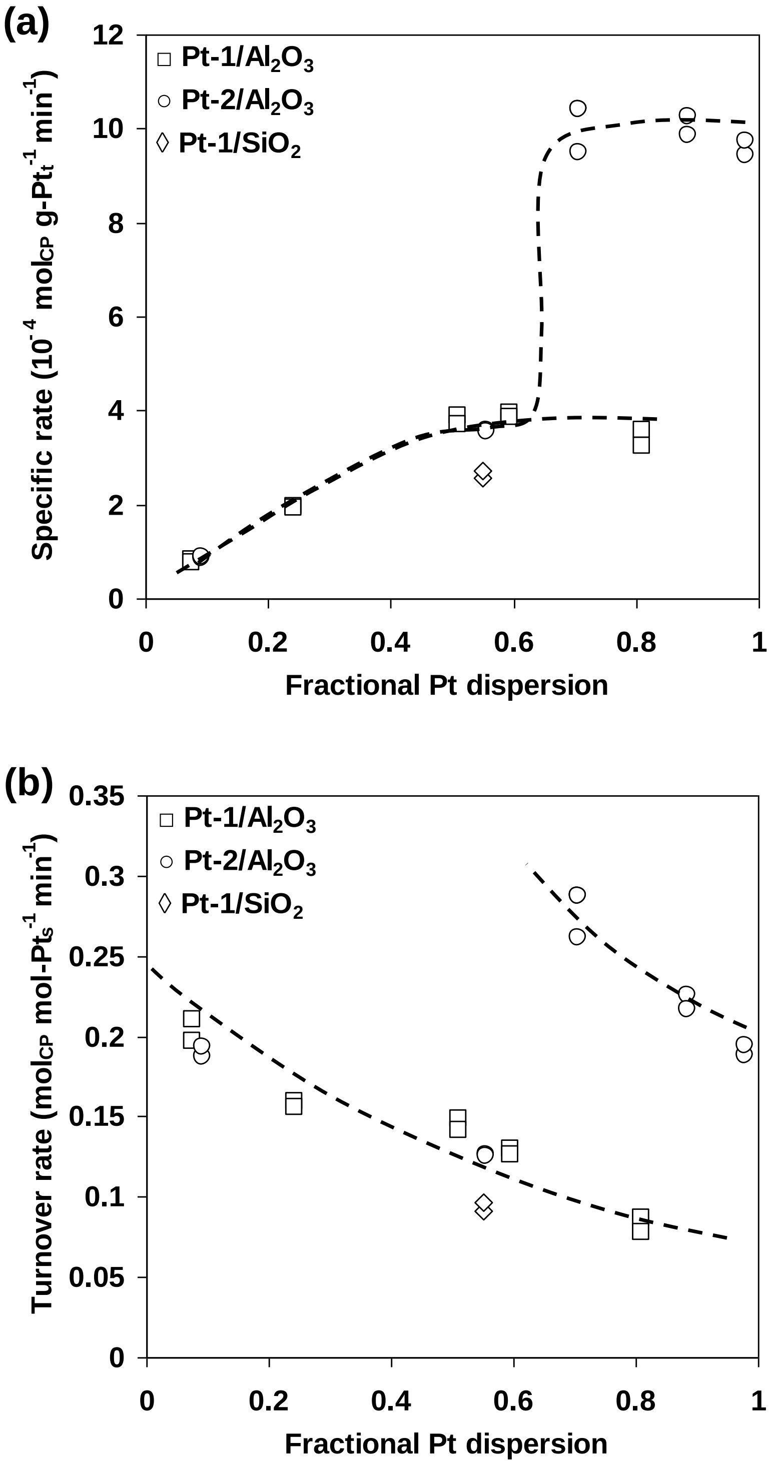

Figure 2-3. Mass specific rates (a) and turnover rates (b) of cyclopentane (CP) ring opening as a function of Pt dispersion, for (□) 0.98%Pt(D)-1/Al_2O_3, (○) 1.08%Pt(D)-2/Al_2O_3 and (◊) 0.41%Pt(0.55)/SiO_2 at 533 K, 8.8 kPa CP and 0.37 MPa H_2.

Figure 2-3 shows the mass specific rates (based on the total mass of Pt) and turnover rates (normalized to the surface atoms) of ring opening of CP as a function of Pt dispersion at 533 K for all the studied Pt catalysts. Divergent data points at the same Pt dispersion reflect the highest and the lowest measured steady-state rates among multiple (at least three times) kinetic measurements (parallel tests) on the same catalyst. The maximum standard deviation is ± 5%. Excellent reproducibilities were achieved in a few cases. For both series of Pt/Al_2O_3 catalysts, the mass specific activities were lower at low dispersions ($D < 0.6$) and remained essentially identical at sufficiently high dispersions (Figure 2-3a). Pt/SiO_2 appeared somewhat less active than the Pt/Al_2O_3 catalysts with similar dispersions ($D = 0.5-0.6$). Notably, for the catalyst series ($Pt\text{-}2/Al_2O_3$) prepared from the Cl-containing precursor, a significant drop of the specific activity was found in a dispersion range of 0.6−0.8.

As far as the turnover frequencies are concerned, two separate trend lines, differing by a factor of 2−3, are noted (Figure 2-3b). They do not correspond simply to the two series of catalysts. Small clusters appear to be less active than larger particles along each trend line, but not within the second catalyst series ($Pt\text{-}2/Al_2O_3$). Along the upper trend lie three Pt/Al_2O_3 catalysts of high dispersions ($D = 0.7-1.0$) prepared from hexachloroplatinic acid and calcined at temperatures below 773 K, whereas the lower one includes all the Pt catalysts (Pt/Al_2O_3 and Pt/SiO_2) prepared from the Cl-free precursor, as well as two Pt/Al_2O_3 catalysts of lower dispersions ($D = 0.09$ and 0.55) prepared from hexachloroplatinic acid and calcined at $T \geq 823$ K. Such antipathetic structure sensitivity is qualitatively in line with some reports on CP ring opening (atmospheric pressure) over Pt and Rh catalysts (not quantitatively in accord with the magnitude) [4,5], but contradicts those observed for MCP ring opening over Pt catalysts [14].

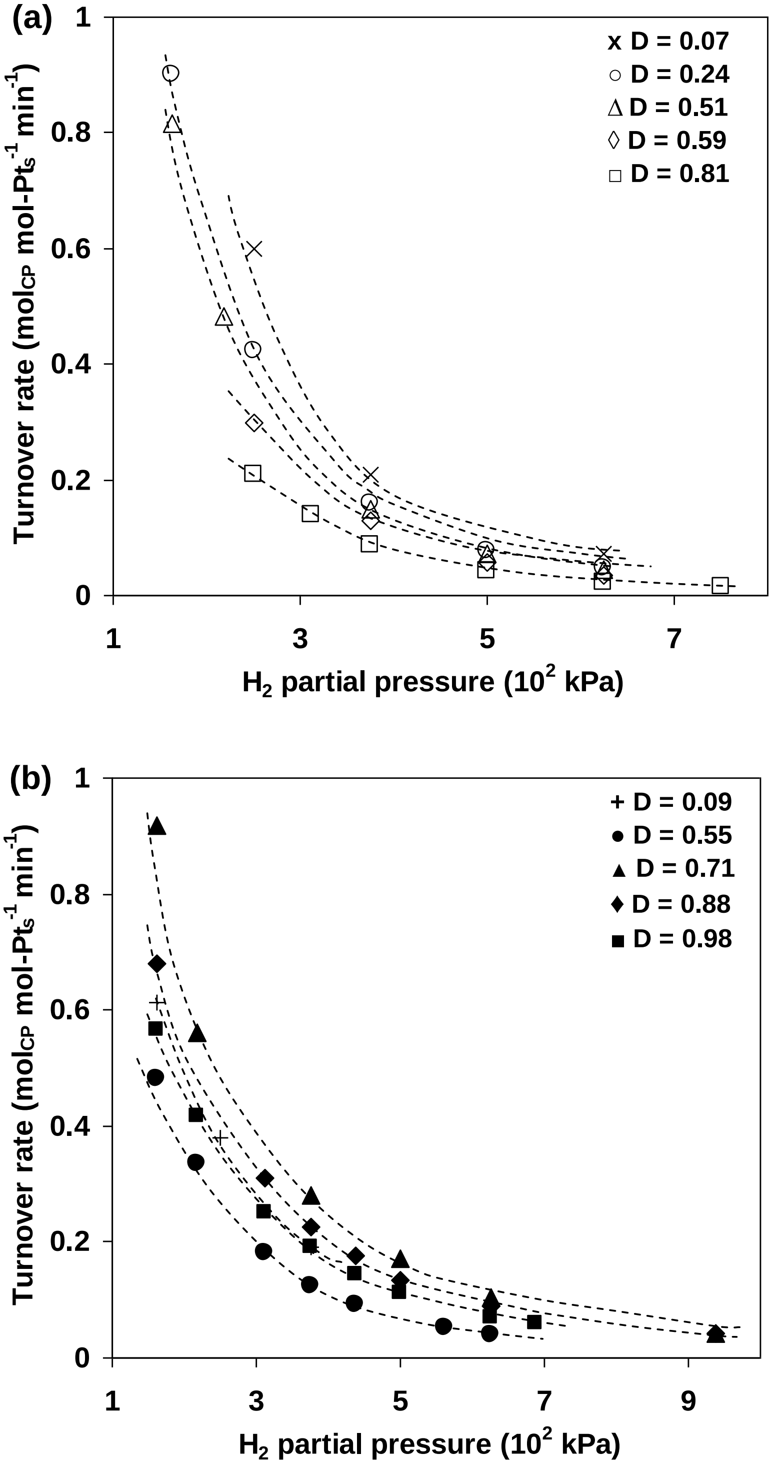

Figure 2-4. Effect of H_2 pressure on turnover rates of CP ring opening on (a) Pt-1/Al_2O_3 and (b) Pt-2/Al_2O_3 catalysts with varying dispersions at 533 K and 8.8 kPa CP.

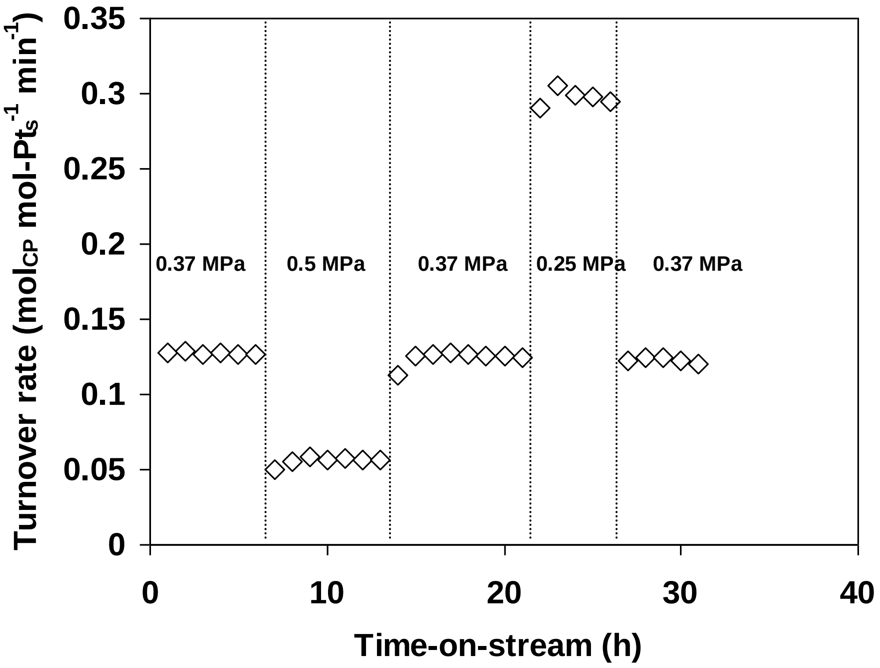

Figure 2-5. Time-on-stream (TOS) behavior of the 0.98%Pt(0.59)-1/Al_2O_3 catalyst and its responsive behavior to (de)pressurization. Reaction conditions: 533 K, 8.8 kPa CP, and indicated H_2 pressures.

Over the whole range of H_2 pressure studied in this work, the ring opening rates decreased with increasing H_2 pressure over all Pt catalysts (Figure 2-4). The regressed reaction order in H_2 in a power-rate-law formalism was found to be slightly more negative in the case of Pt-1/Al_2O_3 (Cl-free) than for most Pt-2/Al_2O_3 (e.g., -2.3 to -2.6 vs. -1.8 to -2.2 at 0.5−0.6 MPa H_2). Moreover, the H_2 reaction order became less negative with decreasing H_2 pressure for both series of catalysts (e.g., -1.6 to -1.8 for Pt-1/Al_2O_3 and -1.1 to -1.6 for Pt-2/Al_2O_3 at 0.1−0.2 MPa H_2), indicative of maximum rates at even lower H_2 pressures (sub-atmospheric) not accessed in this study. No clear trend in the H_2 order was observed on different particle sizes, being rather insensitive to the particle size on the Pt-1/Al_2O_3 series. The time-on-stream (TOS) behavior, taking 0.98%Pt(0.59)-1/Al_2O_3 as an example, clearly shows that practically no activity loss was observed upon changing the pressure up and down (Figure 2-5).

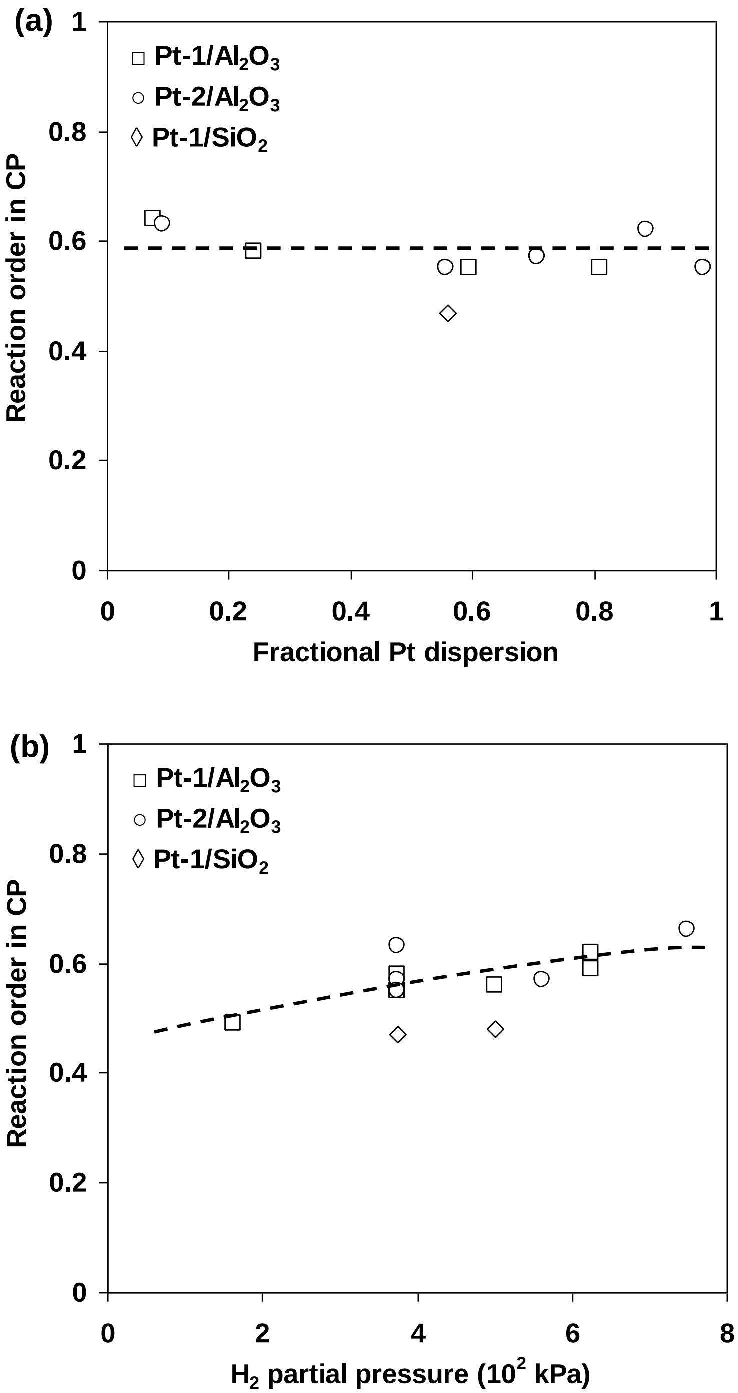

Figure 2-6. Effects of (a) Pt dispersion (533 K, 6−12 kPa CP and 0.37 MPa H_2 pressure, He balance) and (b) H_2 pressure (533 K, 6−12 kPa CP, He balance) on the formal reaction order in CP. Divergent symbols at the same H_2 pressure were obtained on catalysts of different dispersions. The reaction order in CP is reproducible within ± 0.04.

At the indicated conditions, the reaction order in the other reactant, cyclopentane, remained 0.6 ± 0.05 in the whole dispersion range for Pt/Al_2O_3 catalysts (Figure 2-6a). Increasing the H_2 pressure consistently increased the reaction order in CP, pointing to the depletion of carbonaceous surface intermediates at higher H_2 pressures. Under no circumstances did the surface coverage of CP-derived species become negligible, in light of the smaller-than-unity reaction order (Figure 2-6b). CP reaction order seems to be slightly lower (ca. 0.47) with the Pt/SiO_2 catalyst (D_{Pt} = 0.55) than all the Pt/Al_2O_3 catalysts.

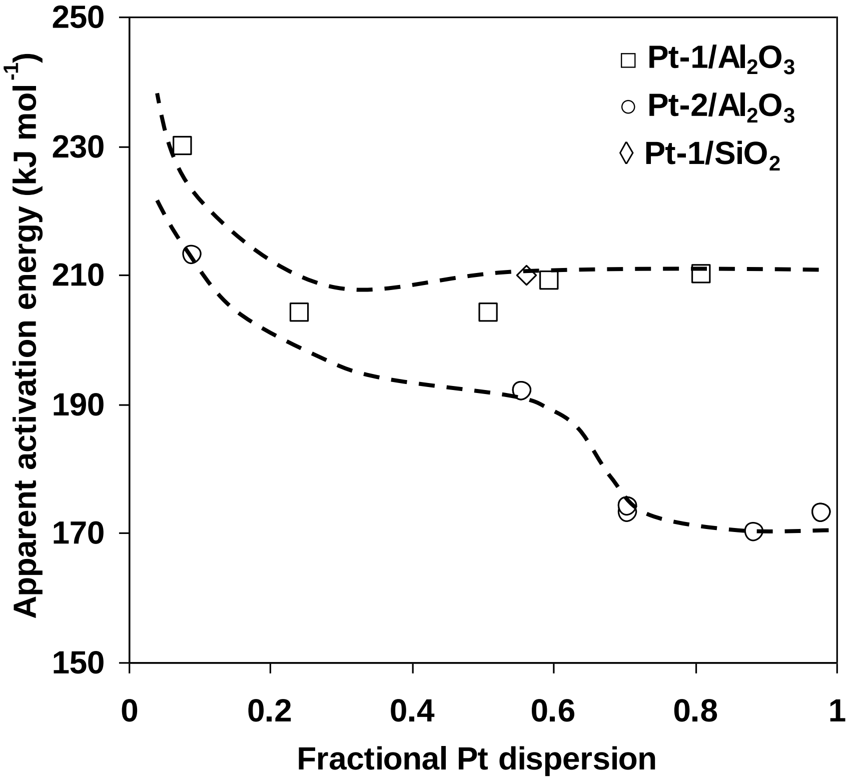

Figure 2-7. Effect of Pt dispersion on apparent energies of activation at 523−563 K, 8.8 kPa CP and 0.37 MPa H_2. The apparent activation energies are reproducible within ± 4 kJ mol^{-1}.

The measured energies of activation for all studied catalysts are shown in Figure 2-7 for a certain combination of reactant pressures. For dispersions higher than 0.7, catalysts prepared from the Cl-free Pt precursor exhibit significantly higher activation energies, i.e., by ca. 40 kJ mol^{-1}, than those prepared from the Cl-containing precursor. The difference became smaller at lower dispersions, but still remained as large as 10−20 kJ mol^{-1}. The activation energies became higher at medium to low Pt dispersions, in stark contrast to the trend in Ir-catalyzed ring opening of cyclohexane, i.e., much lower apparent activation energies at low Ir dispersions [15]. The activation energies measured at varying reactant pressures are compiled in Table 2 for most catalysts. At similar Pt dispersions, apparent activation barriers on Pt-1/Al_2O_3 catalysts remain higher than those observed with Pt-1/Al_2O_3 catalysts at all conditions studied. The difference between the two series of catalysts, however, seems to be less pronounced at sufficiently low H_2 pressures, e.g., < 0.2 MPa. In contrast to cyclohexane ring opening on Ir/Al_2O_3 catalysts [15], where continuous increases in activation energies were observed with increasing H_2 pressure up to the highest pressure studied (1.0 MPa), the activation barriers increased only slightly with increasing H_2 pressure (when > 0.4 MPa) for CP ring opening over Pt/Al_2O_3 catalysts.

Bare Al_2O_3 impregnated with similar amounts of chlorine (in the form of NH_4Cl), followed by thermal treatments in the same way as the Pt-containing catalysts, did not show any detectable ring opening activity at temperatures up to 573 K, which is the highest temperature we studied while being much lower than the typical temperatures for acid-catalyzed cracking of alkanes and cycloalkanes (Table 2-2). A lower β-scission rate in cyclopentyl cations, caused by an unfavorable orientation of the p-orbital at the positively charged carbon atom and the β-bond to be broken, or a higher tendency of the pentyl cation (formed by β-scission of the cyclopentyl cation) to recyclize [16], is thought to be responsible here for the absence of acid catalysis at this temperature. Moreover, hardly any rate enhancement was observed with a mechanical mixture of Pt/SiO_2 (non-acidic) and the above Cl-Al_2O_3, compared to Pt/SiO_2 (Table 2-2). We argue, therefore, that the Brönsted acidity on any of the Pt/Al_2O_3 catalysts does not influence the ring opening activity via bifunctional catalysis, or any mechanism alike, that involves acid-catalyzed C−C bond cleavage as the rate determining step. The acidity (can be either Brönsted or Lewis) associated with the hydroxyl groups or residual chlorine in the catalyst only affects the ring opening catalysis in an indirect way, possibly imposing its effect on the vicinal surface Pt atoms (and adsorbed intermediates) that catalyze the reaction.

Table 2-2. Proof of the little direct impact of acidity in the ring opening activity of cyclopentane at 533 and 553 K (8.8 kPa CP and 0.37 MPa H_2).

Catalyst bed (mg)		TOR (mol-CP mol-Pt_s^{-1} min^{-1})	
Pt/SiO_2	$Cl\text{-}Al_2O_3$	T_{rxn} = 533 K	T_{rxn} = 553 K
0	40	—[a]	—[a]
20	20	0.093 ± 0.005	0.53 ± 0.02
8	30	0.091 ± 0.004	0.54 ± 0.03
40	0	0.089 ± 0.004	0.51 ± 0.02

[a] Below GC detection limit even at the lowest achievable space velocity.

In summary, the above results show that the TOF increased with the particle size in the absence of Pt-associated chlorine, and that the TOFs for CP ring opening differed by a factor of 2−3 for small Pt clusters obtained from different precursors, accompanying remarkable differences in the activation energy and the reaction order in H_2. These observed changes in the TOF appear to be much smaller than the effects observed for changes in support acidity [17,18]. For example, TOF increases of about 10^2 in neopentane conversion have been reported for Pt encapsulated in acidic HY compared to Pt/γ-Al_2O_3 [18]. In principle, if the reaction behavior is not disguised by deactivation or experimental artifacts, changes in the activity of this magnitude may result from changes in the Pt particle size, the particle morphology, or from the intrinsic activity of the Pt atoms, i.e., the electronic properties [12]. Since the particle sizes are quite similar for small clusters (0.8−1.0 dispersion) where TOFs varied by more than a factor of 2 between the two series of catalysts, we consider the electronic state of Pt as the major responsible factor in affecting the activity of CP ring opening. Next, we provide evidence for this hypothesis, and address its microscopic origins based on a qualitative analysis of the Temkin relation.

2.3.3. Understanding the effect of Pt precursor on ring opening activity by probing the electronic states of small Pt clusters in competitive hydrogenation of benzene and toluene

Depending on the nature of Pt precursor salts, similarly small (D = 0.71, 0.81, 0.88) Pt particles show remarkably different activities in the ring opening of CP (Figure 2-3). Pt/Al_2O_3 catalysts prepared from chloroplatinic precursors (acids or salts) are often concluded to comprise a fraction of electron-deficient Pt species even after reduction, for which most evidence was obtained from XPS studies [19−21]. For instance, the binding energy of the Pt $4d_{5/2}$ signal was ca. 0.4 eV higher with Pt/Al_2O_3 prepared from H_2PtCl_6 than with the catalyst prepared from $Pt(acac)_2$, though both contain similar average Pt particle sizes (1.6−2.0 nm) [21].

In this work, we have taken a kinetic approach, i.e., competitive hydrogenation of benzene and toluene, to assessing the electronic density of surface Pt atoms on small clusters, derived from Cl-free or Cl-containing precursors. This methodology proves to correctly reveal the electron density of Pt nanoparticles in the presence of electronic promoters, as effectively as physicochemical techniques such as XPS and X-ray absorption measurements [22]. Benzene and toluene are bonded to the metal surface via π-bonds involving electron transfer from the aromatic ring to the unoccupied metal d-orbitals. Since toluene is a better electron donor than benzene, as a result of the inductive effect of the methyl group, it is supposed to be more strongly bonded than benzene ($K_{T/B} > 1$, where K is the adsorption equilibrium coefficient) [23]. Following this idea, Larsen and Haller showed that this $K_{T/B}$ value could also be used to disclose the electronic states of Pt in zeolite cages [24]. In principle, a larger value of $K_{T/B}$ indicates a lower electron density of the surface Pt atoms [23].

Before studying the competitive hydrogenation of benzene and toluene, the kinetics of benzene hydrogenation in the absence of toluene were investigated in detail, in order to compare our results with reported paradigms under similar conditions [25−27], and to validate the extraction of relative adsorption coefficients of benzene and toluene on Pt surfaces from hydrogenation rates of benzene in benzene/toluene mixtures of different compositions [23,24].

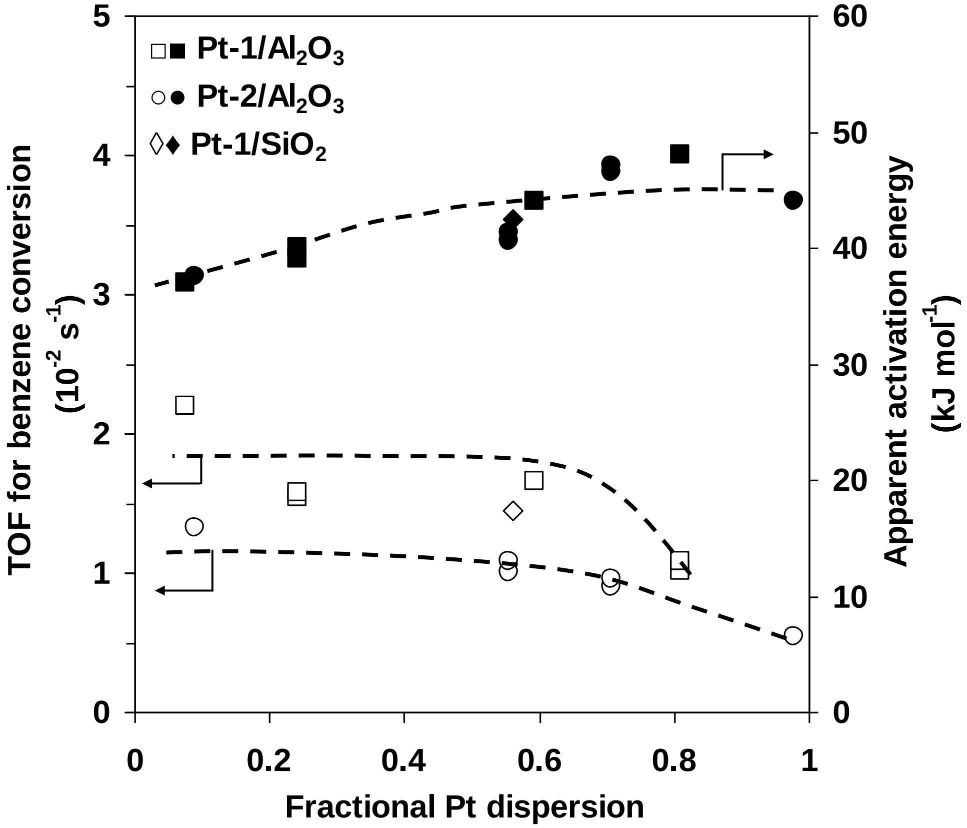

Figure 2-8. Effect of Pt dispersion on the turnover rates of benzene (Bz) hydrogenation at 308 K and activation energies (2.8 kPa Bz and 62.5 kPa H_2, 36 kPa He as balance). The apparent activation energies are reproducible within ± 2 kJ mol^{-1}.

Small differences in the turnover rates were observed in the hydrogenation of pure benzene, in keeping with the generally claimed low sensitivity to the particle size for this reaction, at least in a wide range of dispersion [28−32]. Large particles seemed somewhat more active, at most by a factor of 2, than small clusters for both series of catalysts, as also found by Flores et al. for Pt/Al_2O_3 catalysts reduced at above 673 K [27]. A closer inspection of the rates reveals that the TOFs for benzene hydrogenation are systematically lower on Pt-2/Al_2O_3 catalysts (chlorinated precursor) than on Pt-1/Al_2O_3 catalysts within experimental accuracy (Figure 2-8), in marked contrast to the more-than-doubled TOFs of Pt-2/Al_2O_3 catalysts than those of Pt-1/Al_2O_3 series for CP ring opening (D > 0.60, Figure 2-3). The measured activation energies and reaction orders in two reactants were almost independent of the Pt precursor (Figures 2-8 and 2-9). The activation energies increased from 37 to 47 kJ mol^{-1} with decreasing particle size, being close (44 ± 4 kJ mol^{-1}) on sufficiently small (D > 0.60) particles (Figure 2-8). The reaction order in benzene was slightly positive (ca. 0.07) over all catalysts, whereas the reaction order in H_2 maintained in the range of 0.7−0.8 on small (D = 0.6−1.0) Pt clusters and increased to ca. 1.0 on large (D < 0.3) particles (Figure 2-9). These values and trends compare well with those in previous reports [25,26,33].

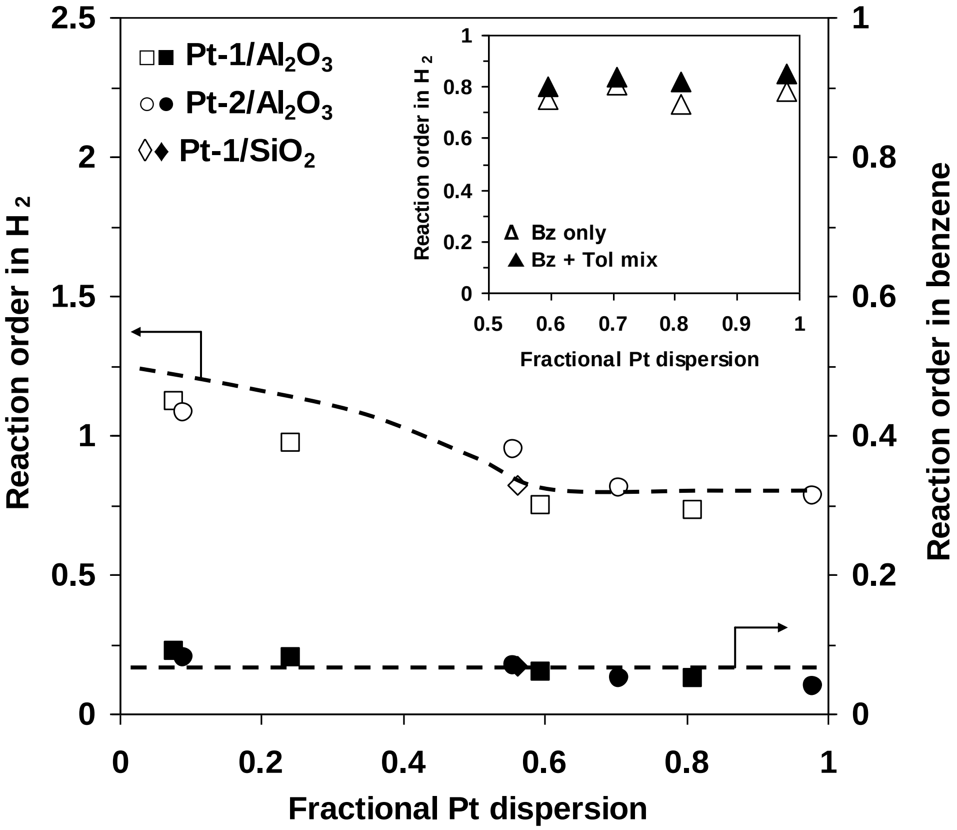

Figure 2-9. Effect of Pt dispersion on the reaction orders with respect to H_2 (empty symbols) and benzene (filled symbols) in Bz hydrogenation at 308 K (2−4 kPa Bz and 45−65 kPa H_2, He as balance in 101 kPa total pressure). The maximum errors in reaction orders are ± 0.01 for Bz and ± 0.04 for H_2. The inset shows that the reaction order in H_2 hardly changed when toluene was present in 0−3.4 kPa.

Previous studies that advocated the competitive hydrogenation of benzene and toluene as a measure of electron deficiency of surface metal atoms cancelled the H-coverage function in the Langmuir-Hinshelwood rate expression without presenting the evidence for this simplification [22−24]. In the present study, we have explored the kinetics of benzene hydrogenation and competitive hydrogenation in greater detail, and found that the reaction order in H_2 indeed remained constant and similar on clusters of similar dispersions (D = 0.6−1.0), irrespective of the origin of Pt precursor (Figure 2-9). Consequently, it should be valid to derive the relative adsorption coefficients of benzene and toluene ($K_{T/B}$) directly from the hydrogenation rates of benzene in its pure form and in a series of compositional mixtures with toluene (Eqs. 1−3).

In a pure benzene feed, the rate for benzene hydrogenation (R_B^0) is given by:

$$R_B^0 = f^0(H_2)k_BK_B/(1 + K_BP_B) \qquad \text{(Eq. 1)}$$

In a mixture of benzene and toluene (P_B and P_T as their partial pressures in the gas phase), the rate for benzene hydrogenation (R_B) is given by:

$$R_B = f(H_2)k_BK_B/(1 + K_BP_B + K_TP_T) \qquad \text{(Eq. 2)}$$

If the functionality of H_2 pressure is identical in both cases, i.e., $f^0(H_2) = f(H_2)$, and the adsorption sites for aromatics are fully covered ($K_BP_B >> 1$ or $K_BP_B+K_TP_T>> 1$), then

$$R_B^0/R_B = 1 + K_{T/B}(P_T/P_B) \qquad \text{(Eq. 3)}$$

where $K_{T/B}$ represents the ratio of adsorption coefficient of toluene over that of benzene on a specific catalyst. For the competitive hydrogenation of benzene and toluene in mixtures of these two, the reaction orders in H_2 were found to be very close to those measured in the hydrogenation of pure benzene (inset of Figure 2-9), validating the assumption of $f^0(H_2) = f(H_2)$.

Figure 2-10 shows a typical experiment that switched the feed between pure benzene and a certain benzene-toluene mixture. The rate of hydrogenation in both cases (R_B^0 and R_B) was measured exactly on the same catalyst and at the same reaction temperature. Such switch experiments also made allowance for the deactivation, and in doing so, could reduce the experimental error, for a single measurement, in the relative ratio of the measured hydrogenation rates (by averaging R_B^0/R_B, $R_B^{0'}/R_B^{'}$ and $R_B^{0''}/R_B^{''}$ in Figure 2-10). At least three gas-phase compositions of benzene and toluene (P_T/P_B = 0.3−1.2) were chosen to evaluate the relative hydrogenation rates (R_B^0/R_B). Particularly, we focused on three Pt/Al_2O_3 catalysts containing similarly small clusters, i.e., $Pt(0.81)\text{-}1/Al_2O_3$, $Pt(0.88)\text{-}2/Al_2O_3$ and $Pt(0.71)\text{-}2/Al_2O_3$, which showed different activities in the ring opening of CP (Figure 2-3). We chose these catalysts with very similar particle sizes (1.1−1.4 nm) because it is well known that the particle size also has a large effect on the electronic state of the particle.

Among these three catalysts, the one with the highest dispersion (D = 0.88), derived from hexachloroplatinic acid, showed the highest $K_{T/B}$ value (4.35), being slightly higher than Pt(0.71)-2/Al_2O_3 ($K_{T/B}$ = 4.18) which was also prepared from the Cl-containing precursor (Figure 2-11). Despite that Pt(0.81)-1/Al_2O_3 has a higher dispersion than Pt(0.71)-2/Al_2O_3, the $K_{T/B}$ value is evidently smaller ($K_{T/B}$ = 3.70) on the former catalyst, suggesting a lower electron density of surface Pt atoms on the latter. This lower electron density is supposed not to arise from the particle size, because the smaller particle size in Pt(0.81)-1/Al_2O_3 would cause the surface Pt atoms to be more ‘electron-deficient’ like [34], which would, in turn, have resulted in a larger $K_{T/B}$ value than on Pt(0.71)-2/Al_2O_3. Since the major difference in these two catalysts is considered to be the level of chlorine associated with the surface Pt atoms, it is reasonable to speculate that electron-withdrawing chlorine species renders the vicinal Pt atoms poorer in the local electron density.

Nevertheless, the observed differences (4.3 and 4.2 vs. 3.7 at 308 K) in the $K_{T/B}$ between Pt(0.88)-2/Al_2O_3, Pt(0.71)-2/Al_2O_3 and Pt(0.81)-1/Al_2O_3 catalysts are much smaller than that (14 vs. 8 at 298 K) between Pt clusters encaged in an acidic Y-zeolite and similarly small Pt clusters on a neutral SiO_2 support [24]. By inference, the electron deficiency of surface Pt atoms, caused by electron-withdrawing Cl-species, is quite small for Pt-2/Al_2O_3 catalysts. Indeed, CO chemisorption on both series of catalysts failed to disclose this difference in the electron availability in Pt d-orbitals in the absence and presence of Cl (see Appendix). Such subtle electronic perturbations induced by Cl to the electronic states of surface Pt atoms do, however, lead to considerably higher (2−3 times) rates in CP ring opening over Pt-2/Al_2O_3 catalysts than over Pt-1/Al_2O_3 catalysts for D > 0.70 (Figure 2-3b). The question, now, arises as to whether the presence of Cl affects mainly the adsorptive properties of surface Pt atoms towards the reactants, or mainly the intrinsic activity of Pt towards the C−C bond cleavage.

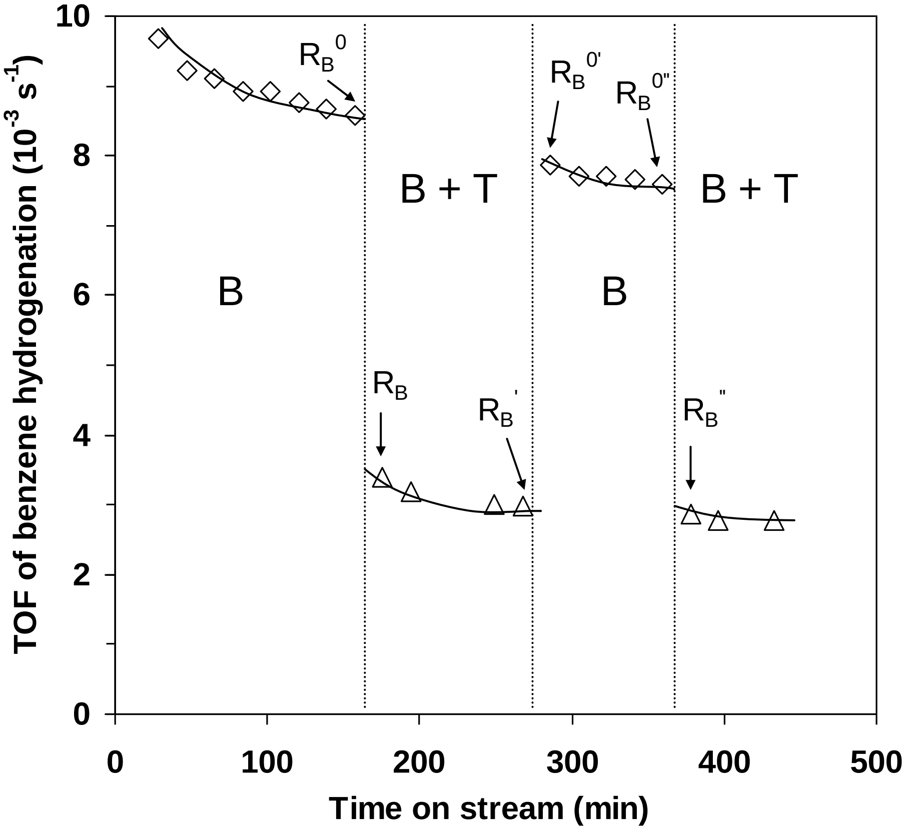

Figure 2-10. Switch experiment between the feed containing only benzene (◊) and that contains benzene and toluene (Δ). Catalyst and reaction conditions: Pt(0.81)-1/Al_2O_3, 308 K, 2.8 kPa Bz, 1.2 kPa Tol, 62.5 kPa H_2 and 34.5 kPa He as balance.

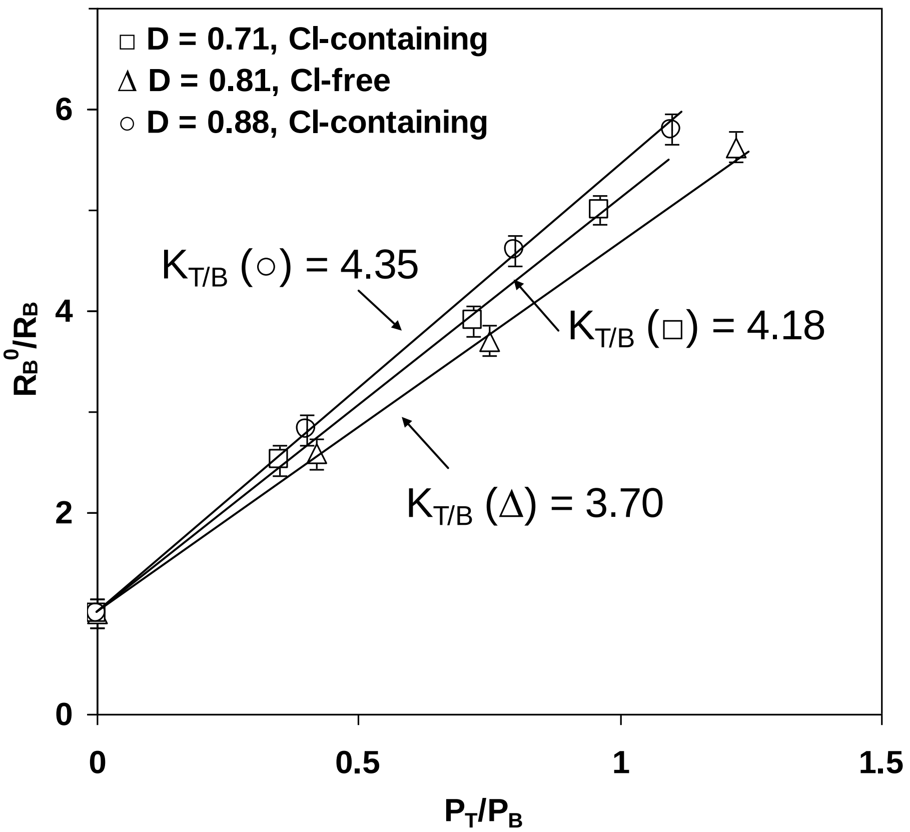

Figure 2-11. Relative ratio of benzene hydrogenation rates in a pure feed and mixtures of benzene (Bz) and toluene (Tol) as a function of the Bz/Tol ratio in the gas phase. Reaction conditions: 308K, 2.8 kPa Bz, 0−3.4 kPa Tol, 62.5 kPa H_2 and He as balance in a total pressure of 101 kPa. The $K_{T/B}$ values are the slopes of the lines.

2.3.4. Effect of chlorine: on the activation barrier or on the reactant coverage?

As the coverage by CP-derived reactive intermediates is only slightly changed (< 10%) by the presence of Cl, the difference in rates between Pt-1 and Pt-2 series apparently stems from the intrinsic rate constant. It is important to note that even a difference of ca. 5 kJ mol^{-1} in the true activation barrier suffices to account for the 3-time difference in the rate or rate constant. This modest difference in the activation barrier is due, very likely, to the subtly changed electronic density of surface Pt atoms induced by Cl. Thus, the presence of chlorine alters the turnover rates mainly by modifying the electronic states of Pt and consequently the true activation barrier.

There is, however, a significant gap in the apparent activation barrier between Pt-1/Al_2O_3 and Pt-2/Al_2O_3 catalysts; the apparent energies of activation are ca. 40 kJ mol^{-1} higher with the former series than with the latter, at high Pt dispersions (Figure 2-7). The apparent ($E_{a,app}$) and the true ($E_{a,int}$) activation barrier are related by the Temkin equation [35]

$$E_{a,app} = E_{a,int} - \Sigma n_i Q_i \qquad \text{(Eq. 4)}$$

where n_i is the order in the reactant i, and Q_i the isosteric heat of adsorption of the reactant i under reaction conditions. It is straightforward from this relation that the enthalpy changes in the activation of reactants play an important role in affecting the apparent reaction energetics.

In the ring opening of CP, H_2 reaction orders (-1.1 to -1.6) observed on Pt-2/Al_2O_3 catalysts (Cl-containing precursor) are generally less negative than those (-1.6 to -1.8) observed on Pt-1/Al_2O_3 catalysts (Cl-free precursor), particularly for small Pt particles (D > 0.70, 0.1−0.2 MPa H_2 in Figure 2-4). This suggests that hydrogen adsorption on Pt is weaker with Pt-2/Al_2O_3 catalyst than with Pt-1/Al_2O_3 catalysts. In the hydrogenolysis of neopentane, Koningsberger and coworkers found that the hydrogen coverage decreases with increasing acidity of the support [36,37]. These authors reasoned that the surface binding of H-atoms undergoes a greater extent of weakening with increasing support acidity than that of C-atoms, because the Pt–H bonding has a greater Pt *sp* component (Pt 6*sp* orbitals) than in the Pt–C bonding [36,38,39]. In line with this explanation, our experimental results show that the reaction order in CP did not differ appreciably between Pt-1 and Pt-2 series for similar average particle sizes (Figure 2-6) [40], while the reaction order in H_2 was less negative (weaker adsorption) on Pt/Al_2O_3 prepared from hexachloroplatinic acid.

If we analyze the apparent activation energy quantitatively by the Temkin relation, the exothermicity term introduced by H_2 adsorption may cause the apparent activation barrier to be lower (smaller heat of adsorption times lower reaction orders in H_2), by at least 20 kJ mol^{-1}, on the Pt-2/Al_2O_3 catalysts that contain mainly small Pt clusters (D > 0.70). The endothermic term for the dehydrogenative activation of CP must be similar, as a result of the similar coverages by CP-derived intermediates indicated by the reaction order in CP. Thus, the presence of chlorine brings down the reaction energetics mainly by weakening the H-adsorption and, in turn, the heat-of-adsorption contribution to the apparent activation barriers.

Moreover, the Cl effect observed in this study seems not to be of a geometric origin, i.e., non-selective blockage of the surface Pt atoms, as this would cause the CP-coverage to change in a more pronounced way than H-coverage as a result of the larger size of CP than a H_2 molecule, which was not the case (vide supra).

Residual chlorine atoms associated with the Al_2O_3 support could not easily be eliminated upon thermal treatment without water vapor [41,42]. It seems, however, that calcination at higher temperatures (823−873 K) followed by H_2 reduction effectively removed the electron-withdrawing chlorine species in the vicinity of exposed Pt atoms in our catalysts, in light of the close activities between Pt-1 and Pt-2 series for similar Pt particle sizes ($D < 0.6$).

2.3.5. Origin(s) of the antipathetic structure sensitivity

We have shown that the turnover rates increased by less than a factor of 3 with increasing the Pt particle size from 1 to 15 nm, when no chlorine effects are present (Pt-1 series in Figure 2-3). Although this was exemplified at a certain set of reaction conditions, it is supposed to hold also for a wider range, due to the temperature and pressure dependences of the kinetics that serve to amplify, or at least not to dampen, this structure sensitivity (Figures 2-4, -6 and -7).

To explain this antipathetic structure sensitivity, we first note that the observed changes of TOFs with dispersion do not correlate with the population of low-coordination atoms (corners and edges), as the latter sharply decreases with increasing particle size (Table 2-3). Therefore, it appears that the higher turnover rates on large particles should be ascribed to a higher population of low-index planes. At high Pt dispersions ($D = 0.8-1.0$), the highest-coordination (111) facet is sparse on the cluster surfaces. The TOFs of CP ring opening, however, were not extremely low on these very small clusters (Figure 2-3), suggesting that the (111) facet is not the sole active domain. This conclusion critically depends on the accuracy of information about the particle size or dispersion. For instance, the fraction of (111) atoms within all the exposed surface atoms increases by a factor of 2.5 when the particle size increases from 1.9 to 13.5 nm (Table 2-3). Thus, if the particle size had been underestimated, it would have become possible that the fraction of (111) face atoms correlates with the change of the surface-normalized TOF. To be rigorous, we need to point out that only if the rate constants, not rates, are found to scale with the fraction of a certain category of surface sites can one proceed to conclude the nature of active sites. Regardless, low-index planes are thought to be important for ring opening catalysis, in accord with a surface science study performed at near-atmospheric pressures [43].

Table 2-3. Estimated population of four types of surface atoms in a cuboctahedral model for five cluster sizes (i.e. shell number m: 3, 5, 10, 20 and 40, respectively)[a]

Type	CN	Fraction of surface atoms				
		Pt_{55} (1.3 nm, D = 0.76)[b]	Pt_{309} (1.9 nm, D = 0.52)[b]	Pt_{2869} (3.5 nm, D = 0.28)[b]	Pt_{24739} (6.8 nm, D = 0.15)[b]	Pt_{205479} (13.5 nm, D = 0.074)[b]
Corner	5	0.286	0.074	0.015	0.003	0.0007
Edge	7	0.571	0.444	0.236	0.120	0.06
(100)	8	0.143	0.333	0.473	0.538	0.569
(111)	9	0	0.148	0.276	0.339	0.370

[a] Numerical formulae: N_t (number of total atoms) = $1/3(2m-1)(5m^2-5m+3)$, N_s (number of surface atoms) = $10m^2 - 20m + 12$; N_{corner} (number of corner atoms) = 12; N_{edge} (number of edge atoms) = $24(m-2)$; $N_{(100)}$ (number of (100) terrace atoms) = $6(m-2)^2$; $N_{(111)}$ (number of (111) terrace atoms) = $4(m-3)(m-2)$.

[b] D (dispersion) = N_s/N_t, d (cluster size) ≈ 1.00/D.

Compared to the above arguments based mainly on a simplistic geometric model, another plausible cause for this antipathetic structure sensitivity focuses on the surface coverages of catalytically relevant species. Classically, the rate of hydrogenolysis (CP ring opening in this case) is dictated by that of the rate determining step involving H-depleted surface species. The high H_2 pressures in this study greatly suppress the coverage of unsaturated active intermediates on the surfaces of both small and large Pt particles, by virtue of dehydrogenation equilibrium preceding the C−C bond cleavage. This suppression, however, could be relatively smaller on larger Pt particles, as a result of a weaker binding energy of H on flat surfaces than on highly undercoordinated surface atoms. Even a slight decrease in the surface H-coverage could remarkably increase the coverage of the active intermediates, which are typically regarded as considerably H-depleted and are therefore highly sensitive to H-coverage changes. Consequently, the turnover rate increases as H-adatoms deplete and active carbonaceous intermediate populate, both to a modest extent, at larger particle sizes. This interpretation seems likely in the ring opening of cyclohexane over Ir/Al_2O_3 catalysts (i.e., lower reaction orders in CP and less pronounced suppression by H_2 pressure on large Ir particles than on small ones) [15], but not supported by the results in this work. The reaction orders in H_2 and in CP almost did not change on small and large Pt particles (Figures 2-4 and 2-6), indicating that the coverages of hydrogen- and CP-derived intermediates are not very different on small and large Pt particles. In this light, a larger intrinsic rate constant seems more likely to be responsible for the higher TOF on large Pt particles. The rate constant (per surface atom) is higher on large particles, partly because the low-index planes become more abundant on the surface of large particles. Moreover, if the difference in the measured activation energies (higher by 20−30 kJ mol^{-1} on large particles) reflects mainly the difference in the barrier heights of the C−C bond cleavage step on small and large particles, the pre-exponential factor must be much larger (e.g., by 10^2−10^3) on large particles than on small ones. Most likely, this implies that transition state structures vary (in terms of lateness or tightness) on the surface of Pt particles of different sizes, leading to different barrier heights and entropy changes (30−70 J mol^{-1} K^{-1} greater on large particles) of the C−C bond cleavage step on small and large particles.

In summary, the observed antipathetic structure sensitivity of the TOF is a result of complex factors, i.e., the fraction of low-index face atoms, the true activation energy and transition-state entropy, and less importantly in this work, the reactant coverages. To allow rigorous conclusions on the relative importance of these factors, future work needs to be conducted under conditions where the coverage by CP-derived reactant pool is negligible to preclude the coverage differences on small and large Pt particles.

2.3.6. Resolving the discrepancies in the observed structure sensitivity between the literature and this work

The antipathetic structure sensitivity for CP ring opening had been observed over Pt/Al_2O_3 catalysts [3,4]. The scale of TOF change with Pt dispersion, however, was much larger (i.e., an order of magnitude) than observed in the present work. Apparently, this quantitative difference in the scale of antipathetic structure sensitivity is due, at least in part, to the different reaction conditions applied in different studies. Instead of simply stating in this way, we detail below how the reaction conditions are expected to influence the observed structure sensitivities. By doing this, we are able to remark that it may be sometimes inappropriate, or not pertinent, to attribute some opposing observations in the literature, e.g. increasing trends in one and decreasing trends in another, simply to the differences in the reaction conditions without even a qualitative analysis, as the conditions may serve to strengthen a certain trend rather than to reverse it.

Let us now come back to our case. First, the temperatures applied in the work of Barbier et al. were higher (e.g., 573 K) than studied in this work (e.g., 533 K) [4]. It has been shown that measured activation energies were larger on low-dispersion catalysts than on high-dispersion ones by 20−50 kJ mol^{-1}, depending on the origin of the Pt precursor (Figure 2-7). The higher activation energies at low Pt dispersions, especially for the Pt-2/Al_2O_3 series, necessarily mean that apparent rate constants at higher temperatures would show more pronounced differences between catalysts containing remarkably different Pt particle sizes. From the activation energies (170 kJ mol^{-1} at high dispersions, 210 kJ mol^{-1} at low dispersions) and reaction temperatures, the contribution from the rate constant to the overall magnitude of the structure sensitivity was estimated to be greater by a factor of 2 at 573 K than at 533 K.

Second, the partial pressures of reactants, especially of H_2, were significantly different between the present study and the previous work [4]. On one hand, the heat of H_2 adsorption is weaker on flat surfaces than on small clusters, at both low and high H_2 pressures. On the other hand, at lower H_2 pressures (< 1 bar) as in Barbier et al.'s work, the H-coverage is not as high as in this work [44], resulting in smaller lateral interactions that reduce the heat of adsorption. Therefore, the difference in the surface H-coverage between large and small Pt particles should be more pronounced at lower H_2 pressures.

As a result, the difference in the coverage of carbonaceous active intermediates between large and small Pt clusters should be greater at lower H_2 pressures, leading to stronger antipathetic structure sensitivity as observed in the work of Barbier et al. [4].

Third, significant coverage by inactive carbonaceous surface species could give rise to the so-called secondary structure sensitivity [12], which is superimposed on the original structure sensitivity to dampen, or to magnify, the original behavior [43,45] In this work, deactivation was much less severe than the previous reports, owing to the lower temperatures and higher H_2 pressures employed. The surface coverage of inactive carbon deposits must be also much lower than in the previous studies.

Nevertheless, we are unable to exclude that highly unsaturated surface Pt atoms, e.g., corners/edges, are rendered inactive in the steady-state catalysis via irreversible titration by carbon at the initial stage of reactant introduction. In contrast to the observations in Ir-catalyzed ring opening of cyclohexane where corners/edges are shown to still participate in the catalytic cycle on the surface of small clusters [15], there appeared no sign for the catalytic activities of these highly reactive surface structures in Pt catalysts. Stronger hydrogenolysis activity of Ir, or a lower affinity (than Pt) towards carbon, may qualify the different observations on Pt and Ir catalysts.

2.4. Conclusions

Ring opening of cyclopentane (CP) has been studied over supported Pt catalysts under pressures above atmospheric, much higher than those in previous studies. The quantitative inconsistency between this work and other contributions, concerning the magnitude of the antipathetic structure sensitivity, has been resolved by a detailed comparison of the reaction conditions.

The limited changes in the reaction orders in CP and H_2 on Pt particles of different sizes lead us to conclude that the higher turnover rates on large Pt particles are mainly due to the higher rate constants (per surface atom), which, in turn, depend on the fraction of catalytically relevant surface structures (not all surface atoms). Although it remains difficult at the present stage to conclude whether surface atoms with different degrees of coordinative unsaturation catalyze the C−C bond cleavage with the same activation barriers, we speculate that the difference in the measured activation energies partly reflect that in the true barrier. If so, the higher activation energies and the higher TOFs on large particles have to be reconciled by much larger activation entropy changes on these large particles.

In this work, the relative adsorption coefficients of toluene and benzene has been utilized as a quantitative measure of the electronic density of surface Pt species in catalysts prepared from the Cl-free and Cl-containing precursors. This reaction is a simpler and more sensitive probe, than CO adsorption measurements, to disclose lower electron densities of surface Pt atoms on particles with similar sizes (1.0−1.5 nm) for the latter series of catalysts than for the former series. Care, however, must be taken with respect to the extraction of the relative adsorption coefficients from measured hydrogenation rates, because the use of these values for interpreting the electronic states of Pt would be rendered invalid, in case different catalysts featured different pressure dependences of the kinetics.

In analogy with a previous contribution by Koningsberger et al., which showed a significant TOF increment (1−2 orders of magnitude in Pt-catalyzed neopentane hydrogenolysis) when altering the support from basic (NaY) to acidic (H-USY), the promotional effect of Cl on the TOF for the ring opening of CP in this work is related to a slightly decreased electron density and an assumedly lower concentration of H-adatoms on the surface Pt atoms by retaining a certain level of Cl in the Pt catalysts. This Cl effect on the electronic states of the active metal may not find a general basis, however, since small or no promotional effects (less than 50%) on the activity and selectivity were observed in the Ir-catalyzed ring opening of cyclohexane as we previously reported.

2.5. Acknowledgements

Hui Shi thanks the Elitenetzwerk Bayern NanoCat for a Ph.D. grant and financial support. The authors are indebted to Dipl.-Ing. Xaver Hecht for technical support and for conducting N_2 physisorption and H_2 chemisorption measurements, to Dipl.-Ing. Martin Neukamm for conducting AAS measurements.

2.6. Appendix

The infrared frequency shift of CO* on different surface structures or in the presence of different electronic promoters is usually attributed to electron availability in the metal particle to participate in backbonding in the anti-bonding orbitals of chemisorbed CO, though such shifts can be complicated by coverage effects [A1−A4].

Infrared spectra for Pt(0.88)-2/Al_2O_3, Pt(0.71)-2/Al_2O_3, and Pt(0.81)-1/Al_2O_3 samples equilibrated with CO ($3.7−4.5 \times 10^{-4}$ mbar, 318 ± 3 K), corresponding to 8−11% of saturation monolayer CO* coverage, are shown in Figure 2A-1 (solid thick lines). This pressure and CO* coverage is chosen as comprise between reasonably good signal intensities and as-low-as-possible CO* coverage to minimize the dipole coupling effects. The saturation of Pt surface with CO* occurs on all these samples at pressures higher than 1.0×10^{-2} mbar.

The band at 2070-2090 cm^{-1} has been assigned to linear on-top CO*. The peaks from the reduced catalysts, however, featured low-frequency inhomogeneous line broadening in addition to a distinct high-frequency shoulder. Infrared CO absorption peaks with a similar shape were also shown by Greenler and co-workers [A5,A6] and Fanson et al. [A7]. There can be many factors contributing to the observed shape of CO adsorption bands on these catalysts, such as a relatively broad particle size distribution, or intensity transfer due to dipole coupling [A1]. While these factors may have their impacts on the wavenumbers and intensity ratios between different peaks resolved from the adsorption band, we believe that the very similar average particle sizes (1.1−1.4 nm) and similarly low CO* coverages among these catalysts render the comparison of electronic states of Pt on the basis of CO-stretching vibrational frequencies/wavenumbers essentially valid for these spectra.

The deconvoluted peaks (thin lines) and the related wavenumbers were shown in Figure 2A-1. Three peak components with different wavenumbers appeared to give good fits to the measured spectra. The full width at half-maximum (FWHM) increased with decreasing wavenumbers for different peaks. Irrespective of the Cl contents in the catalyst, the three peaks appeared at 2083−2089, 2069−2070, 2033−2035 cm^{-1}. The FWHM for these peaks were 65−68, 29−30 and 11−12 cm^{-1}, respectively. Greenler and coworkers determined that the high-, medium-, and low-frequency components were due to crystallite facet faces, corners, and edges, respectively [A6]. More generally, the wavenumbers increase with the coordination number of surface sites [A5]. Regardless, the results in Figure 2A-1 seem to suggest that the CO stretching frequencies cannot discriminate the difference in the electron density of surface Pt atoms in these catalysts which have similar particle sizes but were prepared from Cl-free and Cl-containing precursors.

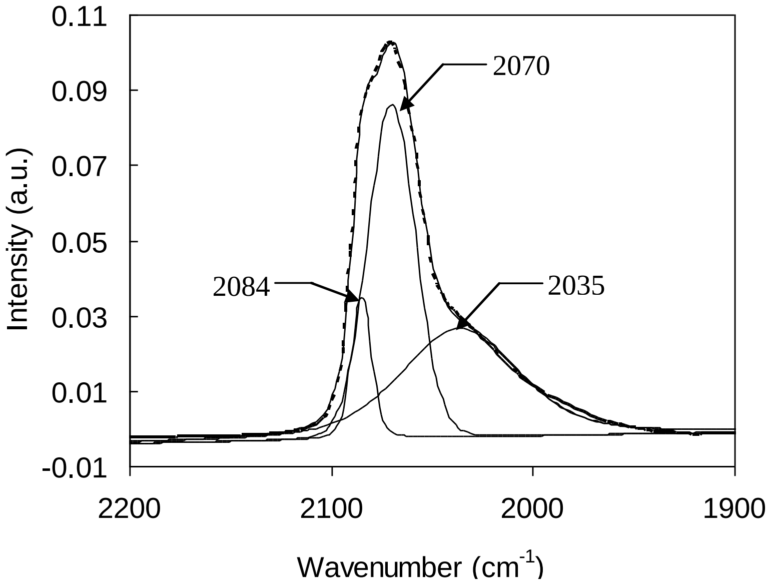

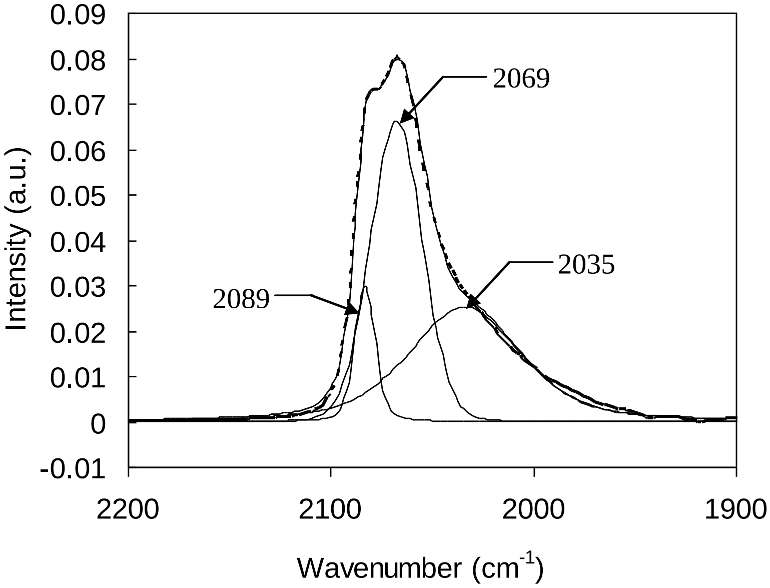

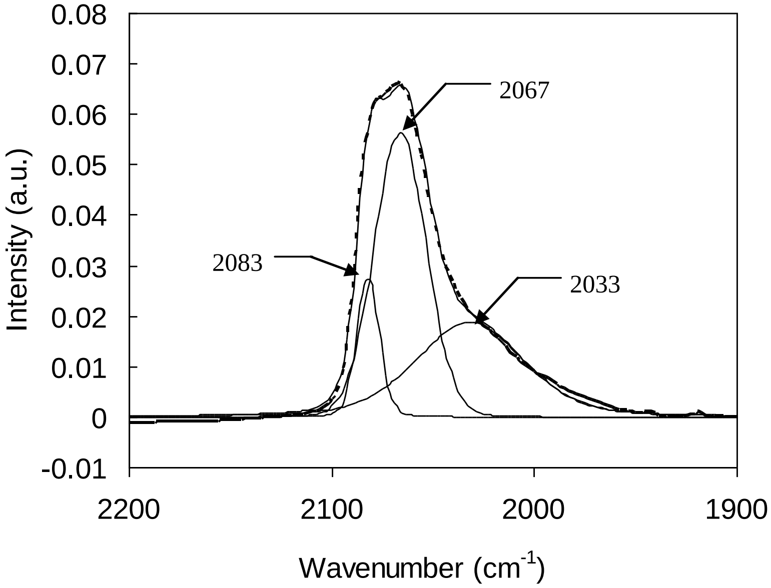

Figure 2A-1. Infrared spectra of CO chemisorbed at 318 (± 3) K for catalysts prepared from hexachloroplatnic acid: (a) Pt-2(0.88)/Al_2O_3, (b) Pt-2(0.71)/Al_2O_3 and that prepared from tetraamine platinum nitrate: (c) Pt-1(0.81)/Al_2O_3.

References in the Appendix

[A1] S.G. Fox, V.M. Browne, P. Hollins, J. Electron Spectrosc. Relat. Phenom. 54/55 (1990) 749.

[A2] A. Crossley, D.A. King, Surf. Sci. 68 (1977) 528.

[A3] P. Hollins, Surf. Sci. Rep. 16 (1992) 51.

[A4] A.D. Allian, K. Takanabe, K.L. Fujdala, X. Hao, T.J. Truex, J. Cai, C. Buda, M. Neurock, E. Iglesia, J. Am. Chem. Soc. 133 (2010) 4498.

[A5] R.K. Brandt, M.R. Hughes, L.P. Bourget, K. Truszkowska, R.G. Greenler, Surf. Sci. 286 (1993) 15.

[A6] R.G. Greenler, K.D. Burch, K. Kretzschmar, R. Klauser, A.M. Bradshaw, B.E. Hayden, Surf. Sci. 152/153 (1985) 338.

[A7] P.T. Fanson, W. N. Delgass, J. Lauterbach, J. Catal. 204 (2001) 35.

2.7. References

1. F.G. Gault, Adv. Catal. 30 (1981) 1.
2. Y. Barron, G. Maire, J.M. Cornet, J.M. Muller, F.G. Gault, J. Catal. 2 (1963) 152.
3. J. Barbier, A. Morales, P. Marécot, R. Maurel, Bull. Soc. Chim. Belg. 88 (1979) 569.
4. J. Barbier, P. Marecot, Nouv. J. Chim. 5 (1981) 393.
5. G.A. del Angel, B. Coq, G. Ferrat, F. Figuéras, Surf. Sci. 156 (1985) 943.
6. S. Fuentes, F. Figuéras, J. Catal. 61 (1980) 443.
7. B. Coq, R. Dutartre, F. Figuéras, T. Tazi, J. Catal. 122 (1990) 438.
8. J. Barbier, P. Marécot, A. Morales, R. Maurel, Bull. Soc. Chim. Fr. 7–8 (1978) I-309.
9. B. Coq, A. Bittar, F. Figuéras, Appl. Catal. 59 (1990) 103.
10. S. Fuentes, F. Figuéras, J. Chem. Soc. Faraday Trans. 174 (1978) 174.
11. U. Wild, D. Teschner, R. Schlögl, Z. Paál, Catal. Lett. 67 (2000) 93.
12. M. Che, C.O. Bennett, Adv. Catal. 36 (1989) 55.
13. M.A. Vannice, J.E. Benson, M. Boudart, J. Catal. 16 (1970) 348.
14. J.R. Anderson, Y. Shimoyama, Proc. Int. Congr. Catal. 5th, 1 (1972) 695.
15. H. Shi, X.B. Li, G.L. Haller, O.Y. Gutiérrez, J.A. Lercher, J. Catal. 295 (2012) 133.
16. J. Weitkamp, in Handbook of Heterogeneous Catalysis, G. Ertl, H. Knözinger, J. Weitkamp (eds.), Vol.2, Wiley-VCH, Weinheim, 1997, p. 439.
17. J.T. Miller, B.M. Meyers, F.S. Modica, M. Vaarkamp, D.C. Koningsberger, J. Catal. 143 (1993) 395.
18. M. Boudart, R.A. Dalla Betta, Proc. Int. Congr. Catal. 5th, 1 (1973) 1329.
19. P. Reyes, M. Oportus, G. Pecchi, R. Fréty, B. Moraweck, Catal. Lett. 37 (1996) 193.
20. S.D. Jackson, J. Willis, G.D. McLellan, G. Webb, M.B.T, Keegan, R.B. Moyes, S. Simpson, P.B. Wells, R. Whyman, J. Catal. 139 (1993) 191.
21. H. Karhu, A. Kalantar, I.J. Väyrynen, T. Salmi, D.Y. Murzin, Appl. Catal. A 247 (2003) 283.
22. Z. Guo, Y.T. Chen, L.S. Li. X.M. Wang, G.L. Haller, Y.H. Yang, J. Catal. 276 (2010) 314.
23. T.T. Phoung, J. Massardier, P. Gallezot, J. Catal. 102 (1986) 456.

24. G. Larsen, G.L. Haller, Catal. Lett. 3 (1989) 103.
25. S.D. Lin, M.A. Vannice, J. Catal. 143 (1993) 539.
26. S.D. Lin, M.A. Vannice, J. Catal. 143 (1993) 554.
27. A.F. Flores, R.L. Burwell, J.B. Butt, J. Chem. Soc. Faraday Trans. 88 (1992) 1191.
28. J.M. Basset, G. Dalmai-Imelik, M. Primet, R. Mutin, J . Catal. 37 (1975) 22.
29. G.C. Bond, Surf. Sci. 156 (1985) 966.
30. R. Maurel, G. Leclercq, J. Barbier, J. Catal. 37 (1975) 324.
31. D.S. Cunha, G.M. Cruz, Appl. Catal. A 236 (2002) 55.
32. C.R. Henry, C. Chapon, S. Giorgio, C. Goyhenex, in R.M. Lambert, G. Pacchioni (Eds.), Chemisorption and Reactivity on Supported Clusters and Thin Films, Kluwer, 1997, pp. 117.
33. V.V. Pushkarev, K. An, S. Alayoglu, S.K. Beaumont, G.A. Somorjai, J. Catal. 292 (2012) 64.
34. M. Vaarkamp, J.T. Miller, F.S. Modica, G.S. Lane, D.C. Koningsberger, T. Uematsu, G.L. Haller, V. Haensel, K. Klier, A. Renouprez, R.W. Joyner, R. Prins, Stud. Surf. Sci. Catal. 75 (1993) 209.
35. M. Temkin, Acta Physicochim. URSS 3 (1935) 312.
36. D.C. Koningsberger, M.K. Oudenhuijzen, J. de Graaf, J.A. van Bokhoven, D.E. Ramaker, J. Catal. 216 (2003) 178.
37. B.L. Mojet, J.T. Miller, D.E. Ramaker, D.C. Koningsberger, J. Catal. 186 (1999) 373.
38. M.K. Oudenhuijzen, J.A. van Bokhoven, J.T. Miller, D.E. Ramaker, D.C. Koningsberger, J. Am. Chem. Soc. 127 (2005) 1530.
39. J. Kua, W.A. Goddard III, J. Phys. Chem. B 102 (1998) 9481.
40. As the H-coverage decreases, the coverage by CP-derived intermediates has to increase, leading to smaller reaction orders in CP. However, this change in the CP reaction order is more difficult to discern compared to the reaction order in H_2, as analyzed in the Supporting Information.
41. A.A. Castro, O.A. Scelza, C.T. Baronetti, M.A. Fritzler, J.M. Parera, Appl. Catal. A 6 (1983) 347.
42. Y.J. Huang, S.C. Fung, J. Catal. 131 (1991) 378
43. R.K. Herz, W.D. Gillespie, E.E. Peterson, G.A. Somorjai, J. Catal. 67 (1981) 386.

44. The H-coverage at 1 bar is ca. 50% smaller than that at 4 bar at the same temperature.
45. W.D. Gillespie, R.K. Herz, E.E. Peterson, G.A. Somorjai, J. Catal. 70 (1981) 147.

Chapter 3

On the active sites and reactive intermediates in the hydrogenolytic cleavage of C–C bonds in cyclohexane over supported iridium clusters

Pressure- and temperature-dependent kinetics of cyclohexane hydrogenolysis have been measured over a series of supported Ir catalysts with varying average particle sizes. The turnover frequency (TOF) exhibited sympathetic and antipathetic trends with decreasing dispersion on small and large Ir particles, respectively. The selectivity to the ring opening product consistently declined with lowering Ir dispersion. The decrease of the TOF with decreasing dispersion for small clusters originates principally from the diminishing population of low-coordination atoms. The increase of the TOF with further decreasing dispersion for large particles is speculated to result from increased population of terrace planes or step sites, or a less unsaturated nature of the most abundant reactive intermediate. The extent of multiple C−C bond cleavage relies mainly on the presence of highly unsaturated atoms and terrace planes in high- and low-dispersion Ir catalysts. Multiple hydrogenolysis also depends on the H_2 *pressure, because single and multiple C−C bond scissions are mediated by surface intermediates with different H-deficiencies. This chapter focuses on the fundamental elementary steps on Ir, devoid of notable effects from support acid-base sites.*

3.1. Introduction

The hydrogenolysis of cycloalkanes is of immense practical and fundamental interest. From an applied point of view, selective ring opening represents an important process following deep hydrogenation of aromatics during the upgrading of light cycle oil (LCO) used for blending in the diesel pool [1−3]. From a fundamental standpoint, the active site requirements and the elementary steps involved in the hydrogenolysis of paraffinic C–C bonds remain partly unresolved for acyclic alkanes even after decades of studies, not to mention the much less explored cycloalkanes in this respect [4].

The structure sensitivity of hydrogenolysis of C–C bonds in alkanes was first demonstrated by Sinfelt et al. for ethane hydrogenolysis over Ni-Cu alloys [5]. Since then, alkane hydrogenolysis is usually assumed to require a large ensemble size, though the evidence arising from particle size effects is actually sparse and contradictory [4−14]. Specifically, only with Ni is the verdict almost unanimous, i.e., the turnover rate (TOR or TOF) decreases with size (above ca. 4 nm) [4]. For ethane hydrogenolysis over Pt/SBA-15 catalysts of different average metal particle sizes in a range of 1−7 nm, the smallest clusters were the most active [6,7]. Over Rh/SiO_2, the TOF of ethane hydrogenolysis increased with dispersion and then fell when particles became smaller than 1.5 nm [8]. A thoughtful investigation of Rh/TiO_2 systems further reveals that the sort of charge transfer between metal and interacting support, either localized or delocalized, could dramatically change the rate variations as a function of percentage exposed [9], justifying the use of non- or weakly interacting supports when particle size effects are being studied in hydrogenolysis reactions. Foger and Anderson reported differences in the specific activities of less than a factor of 3 on Al_2O_3- and SiO_2-supported Ir catalysts with average particle sizes of 1.5−7.0 nm for ethane hydrogenolysis [10]. Having applied a much wider variety of reaction conditions, Engstrom et al. found differing trends of structure sensitivity for hydrogenolysis of ethane or butanes over Ir(111) and Ir(110)-(1×2) surfaces [11]. Thus, it appears that the findings on the structure sensitivity are rather inconclusive for Pt, Rh and Ir even in hydrogenolysis of the seemingly simple ethane molecule. Note that reaction conditions may significantly alter the observations. A study over different Pt model surfaces showed that terraces of Pt(111) without steps and kinks are the most active for C–C bond breaking of cyclohexane (CH) in 100 Torr H_2 [12], in apparent opposition to the trend observed by the same group at very low CH (5×10^{-6} Pa) and H_2 (10^{-4} Pa) pressures where kinks in the steps appeared the most active [13,14].

Compared to the extensively studied ring opening reaction of methylcyclopentane (MCP) [15−22], far less fundamental knowledge is available for the direct endocyclic C–C bond cleavage of the much more stable C_6-naphthenic structures, which are more relevant to the real LCO feeds. Due to the low reactivity of the cyclohexyl ring, bifunctional catalysis, which involves an acid-catalyzed ring contraction step to much more reactive C_5-backbones, is more often applied [1,23−28]. The factor of metal/acid balance is taken into account in such a “bifunctional” scenario, together with the variables (e.g., metal particle size) under investigation [25,28]. This results in a complexity which hampers any attempts to establish an unequivocal structure performance relationship with respect to the metal component. Since the nature of the noble metal appears unlikely to exert a significant influence on the activities or selectivities of the catalysts according to a classical bifunctional mechanism [27,28], fundamental insights exclusively into the metallic function have largely not been acquired.

In spite of being beneficial in terms of enhanced activity and catalyst stability when applied in combination with acidic zeolites [23], Pt particles in the absence of appropriate acidity catalyze predominantly dehydrogenation and isomerization reactions of six-membered-ring hydrocarbons [4]. Monometallic Ru- and Pd-based catalysts exhibit either too high or too low ability, respectively, to cleave C–C bonds. Therefore, non-acidic Ir-based catalysts hold the best promise among all of the monofunctional metal catalysts for achieving selective ring opening of C_6-carbocycles in a single, direct scission [1], as long as C–C bond ruptures at unwanted positions and for multiple times are minimized. In a recent study by Resasco and coworkers [29], intriguing trends, in relation to Ir dispersion, concerning different endocyclic C–C bond cleavage modes of di-substituted cyclohexanes were shown over a series of monofunctional Ir catalysts on non-acidic or weakly acidic supports. This study points to a promising possibility of maximizing C–C bond ruptures at sterically hindered positions (gaining in cetane number) by tailoring Ir dispersion and support characteristics. Nevertheless, detailed kinetic features of such systems, especially those associated with changes in H_2 pressure, remain unexplored [29].

In this context, a detailed kinetics study has been undertaken, using supported Ir clusters of different sizes on non-acidic carriers and applying a wide range of reaction conditions. The catalytic consequences of modulating Ir dispersion and H_2 pressure have been addressed in regard to various reaction probabilities, i.e., ring opening, and multiple hydrogenolysis (internal and terminal modes). The mechanistic and structural origins of cyclohexane hydrogenolysis on Ir are also discussed. Distinct from previous knowledge accumulated on bifunctional Ir catalysts, where a delicate acid-metal balance is more important than metal characteristics [25,28,30], this chapter addresses the catalytic role of metallic Ir in the hydrogenolysis of endocyclic C–C bonds. The role of Ir, in this case, is beyond serving to attain dehydrogenation-hydrogenation equilibrium between cyclic reactants, acyclic products and their carbocations, as suggested in a bifunctional mechanism.

3.2. Experimental

3.2.1. Catalyst preparation

A chlorine-free precursor, iridium(III) acetylacetonate ($Ir(acac)_3$, Aldrich, 97%) was dissolved in toluene before use [31]. Fumed γ-alumina (Alu C, 104 m^2 g^{-1}, Evonik Degussa) was used as the support for preparation of the catalysts. In a typical procedure of incipient wetness impregnation, aliquots of the solution were added dropwise to a beaker containing γ-Al_2O_3 while stirring with a quartz rod. The as-prepared sample was first dried in synthetic air at 393 K overnight and subsequently treated in H_2 at 723 K for 5 h. The reduced material was divided into six portions treated at varying temperatures (473−873 K) for 5 h in dry synthetic air flow and treated again in H_2 at 723 K for 4 h. A temperature increment of 1 K min^{-1} was applied for all thermal treatments. Samples, thus obtained, are denoted as m%Ir(D)-1/Al_2O_3, where m%, D and 1 are the actual Ir loading by wt.% determined by ICP-OES, the fractional Ir dispersion obtained from H_2 chemisorption measurements, and a denotation of the Cl-free precursor, respectively.

A chlorine-containing precursor, ammonium hexachloroiridate ($(NH_4)_2IrCl_6$, Aldrich, 99.99%) was used instead of $Ir(acac)_3$ in order to examine the effects of chlorine on the catalytic activity and selectivity. The procedure for incipient wetness impregnation was the same as that for Cl-free catalysts except that the precursor was dissolved in doubly-distilled deionized water beforehand. After impregnation, the samples were left at ambient conditions (parafilm covered) overnight and then dried in synthetic air at 393 K overnight and reduced in H_2 at 723 K for 5 h. This batch was then divided into four aliquots, which were treated at different temperatures (673−823 K) for 5 h in dry synthetic air flow and reduced at 723 K for 4 h in pure H_2 flow. A high-Ir-loading batch was prepared by wetness impregnation using the same $(NH_4)_2IrCl_6$ solution at a 5-fold-excess volume relative to that in incipient wetness impregnation. After evaporating the solution and drying at 393 K for 12 h, the high-loading batch was reduced at 723 K for 4 h in pure H_2 flow without air-calcination. Samples thus obtained are denoted as m%Ir(D)-2/Al_2O_3, m%, D and 2 are the actual Ir loading by wt.% determined by ICP-OES, the fractional Ir dispersion obtained from H_2 chemisorption measurements, and a denotation of the Cl-containing precursor, respectively. Residual chlorine contents were qualitatively determined to be below 1000 ppm for all catalysts (elemental analysis, Metrohm 686 Titroprocessor).

3.2.2. Catalyst characterization

3.2.2.1. H_2 chemisorption and N_2 physisorption

Weakly and strongly adsorbed fractions of hydrogen uptakes were determined volumetrically by a Sorptomatic 1990 instrument. It had been realized that Ir/Al_2O_3 samples, especially those containing primarily small clusters, were highly susceptible to surface re-oxidation during ambient storage (possibly because iridium adsorbs oxygen strongly [32]), producing irreproducible dispersion results. Therefore, catalyst samples were pretreated in 100 kPa of static H_2 at 723 K for 2−3 h and then evacuated at the same temperature for 0.5 h before chemisorption measurements were carried out. Only by this means could reproducible results be obtained (± 2−5% relative standard deviation). Hydrogen adsorption was conducted at 307 K in a pressure range of 0.5−13.2 kPa with an equilibrating time of 2−5 min for each pressure increase step. After completing the first isotherm, the sample was evacuated to 10^{-4} kPa for 1 h and the second isotherm was measured. The second isotherm (physisorption) was subtracted from the first one (chemisorption + physisorption). The amount of adsorbed hydrogen was determined by extrapolating the linear part of the difference isotherm ($P > 6.5$ kPa) to zero pressure. Dispersions (*D*), defined as the fraction of Ir atoms exposed at surfaces, were estimated by assuming a H_{strong}/Ir stoichiometry of two [33−35]. This ratio was rationalized by multiple hydrogen adsorption on under-coordinated Ir atoms [35]. Correction for chemisorption contribution from the γ-Al_2O_3 support was unnecessary, because the extrapolated values of the isotherms for bare γ-Al_2O_3, pretreated in the same way as the catalysts, were close to zero within the uncertainty of the measurements.

The porosity of the catalyst samples was measured by N_2 physisorption at 77 K on the Sorptomatic 1990 instrument. Prior to the measurements, all samples were outgassed at 523 K for 2 h. The specific surface area was calculated by applying BET theory to the adsorption isotherms over a relative pressure range (p/p^0) between 0.03 and 0.10, assuming a cross-sectional area of 0.162 nm^2 for a N_2 molecule.

3.2.2.2. Transmission electron microscopy

Transmission electron microscope (TEM) images of the materials were recorded with a JEM-2010 JEOL transmission electron microscope operating at 120 kV. Before being transferred to the vacuum system, the samples were ground, suspended in ethanol and ultrasonically dispersed for 2 min. Drops of the dispersions were applied on a copper grid-supported carbon film.

3.2.2.3. ICP-OES

The iridium contents of the samples were determined by inductively-coupled plasma optical emission spectroscopy (ICP-OES). Before measurement, 60−100 mg of the solid sample was mixed with 2.0 cm^3 hydrofluoric acid (10 wt.%), 0.1 cm^3 hydrochloric acid and 0.1 cm^3 nitric acid and boiled until the solution was clear. The iridium concentration of the solution was measured on a Spectroflame FTMOA81A ICP-OES spectrometer

(Spectro Analytic Instruments). Standard solutions containing 0, 50, 100 and 200 ppm Ir in 25 cm^3 6.5 wt.% nitric acid were used for calibration.

3.2.3. Steady state kinetic measurements

The hydrogenolysis of cyclohexane (CH) was studied in a stainless steel packed-bed tubular reactor with an inner diameter of 4 mm. Compacted and crushed catalyst powders sieved to 180−280 μm were diluted with appropriate amounts of quartz sand of identical sieve fractions to ensure sufficient bed lengths for plug-flow hydrodynamics. A K-type thermocouple was attached to the external surface of the reactor (within the isothermal region) to measure and control reaction temperatures. Little difference (< 1 K) was detected at the reaction temperature, when the thermocouple was brought in contact with the catalyst bed. Preliminary tests had confirmed the absence of transport artifacts (Figure 3-1). Prior to reactions, catalysts were pretreated in a pure H_2 flow of 20 cm^3 (STP) min^{-1} (from room temperature to 623 K, 0.2 K s^{-1} ramp and 2 h dwell) and then cooled to the reaction temperature (503−563 K). The hydrocarbon was introduced using a flow of helium (Westfalen AG, 99.996%) passing through a series of bubblers immersed in a thermostatted water bath which contained liquid CH (Aldrich, ≥ 99%). Upon switching of flow configurations, the helium flow carrying saturated vapor of CH at the bath temperature mixed with a flow of H_2 (Westfalen AG, 99.999%) in a co-current mode and contacted the catalyst bed to initiate the reaction at the set temperature. Flow rates of gases and total pressures of the reactor system were modulated by electronic mass flow controllers and back pressure regulators. The typical H_2/CH ratio was tuned from 20 to 350. The kinetic measurements were conducted under total pressures of 0.1−2.0 MPa. The products were analyzed online by a Hewlett-Packard 6890 Plus GC equipped with a DB Petro column (320 μm × 100 m) connected to a flame ionization detector (FID). Initial rates and selectivities were reported as values derived by extrapolation of measured steady-state rates and selectivities to zero contact time. Deactivation, losing at most 15% of the initial activities, was observed for low-dispersion catalysts during high pressure experiments for 5 days below 543 K.

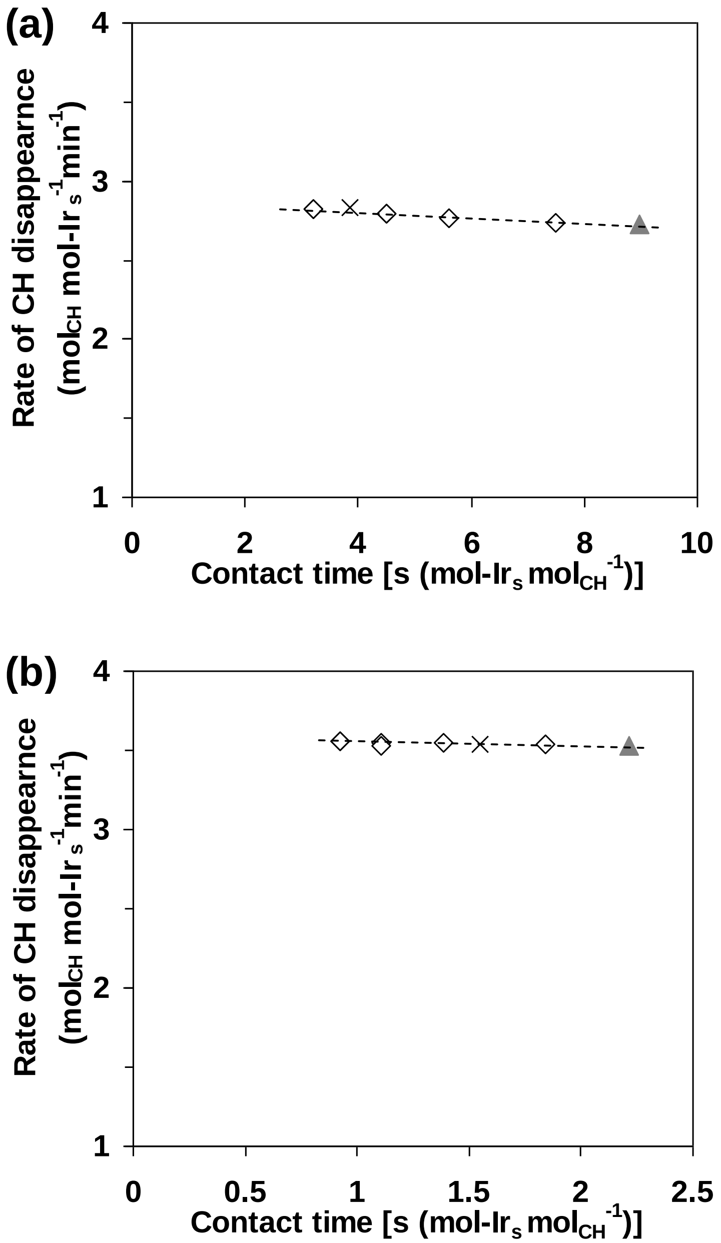

Figure 3−1. Effects of contact time and pellet size on the reaction rates over (a) 0.5%Ir(0.65)-1/Al_2O_3 and (b) 0.5%Ir(0.16)-1/Al_2O_3 at 523 K, 3.1 kPa CH, 0.56 MPa H_2 and conversion levels < 30%. Symbols represent: 280-400 μm, 20 mg (×); 180-280 μm, 20 mg (◊); 180-280 μm, 40 mg (▲).

3.3. Results

3.3.1. Catalyst characterization

All catalysts used in the kinetic studies are listed in Table 3-1. These samples had been treated in H_2 at 723 K, i.e., higher than those (< 570 K) used in the hydrogenolysis reactions, to avoid further structural changes during catalysis. Indeed, significant coalescence was not observed after comparing the metal particle size in spent catalysts with that before reaction (not shown). The actual loadings of Ir in all prepared samples are in excellent agreement with the intended values owing to the impregnation approach used. Up to a loading of ca. 2 wt.%, the surface areas of the resultant materials shrink by at most 10% relative to bare Al_2O_3 support. Neither air-calcination (T = 393−873 K) nor H_2-reduction at 723 K imposes a considerable impact on the BET surface areas of the Ir/Al_2O_3 samples, apparently due to the thermo-stability of γ-Al_2O_3 synthesized by flame pyrolysis and the low surface density of Ir atoms.

The effect of calcination temperature on Ir dispersion is shown in Figure 3-2. Increasing the calcination temperature from 393 to 873 K, followed by reduction at 723 K, decreased the Ir dispersion from ca. 60% to lower than 20% for the low-loading (0.50−0.54%) samples. Notably, the Ir/Al_2O_3 samples prepared from Cl-free precursor featured a sharp loss of Ir dispersion from 52% to 24% within a narrow temperature window of 623−673 K, possibly because of a much enhanced mobility of surface iridium oxide species (close to the Tammann temperature of IrO_2, 686 K). By contrast, the Ir dispersion of those prepared from Cl-containing precursor showed a relatively gradual decrease and began to approach that of the Cl-free counterpart at high calcination temperatures (> 800 K). The presence of chlorine was proposed to be responsible for re-dispersion of Pt in O_2-containing atmosphere [36], a situation likely to also occur with the Cl-containing Ir/Al_2O_3 catalysts.

Table 3-1. Physicochemical and textural properties of all of the studied Ir catalysts.

Catalysts	BET surface area (m^2 g^{-1})	H_2 chemisorption at 307 K		
		Weak (µmolH_2 g^{-1})	Strong (µmolH_2 g^{-1})	Fractional dispersion[a]
0.50%Ir(0.65)-1/Al_2O_3	97	10	17	0.65
0.50%Ir(0.61)-1/Al_2O_3	—[b]	10	16	0.61
0.50%Ir(0.58)-1/Al_2O_3	99	10	15	0.58
0.50%Ir(0.52)-1/Al_2O_3	—[b]	9	13	0.52
0.50%Ir(0.24)-1/Al_2O_3	90	7	6	0.24
0.50%Ir(0.16)-1/Al_2O_3	—[b]	6	4	0.16
0.50%Ir(0.04)-1/Al_2O_3	85	3	1	0.04
0.54%Ir(0.58)-2/Al_2O_3	100	13	15	0.58
0.54%Ir(0.46)-2/Al_2O_3	96	11	13	0.46
0.54%Ir(0.30)-2/Al_2O_3	92	8	8	0.30
0.54%Ir(0.18)-2/Al_2O_3	88	5	5	0.18
1.92%Ir(0.11)-2/Al_2O_3	95	10	11	0.11
0.98%Ir(0.20)-2/SiO_2[c]	186	13	10	0.20
Ir black (0.01)[d]	—[b]	23	75	0.014

[a] Values are obtained by assuming two strongly adsorbed hydrogen atoms on one surface iridium atom, a chemisorption stoichiometry adopted throughout this work.

[b] Not determined.

[c] This catalyst was prepared by incipient wetness impregnation using $(NH_4)IrCl_6$ as the precursor salt. After impregnation, it was calcined in air at 673 K and reduced in H_2 at 723 K (the same treatment procedure as for the other catalysts).

[d] Commercially available from Aldrich (≥ 99.9% trace metal).

Representative TEM micrographs are presented in Figure 3-3. For 1.92%Ir/Al_2O_3, a surface weighted mean particle size was analyzed statistically to be 11.7 nm by sampling a number of 210 Ir particles from a collection of 24 different areas. Note that this value, when translated into dispersion ($D = 0.99/d \approx 0.09$), is in reasonable agreement with that determined by H_2 chemisorption ($D_{Ir} = 0.11$). Hence, the H_{strong}/Ir stoichiometry of two seems to be valid on this low-dispersion sample. On 1.92%Ir/Al_2O_3, particles larger than

10 nm became common, and a broad distribution (11.7 ± 6.9 nm) was observed. Unlike the low-loading samples, small clusters of 1−2 nm were rarely seen in this case (Figure 3-3e). For all low-loading (0.50−0.54%) samples, unfortunately, a sufficient number (say, at least 150) of visible metal particles were not available for performing a convincing analysis of particle size distribution. However, the trend that Ir dispersion decreases as calcination temperature and Ir loading increase is qualitatively supported by TEM (Figure 3-3).

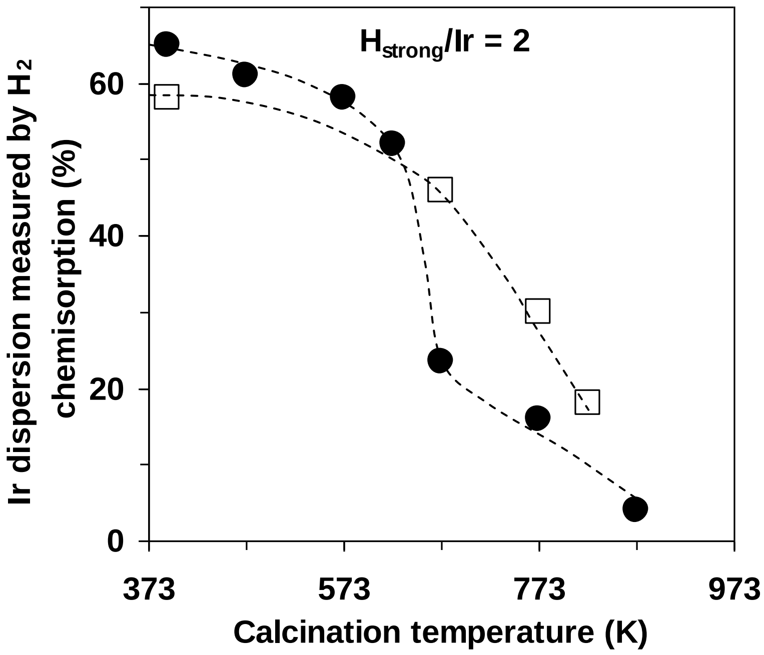

Figure 3−2. Ir dispersion as a function of calcination temperature in synthetic air. Filled circles represent the dispersions of Ir/Al_2O_3 catalysts prepared from Cl-free precursor and empty squares correspond to those prepared from a Cl-containing precursor.

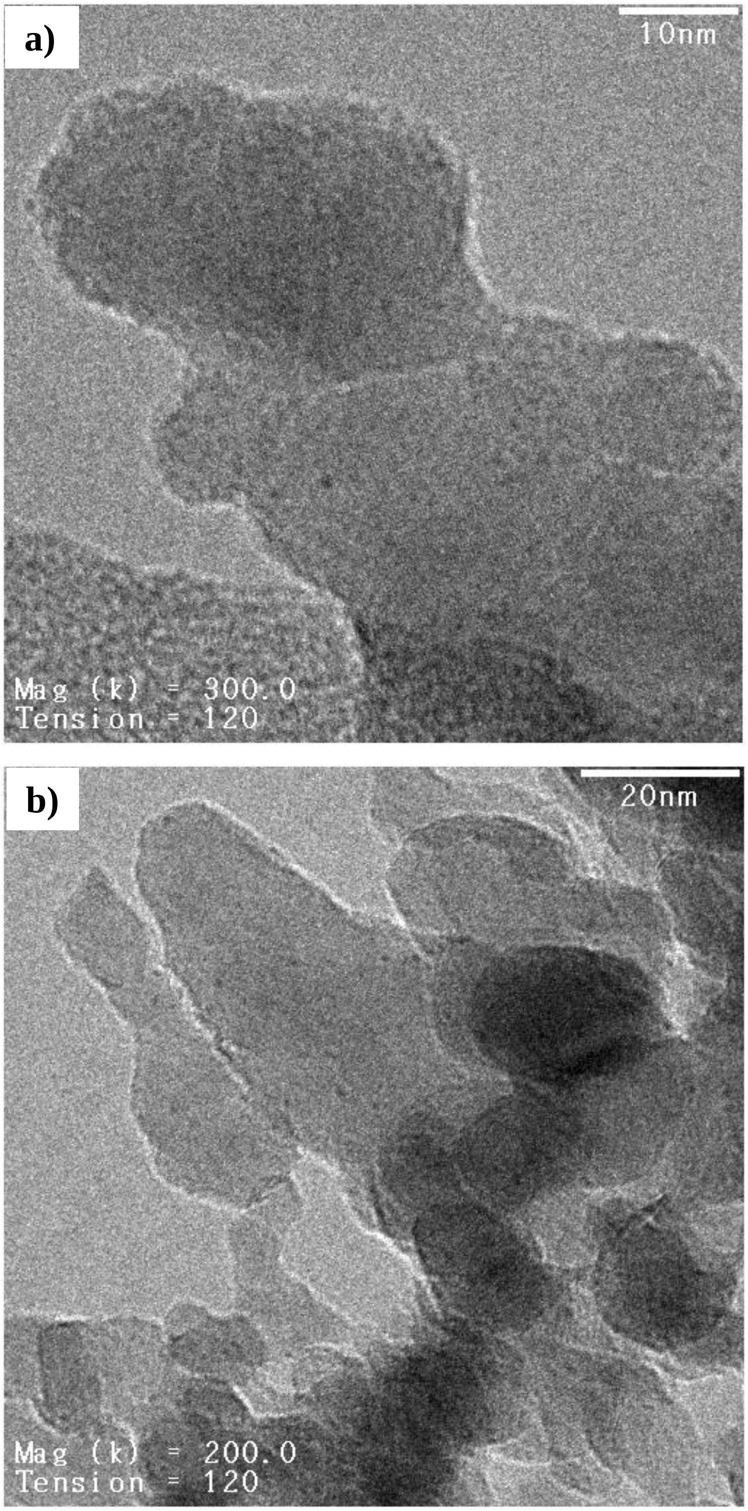
a)
10nm
Mag (k) = 300.0
Tension = 120
b)
20nm
Mag (k) = 200.0
Tension = 120

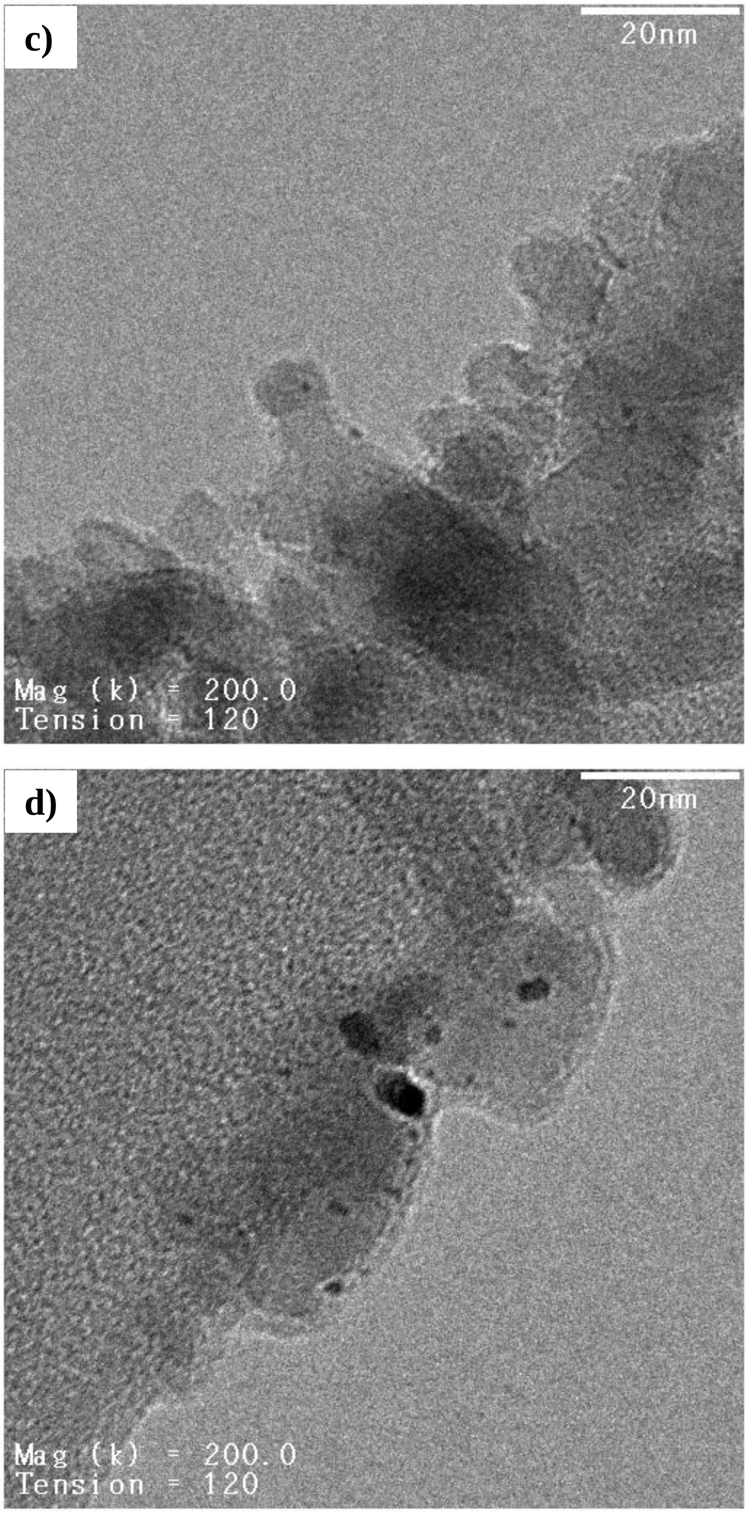
c)
20nm
Mag (k) = 200.0
Tension = 120
d)
20nm
Mag (k) = 200.0
Tension = 120

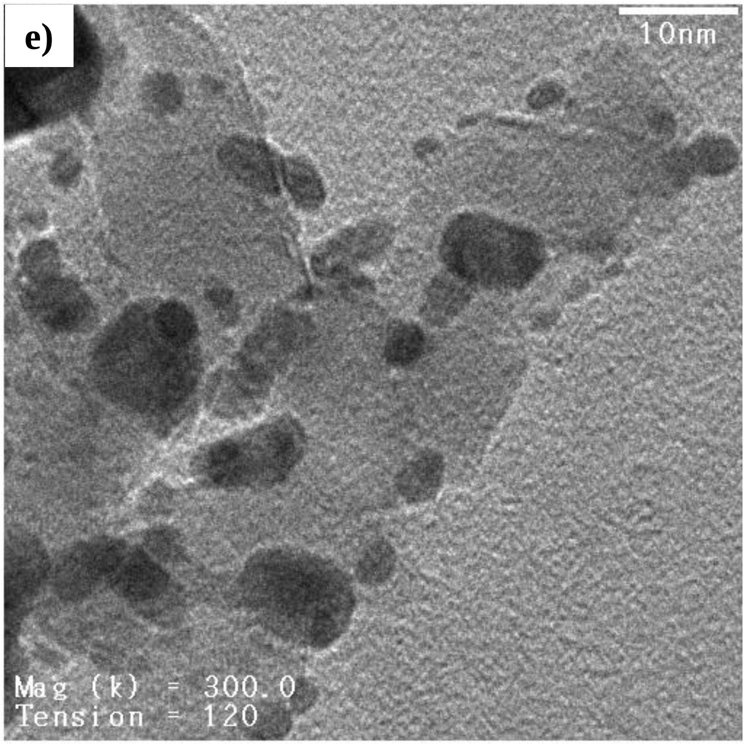

Figure 3−3. Typical TEM micrographs for some supported Ir catalysts applied in this study: (a) 0.50%Ir(0.65)-1/Al_2O_3; (b) 0.54%Ir(0.58)-2/Al_2O_3; (c) 0.54%Ir(0.46)-2/Al_2O_3; (d) 0.54%Ir(0.30)-2/Al_2O_3; (e) 1.92%Ir(0.11)-2/Al_2O_3.

3.3.2. Thermodynamics and kinetics of minor reaction channels in CH conversion

Methylcyclopentane (MCP), a potential intermediate product from ring contraction (RC) of cyclohexane (CH), was observed only in traces (< 0.3% within converted fractions) over all Ir/γ-Al_2O_3 catalysts studied. This is indicative of a negligible contribution of indirect ring opening (RO) following RC catalyzed by acid functions. Do et al. reached the same conclusion that indirect RO makes little contribution to the overall conversion of dimethylcyclohexane on Al_2O_3-, SiO_2-, and TiO_2-supported Ir catalysts [29]. In the present work, a more convincing piece of evidence against the presence of indirect RO stems from the observed distribution of C_6-isomers. If the indirect RO had occurred to form MCP that was rapidly ring-opened, methylpentanes would have been formed in much larger quantities compared to n-hexane, due to the well-known preference of iridium to cleave unsubstituted C–C bonds. In contrast to such a scenario, n-hexane was the dominant C_6-alkane product (> 95% within all C_6-alkanes). Thus, residual chlorine, if it exists at the surface, does not introduce an additional pathway of CH conversion via acid induced catalysis.

The only reactions detected fall into three major categories, namely isomerization, dehydrogenation and hydrogenolysis (Scheme 3-1). Their relative significance depends on the H_2 pressure and temperature applied, as well as on the Ir dispersion. The basic thermodynamic and kinetic characteristics of the first two reaction channels will be described below in brief, while the hydrogenolytic scission of C−C bonds is the focus in the sections to follow.

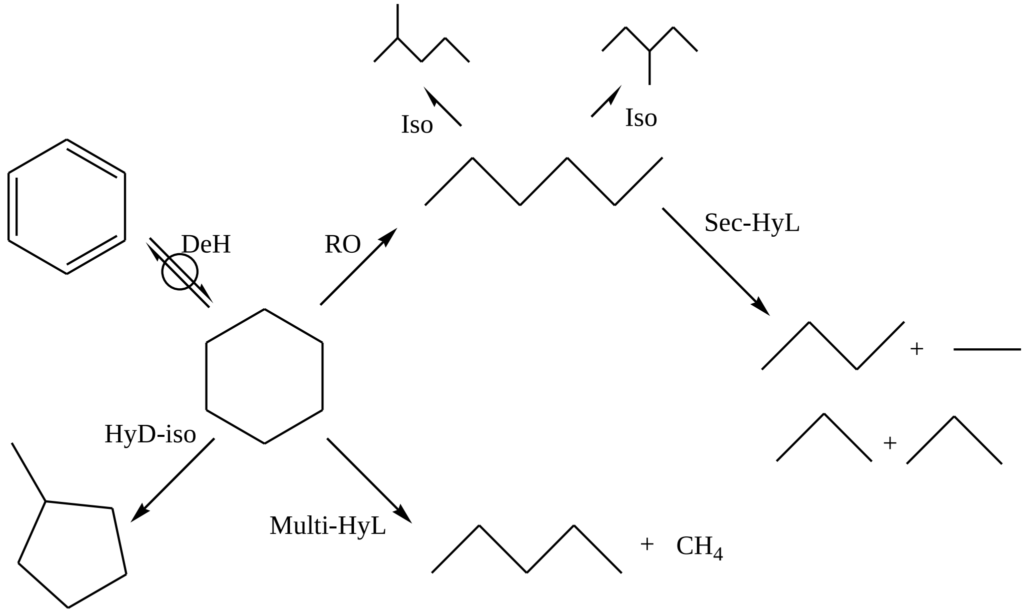

Scheme 3-1. Reaction network of CH conversion over Ir/Al_2O_3 catalysts in presence of high-pressure H_2. Minor modes of multiple scissions in primary and secondary hydrogenolysis are not shown for the sake of brevity. DeH = dehydrogenation, RO = ring opening, Iso = isomerization (metal-catalyzed), HyD-iso: Hydroisomerization (acid-catalyzed), Multi-HyL: multiple hydrogenolysis, Sec–HyL: secondary hydrogenolysis.

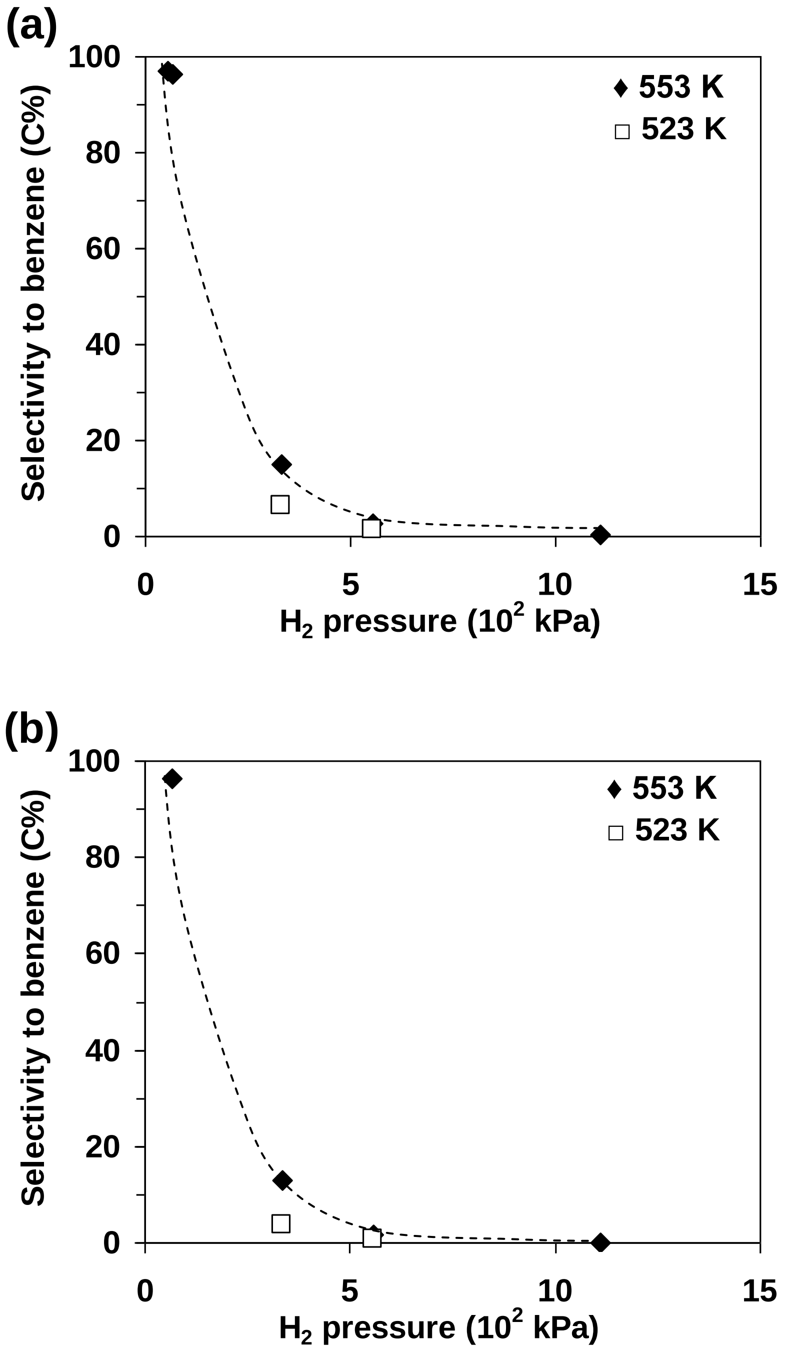

Figure 3-4. Selectivity to benzene as a function of H_2 pressure at 523 (□) and 553 K (♦) over (a) 0.54%Ir(0.46)-2/Al_2O_3 and (b) 0.50%Ir(0.24)-1/Al_2O_3.

3.3.2.1. Dehydrogenation

As expected on the basis of its endothermic nature and the equilibrium-induced inhibition by H_2, dehydrogenation occurred preferably at lower H_2 pressures and higher temperatures (Figure 3-4). For example, over 0.54%Ir(0.46)-2/Al_2O_3, ca. 96% of reacted CH was converted to benzene at 0.07 MPa H_2 and 503−553 K. In contrast, aromatization accounted for 14% selectivity at 0.33 MPa H_2, 553 K and further down to 6% at 523 K. Cyclohexene was barely detected possibly arising from both a too low equilibrium constant (2−4 orders of magnitude lower than that for benzene formation in the studied temperature range) and its fast consecutive conversion once formed. At H_2 pressures above 1.0 MPa, the dehydroaromatization route became negligible at all temperatures studied. Moreover, the gas-phase chemical equilibrium appeared to be established in presence of high pressure (> 1 MPa) H_2, as told by the virtually invariant pressure quotients when the contact time was varied. These pressure quotient values (around 0.3) approximated the equilibrium constant of dehydrogenation calculated from thermo-chemistry data without correction by fugacity coefficients (Figure 3-5).

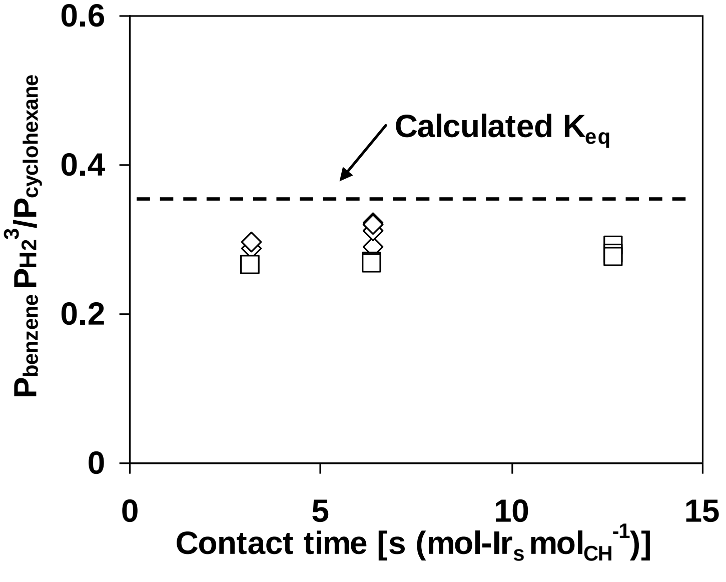

Figure 3-5. Effect of contact time on the approach to equilibrium of CH dehydrogenation shown over 0.54%Ir(0.46)-2/Al_2O_3 (◊) and 0.54%Ir(0.30)-2/Al_2O_3 (□). Reaction conditions were 543 K, 1.1 MPa H_2, 3.1 kPa CH.

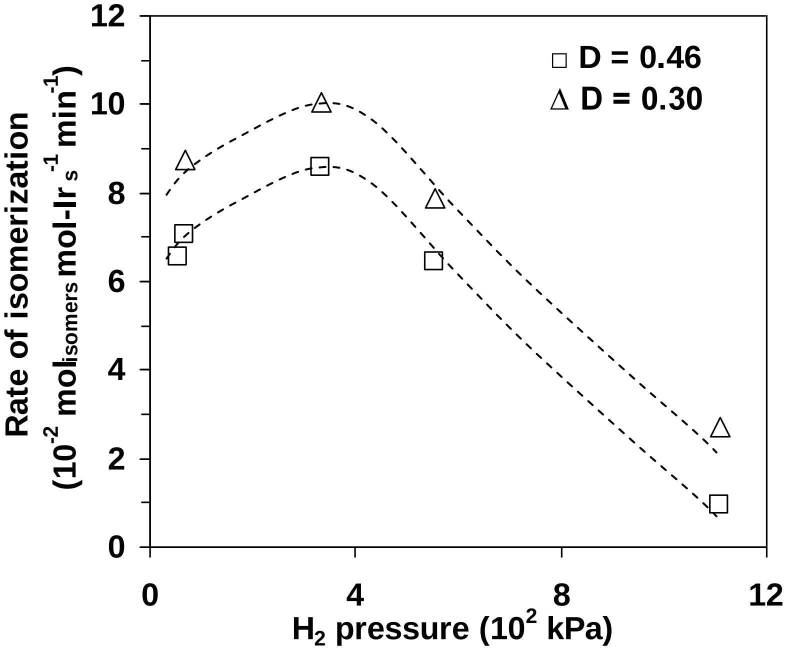

Figure 3-6. Influence of H_2 pressure on the rate of isomerization in CH conversion over 0.54%Ir(0.46)-2/Al_2O_3 and 0.54%Ir(0.30)-2/Al_2O_3 at 553 K and 3.1 kPa CH.

3.3.2.2. Isomerization

At all conditions studied in this work, isomerization of n-hexane always occurs, but is far from equilibrium, as assessed by the approach-to-equilibrium index [37]. The isomerization activity of Ir is much lower than that of Pt [10]; accordingly, the two branched hexane isomers, 2- and 3-methylpentanes, formed in a ratio of ca. 2−3, were found only in low quantities (< 2% within all products) even up to conversion levels around 40%. Isomers of lower alkanes, i.e., isopentane and isobutane, became detectable above 533 K and conversions higher than 20%, but only to a marginal degree. The rates of all isomerization reactions were further suppressed by elevating H_2 pressures (Figure 3-6). Thus, isomerization is only a minor reaction channel on all catalysts at all conditions.

3.3.3. Structure sensitivity of CH hydrogenolysis: rates and selectvities

Cyclohexane turnovers showed very high selectivity (> 95%) to ring opening (RO) and fragmentation as H_2 pressures are elevated sufficiently high to suppress dehydroaromatization and isomerization, as discussed above. The two kinds of hydrogenolytic reactions possess high equilibrium constants (on the order of 10^2 for RO, and of 10^6–10^8 for fragmentation in the studied temperature range, see Table 1-1) and are, therefore, irreversible in light of their overall remoteness from equilibrium at all conditions. n-Hexane was practically the exclusive ROP from CH, whereas lower n-alkanes, arising from multiple C–C bond cleavage and secondary reactions of re-adsorbed n-hexane, existed in different quantities depending on the temperature, H_2 pressure, Ir dispersion, and contact time.

3.3.3.1. General trend of the activity-dispersion relation over Cl-free catalysts

Figure 3-7 displays the mass specific rates and turnover frequencies (TOFs) for hydrogenolysis of CH over Cl-free Ir/Al_2O_3 catalysts as a function of Ir dispersion measured by H_2 chemisorption. We emphasize that special care has been taken of the reproducibility of kinetic and chemisorption experiments and that reaction rates reported hereinafter are extrapolated values at zero contact time which rigorously preclude any contributions from the kinetics of secondary reactions. Moreover, deactivation was suppressed to low extents (< 10%) during data collection.

Interestingly, the turnover rate first declined with decreasing Ir dispersion in a range corresponding to average cluster sizes between 1 and 2 nm, but increased again when further decreasing Ir dispersions at values lower than 25% (Figure 3-7b). Keeping in mind the higher mass-specific rate on 0.50%Ir(0.16)/Al_2O_3 than 0.50%Ir(0.24)/Al_2O_3 (Figure 3-7a), we exclude the reason for the antipathetic branch of TOFs in the low-dispersion range to be related to an inaccurately determined number of surface Ir atoms. In marked contrast with the current monofunctional catalytic system, the TOFs for tetralin hydroconversion (RO plus RC) over Ir/ASA catalysts remained essentially constant in an Ir size range of 1.5 to 7.8 nm, suggesting that metal components in bifunctional catalysts were not involved in the rate-controlling steps [28].

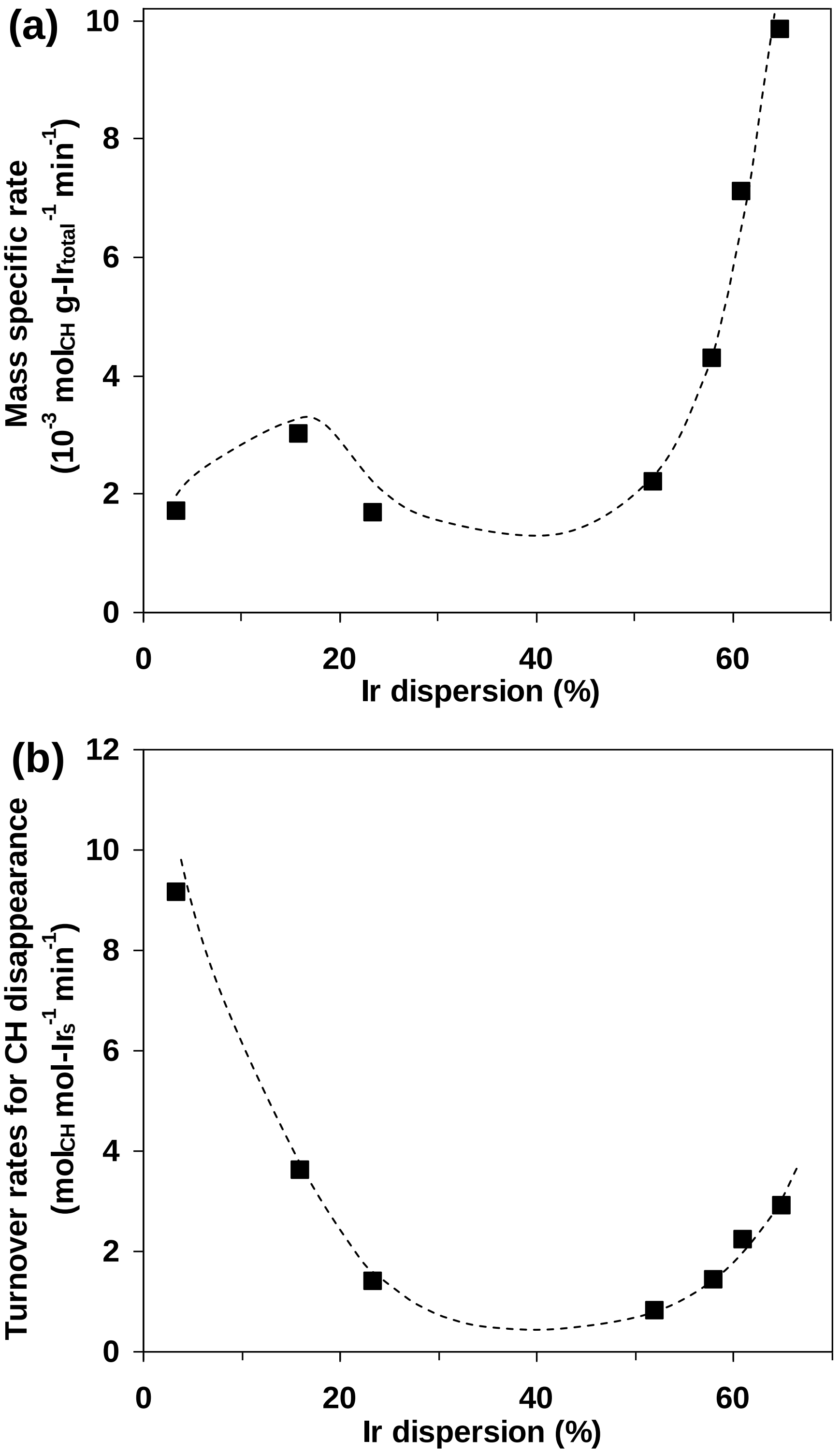

Figure 3-7. Apparent dispersion sensitivities of (a) total-Ir-mass-based rates and (b) surface-exposed-Ir-based rates for cyclohexane (CH) hydrogenolysis at 523 K, 3.1 kPa CH and 0.56 MPa H_2 on 0.50%Ir(*D*)-1/Al_2O_3 catalysts.

3.3.3.2. Effect of precursor and support on the activity-dispersion relation

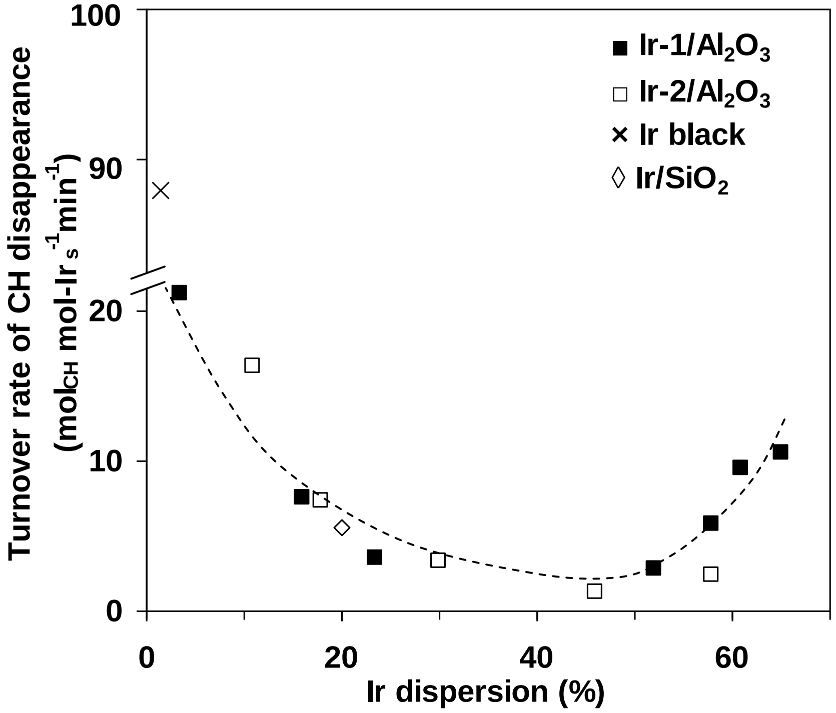

Figure 3-8. Apparent dispersion sensitivity of turnover rates (based on the exposed fraction of Ir atoms) for CH conversion via hydrogenolytic pathways on all studied catalysts at 543 K, 3.1 kPa CH and 0.56 MPa H_2. Catalysts prepared from Cl-free (Ir-1/Al_2O_3) and Cl-containing (Ir-2/Al_2O_3) precursors. Extrapolated reaction rates to zero contact time were used to preclude any kinetic effects of reactant depletion or product inhibition.

Figure 3-8 shows the CH turnover rates at 543 K over all studied Ir catalysts. The nature of the precursor salt, either Cl-free or Cl-containing, was found to evidently affect only the high-dispersion Ir/Al_2O_3 catalysts. For instance, the presence of chlorine in the precursor caused the TOF to be lower by a factor of 2.5, when both catalysts contained small Ir clusters of 0.58 dispersion, whereas the low-dispersion branch (D_{Ir} < 0.30) exhibited comparable TOFs for both types of Ir/Al_2O_3 catalysts. Besides Ir/Al_2O_3, a purchased Ir black (D = 0.01) and a 1.0%Ir/SiO_2 catalyst (D = 0.20) are also plotted in this graph. Qualitatively, the TOFs of all catalysts spread around the two branches with opposite trends, with limited influence of the support identity.

3.3.3.3. Product selectivities: primary and secondary pathways

Space velocities were varied to probe the kinetically primary and secondary nature of different C−C bond cleavage products. The non-zero selectivities for n-hexane and n-pentane/methane, when extrapolated to zero conversion (Figures 3-9 and 3-10), indicate that these two are both kinetic primary products, irrespective of the catalysts used. In contrast, the selectivity trends for the other products, i.e., n-butane, propane and ethane, indicate that they are primarily produced via secondary reactions of re-adsorbed n-hexane. However, their formation via multiple hydrogenolysis of CH before desorbing the primary product n-hexane seems also plausible. Interestingly, the selectivities to n-pentane and methane stayed essentially unaffected with increasing conversions, particularly over catalysts of lower Ir dispersions. This suggests that the secondary reactions of re-adsorbed n-hexane proceed mainly via internal C–C bond cleavages while largely bypassing terminal cleavage pathway. Clearly, the catalysts that contain small and large particles substantially differ between each other in terms of the initial selectivities to n-pentane and methane, pointing to enhanced probabilities of terminal multiple-scission (of intermediately formed n-hexane before it leaves the surface) on larger Ir particles. The increased preference for multiple hydrogenolysis over lower-dispersion catalysts was also manifested in the larger disparity of the initial pentane to methane ratio, e.g., 0.6−0.8.

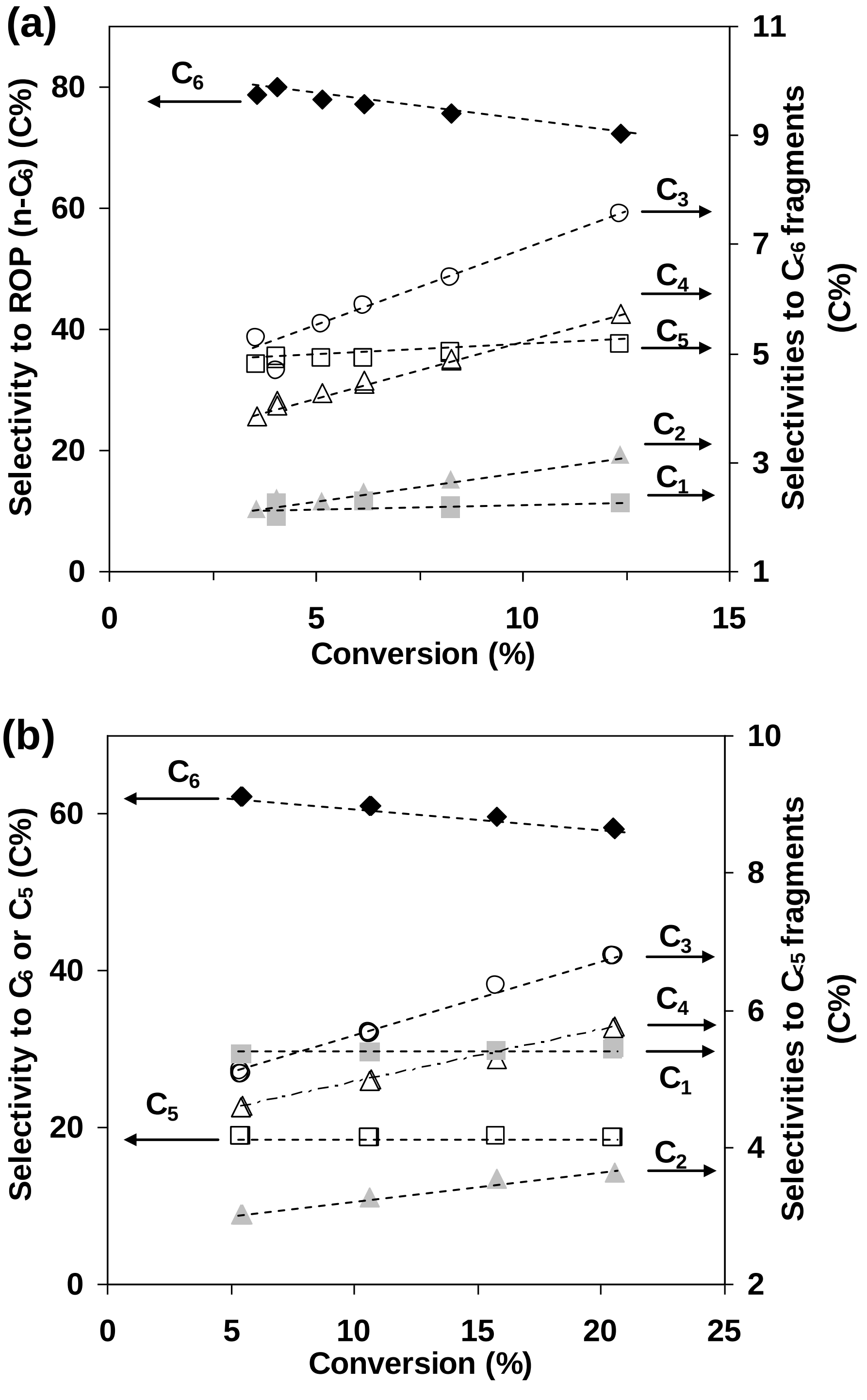

Figure 3-9. Product selectivity as a function of conversion for the hydrogenolysis of CH over (a) 0.54%Ir(0.46)-2/Al$_2$O$_3$ and (b) 0.54%Ir(0.30)-2/Al$_2$O$_3$ at 543 K, 3.1 kPa CH and 0.56 MPa H$_2$. The contact time varied from 2.1 to 6.4 s (mol-Ir$_s$ mol$_{CH}^{-1}$) in (a) and from 1.0 to 4.0 s (mol-Ir$_s$ mol$_{CH}^{-1}$) in (b).

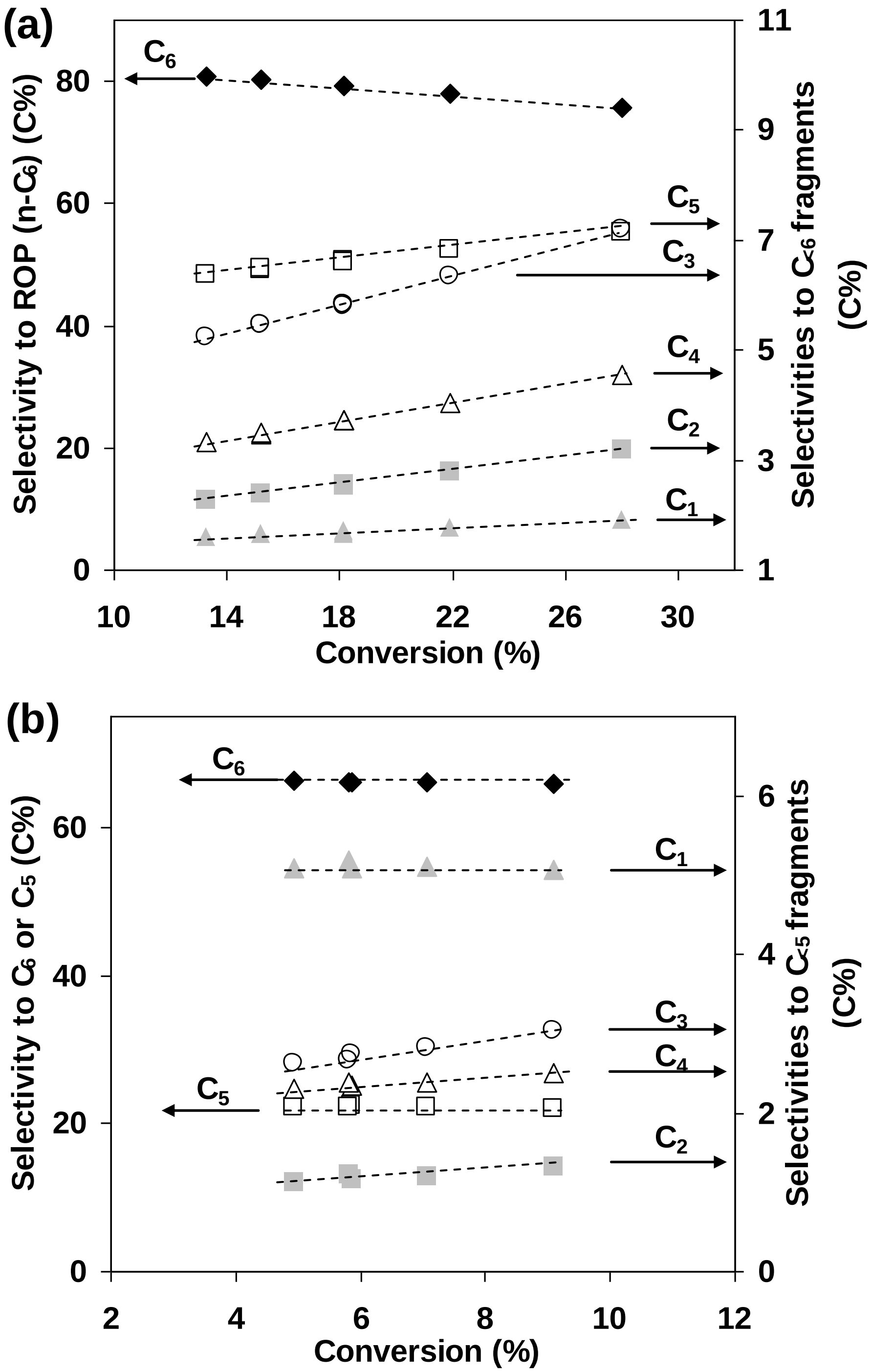

Figure 3-10. Product selectivity as a function of conversion for the hydrogenolysis of CH over (a) 0.50%Ir(0.65)-1/Al_2O_3 and (b) 0.50%Ir(0.16)-1/Al_2O_3 at 523 K, 3.1 kPa CH and 0.56 MPa H_2. The contact time varied from 3.2 to 7.5 s (mol-Ir_s mol_{CH}^{-1}) in (a) and from 0.9 to 1.9 s (mol-Ir_s mol_{CH}^{-1}) in (b).

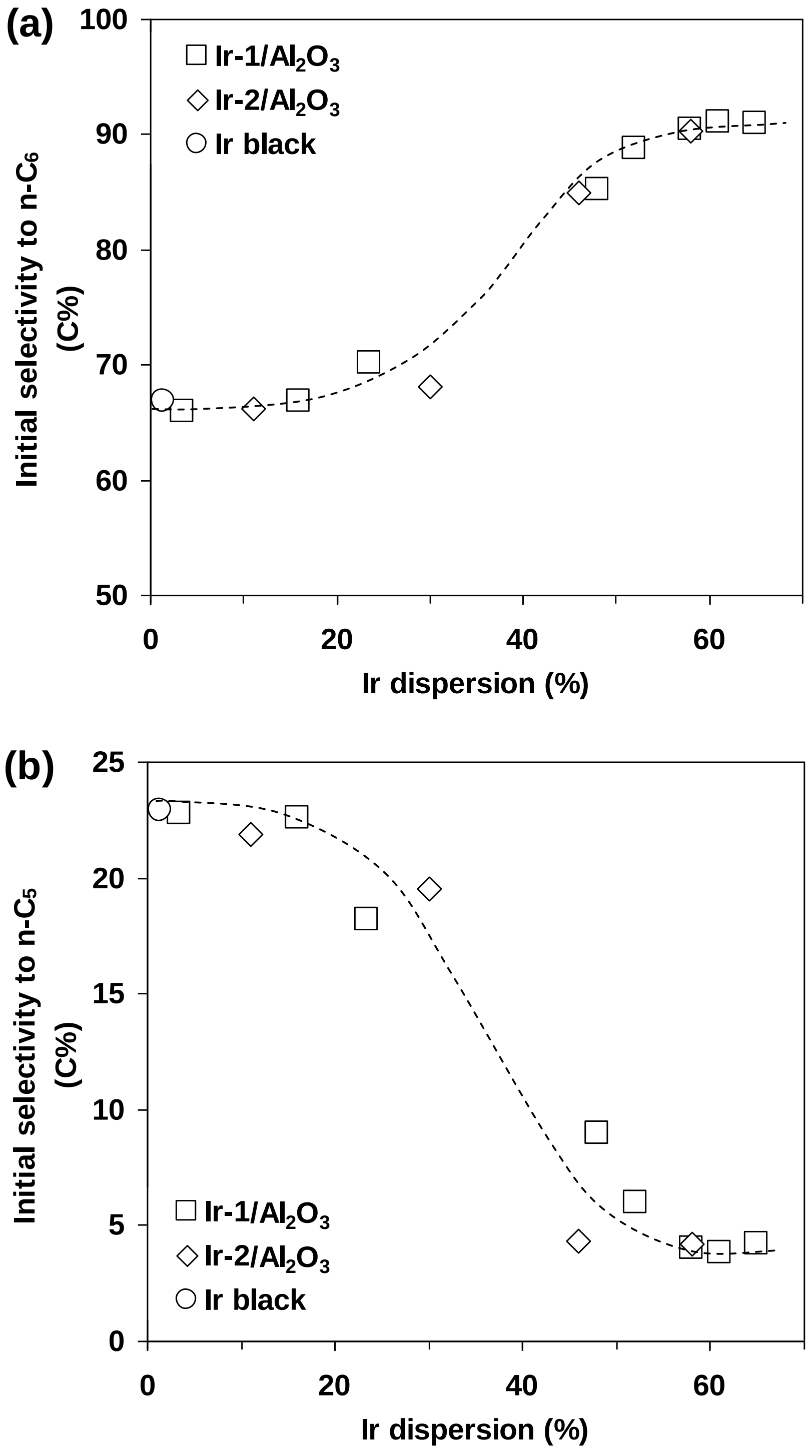

Figure 3-11. Initial selectivities to (a) n-hexane and (b) n-pentane in CH hydrogenolysis as a function of Ir dispersion at 523 K, 3.1 kPa CH and 0.56 MPa H_2 over Ir/Al_2O_3 catalysts prepared from Cl-free (□) and Cl-containing (◊) precursors and over a commercial Ir black (○).

The initial selectivity to n-hexane increased with increasing dispersion, as shown in Figure 3-11a. The selectivity shown on an iridium black (D = 0.01) was the same as that on supported Ir clusters with the largest average size (D = 0.04). By contrast, the initial selectivities to smaller alkanes, most prominently for n-pentane that is formed via a terminal cleavage of the ring-opened intermediates before desorption, decreased with increasing Ir dispersion (Figure 3-11b). For both n-hexane and n-pentane, two plateaus were observed towards the low and high ends of the studied dispersion range. These plateaus suggest the selectivity limits at given reaction conditions over terrace planes and low-coordination atomic arrangement, which have to be the prevalent surface structures on large and small particles, respectively. Initial selectivities to ethane, propane and n-butane that are formed via internal multiple cleavages remained low (ca. 4−6%), and also decreased slightly with increasing dispersion. Strictly speaking, the presence of chlorine induced some deviation from Cl-free counterparts with similar dispersions, which can be more clearly seen from Figure 3-11 at high dispersions. The qualitative trends, however, appeared comparable between the two types of Ir/Al_2O_3 catalysts. As we discuss in detail later, the competition between single and multiple scissions, as well as between terminal and internal scissions, is closely linked to the predominant surface structures on Ir clusters of various average sizes.

3.3.4. H_2-pressure dependences of rates, reaction orders and selectivities over Ir clusters of different sizes

Figure 3-12 depicts the significant impact of Ir dispersion on the conversion rates as a function of H_2 pressure. The H_2 pressure at which the maximum rates were observed, as well as the steepness of rate decline after the optimum pressure, differ significantly between smaller (D > 0.50) and larger particles (D < 0.25). For small clusters with broadly differing activities, the maximum TOF seemed to always appear at H_2 pressures between 0.2−0.3 MPa (Figure 3-12a). The steepness of rate decline after this maximum was quantified by comparison of TOFs at different H_2 pressures (see Table 3-2). The activity ratios among different catalysts that contain small clusters remain essentially identical at any given H_2 pressure, indicating the same curvature of H_2 pressure dependences of TOFs for all of these small clusters, regardless of their relative magnitude of activity and the level of catalyst chlorine concentration (up to several hundred ppm). For large particles (Figure 3-12b), the H_2 pressure for maximum TOFs shifted to higher values (0.3−0.6 MPa). Moreover, the curvatures of TOF-H_2 pressure functions flatten compared to those exhibited by small clusters. In a power rate law expression, the flattened curvature translates to reaction orders in H_2 typically smaller in magnitude on large Ir particles than on small ones. In addition, the increase in H_2 pressure is accompanied by an increase in the reaction order with respect to CH partial pressure (Figure 3-13), suggesting a decrease in the coverage of the CH-derived reactive species by increasing the chemical potential of H_2. It appears that small clusters sense this H_2-pressure effect on coverage more strongly than the large clusters. Note that a reaction order of unity in CH seems hardly accessible unless much higher H_2 pressures and/or lower temperatures are applied.

Table 3-2. Steepness of decline after maximum TOF for CH hydrogenolysis as a function of H_2 pressure over small Ir clusters (D = 0.52−0.65) at 523 K, 3.1 kPa CH.

Ir dispersion	Normalized TOF at $P_{H_2} = p$ MPa[a]			
	$p = 3.33$	$p = 4.44$	$p = 5.56$	$p = 8.33$
0.65	3.3	3.4	3.6	−
0.61	2.8	−	2.8	2.7
0.58	1.8	−	1.8	−
0.52	1.0	1.0	1.0	1.0
0.58[b]	1.1	−	1.2	1.2

[a] Normalized to the TOF over 0.50%Ir(0.52)-1/Al_2O_3 at each given P_{H_2}.

[b] 0.54%Ir(0.58)-2/Al_2O_3.

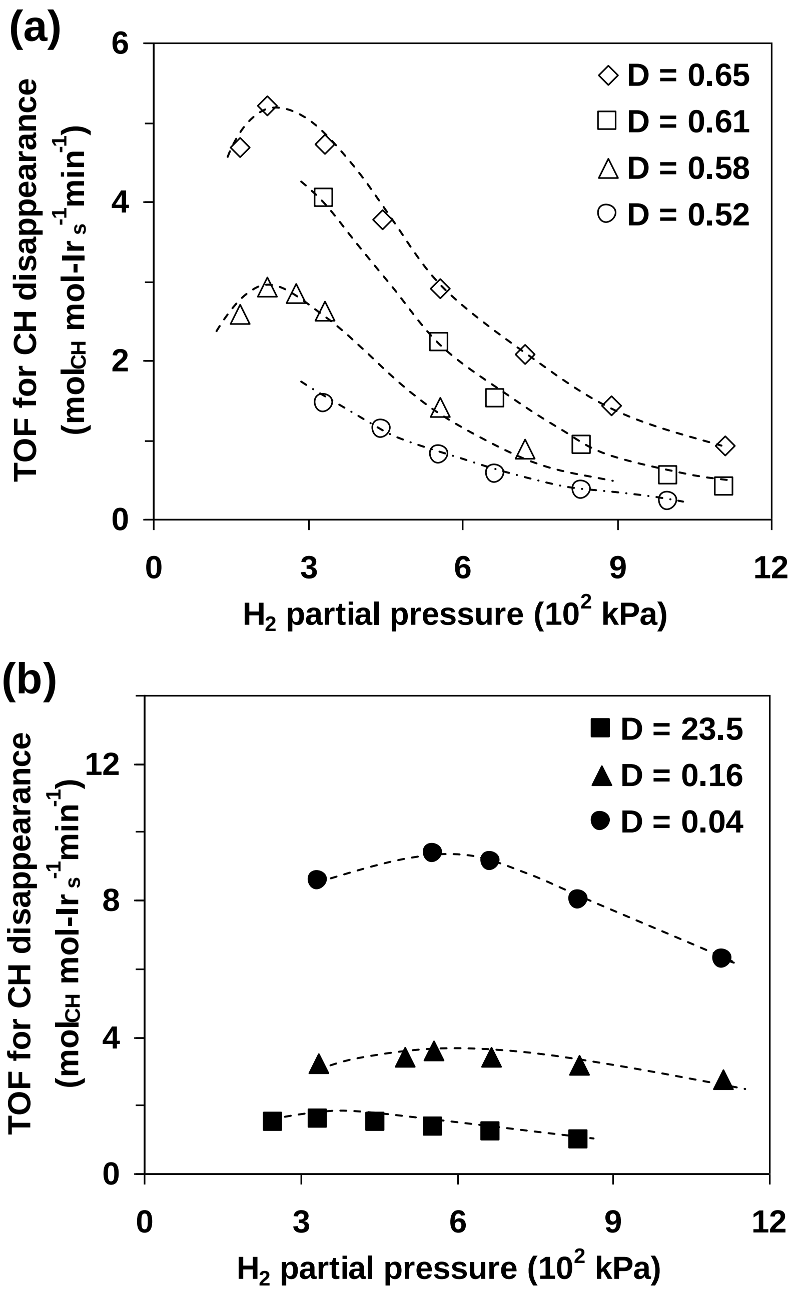

Figure 3-12. Turnover rate dependences on H_2 pressure over 0.50%Ir(*D*)-1/Al_2O_3 catalysts with fractional dispersions of (a) 0.52−0.65 and (b) 0.035−0.235 at 523 K, 3.1 kPa CH.

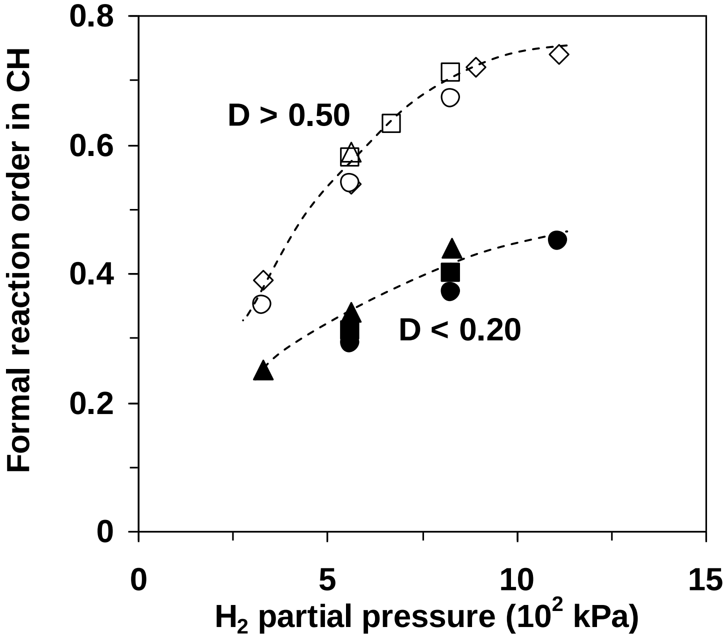

Figure 3-13. Formal reaction order in CH as a function of H_2 pressure on small (open symbols) and large (closed symbols) Ir particles at 523 K and 1.9−4.5 kPa CH.

Analyzing formation rates of different products separately in relation to the cluster size and the H_2 pressure reveals marked differences (Figure 3-14). Before discussing these, we would like to reiterate that the rates reported here reflect only those of kinetically primary cleavage pathways and do not comprise contributions of C−C bond cleavage rates of the primary products.

Over small Ir clusters, the formation rate of the single-scission product, i.e., n-hexane, exhibits a higher optimum H_2 pressure than the maxima of all other products (Figure 3-14a). In contrast, the H_2 pressure dependence of n-pentane (and also methane) formation parallels that of n-hexane over large particles, both showing much higher optimal H_2 pressures than the other fragments (C_2−C_4) formed via internal multiple scissions (Figure 3-14b).

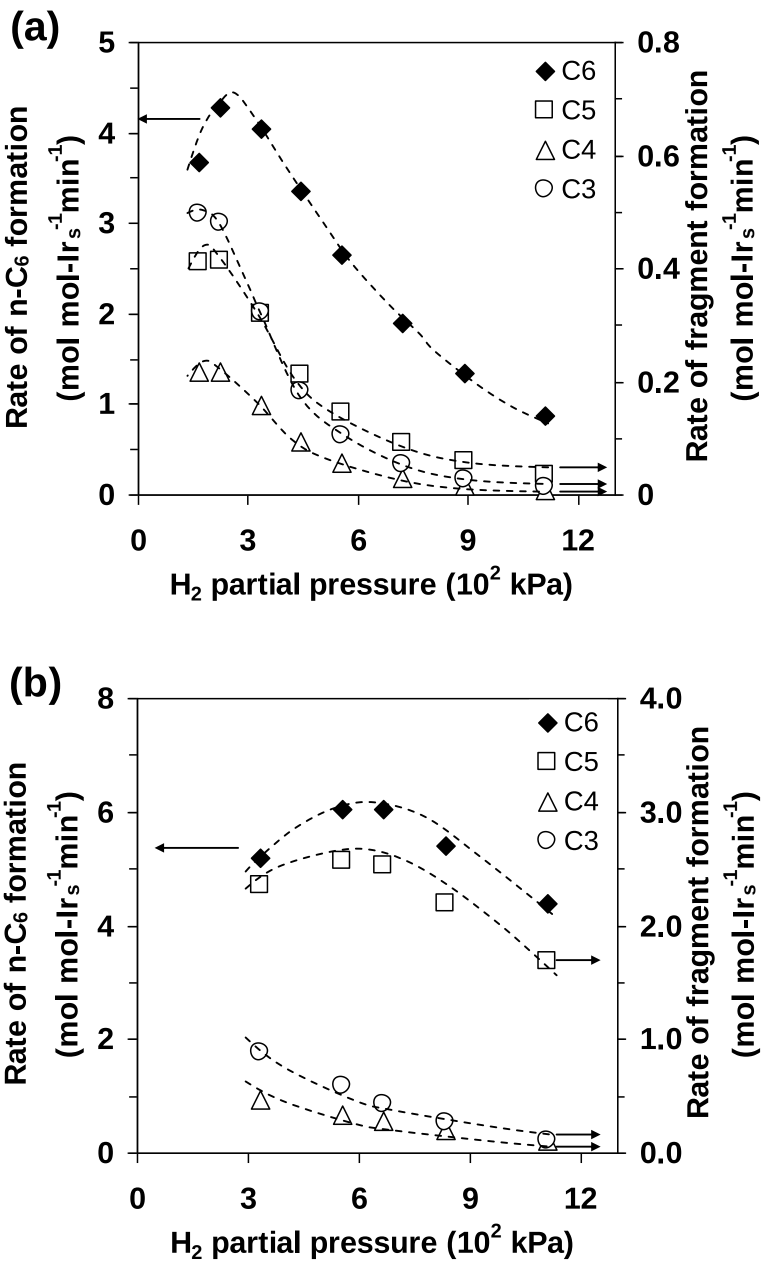

Figure 3-14. Rate dependences on H_2 pressure of the ROPs, n-hexane (♦) and fragments, n-pentane (□), n-butane (Δ) and n-propane (○) over Cl-free Ir/Al_2O_3 catalysts with Ir dispersion of (a) 0.65 and (b) 0.035, respectively. Reaction conditions were 523 K, 3.1 kPa CH. Rates were reported as values obtained after extrapolation to zero contact time. Formation rates of CH_4 and C_2H_6, revealing similar trends as their pairing products (C_5H_{12} and C_4H_{10}, respectively) with changes in H_2 pressure, are omitted for the sake of clarity.

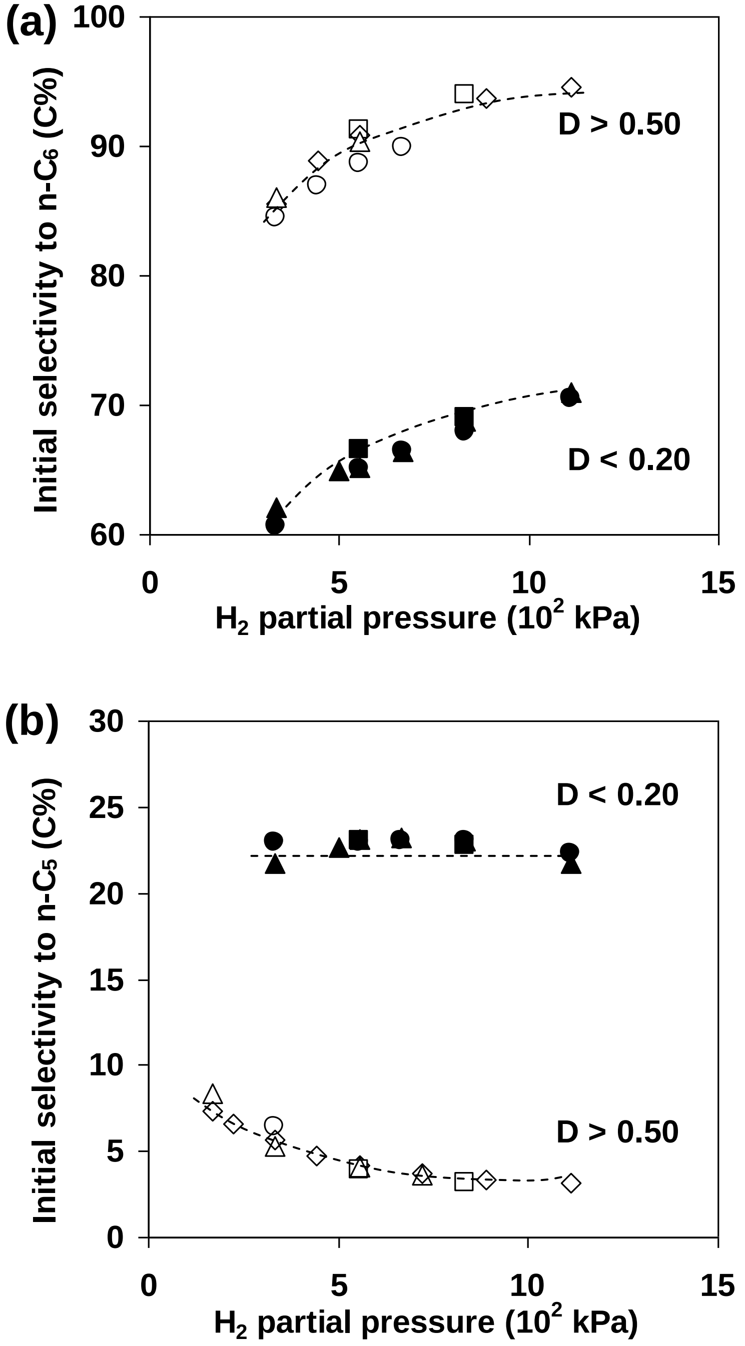
(a)
Initial selectivity to n-C6 (C%)
100
90
80
70
60
0
5
10
15
H2 partial pressure (10^2 kPa)
D > 0.50
D < 0.20
(b)
Initial selectivity to n-C5 (C%)
30
25
20
15
10
5
0
0
5
10
15
H2 partial pressure (10^2 kPa)
D < 0.20
D > 0.50

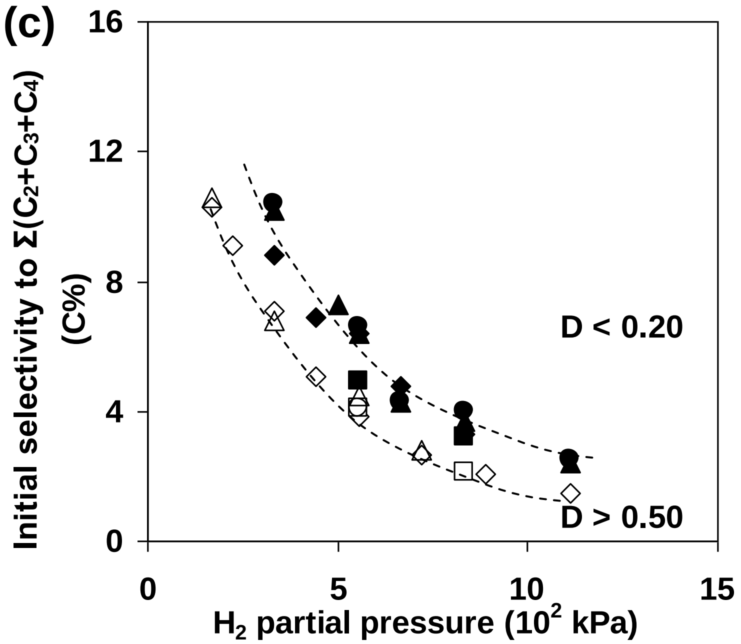

Figure 3-15. Initial selectivities to (a) n-hexane, (b) n-pentane and (c) lumped C_2-C_4 products as a function of H_2 pressure over small (D = 0.52−0.65) and large Ir particles (D = 0.014−0.16) at 523 K, 3.1 kPa CH.

The less pronounced dependence of the rate on the H_2 pressure function for n-hexane than for smaller alkanes leads in consequence to its enhanced selectivity at higher H_2 pressure on both small and large particles (Figure 3-15). The selectivity gap greater than 20% between small and large particles (already exemplified in Figure 3-11 at 0.56 MPa H_2) persists at all H_2 pressures studied, mainly due to the enhanced terminal multiple hydrogenolysis on larger particles and the slightly divergent trends over small and large clusters in response to the H_2 pressure increase (Figure 3-15). We note, however, that the selectivities to internal multiple cleavages consistently decrease with increasing H_2 pressure, hardly dependent on the cluster size (Figure 3-15c).

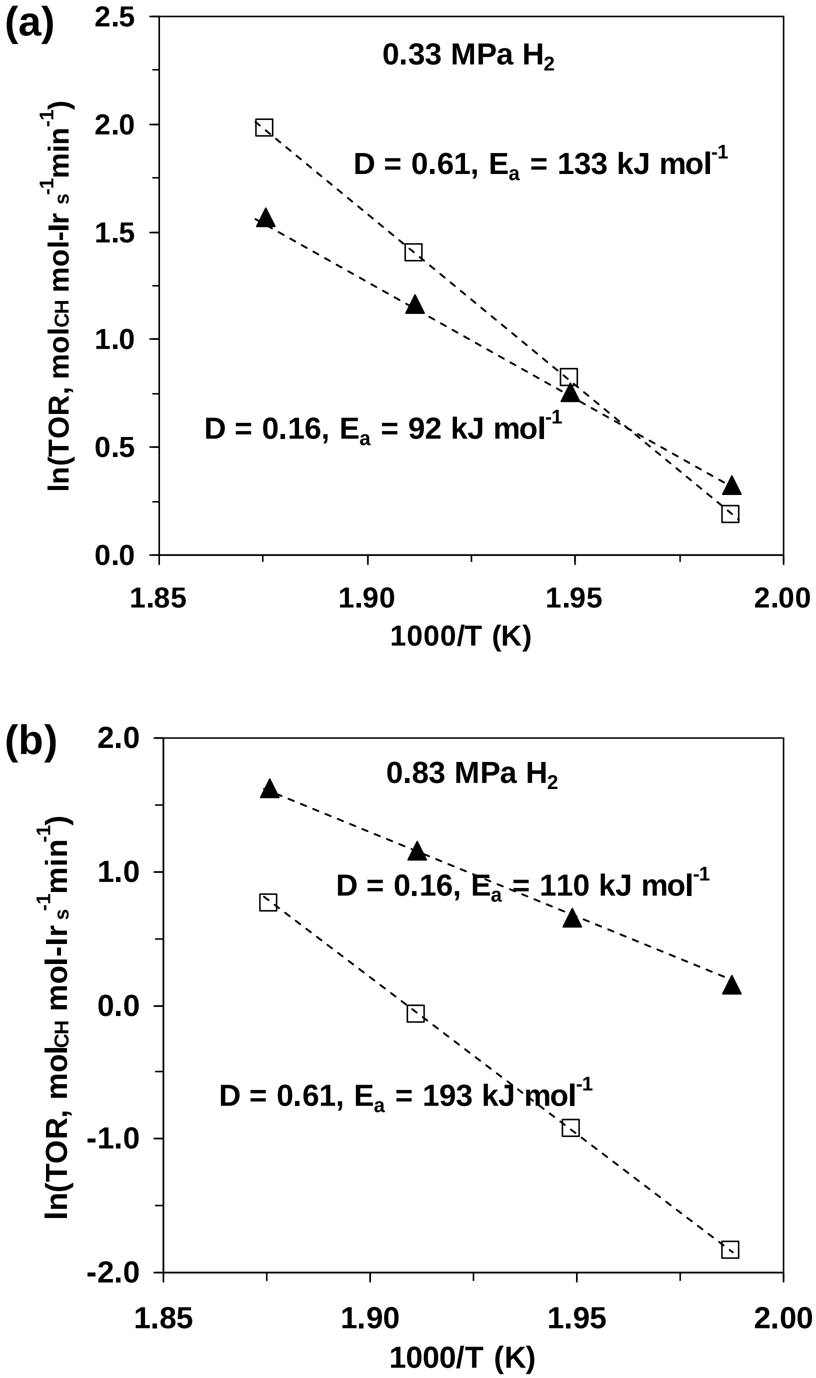

Figure 3-16. Arrhenius plots of turnover rates for CH hydrogenolysis over typical small (□) and large (▲) particles at 3.1 kPa CH and H_2 pressures of (a) 0.33 MPa H_2 and (b) 0.83 MPa H_2.

3.3.5. Temperature dependences of rates and selectivities over Ir clusters of different sizes

The Arrhenius plots of TOFs for CH hydrogenolysis over typical small and large particles are depicted in Figure 3-16 at two widely differing H_2 pressures. Clearly, the large clusters exhibit remarkably lower apparent energies of activation than those on small clusters. Moreover, the H_2 pressure increases apparent energies of activation, most significantly for small clusters. The temperature effect on the reaction order in CH was not for every catalyst measured, but the CH reaction order generally decreased with increasing temperature (not shown).

Table 3-3 summarizes the main kinetic parameters for separate product formation routes at varying H_2 pressures over small and large Ir particles. Note that almost only kinetically primary pathways are concerned at these low conversions. The apparent activation energy decreases with the cluster size for each cleavage mode at the same reaction conditions, but increases on the same cluster size with increasing H_2 pressure and in the order of $n\text{-}C_6 < n\text{-}C_5 < n\text{-}C_4 < C_3$. To be more specific, the apparent activation energies for the ring opening to n-hexane are typically 20−30 kJ mol^{-1} lower than for those for hydrogenolysis at the terminal C−C bond of n-hexane (surface intermediate from CH ring opening). Hydrogenolysis of the internal C−C bonds of n-hexane (surface intermediate from CH ring opening) has even higher activation energies than n-hexane and n-pentane formation. As a result, n-hexane selectivity decreases with increasing reaction temperature (Figure 3-17). The slope of the n-hexane selectivity with the temperature shows that the selectivity losses are independent of the cluster size, e.g., a decrease of ca. 9% from 513 to 543 K. Also shown in Table 3-3, the typically larger activation energies for multiple hydrogenolysis on all clusters and for all rates on small clusters are compensated by the greater pre-exponential factors in the respective case. Such compensation phenomena are common for the hydrogenolysis of alkanes [38]. Noticeably, apparent pre-exponential factors closely resemble each other on sufficiently large Ir particles (e.g., 10^7−10^8 s^{-1} for ring opening at 0.56 MPa H_2 on catalysts of $D = 0.035$−0.30).

Table 3-3. Kinetic parameters over Ir/Al_2O_3 catalysts with varying dispersions.

Catalysts	P_{H_2} (bar)	$E_{a,app}$ (kJ mol^{-1})[a]				A_{app} (s^{-1})[b]			
		C_6	C_5	C_4	C_3	C_6	C_5	C_4	C_3
0.50%Ir(0.65)-1	3.3	121	147	175	187	8.2×10^{10}	2.6×10^{12}	8×10^{14}	3×10^{16}
	5.6	154	174	216	218	1.1×10^{14}	5.8×10^{14}	4×10^{18}	1×10^{19}
	11.1	179	199	–[c]	–[c]	1.1×10^{16}	4.3×10^{16}	–[c]	–[c]
0.50%Ir(0.52)-1	5.6	146	170	208	210	4.6×10^{12}	9.3×10^{13}	2×10^{17}	5×10^{17}
0.54%Ir(0.46)-2	3.3	116	145	155	158	2.9×10^{9}	1.6×10^{11}	2×10^{12}	5×10^{12}
	5.6	138	168	197	208	2.8×10^{11}	1.7×10^{13}	1×10^{16}	1×10^{17}
	11.1	158	180	–[c]	–[c]	8.3×10^{12}	7.0×10^{13}	–[c]	–[c]
0.54%Ir(0.30)-2	5.6	95	98	160	170	4.3×10^{7}	3.0×10^{7}	8×10^{12}	1×10^{14}
	11.1	102	118	176	210	1.8×10^{8}	2.5×10^{9}	1×10^{14}	2×10^{17}
0.50%Ir(0.16)-1	5.6	87	105	157	163	1.9×10^{7}	5.0×10^{8}	3×10^{12}	6×10^{12}
	8.3	95	117	167	200	1.1×10^{8}	7.1×10^{9}	5×10^{13}	1×10^{17}
0.50%Ir(0.035)-1	5.6	85	106	152	154	3.1×10^{7}	1.6×10^{9}	8×10^{12}	2×10^{13}
	8.3	94	116	169	185	2.2×10^{8}	1.4×10^{10}	2×10^{14}	1×10^{16}

[a] Reaction conditions were 3.1 kPa CH and 513−553 K; these reported values, with maximum error of ± 5 kJ mol^{-1} for butanes and propane and ± 3 kJ mol^{-1} for hexanes and pentanes, were derived by taking the slopes from semilogarithmic Arrhenius plots of formation rates of different products as a function of reciprocal temperature.

[b] The pre-exponential factors were derived from the r (TOF) = $A_{app} \times \exp(-E_{a,app}/RT)$. The errors depend on the accuracy of values for activation energies. Therefore, the relative standard deviation is ± 30−60% for n-hexane and n-pentane and ± 300−500% for n-butane and propane.

[c] These values are overestimated due to the inaccuracy of the low extrapolated initial rates at lower temperatures.

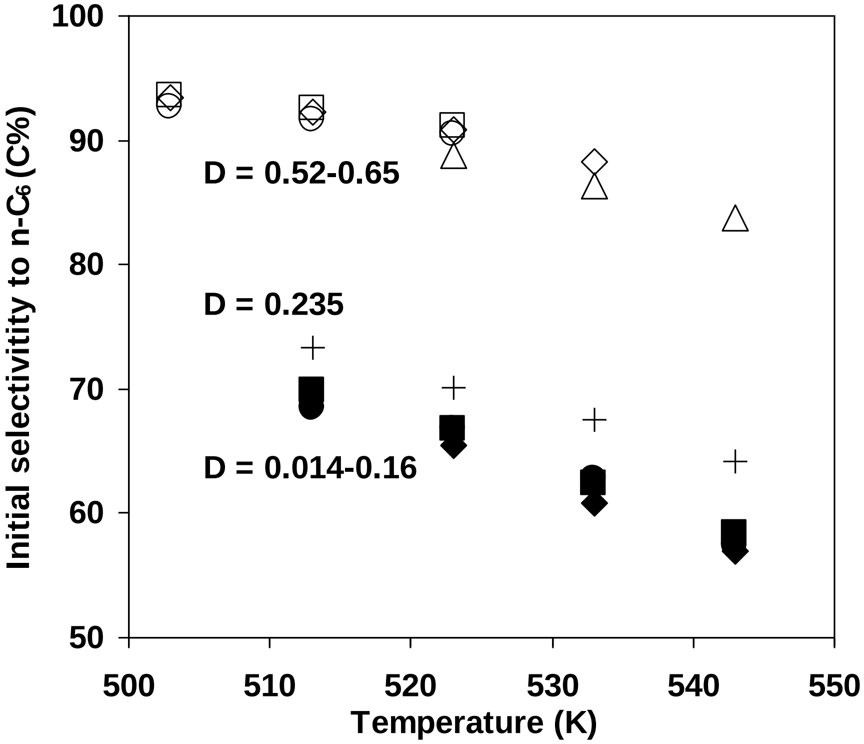

Figure 3-17. Effect of reaction temperature on the initial selectivity to n-hexane over small (open symbols), medium (cross) and large (filled symbols) Ir clusters at 3.1 kPa CH, 0.56 MPa H_2.

3.4. Discussion

Hydrogenolytic C−C bond cleavage of cyclohexane over supported Ir catalysts leads to n-hexane as the sole mechanistically primary product. Some n-hexane molecules formed in this process undergo further hydrogenolysis before vacating the surface. As a result, a fraction of the smaller alkanes formed from these non-desorbed n-hexane molecules are discerned as apparent primary products in light of their non-zero selectivities at zero contact time (Figures 3-9 and -10). The majority of n-hexane, however, desorbs (leading to the measured initial selectivity to n-hexane at zero contact time) and a fraction (depending on the contact time) of the desorbed hexane molecules re-adsorbs and is hydrogenolytically cleaved.

3.4.1. Cleavage patterns of cyclohexane in primary and secondary pathways

The initial selectivity, i.e., the selectivity at zero contact time, to products from multiple C–C bond hydrogenolysis decreased with increasing H_2 pressure, and with decreasing temperature and decreasing cluster size (Figures 3-11, -15 and -17). In line with literature [39], single C−C bond scission is favored at higher hydrogen coverages. Conceptually, it is straightforward to accept that as the concentration of available surface hydrogen decreases, more and more molecules are able to undergo multiple C−C bond scissions. Desorption slows down at lower vicinal H* concentrations, to an extent greater than that for C–C bond cleavage rates. Once the desorption rate slows down to a level commensurate with that of C–C bond rupture, the ring-opened intermediate state (different from the adsorbed state of re-adsorbed n-hexane, as discussed later) would have increased chances of experiencing further hydrogenolysis before desorption. As the H_2 pressure and temperature determine the surface coverage of H* involved in C–C bond cleavage and product desorption steps, they indirectly determine also the concentration of vacancies for the sorption and C−H bond activation of the cycloalkane. Thus, reaction variables that deplete the adsorbed hydrogen should increase the selectivities to multiple C–C bond cleavage.

As the influence of the external parameters on the surface concentration of hydrogen appears to be obvious, let us analyze whether or not the size of Ir particles also affects its concentration. The binding energy of H* is higher on surface defects such as step edges [40]. Thus, it is inferred that the steady-state H* coverage is lower on large Ir crystallites than on small ones [10]. This in turn suggests that the observed lower selectivity to hydrogenolysis of the intermediately formed n-hexane on small Ir particles is partly related to higher H* concentrations, in keeping with the suggestions by Paál and coworkers [39]. Alternatively, a rationale might be found in the increased probability of finding neighboring sites on terrace planes over large particles to accommodate reactive states (and prolong their surface lifetime) for multiple scissions (see next).

Next, let us discuss the finding that primary and secondary pathways show different preferences to terminal and internal cleavage modes. Based on the observed changes of product selectivities with contact time (Figures 3-9 and -10), we infer that the active species derived from cyclohexane first undergoes a single-scission leading to an n-hexane adsorbed species. This intermediate, before desorption, has a certain probability of undergoing further cleavage of a terminal C−C bond, as well as a lower probability of hydrogenolysis at internal C_{II}–C_{II} (bi-secondary) bonds. This low selectivity to hydrogenolysis of internal C−C bonds is likely related to the interaction of the $C^{1,6}$-atoms in the proposed structure of the intermediate with the surface atoms (see Scheme 3-2). Both interacting carbon atoms would likely assume a sorbate configuration (most probably the bonding at a three-fold hollow site in a quite rigid sp^3 configuration) that makes access of inner carbon atoms ($C^{2,3,4,5}$) to neighboring metal atoms highly improbable. For achieving cleavage of the terminal C−C bond, only one of these carbon atoms (i.e., C^1, C^6) needs to become more mobile via partial detachment from the surface (Scheme 3-2), while both metal-C bonds need to become flexible to cleave an inner C−C bond. It was also observed that the apparent activation energies were significantly larger for products from internal C−C bond scissions and increased progressively with increasing H_2 pressures (Table 3-3). This reflects the lower coverages of reactive species for multiple C−C bond scissions at internal positions and the greater suppression effects of H_2 pressure on their coverages. It will be further shown in later sections that the factors that govern the selectivities of these C–C bond scissions are the degree of coordinative unsaturation of exposed Ir atoms and the fundamental thermodynamics (e.g., C–H bond strengths) that in turn determine the dehydrogenation depths of reactive species relevant to different cleavage routes.

On large Ir particles, the probability of terminal C–C bond cleavage in kinetically primary pathways is remarkably higher than that for hydrogenolysis of internal C−C bonds (Figures 3-9b and -10b), whereas the difference is much smaller on small particles (Figure 3-9a and -10a). This might point to the fact that on small particles the sp^3 configuration of the ring-opened intermediate is less favored (lower concentration of three-fold hollow sites) than the more flexible bonding in two-fold and in on-top configurations. As discussed above, the favorable adsorbed state after the first C–C bond scission enabling further hydrogenolysis is one in which a higher flexibility of the metal–carbon bond is assumed. Alternatively, this difference can be tentatively attributed to the higher concentration of more reactive undercoordinated surface Ir atoms (corners, edges) on smaller Ir particles which discriminate less between the difficulties to cleave the first C−H bond than the sites with higher coordination on the surface of larger particles.

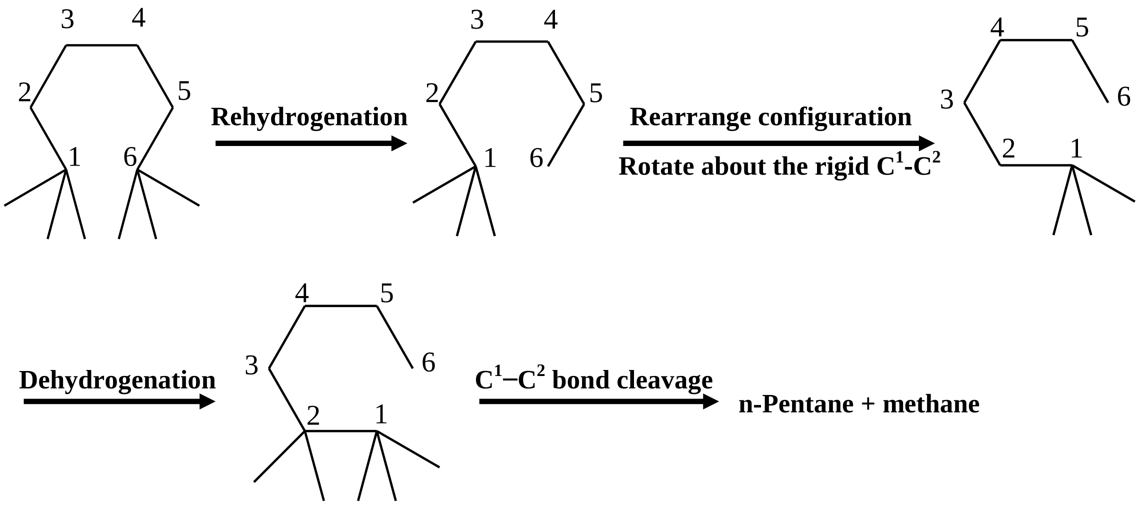

Scheme 3-2. Terminal C−C bond cleavage prevails in chemisorbed n-hexane intermediate formed from cyclohexane ring opening on flat surfaces (C^1−C^2 bond cleavage as an example). Carbon atoms at 2−5 positions cannot access the surface effectively. Surface metal atoms are not shown.

In stark contrast to kinetically primary reactions (analyzed by selectivities at zero contact time), less than 15 mol% of secondary C–C bond scission reactions (analyzed by changing contact times) yield n-pentane/methane on small Ir clusters, and only ca. 1−2 mol% on large particles (Figures 3-9 and -10). As the kinetically secondary reactions largely bypassed the cleavage of a terminal C−C bond, the associated adsorbed states of the mechanistically primary product (n-hexane) directly reacting further and those formed upon its re-adsorption must be radically different from each other. This suggests that upon re-adsorption on the metal, the collision and activation of the C−H bond (which is progressively easier for the carbon atoms at inner positions) in the n-hexane molecule on the surface becomes more important in affecting the C−C bond cleavage reactivities through the coverage term. Also, adsorption via the internal C–C bonds seems to be the preferred adsorption geometry of hexane molecules over Ir surface under the high H_2 pressures used in this study (most studies in the literature were performed at H_2 pressures lower than 100 kPa).

Overall, the results demonstrate the preference of Ir surfaces for hydrogenolysis of internal C−C bonds [4]. We have not considered the differences in electron transfer directions with internal and terminal adsorption as previously put forward by Clarke and Rooney [41], since these factors are regarded to be more subtle and require an explicit understanding of changes in the electronic structure with varying Ir cluster sizes.

3.4.2. Implications of H_2 pressure effects on product formation rates and apparent activation energies in cyclohexane hydrogenolysis

Although the surface concentration of hydrogen plays a crucial role for hydrogenolysis (metals with high surface concentrations of hydrogen such as Pt or Pd tend not to be good hydrogenolysis catalysts [4,42]), a detailed mechanistic analysis under conditions relevant to industrial applications, i.e., higher pressures, has been lacking. In the present work, the presence of H_2 exerts a remarkable impact on activity, selectivity and activation barriers (Figures 3-12 to 3-15 and Table 3-3). The reaction rate passes through a maximum, the position of which with respect to H_2 pressure depends on the Ir dispersion (Figure 3-12), the reaction temperature, as well as the hydrocarbon pressure (Figure 3-14). The decrease in Ir dispersion, especially from very high ($D > 0.50$) to low values ($D < 0.20$), shifts the optimal H_2 pressure to higher values for product formation and leads to less pronounced variations for primary ring opening (n-hexane) and for the subsequent hydrogenolysis (n-pentane) on large (average size > 5 nm) Ir clusters. This is radically different from the steep decline after the rate maxima on small (1−2 nm) Ir clusters. At first glance, the decline can be due to competition in reactant adsorption. Hence, it appears that small Ir clusters respond to the H* coverage variations more than large particles, possibly reflecting that both hydrocarbon-derived reactive species and H* strongly compete for the low-coordination sites.

Alternatively, we would like to speculate that the relative percentage of reactive intermediates, i.e., the concentrations of the H-deficient reaction intermediates and the concentration of vicinal H*, may cause the maximum in a relation between the H_2 pressure and the formation rate. Conceptually, it is conceivable that surface species that are more extensively dehydrogenated require more empty sites to accommodate their dissociated hydrogen atoms. Hence, an increase of H* coverage will decrease the population of such deeply dehydrogenated species. Therefore, we conclude (for a more rigorous discussion, refer to Sections 3.4.4 and 3.4.5), that the lower pressure dependence and the higher optimum H_2 pressures on large particles (Figures 3-12b and -14b) mainly point to the less H-deficient nature of the most abundant reactive intermediates (MARIs) than on small clusters.

Additionally, it is important to consider that the dehydrogenation depth also depends on the nature of the hydrocarbon and the position of the C–C bond (terminal or internal) in the reactant or in the ring-opened intermediate, i.e., the weaker the strength of C–H bonds, the greater the ease of H-abstraction and the stronger the suppression by H_2 of pathways that require more unsaturated active species. Along this line, the lower values of optimum H_2 pressure at maximum rates for internal multiple cleavages (Figure 3-14) can be understood by greater dehydrogenation depths as a result of the slightly weaker secondary C−H bonds (13 kJ mol^{-1} lower than primary C−H bonds in bond dissociation energy) [43]. We develop this discussion in more detail in Section 3.4.6.

Let us discuss next the effect of H_2 pressure on the measured energies of activation, $E_{a,app}$. The functional relation between $E_{a,app}$ and reactant pressures was first derived by Temkin [44] and expressed as follows:

$$E_{a,app} = E_{a,int} + \Sigma n_i \Delta H_i \qquad \text{(Eq. 1)}$$

where n_i is the reaction order in the reactant i. The enthalpy change for H_2 chemisorption is negative, and the reaction order in H_2 is also negative after the optimum H_2 pressure. The activation (adsorption plus dehydrogenation) of cyclic hydrocarbons prior to C–C bond scission is endothermic (weaker C–M bonds than C–H bonds) when dissociated hydrogen atoms recombine and desorb as gas phase H_2 (i.e., no net effect from M−H bond strength), and the reaction order in hydrocarbon is fractional and tends to approach unity with increasing H_2 pressures.

It follows from Equation 1 that over much of the H_2 pressure range $E_{a,app}$ would be greater than $E_{a,int}$. For catalysts of higher dispersions ($D \geq 0.46$), the reaction order in H_2 goes more negative at higher H_2 pressures, while the reaction order in cyclic hydrocarbon stays always positive and increases with H_2 pressures, both factors weighing on the increase of apparent activation energies (Table 3-3). Taking advantage of the Temkin relation (Eq. 1), the slightly changed $E_{a,app}$ with increasing H_2 pressure for hydrogenolysis of CH over large Ir particles (D < 0.20), is qualitatively attributed to the lower sensitivity of the H_2 reaction order in the studied pressure range (Figures 3-12 and -14). The markedly lower apparent activation barriers for primary C–C bond cleavage over the large Ir particles are attributed to the much smaller reaction orders in H_2 (-0.8~0.3) and in CH (0.2~0.5) compared to those (-2.5~-0.8 and 0.4~0.7, respectively) shown by high-dispersion catalysts. These variations in reaction orders reflect a lower coverage of hydrogen adatoms and a higher coverage of CH-derived intermediates on the surface of large particles than on small clusters. The intrinsic activation barrier for CH hydrogenolysis on large particles was estimated to be 85 ± 10 kJ mol^{-1}, by applying Eq. 1 at conditions where reaction orders in H_2 and CH are both close to zero (e.g., at 523 K, 3.1 kPa CH, 0.5−0.6 MPa H_2). Despite that the precision of the Temkin equation may be questioned in fractional-reaction-order cases, the estimation was attempted also for results on small clusters, which led to $E_{a,int}$ values typically larger than 100 kJ mol^{-1}. In comparison, kinetic modeling of rates at different temperatures (not shown) suggested that the intrinsic activation energy is about 100 ± 10 kJ mol^{-1}, i.e., rather similar to the value for the large particles.

3.4.3. Mechanistic considerations based on a classical microscopic model for alkane hydrogenolysis

Before discussing a plausible nature of active sites and catalytically relevant species that give rise to the observed structure sensitivities and H_2-pressure dependent kinetics for endocyclic C−C bond cleavages, we would like to first outline some mechanistic considerations.

It is well accepted that the (non-activated) dissociative chemisorption of dihydrogen, as well as the chemisorption of all alkanes involved, proceeds much faster than the C–C cleavage and, therefore, both remain quasi-equilibrated in the time scale of hydrogenolysis turnovers [4,45−50]. In accordance with this, adsorption-limited kinetics failed to satisfactorily predict the experimental observations in our preliminary modeling attempts. The question remains, if the two reactants compete for the same adsorption sites. For the current work we propose that H* and alkanes (as well as reactive intermediates) compete for the sites active in hydrogenolysis [4], a hypothesis seen valid in MCP and ethane hydrogenolysis over Pt and Ru catalysts, respectively [17,45].

A generalized catalytic sequence, containing quasi-equilibrated steps of H_2 and hydrocarbon activation, an irreversible C–C bond rupture rate-determining step (RDS), and kinetically insignificant re-hydrogenation and desorption steps, is shown in Scheme 3-3, and the derivation of the rate equation for this mechanistic sequence is shown in the Appendix. It is implied in the kinetic treatment that the most abundant surface intermediates are directly involved in the primary reaction pathways. In a rigorous sense, the molecularity of the RDS has remained elusive in hydrogenolysis reactions. Engstrom et al. suggested that the activated C−C bond spontaneously breaks without involving other species or empty sites [11]. Zhuang and Frennet found that better fits in kinetic modeling of a rate expression were obtained when assuming a gas-phase (weakly adsorbed) H_2 molecule is required in the RDS [17]. Shang and Kenney considered no less than ten rate equations and concluded that the involvement of an empty site in the RDS offered the best option for modeling their results on ethane hydrogenolysis over Ru/SiO_2 [45]. For the moment, let us be concerned with a more reasonable model for alkane hydrogenolysis as suggested by Bond [4] and considered by some others [17,45,48], with a few modifications of the original site balance equation (Appendix). This model assumes a surface H* acting as the splitting agent in the rate-controlling C−C bond cleavage. Here, we consider that the H*-assisted RDS may be favored over the non-assisted C−C bond cleavage, which can be understood by kinetic coupling of C−H bond formation in the transition state with the C−C bond cleavage that brings down the activation barrier.

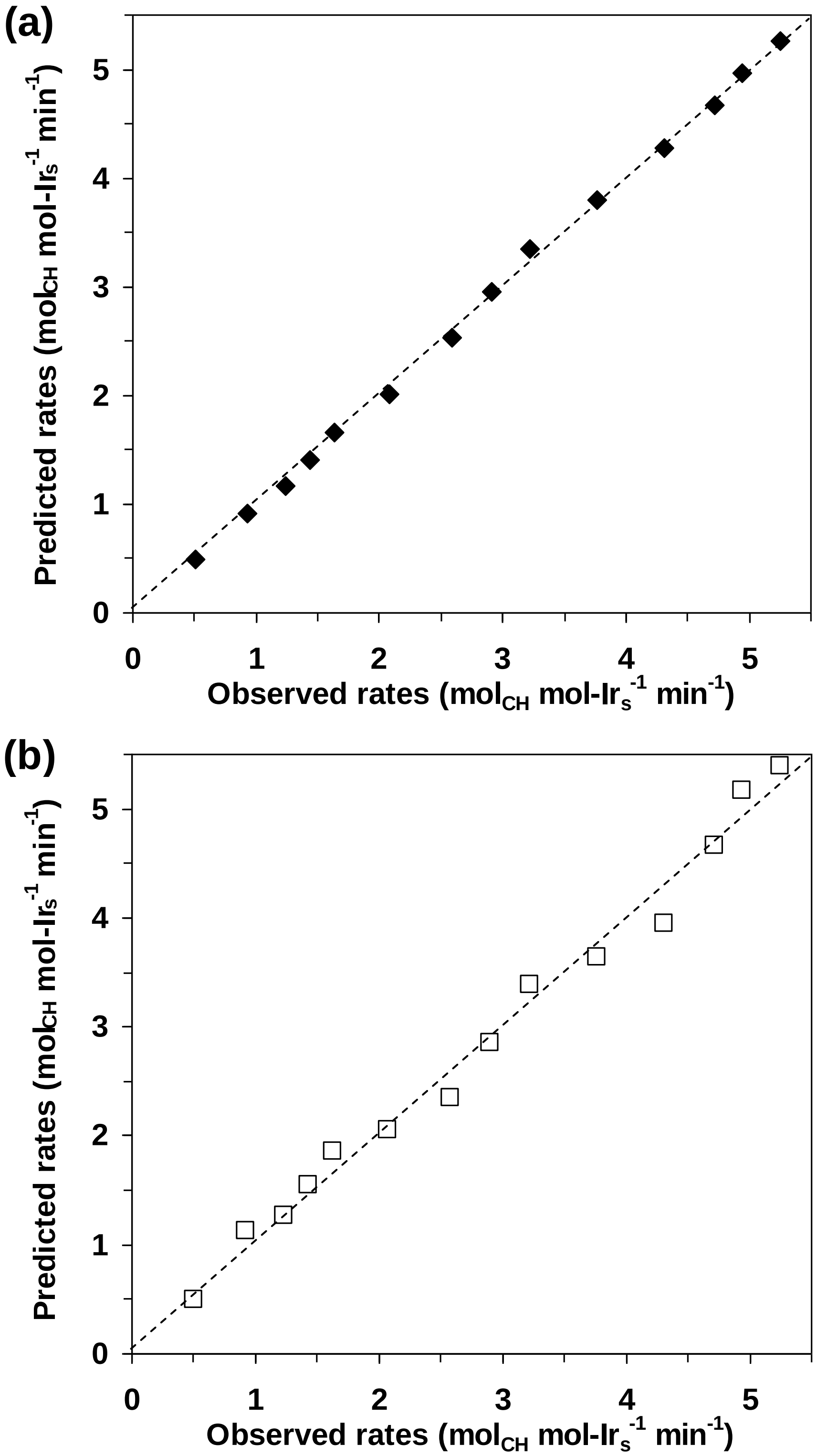
(a)
Predicted rates (mol$_{CH}$ mol-Ir$_s^{-1}$ min^{-1})
0
1
2
3
4
5
Observed rates (mol$_{CH}$ mol-Ir$_s^{-1}$ min^{-1})
0
1
2
3
4
5
(b)
Predicted rates (mol$_{CH}$ mol-Ir$_s^{-1}$ min^{-1})
0
1
2
3
4
5
Observed rates (mol$_{CH}$ mol-Ir$_s^{-1}$ min^{-1})
0
1
2
3
4
5

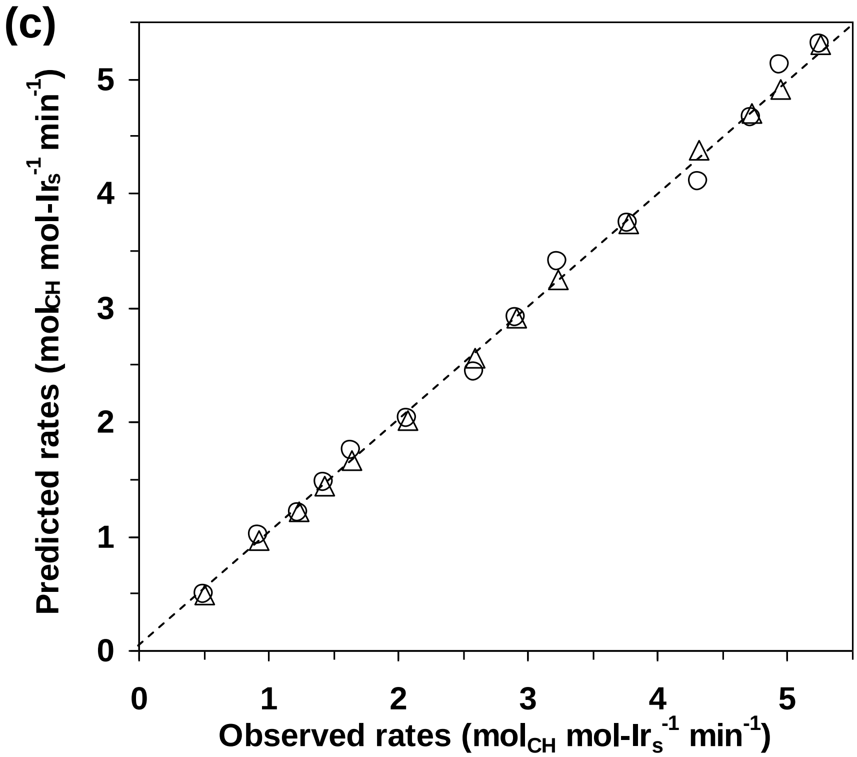

Figure 3-18. Parity plots for the predicted and measured CH hydrogenolysis rates over 0.50%Ir(0.65)-1/Al_2O_3 at 523 K (0.15−1.5 MPa H_2, 2.0−5.0 kPa CH) for different assumptions of the splitting agent in the rate-determining step. The splitting agent is an adsorbed hydrogen in (a), while being gas-phase H_2 (□) in (b) and being empty site (Δ) or gas-phase H_2 + empty site (○) in (c). See the Appendix for the predicted dependences of rate on CH pressure.

The parity plot in Figure 3-18a exemplifies that the H*-assisted RDS hypothesis accurately describes the measured activities of CH hydrogenolysis on Ir/Al_2O_3 catalysts over a 10-fold range in turnover rates ($R^2 > 0.99$). In comparison, the assumption that gas-phase H_2 acts as the splitting agent gives an inferior quality of fitting ($R^2 = 0.97$, Figure 3-18b). Moreover, assuming either a vacancy or a gas-phase H_2 molecule with a vacancy to be involved in the C−C bond cleavage provides as excellent correlation coefficients as the H*-assisted one ($R^2 > 0.99$, Figure 3-18c). We are aware that the mechanistic soundness of all assumptions is to be subjected to the scrutiny of further experimental studies (e.g., evaluation of isotope effects, which will discussed in a separate contribution) as well as theoretical assessments. Note, however, that most of the other competing proposals lack precision in predicting the reaction order of CH compared to the ‘H*-assisted C−C bond cleavage’ model (Figure 3-19), and that the ‘vacancy-involved” RDS assumption results in much lower values of the H_2 adsorption constant (1.6×10^{-5} kPa^{-1}) and the estimated coverage of H* (0.04−0.11) than the ‘H*-assisted’ RDS assumption.

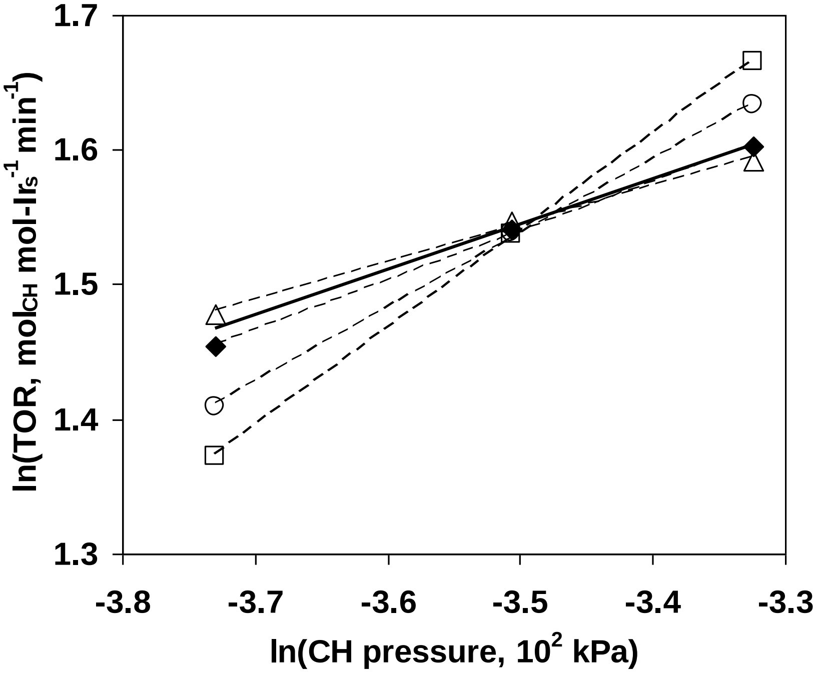

Figure 3-19. Predicted dependences (dashed lines) of turnover rate on CH pressure with different assumptions of the splitting agent involved in the C−C bond cleavage: (♦) adsorbed hydrogen; (Δ) vacancy; (○) gas-phase H_2 + vacancy; (□) gas-phase H_2. The continuous line is drawn with the measured data.

(i) H_2 chemisorption:

$$H_2\ (g) + 2^{*} \rightleftarrows 2H^{*} \qquad K_H = \frac{\theta_H{}^2}{P_{H2}\theta_v{}^2}$$

(where θ_V, θ_H are the vacancy coverage and H*-coverage, respectively)

(ii) Hydrocarbon activation (lumped with recombination of H^* into gas phase H_2):

$$c\text{-}C_6H_{12}\ (g) + n^{*} \rightleftarrows (c\text{-}C_6H_{12\text{-}2x})_n{}^{\#} + xH_2\ (g) \qquad K_{cyc} = \frac{\theta_{cyc}P_{H2}{}^{x}}{P_{cyc}\theta_v{}^{n}}$$

(where θ_{cyc}, *n* and *x* are the coverage by the most abundant CH-derived surface intermediates, the number of free surface atoms and the depth of dehydrogenation)

(iii) C–C bond cleavage (rate determining)

$$(c\text{-}C_6H_{12\text{-}2x})_n{}^{\#} + \text{‘}\mathbf{S}\text{’} \longrightarrow (C_6H_{12\text{-}2x})_n{}^{\#} \qquad R_{rds} = k_{rds}\,\theta_{cyc}\,['s']$$

(where *x* is the depth of dehydrogenation and ‘**S**’ can be an empty site (*), an adsorbed hydrogen (H^*), molecular H_2, a combination of H_2 + *, or even non-existent for non-assisted C–C bond scission; ‘S’ was taken as H^* in the present study; any potential release of sites previously covered by ‘S’ is not shown in the product side)

(iv) Rehydrogenation and desorption (kinetically irrelevant steps, not necessarily quasi-equilibrated, can be reversible or irreversible)

$$(C_6H_{12\text{-}2x})_n{}^{\#} + (2x+2)H^{*} \rightleftarrows C_6H_{14}\ (g) + (2x + 2 + n)^{*}$$

Scheme 3-3. Sequence of steps (not elementary for quasi-equilibrated steps) proposed for cyclohexane hydrogenolysis on Ir/Al_2O_3 catalysts.

3.4.4. Structure sensitivity of cyclohexane hydrogenolysis: the sympathetic branch

The TOF of structure-sensitive reactions [37] may vary in two opposite ways: it may decrease when the dispersion increases, which is defined as antipathetic structure sensitivity. If the TOF increases with increasing dispersion, it is then termed as sympathetic structure sensitivity [51]. Despite that some of the observed more complex structure sensitivities prove to arise from unintended artifacts, there certainly exist cases where the TOF passes through a maximum [51]. The contribution of Del Angel et al. showing that the TOF for MCP hydrogenolysis had a minimum with varying Rh dispersion at 493 K and atmospheric pressure [52] is the only case we have found in the literature in which the TOF of a reaction passed through a minimum as a function of metal dispersion. To the best of our knowledge, there has been no open literature on the structure sensitivity of CH hydrogenolysis over supported Ir catalysts or model Ir surfaces. In this and the next sections, we separately address the possible mechanistic and structural origins for the sympathetic and antipathetic branches of TOF variation with Ir dispersion in CH hydrogenolysis (Figures 3-7 and -8).

Table 3-4 presents the four parameters derived from non-linear regression analysis of measured CH hydrogenolysis rates at 523 K on Ir/Al_2O_3 catalysts containing small clusters. The thermodynamic properties that govern the equilibrium concentration and distribution of surface species do not vary to a substantial degree on different catalysts containing predominantly 1−2 nm Ir clusters, as is also seen by the similar estimated coverages. Indeed, as expected from their closely-resembled curvatures (Table 3-2) and the nearly equivalent H_2 pressure values at rate maxima (Figure 3-12a), the differing activities of these small clusters should primarily stem from the different scaling properties, i.e., intrinsic rate constants of the RDS. More remarkably, the number of cleaved C–H bonds before C–C bond scission is predicted to be nearly four ($x \approx 2$ (H_2 molecules)) on small clusters of $D > 0.50$, which corresponds exactly to the widely proposed C_2-unit mode, or the so-called dicarbene structure, over Ir [1,10,29,53].

Table 3-4. Fitting parameters for CH hydrogenolysis at 523 K on 0.50%Ir(*D*)/Al_2O_3 catalysts with D_{Ir} = 0.52−0.65 for the mechanistic model proposed in Scheme 3. The number of *n* is 2, and the splitting agent is a hydrogen adatom in this case, which corresponds to the rate equation:

$$r = \frac{k_{rds} K_H^{0.5} P_H^{0.5+2x} [\sqrt{(K_H^{0.5} P_H^{0.5} + 1)^2 + \frac{4K_{cyc}P_{cyc}}{P_H^{x}}} - K_H^{0.5} P_H^{0.5} - 1]^3}{8K_{cyc}^2 P_{cyc}^2}$$

Fitting parameters	D_{Ir} = 0.52	D_{Ir} = 0.61	D_{Ir} = 0.65
k_{rds} (s^{-1})	0.7	2.0	2.5
K_H (10^{-4} kPa^{-1})	7.8	7.2	6.0
K_{cyc} (10^4 kPa)[a]	2.2	1.8	2.0
x	2.1	2.0	2.0
Estimated coverages[b]			
θ_v[c]	0.47−0.55	0.50−0.56	0.47−0.56
θ_H[c]	0.24−0.46	0.25−0.46	0.15−0.41
θ_{cyc}[c,d]	1.2×10^{-2}−0.14	1.2×10^{-2}−0.12	1.9×10^{-2}−0.20

[a] The units are only valid at strictly $x = 2$.

[b] CH partial pressure: 2.4−3.6 kPa, H_2 partial pressure 0.33−1.1 MPa.

[c] θ_v: surface coverage of empty site; θ_H: surface coverage by H*; θ_{cyc}: surface coverage by cyclic reactive intermediates. The site balance equation is $\theta_v + 2\theta_{cyc} + \theta_H = 1$ because it is assumed that adsorption of cyclic hydrocarbon occupies two surface atoms.

[d] The lower boundary of estimated coverage which corresponds to high H_2-pressure conditions (> 0.4 MPa) may have been underestimated as evidenced from the worse fitting (overestimation relative to experimentally determined values) of the reaction order in CH under these conditions.

Now that the observed structure sensitivity has been deprived of slight coverage effects, it becomes valid to base the interpretation of the sympathetic branch simply on the decrease of the RDS rate constant with increasing cluster size. The decrease in the RDS rate constant can have different microscopic origins, geometric, electronic or both. Since hydrocarbon hydrogenolysis is often cited to require multi-atom sites, the ensemble size requirement for the C_2-unit mode must have been met on clusters of D = 0.5−0.7. Otherwise, it would have been rendered impossible to have the TOF increase as dispersion increases. It is also implied that there would be a maximum to be observed as the Ir dispersion tends further towards unity. At the present stage, we consider that the population of low-coordination atoms is most consequential to catalysis owing to their greater coordinative unsaturation. As first quantified by van Hardeveld and Hartog [54], the population of low-coordination atoms among all types of surface atoms decreases sharply in this narrow range (1−2 nm).

Table 3-5. Estimated population of four types of surface atoms in a cuboctahedral model for four cluster sizes (i.e. shell number: 3, 4, 5 and 6, respectively)[a].

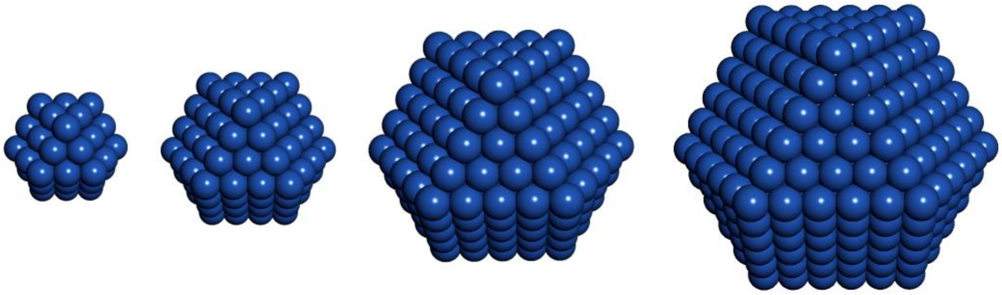

Type	CN	Fraction of surface atoms			
		Ir_{55} (D = 0.76)[b]	Ir_{147} (D = 0.63)[b]	Ir_{309} (D = 0.52)[b]	Ir_{561} (D = 0.45)[b]
Corner	5	0.286	0.130	0.074	0.048
Edge	7	0.571	0.521	0.444	0.381
(100)	8	0.143	0.261	0.333	0.381
(111)	9	0	0.087	0.148	0.190

[a] Numerical formulae: N_s (number of surface atoms) = $10m^2 - 20m + 12$; N_{corner} (number of corner atoms) = 12; N_{edge} (number of edge atoms) = 24(m-2); $N_{(100)}$ (number of (100) terrace atoms) = $6(m-2)^2$; $N_{(111)}$ (number of (111) terrace atoms) = $4(m-3)(m-2)$.

[b] D (dispersion) = N_s/N_t.

Table 3-5 shows a quantitative estimation of the population of different types of surface atoms in closed-shell cuboctahedral Ir clusters. For example, with a slight increase of cluster size from 1.6 to 2.2 nm, the percentage of corner atoms could reduce almost by a factor of 3. This magnitude is similar to the difference in rate constants, i.e., a factor of 3−4, in this dispersion range (D = 0.52−0.65). The stronger suppression effects of H_2 pressure on the reaction rates over small clusters than over large clusters reflect the greater competition of kinetically relevant species on these under-coordinated atoms.

3.4.5. Structure sensitivity of cyclohexane hydrogenolysis: the antipathetic branch

Table 3-6. Fitting parameters for CH hydrogenolysis at 523 K on 0.50%Ir(*D*)-1/Al_2O_3 catalysts with D_{Ir} = 0.04−0.24 for the mechanistic model proposed in Scheme 3. The number of *n* is 2, and the splitting agent is a hydrogen adatom in this case, which corresponds to the rate equation:

$$r = \frac{k_{rds} K_H^{0.5} P_H^{0.5+2x} \left[\sqrt{(K_H^{0.5} P_H^{0.5} + 1)^2 + \frac{4K_{cyc} P_{cyc}}{P_H^{x}}} - K_H^{0.5} P_H^{0.5} - 1 \right]^3}{8 K_{cyc}^2 P_{cyc}^2}$$

Fitting parameters	D_{Ir} = 0.24	D_{Ir} = 0.16	D_{Ir} = 0.04
k_{rds} (s^{-1})	1.0	2.1	5.4
K_H (10^{-4} kPa^{-1})	2.6	2.0	1.7
K_{cyc} (10^{2x} kPa^{x-1})[a]	1.8	1.6	3.0
x	1.6	1.2	1.6
R^2	0.99	0.93	0.98
Estimated coverages[b]			
θ_v[c]	0.47−0.61	0.37−0.58	0.42−0.61
θ_H[c]	0.14−0.32	0.09−0.27	0.10−0.26
θ_{cyc}[c,d]	4.1×10^{-2}−0.20	7.7×10^{-2}−0.27	6.9×10^{-2}−0.24

[a] Complex unit depending on the value of *x*.

[b] CH partial pressure: 2.4−3.6 kPa, H_2 partial pressure 0.33−1.1 MPa.

[c] θ_v: surface coverage of empty site; θ_H: surface coverage by H*; θ_{cyc}: surface coverage by cyclic reactive intermediates. The site balance equation is $\theta_v + 2\theta_{cyc} + \theta_H = 1$ because it is assumed that adsorption of cyclic hydrocarbon occupies two surface atoms.

[d] The lower boundary of estimated coverage which corresponds to high H_2-pressure conditions (> 0.4 MPa) may have been underestimated as evidenced from the worse fitting (overestimation relative to experimentally determined values) of the reaction order in CH under these conditions.

Large Ir particles employed in this work exhibit the following kinetic features. First, compared to the high-dispersion catalysts, the optimum H_2 pressures for maximum rates are higher and the suppression of activity by H_2 pressure after the optimum is less distinct (Figure 3-12). Second, the reaction order in CH is lower than that measured over small clusters (Figure 3-13). Third, the temperature dependence of rates (i.e., $E_{a,app}$) is lower than in the case of the high dispersion catalysts (Figure 3-16). As argued above, the first feature suggests a less-dehydrogenated nature of the catalytically relevant species for C−C bond cleavage on large clusters. According to a Langmuir-Hinshelwood formalism, the second feature points to a higher equilibrium coverage of CH-derived reactive intermediates and/or a less severe competition with H* adsorption sites. And the third can be understood from Temkin relation as a result of smaller contributions from the exothermicity term for H_2 chemisorption and the endothermicity term for CH chemisorption. Consequently, the apparent energies of activation on large particles would be close to the intrinsic activation barrier for C−C bond cleavage. It is unclear at present, if the true barrier for C−C bond cleavage is identical on smaller cluster or if it is slightly (e.g., 10-20%) higher.

Compatible with the above qualitative analysis, dehydrogenation depths (denoted as x in Scheme 3-3) lower than those on small clusters were predicted by kinetic modeling of TOFs measured on low-dispersion catalysts when the same mechanistic sequence was applied (Table 3-6). The values of x (1.2−1.6) are, however, less definitive on large particles partly because the range of measured rates over the low-dispersion catalyst varied at most by two-fold only. The dehydrogenation depth could be even less pronounced (smaller x), if the adsorption strength of H* on these large particles had been underestimated by the kinetic modeling (Table 3-7). We further note that any attempts to constrain the dehydrogenation depth at $x = 2$ and model the other three parameters only lead to unreasonable estimates of H* adsorption equilibrium constant and H* coverage (Table 3-7). It is interesting to note that Engstrom et al. [11] explained the differences in the apparent reaction kinetics and preexponential factors of ethane hydrogenolysis on Ir(111) and Ir(110)-(1×2) surfaces also by different reaction intermediates, namely, C_2H_4(ads) on the former and C_2H_2(ads) on the latter. That is, an extensively dehydrogenated species was the MARI on the Ir(110)-(1×2) surface containing a large faction (25%) of low-coordination atoms, while a less unsaturated species was the MARI on terrace sites. It is speculated that the underlying driving forces for various surface structures to effect different H-deficiencies of MARIs root in the different degrees of coordinative unsaturation of surface atoms.

Table 3-7. Effect of varying H_2-adsorption equilibrium constant (K_H) on the modeling results for 0.50%Ir(0.24)-1/Al_2O_3. The number of *n* is 2, and the splitting agent is a hydrogen adatom.

Fitting parameters				
k_{rds} (s^{-1})	3.9	1.4	1.0	0.6
K_H (10^{-4} kPa^{-1})[a]	0.1	1.0	2.6	7.8
K_{cyc} (10^{2x} kPa^{x-1})[b]	2.0	1.7	1.8	2.1
x	2.0	1.7	1.6	1.4
R^2	0.99	0.99	0.99	0.99
Estimated coverages[c]				
θ_v[d]	0.56−0.84	0.51−0.70	0.47−0.61	0.39−0.49
θ_H[d]	0.03−0.09	0.09−0.23	0.14−0.32	0.20−0.44
θ_{cyc}[d,e]	3.5×10^{-2}−0.20	3.8×10^{-2}−0.20	4.1×10^{-2}−0.20	4.5×10^{-2}−0.20

[a] Preset values.

[b] Complex unit depending on the value of *x*.

[c] CH partial pressure: 2.4−3.6 kPa, H_2 partial pressure 0.33−1.1 MPa.

[d] θ_V: surface coverage of empty site; θ_H: surface coverage by H*; θ_{cyc}: surface coverage by cyclic reactive intermediates. The site balance equation is $\theta_v + 2\theta_{cyc} + \theta_H = 1$ because it is assumed that adsorption of cyclic hydrocarbon occupies two surface atoms.

[e] The lower boundary of estimated coverage which corresponds to high H_2-pressure conditions may have been severely underestimated as evidenced from the overestimated reaction orders in CH relative to experimentally determined values under these conditions.

Besides the above considerations, it is also possible that not the adsorption normal to the surface, but rather an adsorption state in which the molecule is parallel to the surface may exist on large Ir particles predominantly terminated with terrace planes. Although the (111) and (100) planes also exist on small clusters, the large ensemble size requirement for the adsorption parallel to the surface would make this mode nearly inoperative. Without further evidence, it remains difficult to clarify whether the increase of intrinsic rate constant (k_{rds}) with decreasing dispersion (D = 0.04−0.24, Table 6) points to higher reactivities of less unsaturated surface intermediates or enhanced chances of finding adjacent open sites to accommodate the active species. Although it is tempting to ascribe the higher intrinsic rate constants on very large Ir particles to larger pre-exponential factors (transition-state entropy changes), rather than to smaller activation barriers, the accuracy (± 10 kJ mol^{-1}) of determining true activation barriers on small and large clusters renders a conclusive statement difficult. At the present stage, the antipathetic branch is tentatively ascribed to a less-unsaturated nature of the MARI and possibly also a different adsorption mode that requires a much larger ensemble size than the dicarbene-like adsorption complex prevalent on small clusters.

3.4.6. H-deficiency of reactive intermediates as the selectivity mediator for single scission and terminal/internal multiple scissions

We interpret here the observed effects imposed by H_2 pressure on the ring opening selectivity, and the selectivity patterns along primary pathways, on the basis of the unsaturation degree of surface intermediates relevant to different cleavage modes.

Within the framework of the kinetic model proposed in Scheme 3-3, we further introduce different H-deficiencies (the value of *x*) of intermediates between single and multiple C−C bond scissions (denoted as S_{RO} and S_{multi}, respectively), and also between internal and terminal modes of multiple scissions (denoted as S_{tm} and S_{im}, respectively). According to step (iii) in Scheme 3-3, the formation rates of single scission product and multiple scission products along primary reaction pathways are given by the rates of their RDS (C−C bond cleavage):

$$r_{RO} = k_{RO}\theta_{S_{RO}}\theta_H \qquad \text{(Eq. 2)}$$

$$r_{multi} = k_{multi}\theta_{S_{multi}}\theta_H \qquad \text{(Eq. 3)}$$

The quasi-equilibrium assumption for hydrocarbon activation (step ii, Scheme 3-3) implies that the MARIs for single and multiple cleavage in kinetically primary pathways also exist in equilibrium:

$$S_{RO} \rightleftharpoons S_{multi} + (x_{multi}-x_{RO})\,H_2 \qquad \text{(Eq. 4)}$$

where x_{RO} and x_{multi} refer to the dehydrogenation depths of the MARIs for single and multiple C−C bond cleavage, respectively, and, thus, gives:

$$\theta_{S_{RO}} = K_{\text{int}}^{-1}\theta_{S_{multi}} P_H^{(x_{multi}-x_{RO})} \qquad \text{(Eq. 5)}$$

where K_{int} is defined as the equilibrium constant for Eq. 4. Thus, a functional relation (Eq. 6) can be established between H_2 pressure and the rate ratio of single and multiple hydrogenolysis (details on the derivation are shown in the Appendix).

$$\ln(\frac{r_{RO}}{r_{multi}}) = \ln(\frac{k_{RO}}{k_{multi}K_{\text{int}}}) + (x_{multi} - x_{RO})\ln P_H \qquad \text{(Eq. 6)}$$

Therefore, the slope of the $\ln(r_{RO}/r_{multi})$-$\ln(P_H)$ plot would point to the difference in the H-deficiency between surface intermediates involved in single and multiple C−C bond scissions, respectively. The double-logarithmic function is plotted in Figure 3-20 for both small and large Ir particles. A comparison of the slopes in Figures 3-20a and b clearly indicates that H-deficiency (x) is less different between S_{RO} and S_{multi} on large than on small particles, thus bringing the reactivities of single and multiple C−C bond scissions closer together (Figure 3-14b). As is shown in a quantitative way (Table 3-8), the active intermediate for single scission possibly has to further lose more than one hydrogen atom, on average, to allow multiple scissions on small Ir clusters, in accordance with a previous report on the hydrogenolysis of lower alkanes over Ru/Al_2O_3 catalysts [55]. In contrast, less than one or even no further hydrogen needs to be abstracted for terminal multiple-scission to occur on large particles before hydrogenative desorption of the ring-opened intermediate (Table 3-8). Moreover, the average H-deficiency of active intermediates for internal multiple-scission seems to be greater than single-scission (RO) and terminal multiple-scission on both small and large particles, accounting for their lower values of H_2 pressure at maximum rates in primary reactions (propane and butane in Figure 3-14) and the constantly decreasing selectivity to internal multiple-scission with increasing H_2 pressure (Figure 3-15c). The rates of those pathways that have greater dehydrogenation depths before the C−C bond scission step exhibit more marked suppression by increasing H_2 pressure (Figure 3-14). Their greater dehydrogenation depths can be seen as a consequence of the slightly weaker secondary C−H bonds [35]. Finally, a deeper unsaturation degree of S_{im} than S_{RO} and S_{tm} would necessitate a higher contribution of the endothermicity term in the Temkin relation, leading to their higher apparent activation energies (Table 3-3).

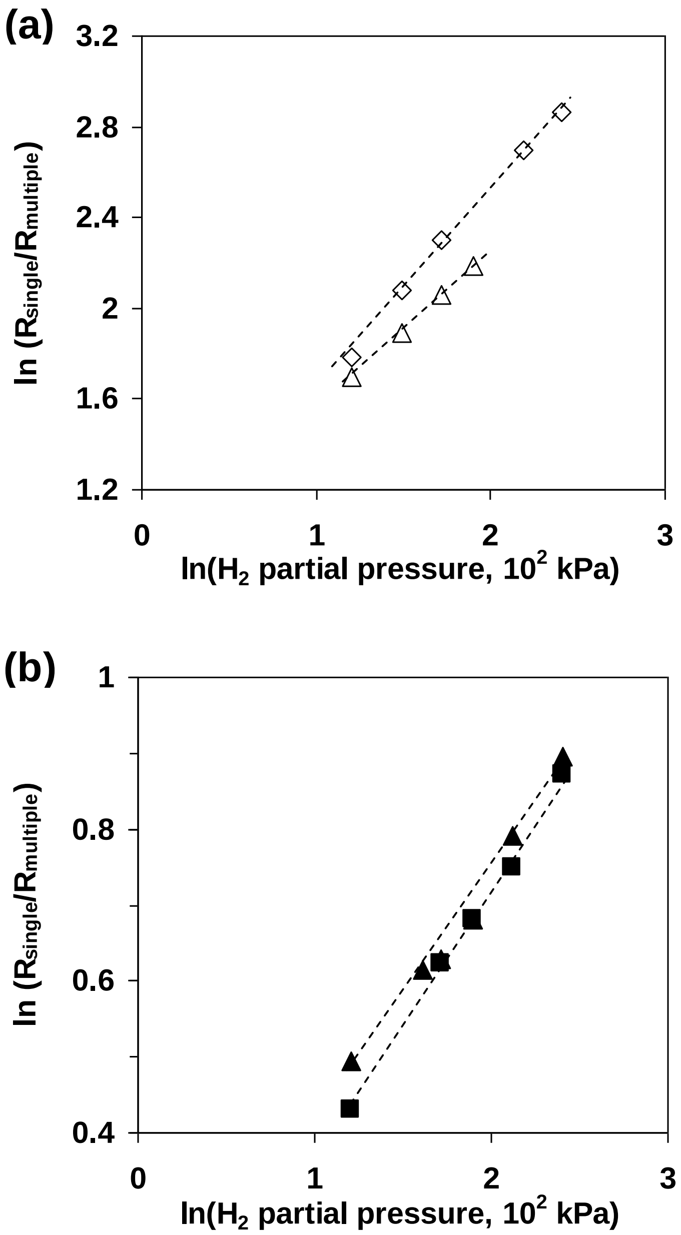

Figure 3-20. Different H-deficiencies of reactive intermediates for single scission (RO) and multiple scissions indicated by the dependences of rate ratios on H_2 pressure over (a) small (D > 0.50) and (b) large (D < 0.20) Ir particles. Reaction conditions: 523 K, 3.1 kPa CH.

Table 3-8. Different extents of H-deficiency of reactive intermediates for single scission, terminal and internal multiple scissions at 523 K on typical small and large Ir particles.

x_m-x_{RO} (H-deficiency difference)[a]	D = 0.65	D = 0.16
Terminal multiple scission	0.5−0.6	0.1−0.2
Internal multiple scission	0.9−1.0	0.4−0.6

[a] The difference in dehydrogenation depth (x) of reactive intermediates between single-scission and multiple-scission (including terminal or internal).

3.5. Conclusions

To explore the intrinsic catalytic specificity of Ir, the present contribution employs a series of Ir catalysts of varying dispersions that catalyze exclusively the direct C−C bond cleavages of cyclohexane.

The pathways for multiple hydrogenolysis in kinetically primary (before desorption of the n-hexane intermediate) and secondary (readsorption of n-hexane) reactions greatly differ. The relative importance of the pathways depends subtly on the Ir cluster size and H_2 pressure and to a lesser degree on the reaction temperature in the studied range. The detrimental effects of lower H_2 pressures, larger particle size and higher temperatures on the selectivity to n-hexane are mainly related to the nature of reactive intermediate for single and multiple C−C bond cleavage, as well as the availability of adsorbed vicinal hydrogen species.

The generally high value of apparent activation barrier for hydrogenolysis that further increases with increasing H_2 pressure is a consequence of the endothermic nature of the activation of cyclic reactants. Moreover, the even higher activation energies for internal C−C bond cleavages are attributable to an energetically more demanding nature as well as a low coverage of the reactive intermediates involved in the rate-determining step.

A dual-branch sensitivity of TOFs to Ir dispersion (D = 0.01−0.65) was observed for the endocyclic C–C bond cleavage. We have provided evidence that the sympathetic structure sensitivity originates from the decrease of the intrinsic rate constant ascribed to the declining population of low-coordination atoms. For larger Ir particles (> 4 nm), an antipathetic trend, i.e., increasing TOFs with decreasing dispersion, has been observed.

On the basis of modeling results, we argue that reactive intermediates of lower H-deficiencies are involved for rate-determining C–C bond cleavage on low Ir dispersion catalysts. The large Ir particles may have intrinsically higher reactivities on terraces or steps on terraces. It is also speculated that a new adsorption mode of cyclohexane that requires a sizable ensemble is more favorably formed on terrace planes.

3.6. Acknowledgments

Hui Shi thanks the Elitenetzwerk Bayern NanoCat for a Ph.D. grant and financial support. The authors are indebted to Dipl.-Ing. Xaver Hecht for the help with construction of the reactor setup and for conducting N_2 physisorption and H_2 chemisorption measurements. Skillful assistances from Dr. Marianne Hanzlik (Technical university of Munich, Germany) and Dr. Andrew DelaRiva (University of New Mexico, USA) are gratefully acknowledged during the TEM measurements.

3.7. Appendix

A1. Derivation of the rate equation for kinetic modeling of cyclohexane hydrogenolysis

A sequence of steps for CH hydrogenolysis on Ir catalysts is shown in Scheme 2.
The quasi-equilibrium assumption for H_2 chemisorption (step i) gives

$$\theta_H = {K_H}^{0.5} {P_H}^{0.5} \theta_v \qquad \text{(E1)}$$

The quasi-equilibrium assumption for hydrocarbon activation (step ii) gives

$$\theta_{cyc} = \frac{K_{cyc} P_{cyc} {\theta_v}^n}{{P_H}^x} \qquad \text{(E2)}$$

A site balance gives

$$\theta_v + \theta_H + n\theta_{cyc} = 1 \qquad \text{(E3)}$$

The rate of CH hydrogenolysis is equal to the rate of the rate-determining step (step iii), thus giving

$$r = k_{rds}\theta_{cyc}\theta_H \tag{E4-1}$$

when an adsorbed H atom is involved in the C−C bond cleavage, or giving

$$r = k_{rds}\theta_{cyc}\theta_v \tag{E4-2}$$

when a vacancy is involved in the C−C bond cleavage, or giving

$$r = k_{rds}\theta_{cyc}P_H \tag{E4-3}$$

when a gas-phase H_2 molecule is involved in the C−C bond cleavage, or giving

$$r = k_{rds}\theta_{cyc}\theta_v P_H \tag{E4-4}$$

when gas-phase H_2 with an open site is involved in the C−C bond cleavage. In our primary attempts of kinetic modeling, the 'H*-assisted' RDS assumption has been chosen. We discuss next two cases differing in the number of binding surface Ir atoms:

(a) For n = 1 and combing (E1), (E2) and (E3)

$$\theta_v = \frac{1}{1 + K_H{}^{0.5}P_H{}^{0.5} + \frac{K_{cyc}P_{cyc}}{P_H{}^x}} \tag{E5}$$

$$\theta_H = \frac{K_H{}^{0.5}P_H{}^{0.5}}{1 + K_H{}^{0.5}P_H{}^{0.5} + \frac{K_{cyc}P_{cyc}}{P_H{}^x}} \tag{E6}$$

$$\theta_{cyc} = \frac{\frac{K_{cyc}P_{cyc}}{P_H{}^x}}{1 + K_H{}^{0.5}P_H{}^{0.5} + \frac{K_{cyc}P_{cyc}}{P_H{}^x}} \tag{E7}$$

Substituing (E6) and (E7) into (E4-1) gives

$$r = \frac{k_{rds}K_H{}^{0.5}K_{cyc}P_H{}^{0.5-x}P_{cyc}}{(1 + K_H{}^{0.5}P_H{}^{0.5} + \frac{K_{cyc}P_{cyc}}{P_H{}^x})^2} \tag{E8}$$

(b) For n = 2 and combing (E1), (E2) and (E3)

$$\theta_v = \frac{-1 - K_H{}^{0.5}P_H{}^{0.5} + \sqrt{(K_H{}^{0.5}P_H{}^{0.5} + 1)^2 + \frac{4K_{cyc}P_{cyc}}{P_H{}^x}}}{\frac{2K_{cyc}P_{cyc}}{P_H{}^x}} \tag{E9}$$

$$\theta_H = \frac{K_H{}^{0.5} P_H{}^{0.5} \left(\sqrt{(K_H{}^{0.5} P_H{}^{0.5} + 1)^2 + \frac{4K_{cyc} P_{cyc}}{P_H{}^x}} - K_H{}^{0.5} P_H{}^{0.5} - 1 \right)}{\frac{2K_{cyc} P_{cyc}}{P_H{}^x}} \tag{E10}$$

$$\theta_{cyc} = \frac{P_H{}^x \left[\sqrt{(K_H{}^{0.5} P_H{}^{0.5} + 1)^2 + \frac{4K_{cyc} P_{cyc}}{P_H{}^x}} - K_H{}^{0.5} P_H{}^{0.5} - 1 \right]^2}{4K_{cyc} P_{cyc}} \tag{E11}$$

Substituing (E10) and (E11) into (E4-1) gives

$$r = \frac{k_{rds} K_H{}^{0.5} P_H{}^{0.5+2x} \left[\sqrt{(K_H{}^{0.5} P_H{}^{0.5} + 1)^2 + \frac{4K_{cyc} P_{cyc}}{P_H{}^x}} - K_H{}^{0.5} P_H{}^{0.5} - 1 \right]^3}{8K_{cyc}{}^2 P_{cyc}{}^2} \tag{E12}$$

In the present work, the site balance has been used as $\theta_v + 2\theta_{cyc} + \theta_H = 1$. Thus, (E12) has been used because of its higher predictive accuracy for the reaction order in CH than (E8). Regardless, both equations (E8 and E12) predict similar values of coverages for vacancy sites, H*-covered sites and the MARI.

A2. Derivation of the functional relation between H_2 pressure and the rate ratio of different cleavage pathways within the kinetic framework of CH hyrdogenolysis proposed in Scheme 2

If the formation rates of single and multiple C−C bond scissions are separately analyzed, their rates are determined by the coverage of the kinetically relevant surface intermediates, the H* coverage and the rate constant of that particular C−C bond cleavage step (step iii, Scheme 3-3). Based on the experimental observations that the H_2 pressure imposes different suppression effects on the single and multiple scission routes, it has been assumed *a priori* that the single and multiple scissions require different H-deficiencies of MARI for their respective C−C bond scission step. The MARI for single scission is denoted as S_{RO}, that for multiple scission as S_{multi}.

According to Scheme 3-3, the formation rate of single scission product along primary reaction pathways is given by the rate of its RDS (C−C bond cleavage):

$$r_{RO} = k_{RO} \theta_{S_{RO}} \theta_H \tag{E13}$$

The formation rate of multiple scission products along primary reaction pathways is given by the rate of its RDS (C−C bond cleavage):

$$r_{multi} = k_{multi} \theta_{S_{multi}} \theta_H \tag{E14}$$

The quasi-equilibrium assumption for hydrocarbon activation (step ii, Scheme 2) implies that there would be a distribution of surface species with varying H-deficiencies on the catalytic surface. Hence, the relative abundance of different surface species is dictated by the equilibrium constants for their inter-transformation. Seen in this light, the MARIs for single and multiple scission exist in equilibrium:

$$\mathrm{S_{RO}} \rightleftharpoons \mathrm{S_{multi}} + (x_{\mathrm{multi}} - x_{\mathrm{RO}})\, \mathrm{H_2} \tag{E15}$$

Thus, the coverages of these two MARIs must satisfy the following:

$$\theta_{S_{RO}} = K_{\mathrm{inter}}{}^{-1} \theta_{S_{multi}} P_H{}^{(x_{multi} - x_{RO})} \tag{E16}$$

Substituting (E16) into (E13) gives

$$r_{RO} = k_{RO} K_{\mathrm{inter}}{}^{-1} \theta_{S_{multi}} P_H{}^{(x_{multi} - x_{RO})} \theta_H \tag{E17}$$

Dividing (E17) by (E14) gives

$$\frac{r_{RO}}{r_{multi}} = \frac{k_{RO}}{k_{multi} K_{\mathrm{inter}}} P_H{}^{(x_{multi} - x_{RO})} \tag{E18}$$

Transforming (E18) into logarithmic scales on both sides gives

$$\ln\left(\frac{r_{RO}}{r_{multi}}\right) = \ln\left(\frac{k_{RO}}{k_{multi} K_{\mathrm{inter}}}\right) + (x_{multi} - x_{RO}) \ln P_H \tag{E19}$$

Therefore, the slope of the double-logarithmic ln($r_{\mathrm{RO}}/r_{\mathrm{multi}}$)-ln($P_H$) plot would point to the difference in the H-deficiency between surface intermediates mediating single and multiple C−C bond scissions, respectively. Along similar lines, H-deficiency of the intermediates relevant to internal and terminal multiple scissions can also be differentiated.

3.8. References

1. G.B. McVicker, M. Daage, M.S. Touvelle, C.W. Hudson, D.P. Klein, W.C. Baird Jr., B.R. Cook, J.G. Chen, S. Hantzer, D.E.W. Vaughan, E.S. Ellis, O.C. Feeley, J. Catal. 210 (2002) 137.
2. A. Corma, V. González-Alfaro, A.V. Orchillés, J. Catal. 200 (2001) 34.
3. H. Du, C. Fairbridge, H. Yang, Z. Ring, Appl. Catal. A 294 (2005) 1.
4. G.C. Bond, Metal-Catalysed Reactions of Hydrocarbons, Springer, Berlin, 2005.
5. J.H. Sinfelt, J.L. Carter, D.J.C. Yates, J. Catal. 24 (1972) 283.
6. H. Song, R.M. Rioux, J.D. Hoefelmeyer, R. Komor, K. Niesz, M. Grass, P. Yang, G.A. Somorjai, J. Am. Chem. Soc. 128 (2006) 3027.
7. R.M. Rioux, H. Song, J.D. Hoefelmeyer, P. Yang, G.A. Somorjai, J. Phys. Chem. B 109 (2005) 2192.
8. D.J.C. Yates, J.H. Sinfelt, J. Catal. 8 (1967) 348.
9. D.E. Resasco, G.L. Haller, J. Catal. 82 (1983) 279.
10. K. Foger, J.R. Anderson, J. Catal. 59 (1979) 325.
11. J.R. Engstrom, D.W. Goodman, W.H. Weinberg, J. Am. Chem. Soc. 110 (1988) 8305.
12. R.K. Herz, W.D. Gillespie, E.E. Peterson, G.A. Somorjai, J. Catal. 67 (1981) 386.
13. G.A. Somorjai, D.W. Blakely, Nature 258 (1975) 580.
14. D.W. Blakely, G.A. Somorjai, J. Catal. 42 (1976) 181.
15. F.G. Gault, Adv. Catal. 30 (1981) 1.
16. M. Chow, G.B. McVicker, J. Catal. 112 (1988) 290.
17. Y. Zhuang, A. Frennet, Appl. Catal. A 134 (1996) 37.
18. D. Teschner, K. Matusek, Z. Paál, J. Catal. 192 (2000) 335.
19. M. Vaarkamp, P. Dijkstra, J. van Grondelle, J.T. Miller, F.S. Modica, D.C. Koningsberger, R.A. van Santen, J. Catal. 151 (1995) 330.
20. W.E. Alvarez, D.E. Resasco, J. Catal. 164 (1996) 467.
21. M. Chow, S.H. Park, W.M.H. Sachtler, Appl. Catal. 19 (1985) 349.
22. P. Samoila, M. Boutzeloit, C. Especel, F. Epron, P. Marécot, J. Catal. 276 (2010) 237.

23. D. Kubička, N. Kumar, P. Mäki-Arvela, M. Tiitta, V. Niemi, H. Karhu, T. Salmi, D.Y. Murzin, J. Catal. 227 (2004) 313.
24. D. Kubička, N. Kumar, P. Mäki-Arvela, M. Tiitta, V. Niemi, T. Salmi, D.Y. Murzin, J. Catal. 222 (2004) 65.
25. S. Lecarpentier, J. van Gestel, K. Thomas, J.-P. Gilson, M. Houalla, J. Catal. 254 (2008) 49.
26. M. Santikunaporn, J.E. Herrera, S. Jongpatiwut, D.E. Resasco, W.E. Alvarez, E.L. Sughrue, J. Catal. 228 (2004) 100.
27. S. Rabl, A. Haas, D. Santi, C. Flego, M. Ferrari, V. Calemma, J. Weitkamp, Appl. Catal. A 400 (2011) 131.
28. S. Nassreddine, L. Massin, M. Aouine, C. Geantet, L. Piccolo, J. Catal. 278 (2011) 253.
29. P.T. Do, W.E. Alvarez, D.E. Resasco, J. Catal. 238 (2006) 477.
30. J.-W. Park, K. Thomas, J. van Gestel, J.-P. Gilson, C. Collet, J.-P. Dath, M. Houalla, Appl. Catal. A. 388 (2010) 37.
31. S. Nassreddine, G. Bergeret, B. Jouguet, C. Geantet, L. Piccolo, Phys. Chem. Chem. Phys. 12 (2010) 7812.
32. F.J.C.M. Toolenaar, A.G.T.M. Bastein, V. Ponec, J. Catal. 82 (1983) 35.
33. G.B. McVicker, R.T.K. Baker, R.L. Garten, E.L. Kugler, J. Catal. 65 (1980) 207.
34. S. Krishnamurthy, G.R. Landolt, H.J. Schoennagel, J. Catal. 78 (1082) 319.
35. B.J. Kip, F.B.M. Duivenvoorden, D.C. Koningsberger, R. Prins, J. Catal. 105 (1987) 26.
36. H. Lieske, G. Lietz, H. Spindler, J. Volter, J. Catal. 81 (1983) 8.
37. M. Boudart, G. Djega-Mariadassou, The Kinetics of Heterogeneous Catalytic Reactions, Princeton University Press, Princeton, NJ, 1984.
38. G.C. Bond, M.A. Keane, H. Kral, J.A. Lercher, Chem. Rev. -Sci. Eng. 42 (2000) 323.
39. A. Majesté, S. Balcon, M .Guérin, C. Kappenstein, Z. Paál, J. Catal. 187 (1999) 486.
40. B.E. Nieuwenhuys, D.I. Hagen, G.A. Somorjai, Surf. Sci. 59 (1976) 155.
41. J.K.A. Clarke, J.J. Rooney, Adv. Catal. 25 (1976) 125.
42. V. Ponec, P.G. Menon, Catal. Rev. -Sci. Eng. 25 (1983) 229.

43. D.F. McMillen, D.M. Golden, Ann. Rev. Phys. Chem. 33 (1982) 493.
44. M. Temkin, Acta Phsiocochim. URSS 3 (1935) 312.
45. S.B. Shang, C.N. Kenney, J. Catal. 134 (1992) 134.
46. J.H. Sinfelt, D.J.C. Yates, J. Catal. 8 (1967) 82.
47. J.H. Sinfelt, Catal. Rev.-Sci. Eng. 9 (1974) 147.
48. G.C. Bond, R.H. Cunningham, J. Catal. 166 (1997) 172.
49. S.A. Goddard, M.D. Amiridis, J.E. Rekoske, N. Cardona-Martinez, J.A. Dumesic, J. Catal. 117 (1989) 155.
50. A. Cimino, M. Boudart, H. Taylor, J. Phys. Chem. 58 (1954) 796.
51. M. Che, C.O. Bennett, Adv. Catal. 36 (1989) 55.
52. G.A. Del Angel, B. Coq, G. Ferrat, F. Figueras, S. Fuentes, Surf. Sci. 156 (1985) 943.
53. F. Garin, G. Maire, Acc. Chem. Res. 22 (1989) 100.
54. R. van Hardeveld, F. Hartog, Surf. Sci. 15 (1969) 189.
55. G.C. Bond, J.C. Slaa, J. Mol. Catal. A 98 (1995) 81.

Chapter 4

Structure sensitivities of hydrogenolytic cleavage of endocyclic and exocyclic C–C bonds in methylcyclohexane over supported iridium clusters

Methylcyclohexane was chosen as a model substrate for studying the hydrogenolytic ring opening of substituted six-membered naphthenes over a series of monofunctional Ir catalysts with varying average cluster sizes. Detailed analyses of major hydrogenolytic pathways were performed in relation to the dependences of their rates on the H_2 pressure and temperature, in order to seek potential strategies for suppression of reactions other than ring opening. Similarities with cyclohexane hydrogenolysis were shown. The rate of endocyclic C–C bond cleavage first decreases and then increases with declining Ir dispersion from 0.65 to 0.035 under the prevalent conditions. The rate and selectivity of demethylation via exocyclic C–C bond cleavage decrease at increasing H_2 pressures and on smaller Ir clusters. The distinct sensitivities to Ir dispersion for endocyclic and exocyclic C–C bond cleavage pathways suggest that they are mediated by surface species with different ensemble size requirements and reactivities. The presence of the methyl substituent exerts two types of steric effects on the formation of ring opening products, resulting in low selectivity to n-heptane via endocyclic C–C bond scission at the hindered position.

4.1. Introduction

Selective ring opening (SRO) represents an essential process following deep hydrogenation of aromatics during the upgrading of the light cycle oil (LCO) fraction [1−3]. Methylcyclopentane ring opening has been extensively studied over various mono- and bimetallic catalysts [4−16]. In contrast, ring opening of substituted six-membered naphthenes and fused ring structures, which are the most relevant components in LCO feeds, have been subjected to fewer studies that involve metallic functions [1,17−26]. Even fewer studies addressed monofunctional metal catalysts [20−22], because the minimal ring strains in six-membered naphthenes (smaller by ca. 25 kJ mol^{-1} than five-membered-ring [1]) have rendered the direct conversion of these substrates unsatisfactorily slow on most pure metal catalysts. Consequently, the most effective SRO strategy to date has been incorporating acid functions into the catalytic system to catalyze isomerization reactions that transform cyclohexyl backbones to much more reactive cyclopentyl ones [1,17,18,22−26]. Unfortunately, the intrinsic features of purely metal-catalyzed hydrogenolyses of six-membered naphthenes have eluded our understanding in such a bifunctional scenario, where the acidic component catalyzes the ring opening step and the metal is conventionally regarded only as a dehydrogenation-hydrogenation function.

Among the metals with moderate to high hydrogenolysis activity (e.g., Rh, Ir, Ru, Ni), iridium was found to be the most selective towards ring opening [1], which spurred further studies of Ir-based catalysts in SRO of naphthenes [19−23,25,26]. In recent studies by Houalla and coworkers [22,25,26], monofunctional Ir/ZrO_2−SiO_2, Ir/Al_2O_3 and bifunctional Ir/WO_3/ZrO_2−SiO_2, Ir/WO_3/Al_2O_3 catalysts have been developed and investigated in ring opening reactions of methylcyclohexane (MCH). The distribution of the ring opening products (ROPs), however, was not reported in their work [22,26]. In comparison, Do et al. devoted intensive effort to analyzing the selectivity trends for various endocyclic C–C bond cleavage modes of di-substituted cyclohexanes over a series of monofunctional Ir catalysts [21]. The effects of support characteristics and Ir dispersion were explored, but detailed kinetic features associated with changes in H_2 pressure were lacking. Hence, our previous study addressed the catalytic consequences of modulating Ir dispersion and H_2 pressure on the relative contributions of single and multiple C−C bond cleavages, as well as their possible mechanistic origins, in hydrogenolysis of cyclohexane (CH) catalyzed by supported Ir clusters of varying sizes (Chapter 3). We have shown in the last chapter that the role played by metallic Ir is distinct from that acknowledged in bifunctional catalytic systems.

Furthermore, we note that in none of the above-mentioned studies with substituted CHs were exocyclic C−C bond scissions mentioned or observed, probably due to the high H_2 pressure applied (> 3 MPa) [21,22,25]. Nevertheless, it is of great importance to explore the active site requirements and pressure/temperature dependences of dealkylation reactions in order to seek appropriate catalyst compositions and process conditions to suppress these undesired pathways. To this end, the present study compares the structure sensitivities of endocyclic and exocyclic C−C bond cleavages on metallic Ir clusters at varying H_2 pressures and temperatures, using MCH as a probe molecule.

4.2. Experimental

4.2.1. Catalyst preparation

The Ir catalysts in this chapter were the same as those in Chapter 3. Two series of Ir/Al_2O_3 catalysts were prepared from Cl-free ($Ir(acac)_3$) and Cl-containing precursors ($(NH_4)_2IrCl_6$), whereas γ-Alumina (Alu C, 104 m^2 g^{-1}, Evonik Degussa) was used as the support. The detailed procedures were described in the Experimental section of Chapter 3.

The first series of samples are denoted as $m\%Ir(D)\text{-}1/Al_2O_3$, where $m\%$, D and 1 are the Ir loading by wt.% (ICP-OES), the fractional Ir dispersion (H_2 chemisorption), and a denotation of the Cl-free precursor, respectively.

The second series of samples are denoted as $m\%Ir(D)\text{-}2/Al_2O_3$, $m\%$, D and 2 are the actual Ir loading by wt.% (ICP-OES), the fractional Ir dispersion (H_2 chemisorption), and a denotation of the Cl-containing precursor, respectively.

4.2.2. Catalyst characterization

4.2.2.1. H_2 chemisorption and N_2 physisorption

Chemisorption uptakes were measured by a volumetric approach on a Sorptomatic 1990 instrument. The catalyst samples (0.2−0.4 g) were pretreated in 100 kPa of static H_2 at 723 K (5 K min^{-1} ramp) for 2−3 h and then evacuated at the same temperature for 0.5 h before chemisorption measurements. Hydrogen adsorption was carried out at 307 K in a pressure range of 0.5−13.2 kPa with an equilibrating duration of 2−5 min for each pressure increment (1.6 kPa). After completing the first adsorption isotherm, the system was evacuated (10^{-4} kPa, 1 h) to measure the second isotherm. A difference isotherm was obtained by subtracting the second isotherm from the first one. The concentration of chemisorbed hydrogen was determined by extrapolating the linear part of the difference isotherm (P > 6.5 kPa) to zero pressure. Dispersion (*D*), defined as the fraction of Ir atoms exposed at surfaces, was estimated by assuming a H_{chem}-to-surface Ir atom stoichiometry of two, a ratio that implies multiple adsorption of hydrogen on surface Ir atoms [27].

The BET surface area of the catalysts was characterized by N_2 physisorption at 77 K on the Sorptomatic 1990 instrument. All samples were degassed at 523 K for 2 h before measurements. The specific BET surface area was calculated from the adsorption isotherms over a relative pressure range (p/p^0) of 0.03−0.10.

4.2.2.2. Transmission electron microscopy

Transmission electron micrographs were recorded on a JEM-2010 JEOL transmission electron microscope (TEM) with an accelerating voltage of 120 kV. Samples of the catalysts were ground, suspended in ethanol and ultrasonically dispersed for 2 min before being transferred to the vacuum system. Drops of the dispersions were applied onto a holey-carbon Cu grid (Quantifoil Micro Tools).

4.2.2.3. ICP-OES

Iridium contents were measured by inductively-coupled plasma optical emission spectroscopy (ICP-OES) on a Spectroflame FTMOA81A ICP-OES spectrometer (Spectro

Analytic Instruments). In order to conduct the measurement, 60−100 mg of the catalyst was dissolved in a mixture of 0.1 cm^3 nitric acid, 2.0 cm^3 hydrofluoric acid and 0.1 cm^3 hydrochloric acid. Standard solutions containing 0, 50, 100 and 200 ppm Ir in 25 cm^3 6.5 wt.% nitric acid were used for calibration.

4.2.3. Steady-state kinetic measurements

Hydrogenolysis of methylcylohexane (MCH) was studied in a stainless steel tubular reactor with an inner diameter of 4 mm. Catalyst powders sieved (grain size of 180−280 μm) were diluted with quartz sand of identical sieve fractions to minimize heat-induced effects and to ensure plug-flow hydrodynamics. A K-type thermocouple was inserted into the isothermal region of the external surface of the reactor. Differences below 1 K were detected when the thermocouple was held in direct contact with the catalyst bed. Transport artifacts have not been detected by preliminary tests where particle size and contact time were varied (Figure 4-1). Prior to reactions, catalysts (typically 20−40 mg) were pretreated in a pure H_2 flow of 20 cm^3 min^{-1} at 623 K (0.2 K s^{-1} ramp and 2 h hold) and then cooled to the reaction temperature. MCH vapor was introduced by flowing helium (Westfalen AG, 99.996%) through a series of bubblers (immersed in a thermostat water bath) containing liquid MCH (Aldrich, ≥ 99%). The helium flow carrying MCH vapor mixed co-currently with a flow of H_2 (Westfalen AG, 99.999%) and contacted the catalyst bed at the set temperature. Electronic mass flow controllers and back pressure regulators were used to regulate flow rates of gases and total pressures of the reactor system. The kinetic measurements were performed under total pressures of 0.35−2.0 MPa. The products were analyzed online by a Hewlett-Packard 6890 Plus GC equipped with a DB Petro column (320 μm × 100 m) and a flame ionization detector (FID). Initial rates and selectivities were derived by extrapolating the measured rates and selectivities to zero contact time (the conversion was typically below 20%). In a majority of cases, the deactivation was kept below 8% during the whole run Deactivation of at most 12% was observed for catalysts with large Ir clusters for time-on-stream (TOS) of 5 days below 543 K. Selectivities did not change with TOS after the steady state was reached.

4.3. Results

4.3.1. Characterization of the supported iridium catalysts

The details of the bulk and surface characterization of the supported iridium catalysts have been reported in the last chapter. Briefly, air-calcination (T = 393−873 K) and H_2-reduction at 723 K hardly decreased the surface areas of the Ir/Al_2O_3 samples, i.e., at most by 10% relative to γ-Al_2O_3 support. As expected using the impregnation approach, the actual Ir loadings in all samples are almost identical to the anticipated 0.5 wt%. TEM-derived particle sizes were confirmed to be in reasonable agreement with the reciprocal of Ir dispersions determined from H_2 chemisorption measurements (see Chapter 3).

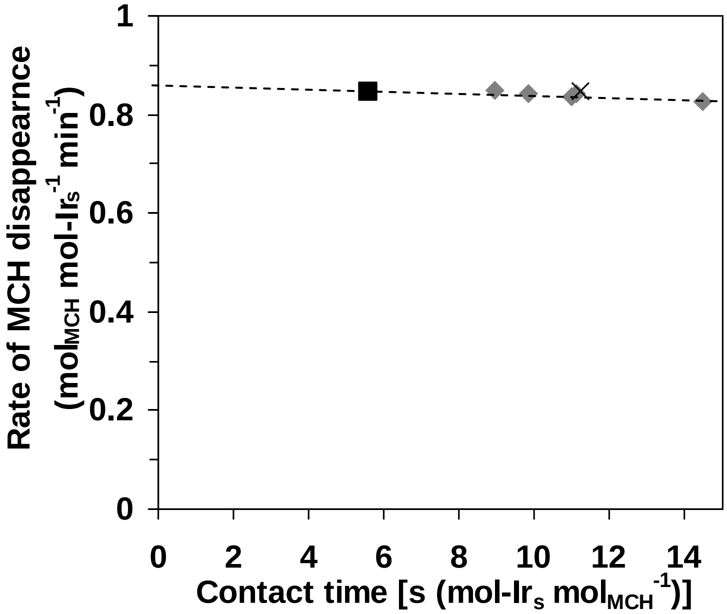

Figure 4-1. Effects of contact time and granule size on the reaction rates over 0.50%Ir(0.61)-1/Al_2O_3 at 523 K, 1.2 kPa MCH, 0.37 MPa H_2 and conversion levels < 15%. Symbols represent: 280-400 μm, 40 mg (×); 180-280 μm, 40 mg (♦); 180-280 μm, 20 mg (■).

4.3.2. Minor reaction channels in methylcyclohexane conversion

Ethylcyclopentane and dimethylcyclopentanes were observed in very low quantities (0.4−0.8% selectivity in total within the converted fraction), indicative of a negligible amount of ring isomerization. If the alkylcyclopentanes had been formed and had subsequently undergone fast ring opening, there would have been a considerable amount of 3-ethylpentane in the C_7 fraction, which was barely detectable. Thus, neither iridium itself nor acidity introduces an additional consumption pathway via isomerization to alkylcyclopentanes and subsequent C_5-ring opening. Likewise, the possibility of indirect ring opening over Ir/Al_2O_3 catalysts was convincingly excluded also in cyclohexane (CH) conversion (see Chapter 3).

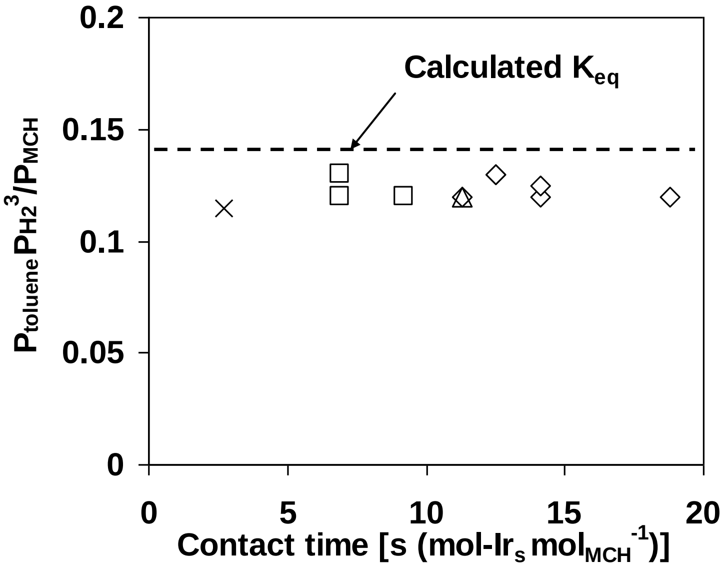

Figure 4-2. Effect of contact time on the approach to equilibrium of MCH dehydrogenation shown over 0.50%Ir(0.61)-1/Al_2O_3 (◊), 0.54%Ir(0.58)-1/Al_2O_3 (Δ), 0.54%Ir(0.30)-2/Al_2O_3 (□) and 0.50%Ir(0.16)-1/Al_2O_3 (×). Reaction conditions were 523 K, 0.63 MPa H_2, 1.2 kPa MCH.

Dehydrogenation of and skeletal isomerization are both minority reaction channels that account for a combined selectivity of less than 4% under prevalent H_2 pressures and temperatures. At H_2 pressures above 0.6 MPa, the dehydrogenation route became negligible at all temperatures studied. Moreover, the gas-phase equilibrium of dehydroaromatization appeared to be attained in presence of high pressure H_2, as suggested by the virtually invariant pressure quotients when the contact time was altered over various catalysts (Figure 4-2). These pressure quotient values approximated the equilibrium constant for the MCH dehydrogenation reaction to toluene (around 0.14 at 523 K) calculated from thermo-chemistry data without correction by fugacity coefficients.

Because of the branchiness introduced by the methyl group, the products formed from MCH contain significant amounts of isoalkanes. With their interconversions potentially possible, the identification of their major formation pathways is rendered difficult. Notably, the three major open-chain C_7 alkanes, i.e., 2- and 3-methylhexanes and n-heptane (2MH, 3MH, nHp), not only have their primary origins from MCH ring opening, but also have a potential likelihood to interconvert between each other via secondary skeletal isomerization. However, other C_7 alkanes with more than one side chain were formed only in trace amounts, and neopentane and neohexane were not even detected, suggesting the unaltered backbone of MCH and its primary products. Furthermore, it was noted in CH conversion that branched C_6 isomers were observed in marginal quantities on Ir/Al_2O_3 catalysts at all conditions studied (Chapter 3). Taken together, these facts have demonstrated the low isomerization activity of Ir [28], and have laid a sound foundation for establishing a simplified reaction network that encompasses a wide spectrum of products in MCH conversion.

4.3.3. Structure sensitivity of methylcyclohexane hydrogenolysis: rates of turnovers via endo- and exocyclic C−C bond cleavages

The conclusion that skeletal isomerization is a minor reaction channel at all conditions studied in this work facilitated the evaluation of initial formation rates of fragments and ROPs, as they can be considered to be produced exclusively from hydrogenolysis. Reaction rates and selectivities reported hereinafter are obtained upon extrapolation to zero contact time which rigorously precludes any contributions from secondary reaction kinetics. Figure 4-3a and b show the turnover frequencies (TOFs) for endo- and exocyclic C−C bond cleavages, respectively, of MCH at 523 K and 0.62 MPa H_2 over Ir/Al_2O_3 catalysts as a function of Ir dispersion. The rate for the exocyclic C−C bond cleavage represents the consumption rate of MCH via demethylation and thus equals the molar formation rate of cyclohexane (CH). The total conversion rate of MCH subtracting the exocyclic cleavage rate is taken as the endocyclic C−C bond cleavage rate.

As shown in Figure 4-3a, the rate of endocyclic C−C bond cleavage declined with decreasing Ir dispersion in a range corresponding to average Ir cluster sizes between 1 and 2 nm (D > 0.40), but increased thereafter when further decreasing Ir dispersion (D < 0.30). An analogous trend was observed in CH hydrogenolysis (Chapter 3). A recent work on MCH hydrogenolysis on Ir/Al_2O_3 catalysts disclosed an increase of TOF for MCH conversion with increasing Ir cluster size in the range of 1.5−3.0 nm [25]. In stark contrast to the endocyclic C−C bond cleavage, the rate of exocyclic C−C bond cleavage persistently increased with decreasing dispersion in the studied range (D = 0.035−0.65), and a significant boost emerged after Ir dispersion dropped below 0.40 (Figure 4-3b). Note that catalysts prepared from different precursors only revealed limited differences.

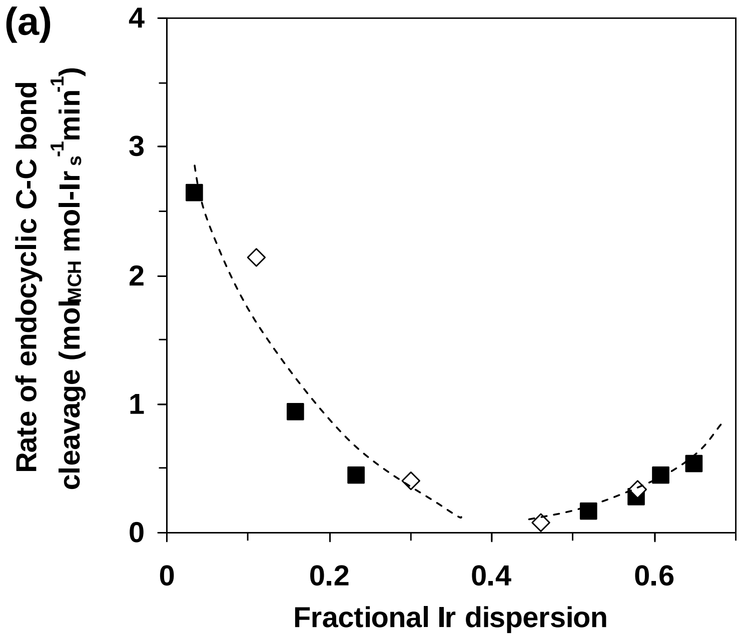

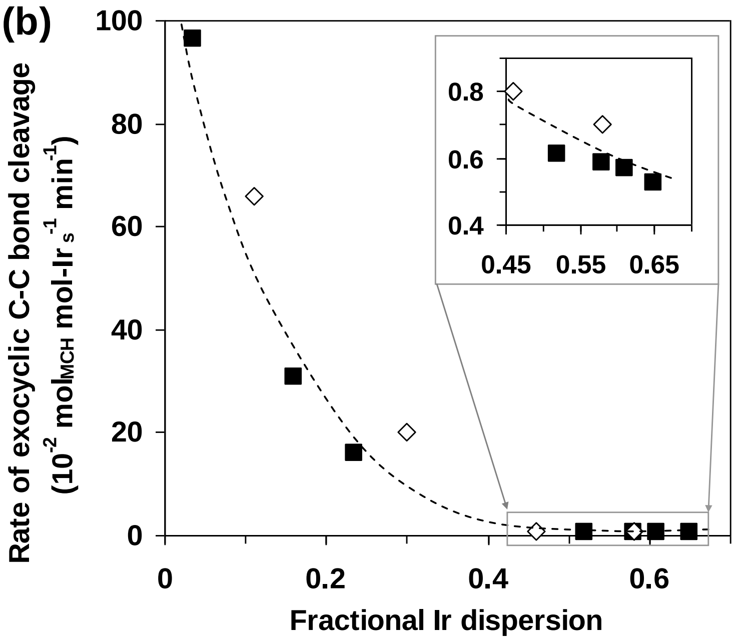

Figure 4-3. Apparent dispersion sensitivities of (a) endocyclic and (b) exocyclic C−C bond cleavage rates (based on the number of surface Ir atoms) of MCH on Ir/Al_2O_3 catalysts at 523 K, 1.2 kPa MCH and 0.63 MPa H_2. Filled squares: catalysts prepared from Cl-free precursor; empty diamonds: catalysts prepared from Cl-containing precursor. The inset of (b) is an enlarged vision of high-dispersion catalysts (D = 0.46−0.65) and shares the same abscissa and ordinate as the main window.

4.3.4. Product selectivities as a function of conversion and Ir dispersion

4.3.4.1. Primary and secondary pathways

Space velocities were varied to probe the kinetically primary and secondary nature of different C−C bond cleavage modes. The single-cleavage products comprise C_7 alkanes formed via ring opening (endocyclic) and CH via demethylation (exocyclic), both requiring C−C bond cleavage only once. The selectivity towards single-cleavage products decreased with increasing conversion, pointing to their mechanistically primary nature. Note that the decrease was smaller on large Ir clusters than on small clusters (Figures 4-4a and 4-5a). Chain alkanes that contain up to six carbon atoms can be formed either via

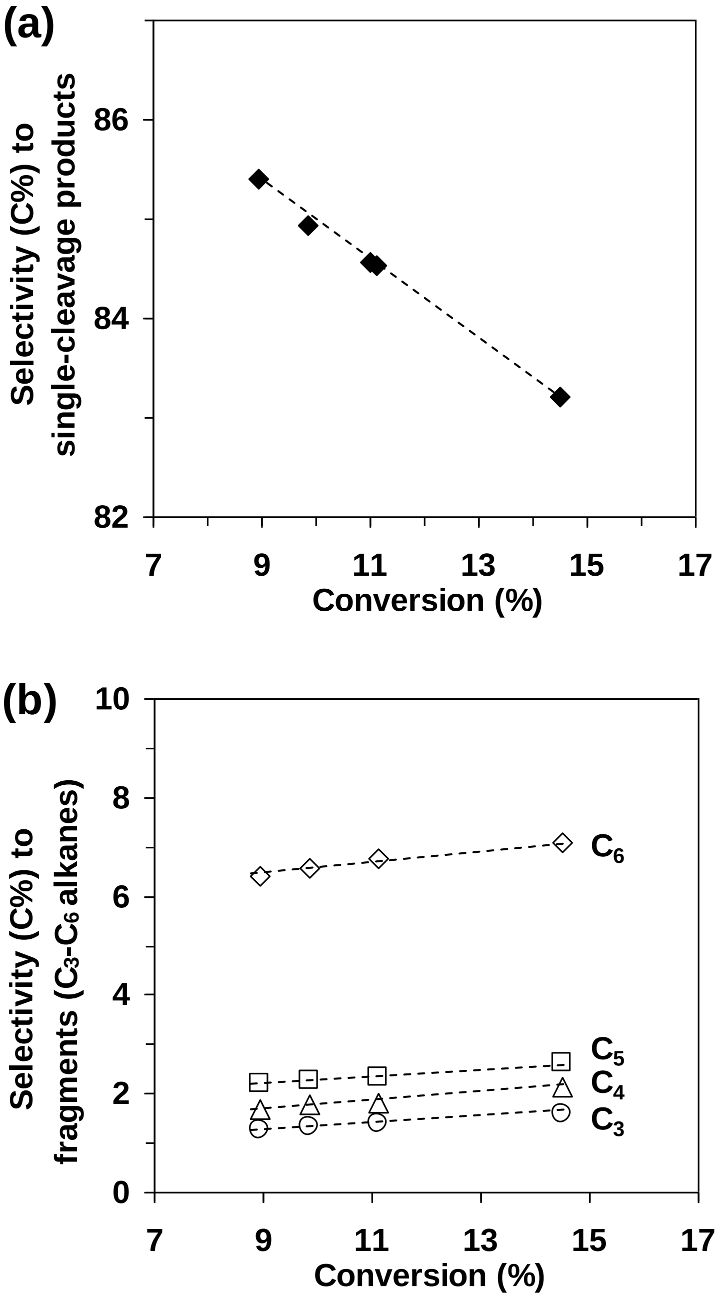

Figure 4-4. Combined selectivities to (a) products formed via a single cleavage of C–C bond (C_7-ROPs and the demethylation product, CH) and to (b) products formed via multiple C–C bond cleavages as a function of conversion over 0.50%Ir(0.61)-1/Al_2O_3 at 523 K, 1.2 kPa MCH and 0.37 MPa H_2. Methane and ethane are omitted for the sake of clarity.

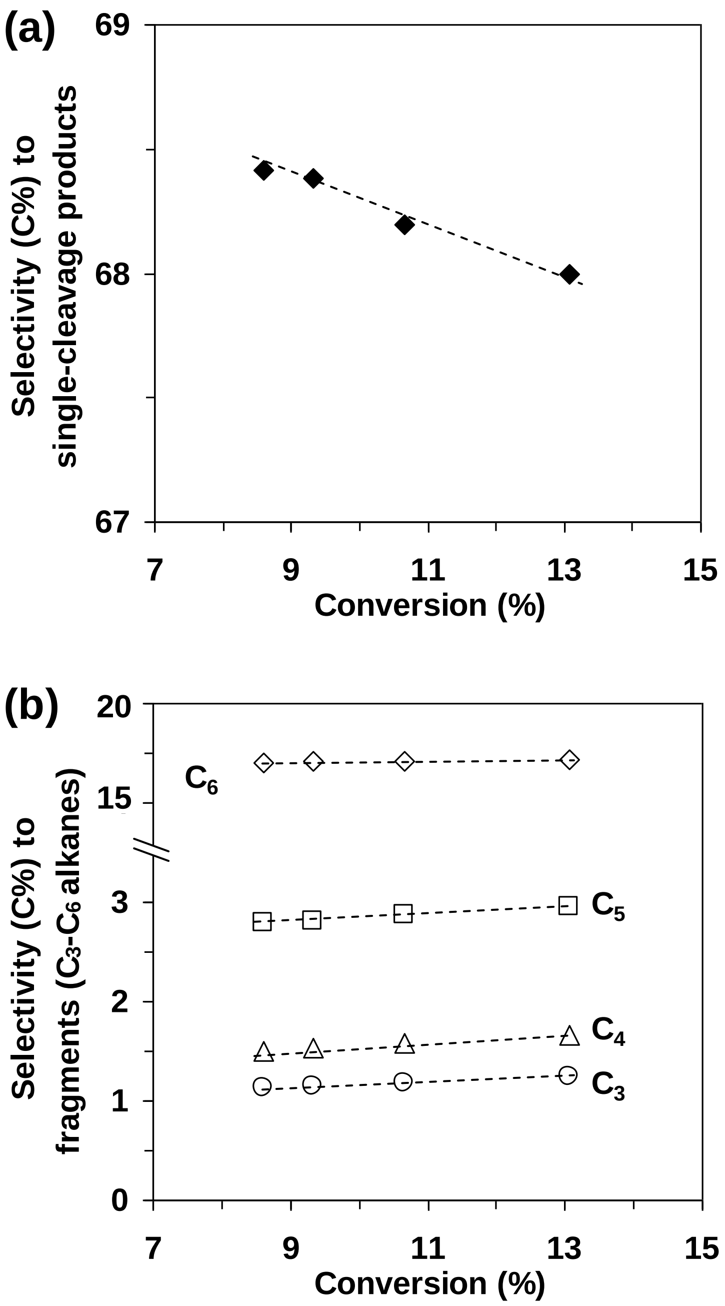

Figure 4-5. Combined selectivities to (a) products formed via a single cleavage of C–C bond (C_7-ROPs and the demethylation product, CH) and to (b) products formed via multiple C–C bond cleavages as a function of conversion over 0.50%Ir(0.16)-1/Al_2O_3 at 523 K, 1.2 kPa MCH and 0.37 MPa H_2. Methane and ethane are omitted for the sake of clarity.

multiple C−C bond cleavage during one surface sojourn of MCH, or via C−C bond cleavage of re-adsorbed primary products.

Small and large Ir clusters substantially differ in their preferences to the modes of multiple and secondary C−C bond cleavage. Over small Ir clusters (Figure 4-4b), the selectivities to $C_{<7}$ alkanes increased with increasing MCH conversion, indicating that a portion of these alkanes are produced via secondary reactions of re-adsorbed single-cleavage products. The formation of $C_{<7}$ alkanes via multiple C−C bond cleavage events of MCH during one surface sojourn seems also plausible as suggested by their low but non-zero intercepts. Over large Ir clusters (Figure 4-5b), the secondary reactions almost exclusively took paths to the formation of C_2−C_5 alkanes, while essentially bypassing the formation of hexanes. In principle, the intercepts and slopes (Figures 4-4 and 4-5) can be used to quantify the C−C bond cleavage selectivities in primary and secondary reactions, respectively. For instance, the selectivities to hexanes in primary multiple-cleavage reactions were estimated to be 5% and 17% on catalysts with fractional Ir dispersions of 0.61 and 0.16, respectively (Figures 4-4b and 4-5b).

4.3.4.2. Single-cleavage products: ring opening and exocyclic C−C bond scission

Due to the well-known preference of Ir-based catalysts to break the unsubstituted C−C bonds at endocyclic positions [1,5], the two methylhexanes (2MH and 3MH) are the major ROPs from MCH and n-heptane (nHp) is the minor ROP. Figures 4-6a and b show the ratios of 3MH/2MH and 3MH/nHp with varying MCH conversion over representative small and large clusters, respectively. The ratio of 3MH/2MH remained more or less invariant on both small and large Ir clusters over the studied range of conversion, indicative of similar rates of secondary reactions of re-adsorbed 3MH and 2MH (Figures 4-6a and b). In comparison, the ratio of 3MH/nHp increased with increasing conversion, particularly over small clusters, suggesting that nHp has a higher hydrogenolysis reactivity than 3MH. A comparison of data over catalysts with similar Ir dispersions but from different precursors shows that the nature of the precursor salt is not consequential to product selectivities, a fact that is further corroborated by more results shown in later sections.

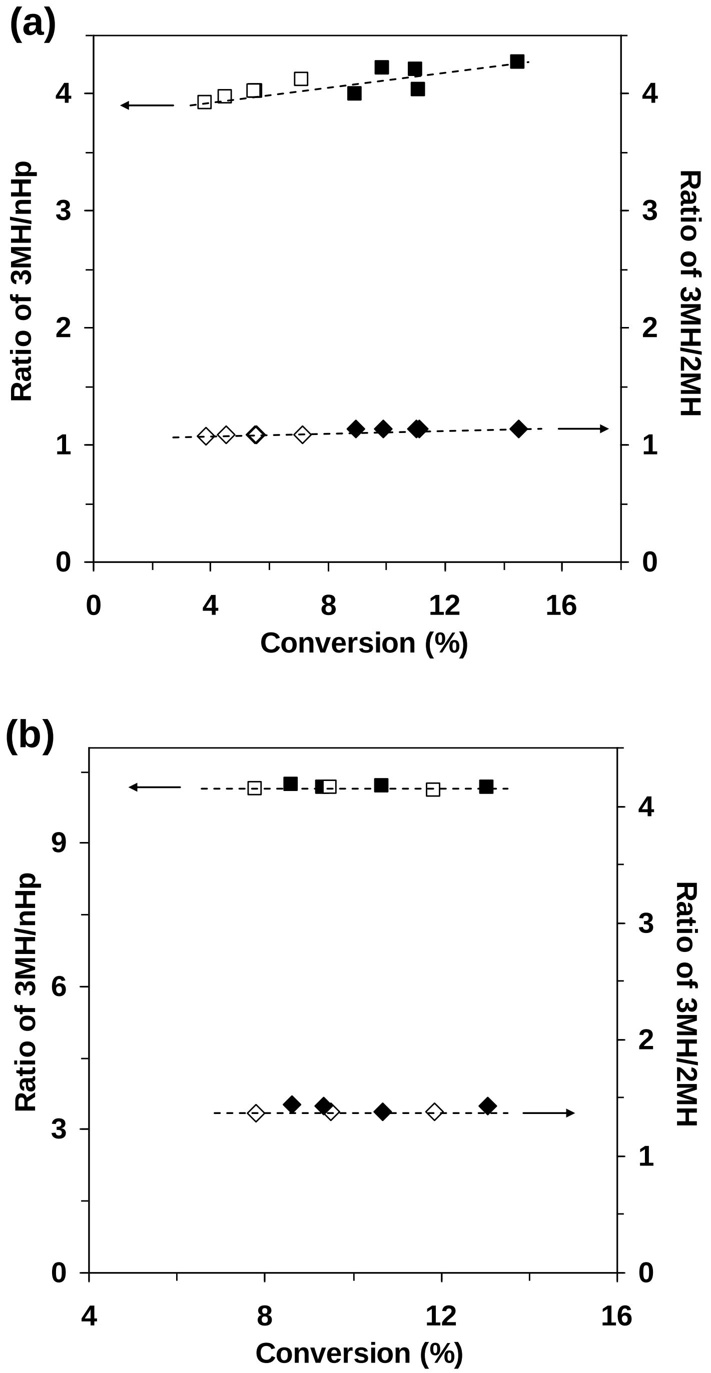

Figure 4-6. Selectivity ratios of 3MH/nHp (squares) and of 3MH/2MH (diamonds) as a function of MCH conversion over (a) small and (b) large Ir clusters at 523 K, 1.2 kPa MCH and 0.37 MPa H_2. Empty and filled symbols in (a) are 0.54%Ir(0.58)-2/Al_2O_3 and 0.50%Ir(0.61)-1/Al_2O_3, respectively; empty and filled symbols in (b) are 0.54%Ir(0.18)-2/Al_2O_3 and 0.50%Ir(0.16)-1/Al_2O_3, respectively.

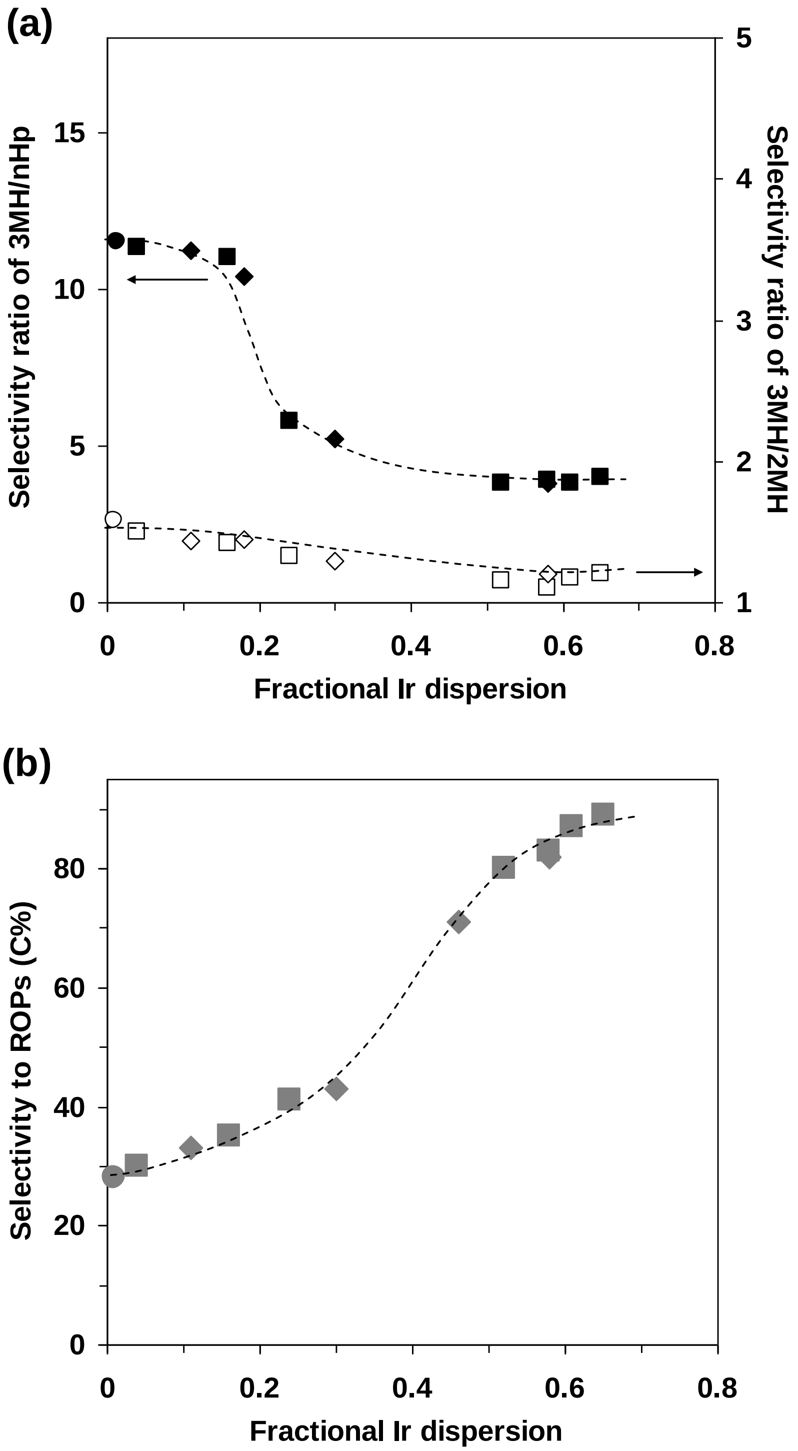

Figure 4-7. (a) Selectivity ratios between 3MH and 2MH (open symbols) and between 3MH and nHp (filled symbols) and (b) lumped selectivity to ROPs (grey symbols) as a function of Ir dispersion at 523 K, 1.2 kPa MCH and 0.37 MPa H_2 over Ir black (circles) and Ir/Al_2O_3 catalysts from Cl-free (squares) and Cl-containing (diamonds) precursors.

The selectivity ratio of 3MH/2MH slightly decreased with increasing Ir dispersion, i.e., from 1.6 over the largest Ir clusters to 1.1 over 1−2 nm clusters (Figure 4-7a). By contrast, the ratio between 3MH and nHp changed significantly with Ir dispersion in the middle range of dispersion and approached 11 and 4, respectively, over the largest and smallest Ir clusters at the given conditions. Note that these selectivity ratios (1.1−1.6 for 3MH/2MH and 4−11 for 3MH/nHp) are apparently different from the equilibrium values for 3MH-2MH and 3MH-nHp interconversions, which are 0.7 and 2.2 at 523 K, respectively, as calculated from the thermochemistry data of the relevant compounds. Decreasing the Ir dispersion resulted in a dramatic loss of selectivity to ROPs (Figure 4-7b), while increasing the selectivities to hexanes and CH.

The selectivity to the exocyclic C−C bond cleavage of MCH to form CH and methane is shown in Figures 4-8a and b as a function of MCH conversion and dispersion, respectively. Over small Ir clusters, the selectivity to exocyclic C−C bond cleavage remained low and decreased slightly with increasing conversion; over large clusters, the selectivity variation with conversion was almost indiscernible over the studied range (Figure 4-8a). Remarkably, the selectivity to the exocyclic C−C bond cleavage monotonically increased with lowering Ir dispersion, reaching more than 40% on the largest Ir clusters (Figure 4-8b). The selectivity trends with changing dispersion appeared closely similar between two types of Ir/Al_2O_3 catalysts prepared from Cl-free and Cl-containing precursors and between supported and unsupported Ir clusters of very large sizes (D = 0.011−0.035). The pronounced preference to exocyclic C−C bond cleavage on large Ir clusters is partly responsible for the more-than-50% selectivity gap between small and large clusters towards the formation of ROPs (Figure 4-7b).

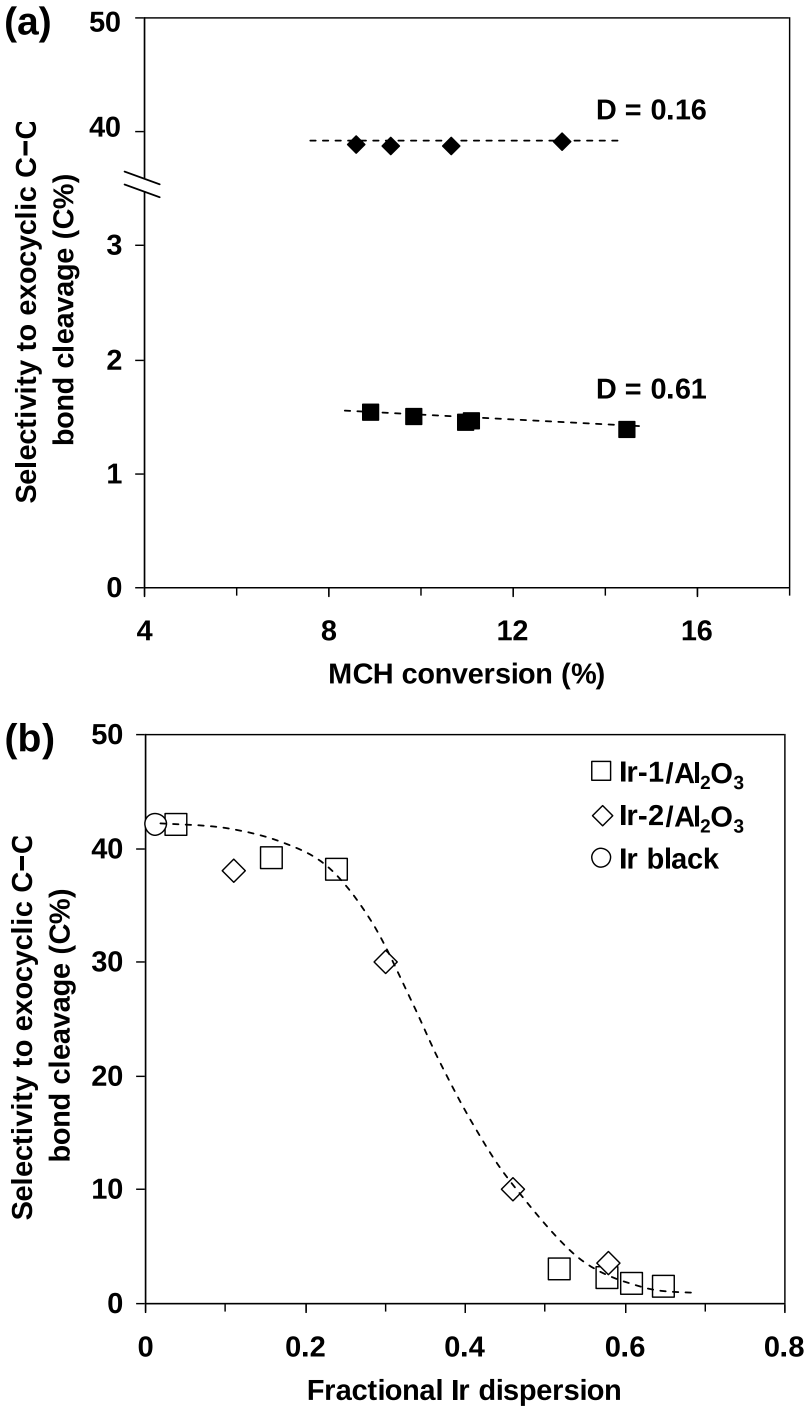

Figure 4-8. Selectivity to the exocyclic C−C bond cleavage (a) as a function of MCH conversion over 0.50%Ir(D)-1/Al_2O_3 catalysts with two dispersions of 0.61 (■) and 0.16 (♦) and (b) as a function of Ir dispersion at 523 K, 1.2 kPa MCH and 0.37 MPa H_2 over Ir/Al_2O_3 catalysts prepared from Cl-free (□) and Cl-containing (◊) precursors and over a commercial Ir black (○).

4.3.4.3. Multiple-cleavage products

Along kinetically primary pathways, C_2−C_6 alkanes (and a portion of methane) are termed as multiple-cleavage products. Hexanes and C_2−C_5 alkanes are defined as "terminal" and "internal" multiple-cleavage products, respectively, each term referring to the position of the cleaved C−C bond in the C_7 ROPs before desorption.

As shown in Figure 4-9a, the selectivity to terminal multiple-cleavage increased with decreasing Ir dispersion, reaching 19% on the largest Ir particles at the indicated condition. Analogous to that exhibited in CH hydrogenolysis, the selectivity to internal multiple-cleavage remained relatively constant with changing dispersion, and was comparable to that of terminal multiple-cleavage on small clusters (Figure 4-9b). Table 4-1 summarizes the product distributions within ROPs and within hexanes that are formed via terminal multiple-cleavage of the ring-opened C_7-intermediates. Over small clusters (D = 0.52−0.65), the product distributions within each of C_6 and C_7 fractions are very close among different catalysts. With decreasing Ir dispersion below D = 0.30, the percentage of nHp in C_7 alkanes decreases from 10% to 5%. The selectivity to n-hexane (nHx) in C_6 alkanes is the highest (i.e., 19%) on the largest Ir clusters of D = 0.035. While the selectivity of 3MH is higher than that of 2MH in C_7 alkanes, 2MP is the main product within C_6 alkanes in all cases.

Concerning the various routes of multiple hydrogenolyses, hexanes with methane, pentanes with ethane and butanes with propane would be three groups of "pairing" fragments if successive scissions do not occur on Ir. Indeed, regardless of the cluster size, pentanes/ethane and butanes/propane pairs substantially equal in terms of their molar formation rates (Figure 4-10). Methane forms at a higher molar rate than hexanes (by at most a factor of 1.5) apparently owing to the demethylation and, to lesser extents, successive scissions. It is important to note that branched $C_{<7}$ alkane products must be formed from C−C bond scissions of the ring-opened intermediates relevant to 2MH and 3MH formation, while the linear alkanes may originate from either MHs or nHp. In addition, for simplicity, we have ascribed the formation of $C_{<7}$ alkanes (except for a portion of methane) to the multiple cleavages of endocyclic C−C bonds in MCH, as it is shown that the exocyclic single-cleavage product CH is much less reactive than the ROPs at least on small Ir clusters (Figure 4-7a). Nevertheless, with an increasing extent of the exocyclic cleavage pathway with decreasing Ir dispersion, the CH concentration at the surface would progressively increase and if followed by C−C bond rupture of CH, yet to desorb, might open up another formation pathway for nHx.

Table 4-1. Product distribution within C_6- and C_7-fractions over Al_2O_3-supported Ir clusters. Reaction conditions: 523 K, 1.2 kPa MCH and 0.37 MPa H_2, conversions < 10%.

D_{Ir}[a]	Percentage within C_6-alkanes (%)			Percentage within C_7-alkanes (%)		
	2MP	3MP	nHx	2MH	3MH	nHp
0.65-1	55	36	9	41	47	12
0.61-1	57	36	7	42	47	11
0.58-1	57	36	7	42	47	11
0.58-2	55	37	8	42	47	11
0.52-1	56	37	7	41	47	12
0.30-2	47	41	12	39	51	10
0.24-1	47	40	13	39	52	9
0.16-1	47	41	12	40	55	5
0.035-1	42	39	19	40	55	5

[a] The number before the hyphen denotes the fractional Ir dispersion and that following the hyphen denotes the type of Ir/Al_2O_3 prepared from a Cl-free precursor (as 1) or a Cl-containing precursor (as 2).

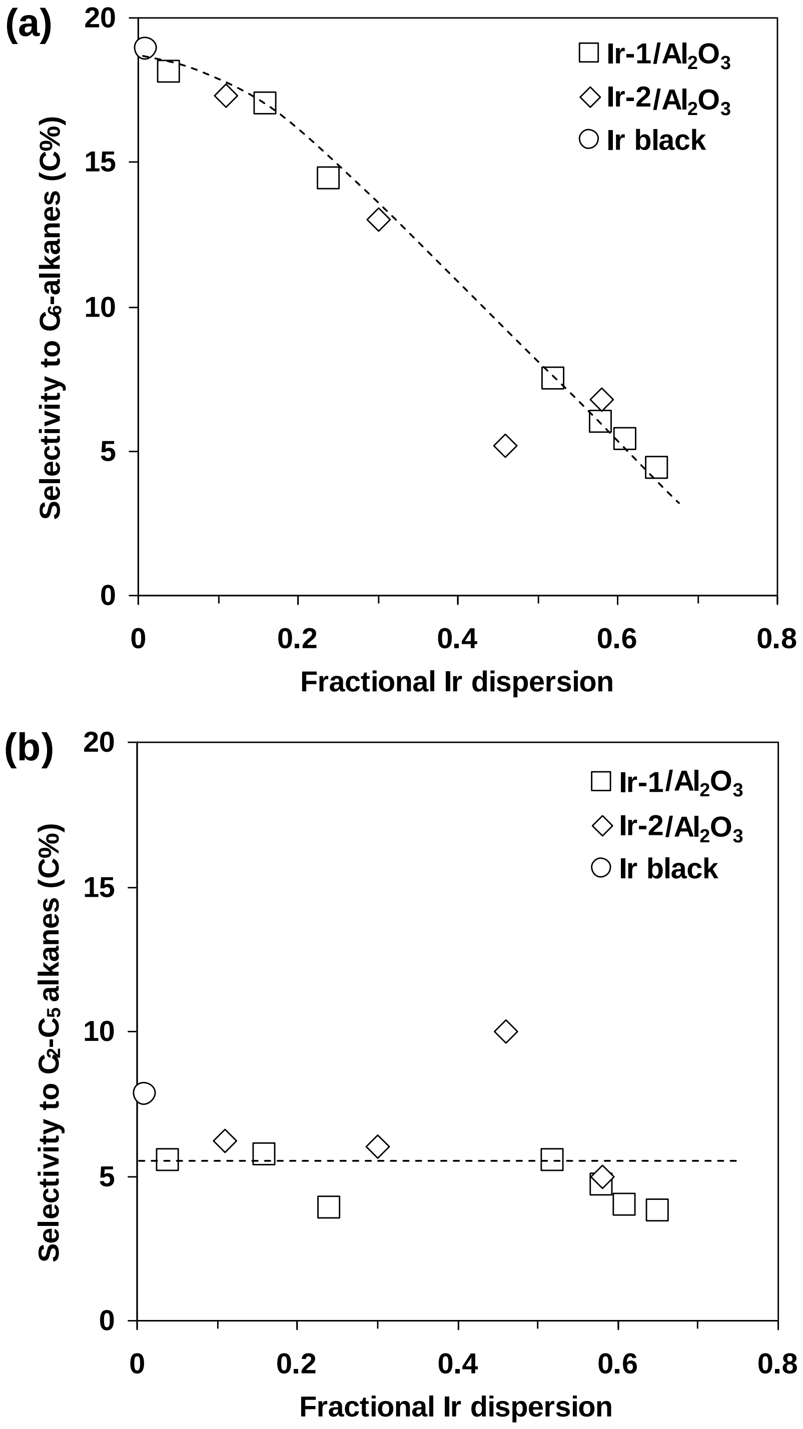

Figure 4-9. Initial selectivities to (a) hexanes and (b) C_2−C_5 alkanes in MCH hydrogenolysis as a function of Ir dispersion at 523 K, 1.2 kPa MCH and 0.37 MPa H_2 over Ir/Al_2O_3 catalysts prepared from Cl-free (□) and Cl-containing (◊) precursors and over a commercial Ir black (○).

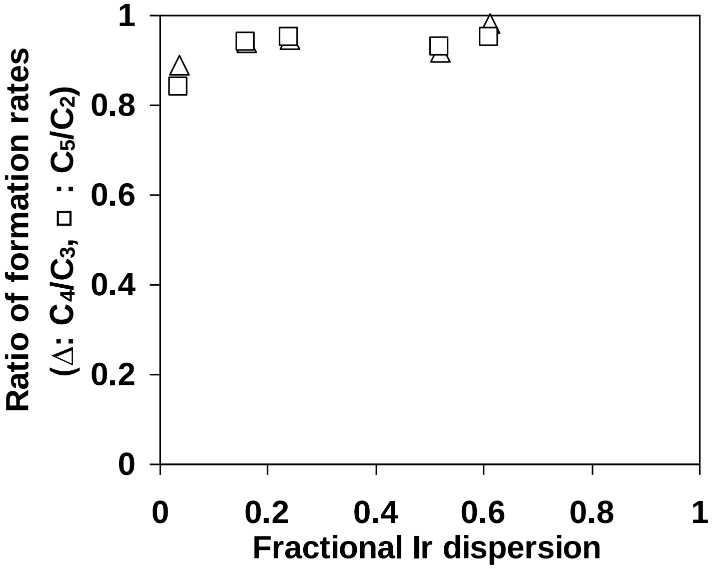

Figure 4-10. The ratios of formation rates between C_4 alkanes and propane (Δ) and between C_5 alkanes and ethane (□) over 0.50%Ir/Al_2O_3 catalysts of varying dispersion. Reaction conditions were 523 K, 0.37 MPa H_2, 1.2 kPa MCH.

4.3.5. H_2 pressure dependences of rates and selectivities over Ir clusters of different sizes

Figure 4-11 shows the H_2 pressure effect on the rates of endocyclic and exocyclic C−C bond cleavage, as well as their ratios, on small Ir clusters (D = 0.52−0.65). For small clusters with broadly differing activities, the maximum TOFs for endocyclic C−C bond cleavage seem to invariably appear at similar H_2 pressures around 0.3 MPa (Figure 4-11a). The activity ratios among different catalysts that contain small clusters remain essentially identical at any given H_2 pressure (not shown), indicating closely resembled curvatures of H_2-pressure dependences of TOFs for all of these small clusters regardless of their relative magnitude of activity. In comparison with the endocyclic C−C bond cleavage, exocyclic cleavage rates are closer on small Ir clusters of different dispersions and exhibit lower optimum H_2 pressures (Figure 4-11b), which were not accessed in the studied range (0.2−1.0 MPa). The ratios between endocyclic and exocyclic C−C bond cleavages increase with H_2 pressure and Ir dispersion, leveling off at H_2 pressures higher than 0.5 MPa for every high-dispersion catalyst (inset of Figure 4-11b).

Figure 4-12 shows the H_2 pressure effect on the rates of endocyclic and exocyclic C−C bond cleavage, as well as their ratios, on large Ir clusters (D = 0.035−0.24). For large clusters, the H_2 pressure for maximum rates of endocyclic C−C bond cleavage shifted to higher values than those on small clusters (Figure 4-12a). Moreover, the curvatures of TOF-H_2 pressure functions flatten compared to those exhibited by small clusters. Note that these features bear resemblance to those shown in CH hydrogenolysis (see Chapter 3). On the other hand, exocyclic C−C bond cleavage rates are higher on large Ir clusters than on small clusters and increase with decreasing dispersion at all H_2 pressures (Figure 4-12b). Optimum H_2 pressures for the exocyclic cleavage were below the low-limit of the studied pressure range (0.37−1.0 MPa). The ratios of endocyclic-to-exocyclic C−C bond cleavage are much lower on large clusters than on small clusters and increase consistently with H_2 pressure, showing parallel values on large Ir clusters of different average sizes at any given conditions (inset of Figure 4-12b). The reaction order with respect to MCH partial pressure is smaller on low-dispersion catalysts ($D < 0.20$) than on high-dispersion ones ($D > 0.50$), and the increase in H_2 pressure is accompanied by an increase in the reaction order for all cluster sizes (Figure 4-13). The much less negative reaction orders in H_2 and the less positive orders in MCH suggest, respectively, lower surface coverages of H_2-derived species and higher coverages of MCH-derived species on large clusters.

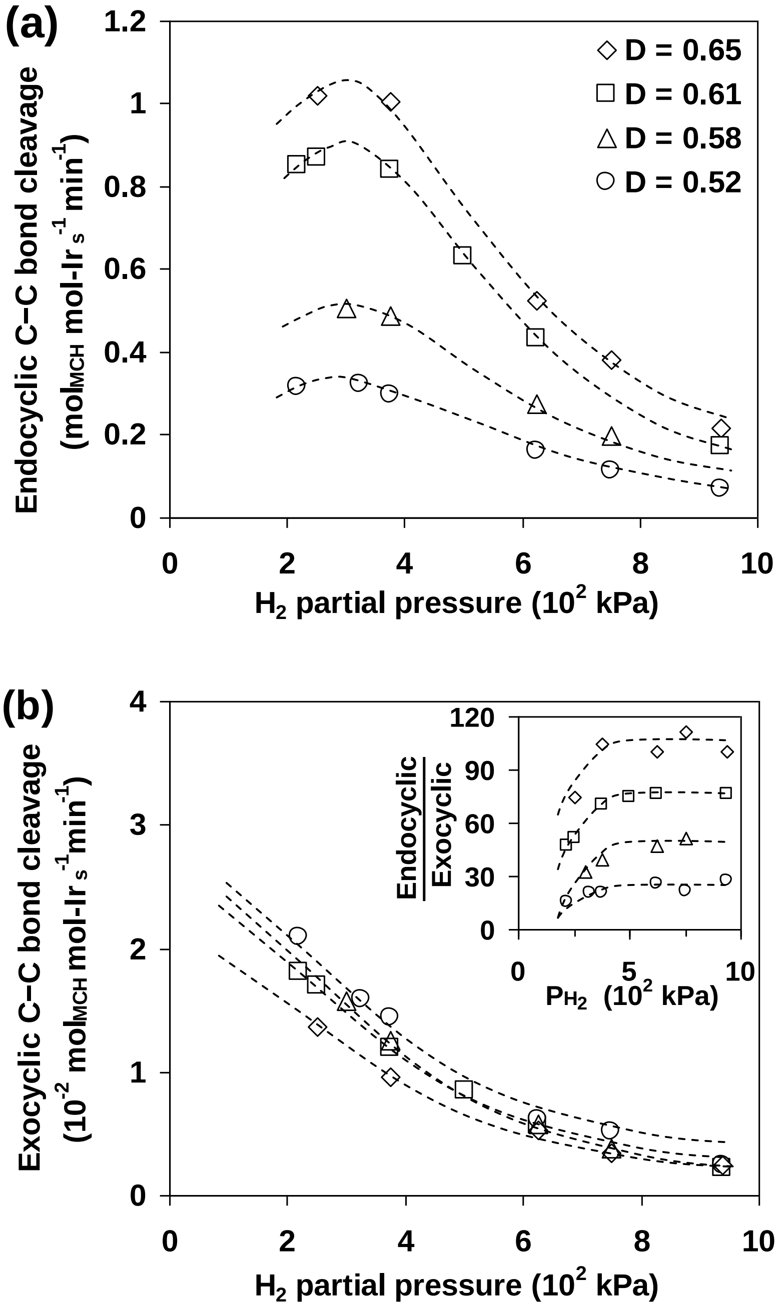

Figure 4-11. Dependences of (a) endocyclic and (b) exocyclic C−C bond cleavage rates on H_2 partial pressure in MCH hydrogenolysis over small Ir clusters (D = 0.52−0.65) at 523 K and 1.2 kPa MCH. Rates are normalized to the number of surface Ir atoms. The inset of (b) shows the ratio between rates of endocyclic and exocyclic C–C bond cleavage as a function of H_2 pressure. Symbols represent: D = 0.65 (diamond), D = 0.61 (square), D = 0.58 (triangle) and D = 0.52 (circle).

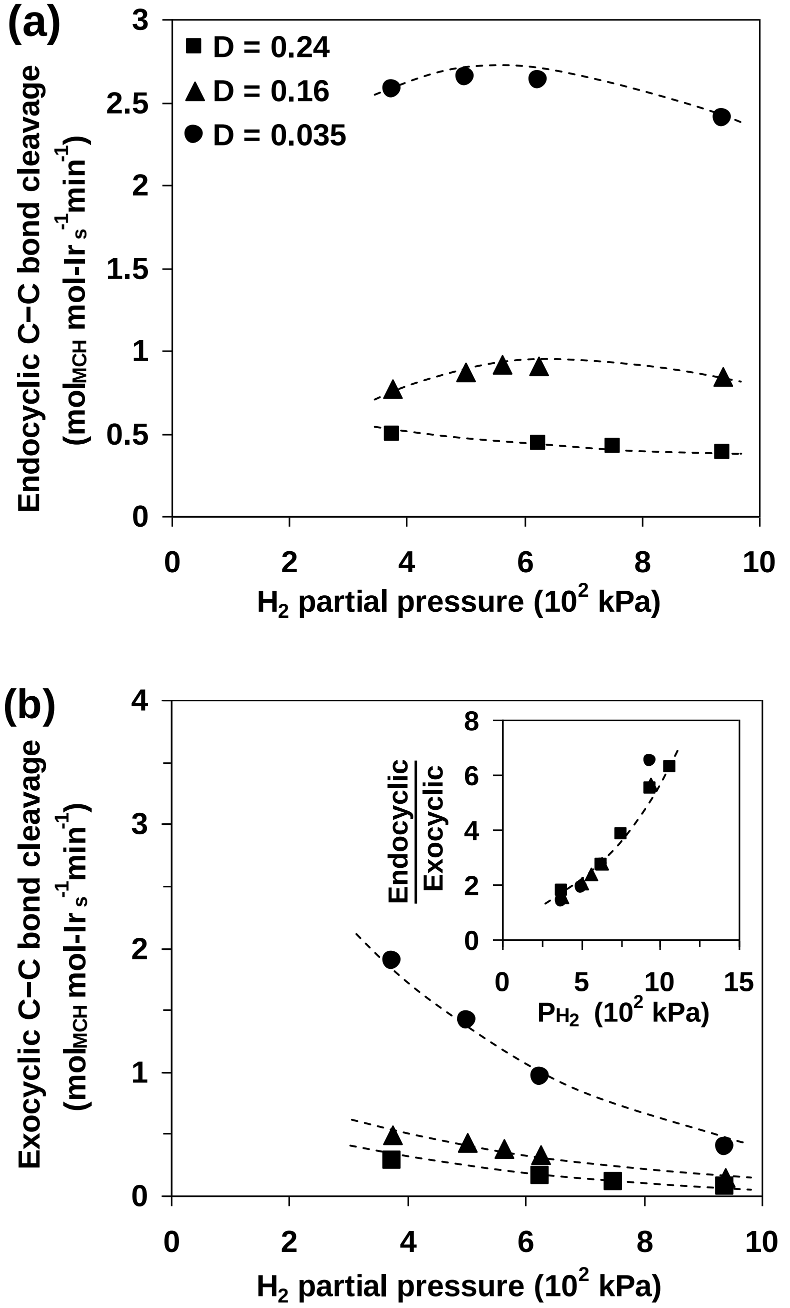

Figure 4-12. Dependences of (a) endocyclic and (b) exocyclic C−C bond cleavage rates on H_2 partial pressure in MCH hydrogenolysis at 523 K and 1.2 kPa MCH over larger Ir clusters (D = 0.035−0.24). Rates are normalized to the number of surface Ir atoms. The inset of (b) shows the ratio between rates of endocyclic and exocyclic C–C bond cleavage as a function of H_2 pressure. Symbols represent: square (D = 0.24), triangle (D = 0.16) and circle (D = 0.035).

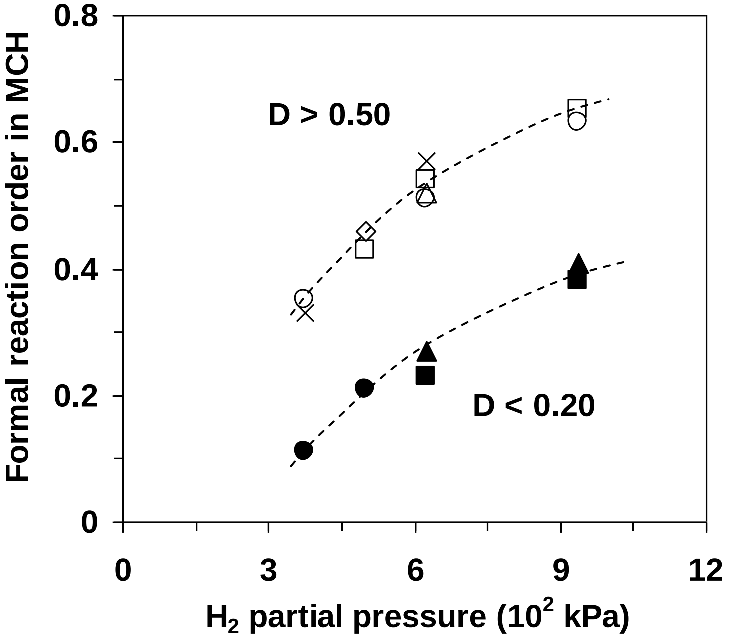

Figure 4-13. Formal reaction order in MCH as a function of H_2 pressure on small (open symbols) and large (closed symbols) Ir clusters at 523 K and 0.9−1.6 kPa MCH.

Figure 4-14 illustrates the formation rates of three ROPs as a function of H_2 pressure over two Ir/Al_2O_3 catalysts that contain typically small and large clusters, respectively. On small clusters (D = 0.61), formation rates of all ROPs exhibited similar optimum H_2 pressures (Figure 4-14a), whereas on large clusters (D = 0.16), the formation rate of 3MH peaked at a much higher H_2 pressure than those of 2MH and nHp (Figure 4-14b). When the relative ratios between ROPs were compared (Figure 4-15), both 3MH/nHp and 3MH/2MH remained fairly constant with varying H_2 pressures over small clusters (D > 0.50), in contrast to the increasing trends of both ratios, particularly 3MH/nHp, with increasing H_2 pressure over large clusters (D < 0.20). Consequently, on large Ir clusters, the increase in H_2 pressure imposed a detrimental effect on the selectivity to nHp, the non-branched ROP via C−C bond cleavage at the sterically hindered position. The selectivity to nHp on large clusters (1−5%) was under all conditions lower than that (10−15%) over the higher-dispersion ones on which the variation of H_2 pressure only induced slight changes to nHp selectivity.

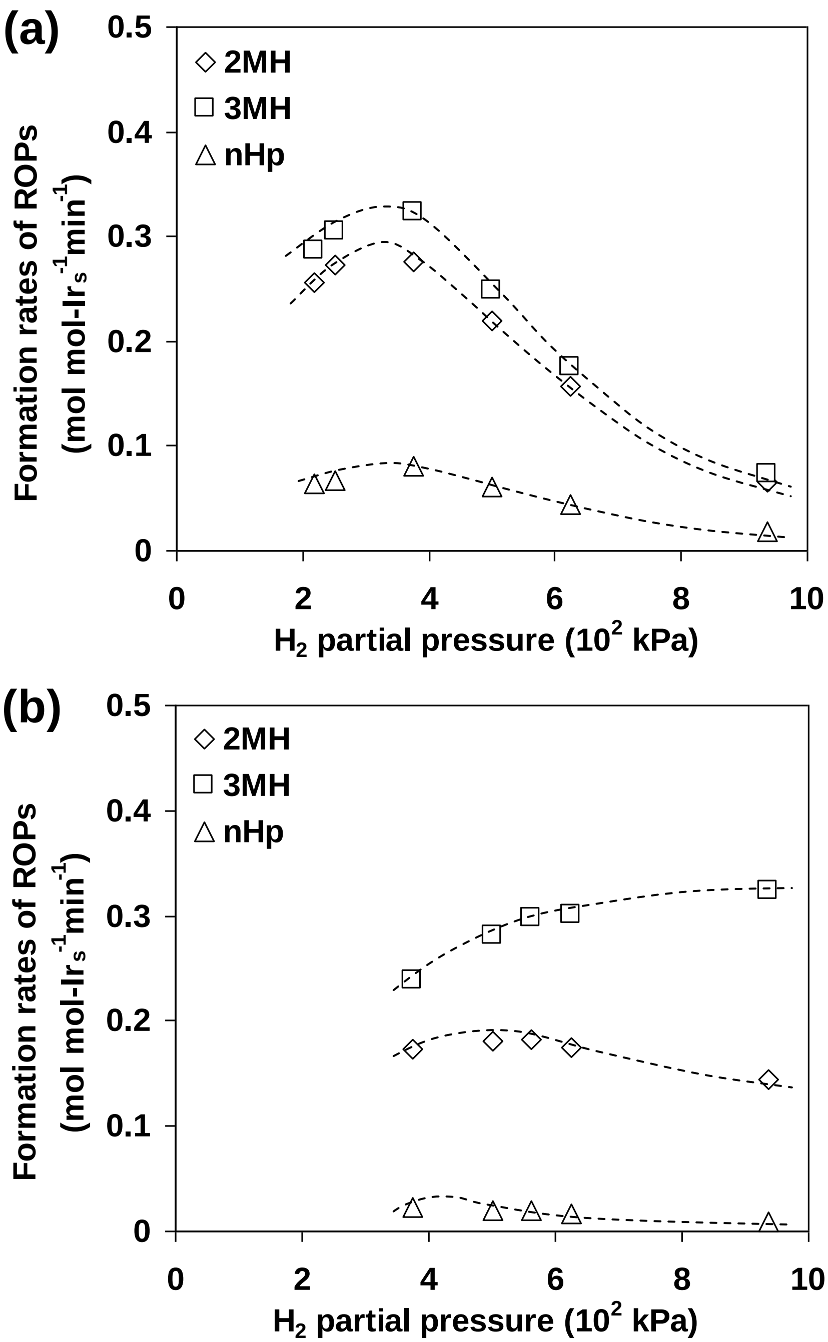

Figure 4-14. Dependences of formation rates of three ROPs from MCH on H_2 pressure over typical (a) small (D = 0.61) and (b) large (D = 0.16) clusters at 523 K, 1.2 kPa MCH.

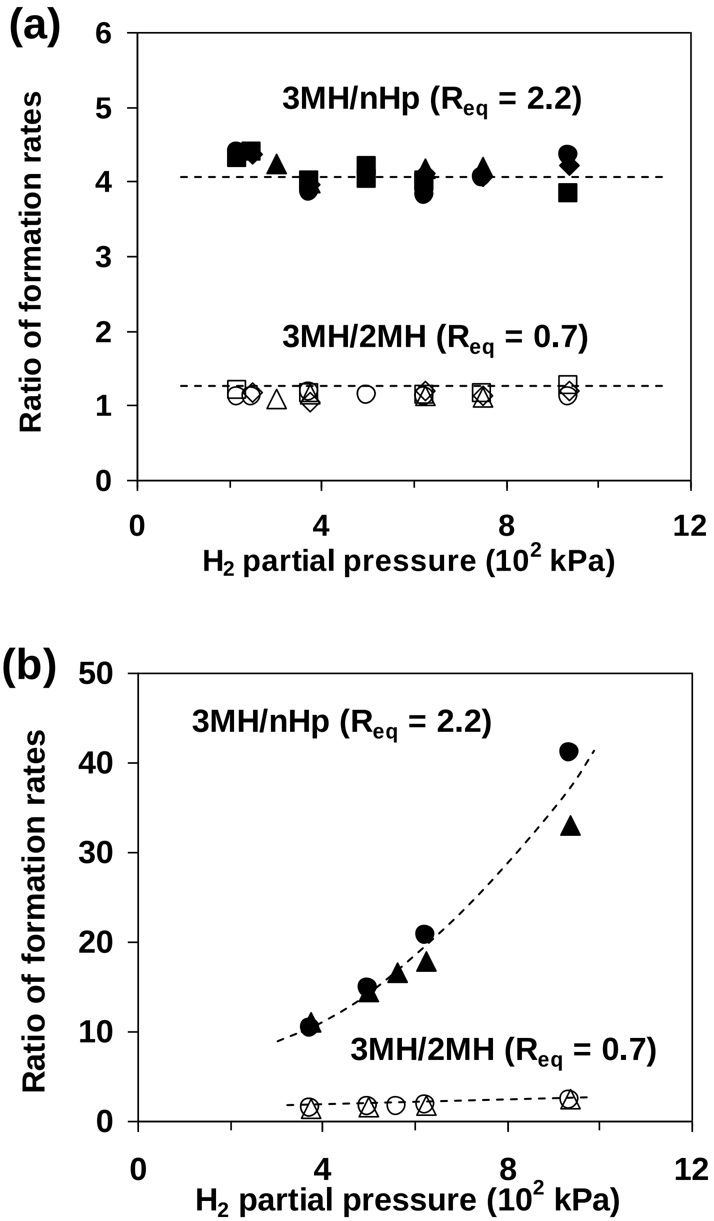

Figure 4-15. The ratios between the formation rates of two methylhexanes (3MH/2MH, filled symbols) and between rates of cleavages at the least-hindered and the most-hindered position (3MH/nHp, open symbols) on (a) small (D > 0.50) and (b) large (D < 0.20) Ir clusters at 523 K, 1.2 kPa MCH. Equilibrium ratios of 3MH/2MH and 3MH/nHp at 523 K are indicated alongside the curves.

The effects of H_2 pressure on the product selectivities on small and large clusters are summarized in Figure 4-16. The selectivity towards ROPs increased with increasing H_2

pressure over both small and large Ir clusters (Figure 4-16a). There was a significant selectivity gap in selectivity of ROPs between small and large clusters, due to the higher extents of exocyclic C−C bond cleavage and terminal multiple-cleavage on large Ir clusters (Figures 4-16b−c). Over small Ir clusters, the selectivities to products formed via exocyclic and multiple C−C bond cleavages were all suppressed by the increase in H_2 pressure (Figures 4-16b−d). By contrast, the terminal multiple-cleavage, which yielded hexanes and a portion of methane, was enhanced by H_2 pressure increase on catalysts containing large Ir clusters (Figure 4-16c). Moreover, the suppression effect of H_2 pressure on the exocyclic C−C bond cleavage was much stronger on large clusters (Figure 4-16b).

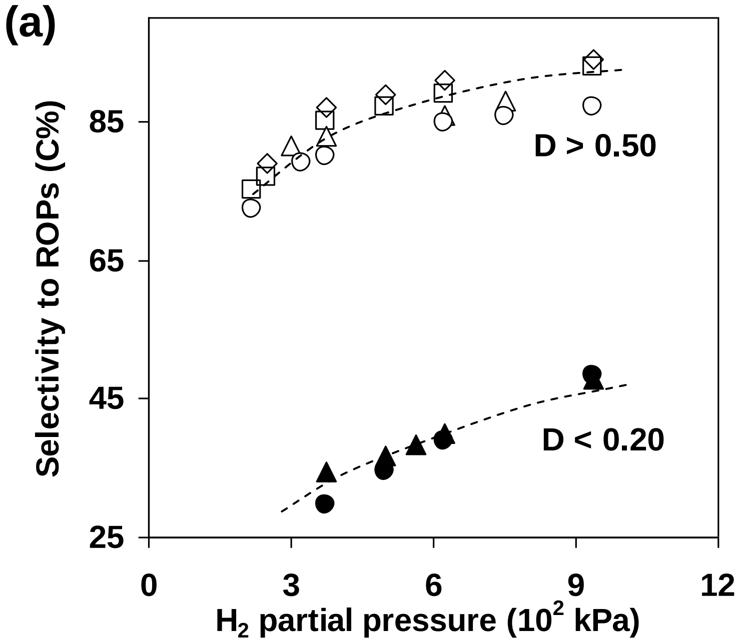

Figure 4-16. Initial selectivities to (a) ROPs, (b) cyclohexane, (c) hexanes and (d) lumped C_2-C_5 alkanes as a function of H_2 pressure over small (D > 0.50, open symbols) and large Ir clusters (D < 0.20, filled symbols) at 523 K, 1.2 kPa MCH.

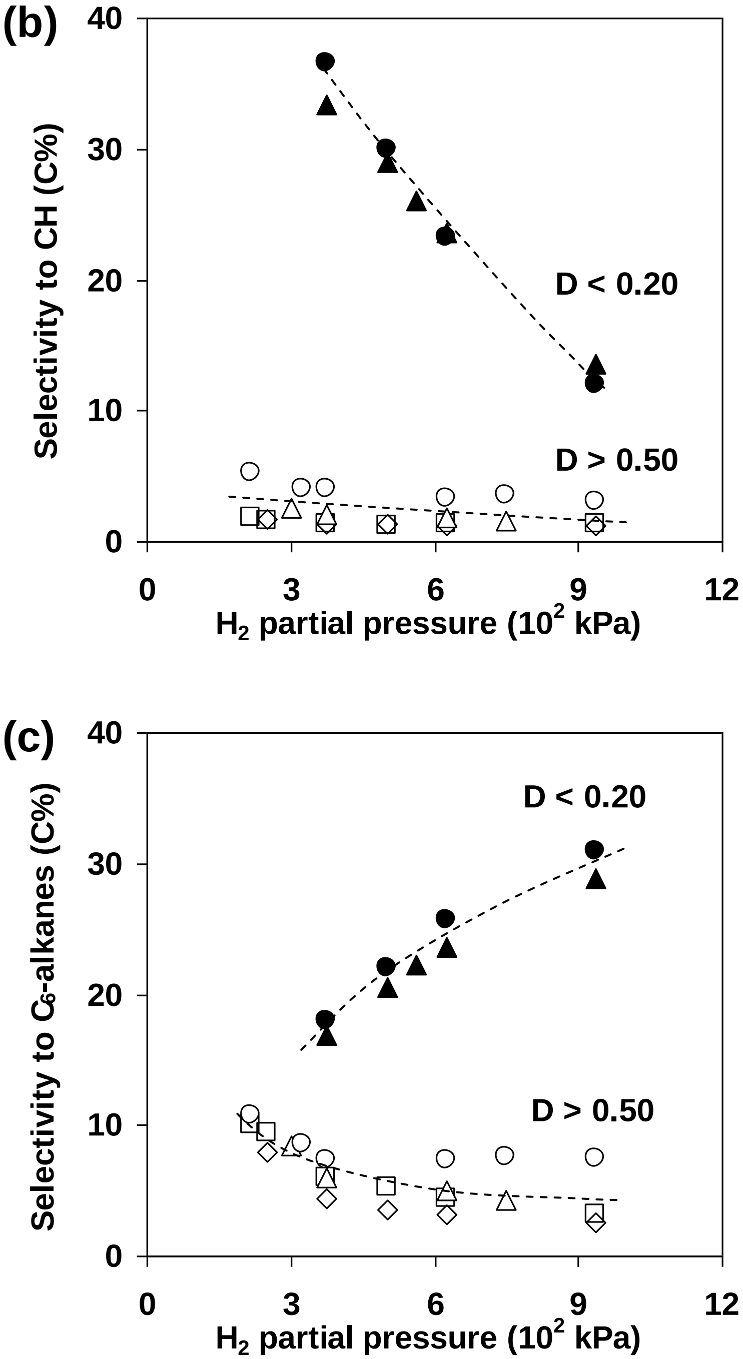

Figure 4-16. (continued)

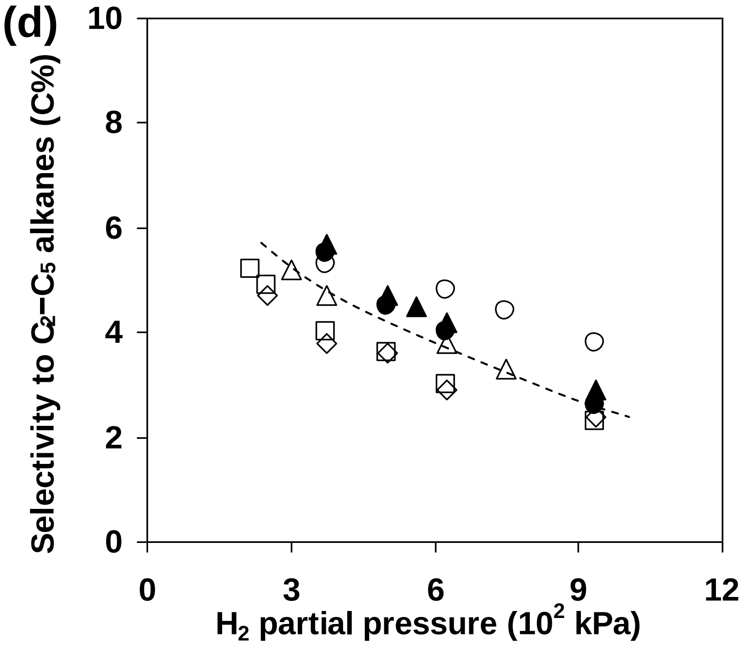

Figure 4-16. (continued)

4.3.6. Temperature dependences of rates and selectivities over Ir clusters of different sizes

Table 3-2 summarizes the apparent activation energies ($E_{a,app}$) for separate product formation routes at varying H_2 pressures over small and large Ir clusters. The increase in H_2 pressure typically elevates the $E_{a,app}$ for all C−C bond cleavage routes. The effect of Ir cluster size is more intricate and differs among various cleavage modes. Within the ROPs, the nHp formation is characterized by a higher $E_{a,app}$ than MHs formation. This is particularly so on large Ir clusters, revealing a difference in activation energy of 80−100 kJ mol^{-1} for nHp and MHs. The cluster size does not influence the $E_{a,app}$ for nHp formation to a substantial extent. In contrast, the apparent energies of activation for the formation of MHs are significantly smaller on large Ir clusters than on small ones at the same reaction conditions. For instance, at H_2 pressure of 0.63 MPa, the $E_{a,app}$ for 2MH formation is 155 kJ mol^{-1} on high-dispersion catalysts, while being ca. 100 kJ mol^{-1} on low-dispersion catalysts. The activation energy is always smaller for 3MH than for 2MH, regardless of the prevalent cluster size and H_2 pressure. On small clusters, the exocyclic

Table 4-2. Apparent activation barriers ($E_{a,app}$) for MCH hydrogenolysis (demethylation, ring opening and multiple C−C bond cleavages), measured at comparable conversions below 5%.

Catalysts	P_{H_2} (bar)	$E_{a,app}$ (kJ mol^{-1})[a]						
		Single cleavage				Multiple cleavage		
		CH	2MH	3MH	nHp	C_6	C_5	C_4
Ir(0.61)-1	5.0	154	138	135	144	155	190	193
	6.3	164	155	150	156	184	226	230
	9.4	171	183	176	185	212	–[b]	–[b]
Ir(0.52)-1	3.7	146	120	112	144	150	183	188
	6.3	182	155	146	166	161	208	210
	9.4	205	183	165	188	170	–[b]	–[b]
Ir(0.18)-2	3.7	135	103	88	147	117	125	158
	6.3	159	106	85	172	120	–[b]	–[b]
Ir(0.16)-1	3.7	140	90	82	140	101	107	150
	5.0	162	103	91	160	108	170	–[b]
	6.3	162	102	84	156	107	177	–[b]
Ir(0.035)-1	6.3	185	107	86	180	111	184	–[b]

[a] Reaction conditions were 1.2 kPa MCH and 513−543 K; these reported values, with maximum errors of ± 7 kJ mol^{-1} for pentanes and butanes, ± 5 kJ mol^{-1} for hexanes and n-heptane, and ± 3 kJ mol^{-1} for methylhexanes and cyclohexane, were derived by taking the slopes from semilogarithmic Arrhenius plots of formation rates of different products as a function of reciprocal temperature.

[b] Not reliable, since these values are overestimated due to the inaccuracy of the rates measured at lower temperatures.

C−C bond cleavage (demethylation to form CH) shows similar or slightly higher $E_{a,app}$ to those of the 2MH and nHp. On large clusters, the activation energy for CH formation is slightly lower than that of nHp and much higher than that of the MHs. On small clusters, the formation of $C_{<7}$ alkanes via multiple C−C bond cleavages typically exhibits larger $E_{a,app}$ values than those of the MHs. The internal multiple-cleavage (yielding C_2 to C_5

alkanes) has higher activation energies than that of terminal multiple-cleavage (yielding hexanes). On large clusters, the apparent activation energy for terminal multiple-cleavage drops to a value very close to those of the MHs, i.e. ca. 100 kJ mol^{-1}. Due to the generally lower $E_{a,app}$ for MHs (the main components of ROPs) than the other products, the selectivity to ROPs declines with increasing reaction temperature over both low- and high-dispersion catalysts (Figure 4-17a). The significantly greater $E_{a,app}$ for demethylation than those for ring opening on low-dispersion catalysts accounts for the drastic increase in CH selectivity with increasing temperature (Figure 4-17b).

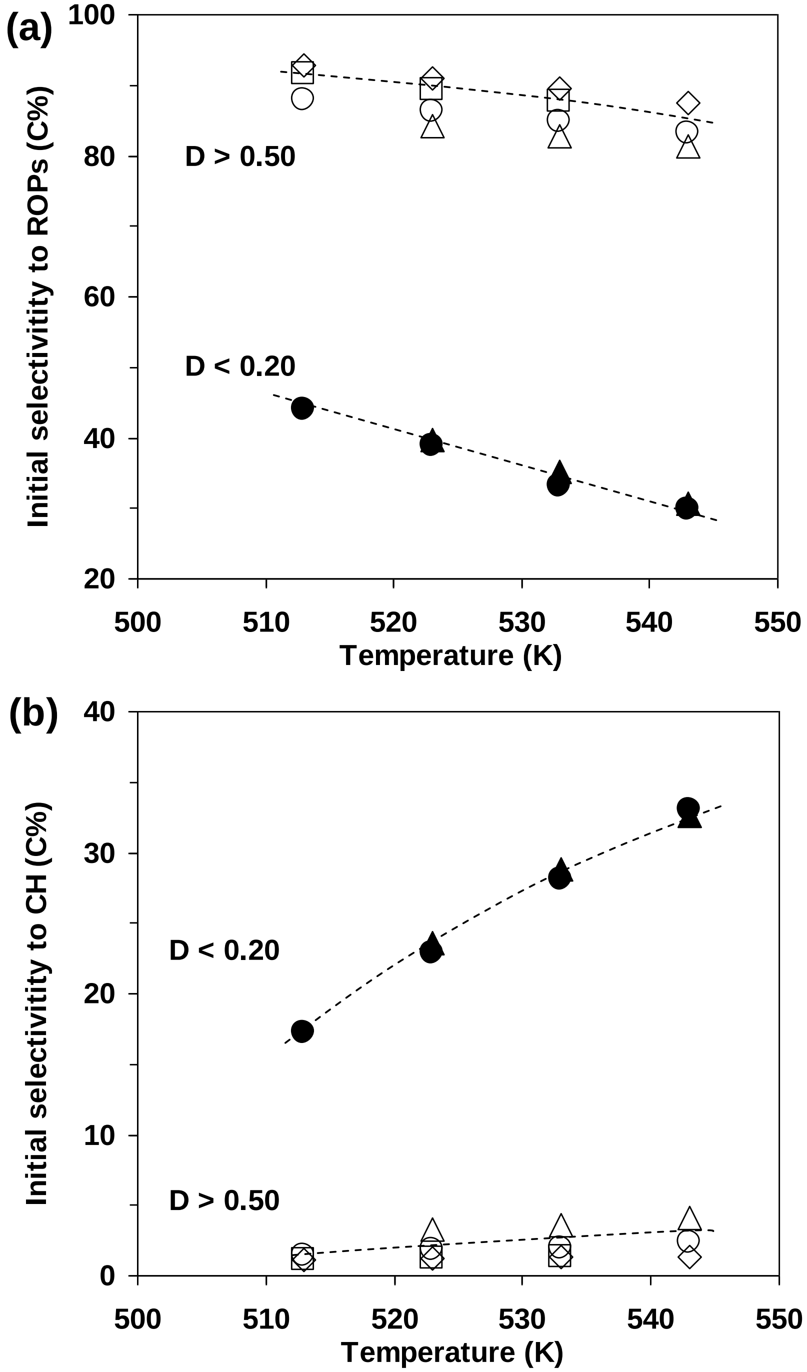

Figure 4-17. Effect of reaction temperature on the initial selectivities to (a) ROPs and (b) cyclohexane over small (open symbols) and large (filled symbols) Ir clusters at 1.2 kPa MCH, 0.62 MPa H_2.

4.3.7. Kinetic simulation based on a classical mechanistic model

We have discussed in the previous chapter the microscopic considerations in the kinetic modeling of CH hydrogenolysis rates over both small and large Ir clusters. These concerns apply also to the MCH hydrogenolysis. A full repetition of them is unnecessary, but the major assumptions adopted are described as follows. Briefly, the classical mechanism involves quasi-equilibrated steps of H_2 and hydrocarbon activation, an irreversible C–C bond rupture rate-determining step (RDS), and kinetically insignificant re-hydrogenation and desorption steps. It is implied in kinetic treatments that the most abundant surface intermediates are directly involved in the primary reaction pathways. The most reasonable C–C bond splitting agent in the RDS was found to be an adsorbed H-atom [4] (also see Chapter 3). After specifying that the active site contains two metal atoms to bind the pair of C–C bond in MCH, the above assumptions lead to the following equation for the turnover rate of MCH hydrogenolysis in terms of H_2, MCH pressures and of the rate or equilibrium constants for the relevant elementary steps (see Appendix in Chapter 3 for derivation of the kinetic equation):

$$r = \frac{k_{rds} K_H{}^{0.5} P_H{}^{0.5+2x} \left[\sqrt{(K_H{}^{0.5} P_H{}^{0.5} + 1)^2 + \frac{4K_{cyc} P_{cyc}}{P_H{}^{x}}} - K_H{}^{0.5} P_H{}^{0.5} - 1\right]^3}{8 K_{cyc}{}^2 P_{cyc}{}^2} \qquad \text{(Eq. 1)}$$

The parity plots in Figure 4-18 demonstrate that the H*-assisted RDS hypothesis satisfactorily describes the measured total rates of MCH hydrogenolysis on high-dispersion Ir/Al_2O_3 catalysts over a 10-fold range in turnover rates ($R^2 > 0.98$).

For the endocyclic C−C bond cleavage, the equilibrium constants for H_2 and MCH activation do not differ much on catalysts that comprise primarily 1−2 nm Ir clusters (Table 4-3). In contrast, the intrinsic rate constants of the RDS decrease from 0.52 to 0.15 s^{-1} with decreasing Ir dispersion from 0.65 to 0.52. The number of cleaved C–H bonds prior to C–C bond scission is predicted to be slightly larger than four ($x \approx 2$ (H_2 molecules)) on small clusters of $D > 0.50$. This stoichiometry corresponds to the widely proposed C_2-unit mode, or the so-called dicarbene species, over Ir surfaces [1,21,25,28].

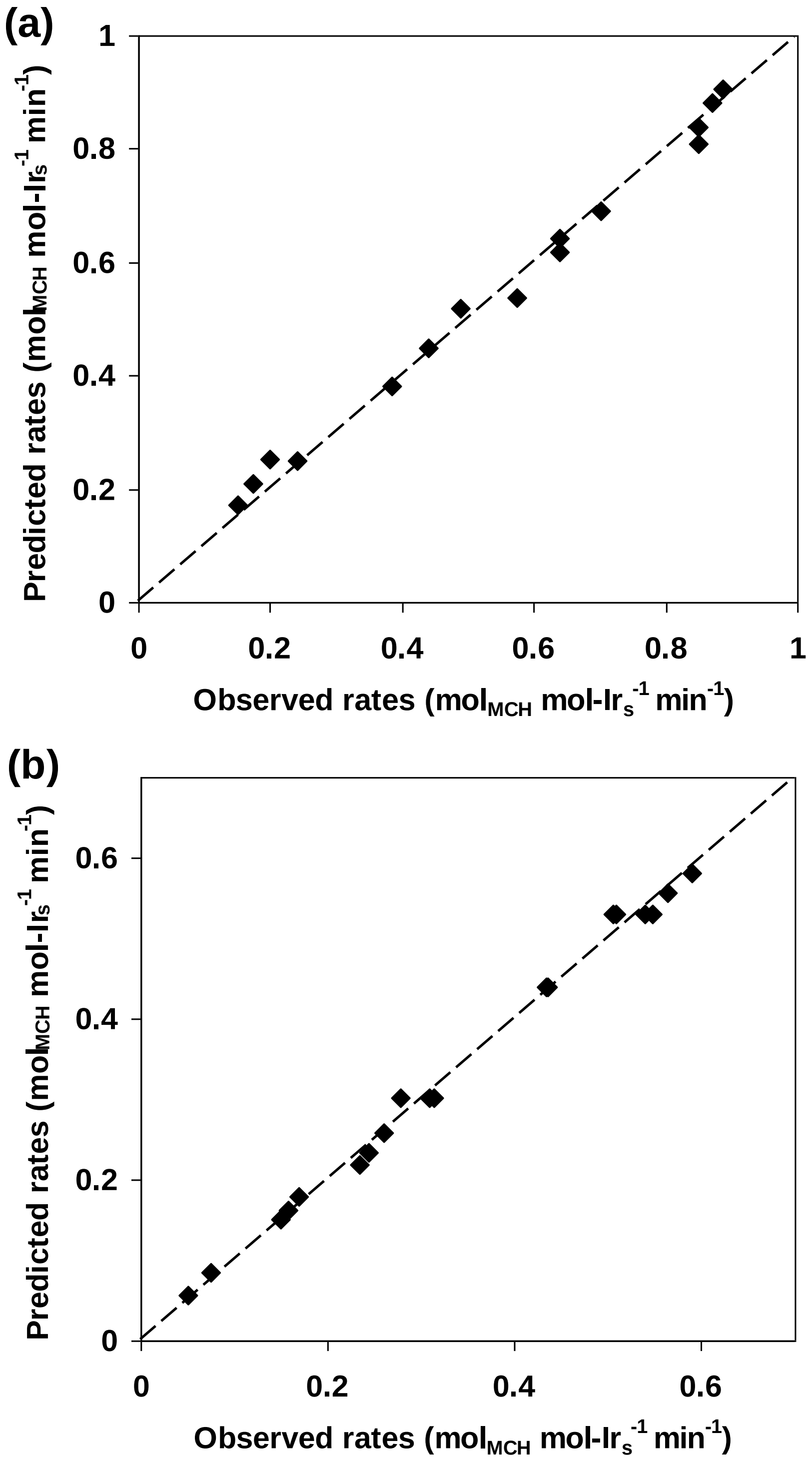

Figure 4-18. Parity plots for the predicted and measured total conversion rates of MCH over (a) 0.50%Ir(0.61)-1/Al$_2$O$_3$ and (b) 0.54%Ir(0.58)-2/Al$_2$O$_3$ at 523 K (0.15−1.3 MPa H$_2$, 0.9−1.6 kPa MCH) for the mechanism proposing an adsorbed H-atom as the splitting agent in the rate-determining step.

Table 4-3. Fitting parameters for the endocyclic C−C bond cleavage in MCH at 523 K on 0.50%Ir(*D*)-1/Al_2O_3 catalysts with D_{Ir} = 0.52−0.65 for the rate equation:

$$r = \frac{k_{rds} K_H^{0.5} P_H^{0.5+2x} \left[\sqrt{(K_H^{0.5} P_H^{0.5} + 1)^2 + \frac{4 K_{cyc} P_{cyc}}{P_H^{x}}} - K_H^{0.5} P_H^{0.5} - 1 \right]^3}{8 K_{cyc}^2 P_{cyc}^2}$$

Fitting parameters	D_{Ir} = 0.52	D_{Ir} = 0.61	D_{Ir} = 0.65
k_{rds} (s^{-1})	0.15	0.41	0.52 (2.5[a])
K_H (10^{-4} kPa^{-1})	8.2	7.3	7.8
K_{cyc} (10^{2x} kPa^{x-1})[b]	10.7	8.4	8.7
x	2.3	2.2	2.2
R^2	0.981	0.985	0.987
Estimated coverages[c]			
θ_v[d]	0.35−0.53	0.37−0.55	0.36−0.54
θ_H[d]	0.15−0.46	0.15−0.44	0.15−0.45
θ_{cyc}[d,e]	1.6×10^{-2}−0.25	1.6×10^{-2}−0.24	1.6×10^{-2}−0.25

[a] The intrinsic rate constant in CH hydrogenolysis reported in Tables 3-4 and 3-6.

[b] Complex unit depending on the value of *x*.

[c] MCH partial pressure: 0.9−1.6 kPa, H_2 partial pressure 0.2−1.2 MPa.

[d] θ_v: surface coverage of empty site; θ_H: surface coverage by H*; θ_{cyc}: surface coverage by cyclic reactive intermediates. The site balance equation is $\theta_v + 2\theta_{cyc} + \theta_H = 1$ because it is assumed that adsorption of cyclic hydrocarbon occupies two surface atoms.

[e] The lower boundary of estimated coverage which corresponds to high H_2-pressure conditions (> 0.4 MPa) may have been underestimated as evidenced from the worse fitting (overestimation relative to experimentally determined values) of the reaction order in MCH under these conditions.

On large Ir clusters, average dehydrogenation depths (*x* values, Table 4-4) were predicted to be lower than those on small clusters (Table 4-3). The values of *x* (1.2−1.4) are, however, less definitive on large clusters, partly because the measured rates over low-dispersion catalysts varied by less than two-fold (Figure 4-12). In spite of the inferior fits, we remark that any attempts to constrain the dehydrogenation depth at *x* = 2 (or even larger) and model the other three parameters only lead to unreasonable estimates of the H_2-adsorption equilibrium constant and H*-coverage (see Chapter 3). Moreover, the dehydrogenation depth could be even shallower if the adsorption strength of H* on these large clusters had been underestimated by the kinetic modeling. All the above trends regarding the endocyclic C−C bond cleavage are very similar to those observed in CH hydrogenolysis. The limitation of the current kinetic model and the uncertainty of modeling results on large clusters, as well as the difficulty of modeling exocyclic C−C bond cleavage rates, are discussed in Section 4.4.2.

Table 4-4. Fitting parameters for the endocyclic C−C bond cleavage in MCH at 523 K on 0.50%Ir(*D*)-1/Al_2O_3 catalysts with D_{Ir} = 0.035−0.16 for the rate equation:

$$r = \frac{k_{rds} K_H^{0.5} P_H^{0.5+2x} \left[\sqrt{(K_H^{0.5} P_H^{0.5} + 1)^2 + \frac{4K_{cyc} P_{cyc}}{P_H^{x}}} - K_H^{0.5} P_H^{0.5} - 1 \right]^3}{8 K_{cyc}^2 P_{cyc}^2}$$

Fitting parameters	D_{Ir} = 0.16	D_{Ir} = 0.035
k_{rds} (s^{-1})	0.47	1.5
K_H (10^{-4} kPa^{-1})	2.3	2.6
K_{cyc} (10^{2x} kPa^{x-1})[a]	8.1	5.0
x	1.4	1.2
R^2	0.932	0.925
Estimated coverages[b]		
θ_v[c]	0.37−0.53	0.43−0.53
θ_H[c]	0.11−0.25	0.13−0.26
θ_{cyc}[c,d]	0.12−0.26	0.11−0.22

[a] Complex unit depending on the value of *x*.

[b] MCH partial pressure: 0.9−1.6 kPa, H_2 partial pressure 0.37−1.0 MPa.

[c] θ_v: surface coverage of empty site; θ_H: surface coverage by H*; θ_{cyc}: surface coverage by cyclic reactive intermediates. The site balance equation is $\theta_v + 2\theta_{cyc} + \theta_H = 1$ because it is assumed that adsorption of cyclic hydrocarbon occupies two surface atoms.

[d] The lower boundary of estimated coverage which corresponds to high H_2-pressure conditions (> 0.4 MPa) may have been underestimated as evidenced from the worse fitting (overestimation relative to experimentally determined values) of the reaction order in MCH under these conditions.

4.4. Discussion

4.4.1. Selectivities of C−C bond cleavages in methylcyclohexane along primary and secondary pathways

Methylcyclohexane possesses four distinguishable pairs of C−C bonds, three at endocyclic positions and one exocyclic. A single cleavage of endocyclic C−C bond in MCH leads to any of the C_7 alkanes, i.e., 2MH, 3MH or nHp, while a single exocyclic C−C bond cleavage leads to equimolar formation of cyclohexane and methane. The selectivities to single-cleavage products decreased with conversion on all catalysts, indicating that they are mechanistically primary products (Figures 4-4a and -5a). Smaller ($C_{<7}$) alkanes are formed via both multiple-cleavage of MCH during one surface sojourn and secondary reactions of re-adsorbed single-cleavage products, whose contributions are suggested from the intercepts and slopes in selectivity-conversion plots, respectively (Figures 4-4 and -5). Therefore, $C_{<7}$ alkanes are of both primary and secondary natures from a kinetics point of view. It is conceptually difficult to imagine the formation of $C_{<7}$ alkanes via multiple-point contact of MCH to the surface followed by concerted C−C bond cleavages. Rather, $C_{<7}$ alkanes should be seen as mechanistically secondary products from a second C−C bond cleavage of ROPs before desorption [22]. Moreover, these small alkanes are basically not formed via successive scissions of ROPs because the formation rates are essentially equal for pairing products (ethane and pentane, propane and butanes, see Figure 4-10).

It is worth mentioning that the slope in selectivity-conversion plots (Figures 4-4a and -5a) does not merely represent the reactivity differences between single-cleavage products and the reactant. Rather, it reflects the difference between formation rates of multiple-cleavage products along primary and secondary pathways. Table 4-5 shows the regressed pseudo-first-order constants for the primary and secondary pathways in a simplified reaction network for MCH hydrogenolysis over high- and low-dispersion catalysts (the differential equations used are listed in the Appendix of this chapter). The reactivities of MCH and single-cleavage products do not differ much on each catalyst in terms of their first-order rate constants (k_1 and k_2), i.e., by a factor of 1−2. The multiple-cleavage rate along secondary pathways (k_2) is substantially larger relative to that along primary reaction pathways (k_3), i.e., by a factor of >5, on high-dispersion catalysts (D = 0.61, 0.52, Table 4-5). Hence, the smaller slope of selectivity change with conversion on large clusters (ca. 0.1 in comparison with 0.3−0.4 on small Ir clusters, see Figures 4-4a and -5a) is not mainly a reflection of lower reactivities of single-cleavage products than the reactant MCH; rather, it principally points to the similar formation rates of multiple-cleavage products along primary and secondary pathways (k_2 and k_3) on large Ir clusters. Clearly, the formation of multiple-cleavage products along primary reaction pathways (k_3 values in Table 4-5) suggests that single-cleavage products are more susceptible to a successive C−C bond cleavage during one surface sojourn (viz. primary pathways) on large clusters than on small ones.

Table 4-5. Pseudo-first-order rate constants for a simplified reaction network (see below) of MCH hydrogenolysis on 0.50%Ir(D)-1/Al_2O_3 catalysts at 523 K, 1.2 kPa MCH and 0.63 MPa H_2. Primary reactions: k_1, k_3; secondary reactions: k_2.

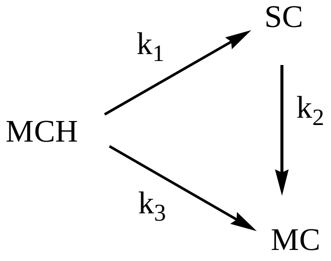

(SC: single-cleavage products; MC: multiple-cleavage products)

Fractional Ir dispersion (D)	Apparent rate constants (mol_{MCH} mol-Ir_s^{-1} min^{-1})		
	k_1	k_2	k_3
0.61	0.39	0.33	0.046
0.52	0.14	0.12	0.021
0.16	0.84	0.37	0.40
0.035	2.2	1.1	1.4

The intercepts extrapolated to zero conversion in selectivity-conversion plots suggest that the probability for terminal-cleavage in primary reactions is remarkably higher than that for internal-cleavage on low-dispersion catalysts (Figure 4-5b). Lecarpentier et al.

also reported that the multiple-cleavage products of MCH consisted primarily of methane and C_6 alkanes in comparable concentrations on Ir/ZrO_2-SiO_2 of 13% dispersion [22]. Mono- and di-branched C_7 alkanes are the main multiple-cleavage products in the hydrogenolytic reactions of 1,2- and 1,3-dimethylcyclohexanes over supported Ir catalysts [21]. In light of these facts, it is conceivable that the favorable adsorbed state after the first C–C bond cleavage of MCH is one that bears partial attachment to the surface and that has to make its next choice between terminal C–C bond cleavage and hydrogen-facilitated desorption. In contrast, secondary reactions, due to re-adsorption of primary products along the catalyst bed, do not particularly show preference to either terminal or internal cleavage modes as for small Ir clusters (slopes in Figure 4-4b). Secondary reactions largely bypass terminal-multiple-cleavage on large clusters (slopes in Figure 4-5b), presumably because the primary products re-adsorb preferentially via internal C−C bonds on large clusters.

The selectivity to ring opening (extrapolated to zero conversion) increased with increasing H_2 pressure, and with decreasing temperature and cluster size (Figures 4-16a, -17 and -7b, respectively), in line with the trends in CH hydrogenolysis. The surface coverage of H* (adsorbed H-atom) is critical to the number of turnovers via single-cleavage routes relative to that via multiple-cleavage routes during a surface sojourn of MCH, because the two cleavage modes are mediated by surface species that are different in the degree of H-deficiency (Chapter 3). In addition, the rates of rehydrogenation and product desorption steps, which affect the surface residence time of relevant intermediates, depend on the concentration of H* vicinal to the adsorbed single-cleavage products. The possibility of multiple C–C bond scissions in primary reactions depends on H_2 pressure and temperature, because they determine the surface coverage of H* (involved in the C–C bond cleavage and product desorption steps), and also the concentration of available vacancies for the landing and activation of hydrocarbon. On the other hand, the lower ROP-selectivities at larger cluster sizes can be interpreted by lower H* coverages on large clusters with lesser coordinative unsaturation (Table 4-4). Alternatively, the low ROP selectivity can be ascribed to the increased probabilities of finding neighboring sites on large clusters (low-index facets) to accommodate more unsaturated multiply-bonded species (the active state for multiple-cleavage requires further dehydrogenation from ROP intermediates), as well as detached hydrogen atoms. These surface species would require larger ensembles than those for ring opening routes, thereby favoring the multiple-cleavage, particularly the terminal modes (Figure 4-9a), over ring opening. Higher H*-coverages depress further dehydrogenation to reach the activated state and ensemble size requirement for multiple-cleavage. The large gap in ROP selectivity between small and large Ir clusters is partly rationalized from the H*-coverage values estimated by kinetic modeling. The H*-coverage at similar H_2 pressures is higher on small clusters ($D > 0.50$) than that on large clusters ($D < 0.20$) by a factor of 2, the magnitude of which is comparable to the effect of H_2 pressure increase (0.37 to 1.0 MPa) on the estimated H*-coverage. The increase in ROP selectivity brought forth by increasing H_2 pressure in this range was smaller than that caused by increasing Ir dispersion from 0.20 to 0.50. Therefore, we conclude that changes in the H*-coverage are insufficient to account for the ROP selectivity gap between small and large clusters. The decisive cause for the much lower ROP selectivity over large clusters than over small clusters has to be the difference in the probability of finding neighboring sites.

The selectivity to internal multiple-cleavage seems always low and rather insensitive to the surface structure (Figure 4-9b), the cause of which is not precisely understood at present. We tentatively focus on the argument that reactive intermediates relevant for internal multiple-cleavage always have greater unsaturation degrees than the other cleavage routes on metallic Ir clusters of any sizes, rendering the scission probability of these internal C−C bonds relatively unaffected by the cluster size. However, we do not fully exclude a slight contribution from carbenium-mediated pathways, which lead to C−C bond activation and scission preferentially at internal positions.

Among the three C_7 ROPs, those formed via C−C bond cleavages at unsubstituted positions, i.e., 3MH and 2MH, exhibited similar selectivities. The 3MH/2MH ratio slightly depended on the Ir dispersion, i.e., from 1.6 over low-dispersion catalysts to 1.1 over high-dispersion ones (Figure 4-7). The ratio between 3MH and nHp, the latter formed via C_{III}−C_{II} bond cleavage, changed significantly with Ir dispersion in the middle range of dispersion and approached 4 and 11, respectively, over the smallest and largest Ir clusters at 523 K and 0.37 MPa H_2 (Figure 4-7). These two extreme values are likely to reflect the relatively larger steric hindrance on more crowded terrace planes, than on small clusters that expose higher fractions of low-coordination atoms. The steric hindrance imposes stronger inhibition on the access and activation of the tertiary carbon atom in MCH by surface Ir atoms. The selectivity to 2MH is always slightly lower than that to 3MH, suggesting that the methyl group on the tertiary carbon is still able to affect the adsorption and activation of the nearest pair of bisecondary C−C bonds which eventually lead to the formation of 2MH (Section 4.4.3). In particular, the steric repulsion between adsorbed H-atoms and the methyl substituent would become progressively important at increasing H_2 pressure, leading to the increased ratios of 3MH/2MH and 3MH/nHp on crowded terrace planes (Figure 4-15b). This effect seems much less pronounced on small clusters, as seen from the constant ratios (Figure 4-15a). However, a further increase of H_2 pressure up to 1.8 MPa evidenced increased ratios of 3MH/2MH and 3MH/nHp to 1.8 and 5.2, respectively, on the 0.50%Ir(0.61)-1/Al_2O_3 catalyst (not shown).

Concerning the multiple-cleavage products, two facts merit consideration. Within C_6 alkanes, 2MP forms with a higher selectivity than 3MP, most prominently on small Ir clusters, apparently because the terminal C−C bond cleavage of 2MH and 3MH can lead to 2MP formation. On the other hand, 3MP can only be produced via C−C bond cleavage at the 5-C and 6-C atoms along the C_6-chain of 3MH. The C−C bond involving a tertiary carbon remains intact during multiple-cleavage on small clusters, as suggested by the non-enriched nHx percentage in C_6 fractions relative to that of nHp within C_7 fractions (Table 4-1). Indeed, the presence of a tertiary carbon atom is reckoned to decrease the reactivity of a C−C bond [4,5,28]. However, it is interesting to observe that despite the decreasing selectivity of nHp in ROPs, the percentage of nHx among C_6 alkanes increases with increasing Ir cluster size (Table 4-1). At first sight, it seems to suggest that the methyl substituent in 2MH or/and 3MH is cleaved off, resulting in enhanced formation of nHx. This line of reasoning would, however, become incompatible with the allegedly lower reactivity of C−C bond involving a tertiary C-atom [4,5,28]. More reasonably, the increased nHx percentage within C_6 alkanes on low-dispersion catalysts is ascribed to lower reactivities of branched C_7 alkanes (2MH and 3MH, which lead to MPs) relative to the non-branched one (nHp, which leads to nHx) on large clusters. Also note that the exocyclic-cleavage product CH could also form nHx, the contribution of which appears to increase on large Ir clusters. A separate investigation into the reaction behaviors of these intermediate products is outside of the scope of the current work, but is of apparent necessity to explicitly understand the reaction patterns mentioned above.

The selectivity to the exocyclic C−C bond cleavage in primary reactions is most sensitive to the change of dispersion in the range of D = 0.25−0.50 (Figure 4-8b). At higher (D > 0.50) or lower (D < 0.20) dispersions, the selectivity to exocyclic C−C bond cleavage reaches the limit value of ca. 2% and 40%, respectively. The greatly pronounced exocyclic C−C bond cleavage on low-dispersion catalysts may be due to a larger ensemble size requirement for this bond cleavage mode relative to that for ring opening routes. More evidence based on H_2 pressure effects is presented in later sections.

4.4.2. Apparent and intrinsic structure sensitivities of endocyclic and exocyclic C−C bond cleavage

The varying activities of catalysts with small clusters in endocyclic C−C bond cleavages should stem mainly from the differences in the intrinsic rate constant of the RDS (the only scaling property that does not come together with the H_2 pressure term). This is expected from the closely-resembled curvatures of small Ir-clusters and the nearly equivalent H_2 pressure at rate maxima (Figure 4-11a). Indeed, the modeling results in Table 4-3 confirm that the thermodynamic properties that dictate the equilibrium concentration and distribution of surface intermediates relevant to endocyclic C–C bond cleavages do not vary to a substantial extent. Now that coverage effects can be neglected, the sympathetic branch (D > 0.45, Figure 4-3a) for the endocyclic C–C bond cleavage is simply ascribed to the decrease of the RDS rate constant with increasing cluster size. The regressed rate constants are lower compared to those in CH hydrogenolysis over the same catalysts (see Tables 3-4 and -6), suggesting that the methyl substituent drastically lowers the ring reactivity. Similarly, McVicker et al. found that MCH conversion was roughly twice that of 1,2,4-trimethylcyclohexane at 10 times higher liquid hourly space velocity at 573 K [1]. In stark contrast, Do et al. observed very similar overall conversions of methylcyclohexane and dimethylcyclohexane at 553 K on the same Ir/Al_2O_3 catalyst containing small clusters (1−2 nm) [21].

Since hydrocarbon hydrogenolysis requires multi-atom sites [4,29], the ensemble size requirement for the C_2-unit mode must have been met on clusters of D = 0.5−0.7. Otherwise, it would have been impossible to see the TOF increase as dispersion increases in this range. As proposed in Chapter 3, the population of low-coordination atoms is considered most consequential to hydrogenolysis catalysis owing to their greater coordinative unsaturation. The population of low-coordination atoms among all surface atoms is known to decrease sharply in this narrow range (1−2 nm) [30]. A quantitative estimation of the population of different types of surface atoms in closed-shell cuboctahedral Ir clusters demonstrates that the percentage of corner atoms is reduced by almost a factor of 3 with only a slight increase of cluster size from 1.6 to 2.2 nm (Table 3-5). This magnitude is remarkably similar to the difference in regressed rate constants, i.e., a factor of 3−4, in this dispersion range (D = 0.52−0.65, Table 4-3).

Predicted dehydrogenation depths are lower on large Ir clusters than on small ones, indicating that different intermediates lead to the endocyclic C–C bond cleavage on small and large clusters. Tentatively, the antipathetic branch of the correlation between rate of C−C bond cleavage and dispersion (D < 0.40, Figure 4-3a) is ascribed to the less-unsaturated nature of the MARI that features a different reactivity and ensemble size requirement. Engstrom et al. [31] explained the differences in the apparent reaction kinetics and preexponential factors of ethane hydrogenolysis on Ir(111) and Ir(110)-(1×2) surfaces also by different reaction intermediates, namely, C_2H_4(ads) on the former and C_2H_2(ads) on the latter. Dominant surface structures on small and large clusters radically differ, which may cause different reactivities for C−H and C−C bond activation by either favoring one transition state structure over another or changing the lateness of the transition states [32]. There are good reasons to believe that the underlying driving force for small and large clusters to induce different H-deficiencies of most abundant reactive intermediates (MARIs) originates from the different degrees of coordinative unsaturation for surface atoms on clusters of broadly varying sizes.

Exocyclic C−C bond cleavage exhibits a strong antipathetic structure sensitivity in the dispersion range of 0.035−0.65 (Figure 4-3b). It would have been most ideal to also model the rate of exocyclic C–C bond cleavage by the same kinetics evaluation as shown above for endocyclic C–C bond cleavage. However, it was recognized from previous modeling attempts that a steric factor might have been missing in the rate equation (Eq. 1) for the exocyclic C–C bond cleavage occurring around the sterically hindered C-atom. We speculate that the H_2 pressure, or H-coverage, not only affects the concentration of reactive intermediates at appropriate dehydrogenation depth, but also imposes a steric impact on the effectiveness of MCH activation at catalytic surfaces, that is, the fraction of MCH molecules that approaches the active center and gets activated is further reduced by a factor of $\sigma(\mathrm{P_H})$:

$$\theta_{cyc}' = \sigma(\mathrm{P_H})\,\theta_{\mathrm{cyc}} = \frac{\sigma(\mathrm{P_H})K_{cyc}P_{cyc}\theta_v{}^n}{P_H{}^x} \qquad \text{(Eq. 2)}$$

where $\sigma(\mathrm{P_H})$ is the newly added term that denotes the H_2-pressure dependent steric factor. As will be discussed in Section 4.4.3, while this factor seems to be unimportant or almost independent of H_2 pressure for the endocyclic C−C bond cleavage on small clusters, it may become more H_2-pressure dependent for the exocyclic C−C bond cleavage and on large clusters. Since its functional dependence on H_2 pressure is unknown, further refinement of the current model requires additional assumptions and is left to our future studies. Regardless, the more than two orders of magnitude difference between the TOFs of the smallest and largest clusters strongly suggests that exocyclic C−C bond scission is intrinsically structure sensitive and features a larger ensemble size requirement than the endocyclic C−C bond cleavage.

4.4.3. Microscopic implications of H_2 pressure effects on product formation rates

Previous studies on MCH hydroconversion over supported Ir catalysts included predominantly the exploration of bifunctional catalysis [22,25,26,33,34]; only a few concerned ‘acid-free’ Ir catalysts [22,25]. However, none of them have addressed the effects of H_2 pressure on the reaction kinetics, nor their implications in mechanistic aspects. In the present work, remarkable H_2 pressure impacts have been shown on reaction rates and product selectivities (Figures 4-11−16). The rates of endocyclic C−C bond cleavage show different H_2-pressure dependences, i.e., the curvature of rate-pressure function and the H_2 pressure at the rate maximum, on small and large Ir clusters (Figures 4-11a and 12a). The higher optimal H_2 pressures and flatter curvatures on large

Ir clusters might suggest that the average unsaturation degree of reactive intermediates for endocyclic C−C bond cleavage is lower on large Ir clusters than on small clusters (Table 4-4). We have discussed this in more rigorous terms by kinetic modeling results in Section 4.4.2.

When the formation rates of the three ROPs were analyzed as a function of H_2 pressure, similar optimum H_2 pressures and curvatures were observed for all ROPs on small Ir clusters (Figure 4-14a). As a result, the formation rates for ROPs at different hydrogen pressures exhibited relatively constant ratios (Figure 4-15a). In contrast, the formation rate of 3MH peaked at a much higher H_2 pressure than those of 2MH and nHp on large Ir clusters (Figure 4-14b). The relative ratios between 3MH and either of 2MH and nHp continued to increase with H_2 pressure (Figure 4-15b). It is not straightforward to account for these differences over clusters of varying sizes simply by invoking the dehydrogenation-depth postulate (Chapter 3), because it is unlikely that dehydrogenation depths for all ROPs are closely similar on small Ir clusters while differing so much between each other on large particles. Instead, it is illustrated in Scheme 4-1 how the different optimum H_2 pressures for the three ROPs on large clusters could be satisfactorily interpreted by steric effects arising from the methyl substituent and co-adsorbed H-atoms. On large clusters terminated by flat terraces, as far as endocyclic C−C bond cleavage is concerned, the adsorption conformation of MCH has to be tilted and the methyl group has to stay away from the surface in order to minimize the steric repulsion. The ring opening at the substituted position, leading to nHp (ca. 5% within the ROPs), would inevitably render the methyl group adjacent to the close-packed surface on large clusters and is therefore the most hindered adsorption mode (Scheme 4-1a). Moreover, any additional H-atoms adsorbed at neighboring sites would increase the repulsive interaction between the H-atoms in the methyl group and the surface (Scheme 4-1b). This latter effect causes the formation rates of 2MH and nHp to decline much earlier than that of 3MH with increasing H_2 pressure (Figure 4-14b). During the formation of 3MH, the methyl in the adsorbed intermediate ‘sticks’ outward from the surface and interacts little with adsorbed H-atoms (Scheme 4-1c), until the effect of appropriate dehydrogenation depth starts to set in at very high H_2 pressures. We further conclude that the steric effects imposed by neighboring Ir atoms or increased H* coverage must be either small or nonconsequential to ring opening catalysis on low-coordination atoms at the surface of small Ir clusters, as the formation rates of all ROPs show the same impact of H_2 pressure (Figures 4-14a and 15a). Indeed, the curved surface on small clusters would effectively reduce the interaction force between the vicinally adsorbed H-atoms and the methyl C−H bonds (Scheme 4-1d). Only in the absence of these steric effects can we infer that the dehydrogenation depths of the catalytically relevant intermediates are similar for different ROPs.

As opposed to the very different endocyclic C−C bond cleavage rates on small clusters of similar dispersions (D = 0.52−0.65, Figure 4-11a), exocyclic cleavage rates are less different and exhibit monotonic declining trends with increasing H_2 pressure (0.2−1.0 MPa) on these small clusters (Figure 4-11b). On large Ir clusters, the rate of exocyclic C−C bond cleavage still decreases with increasing H_2 pressure (Figure 4-12b). Different ensemble size requirements for the endo- and exocyclic C−C bond cleavage, rather than different dehydrogenation depths for the relevant catalytic intermediates, play the major role here. Considering the extremely antipathetic sensitivity to the Ir dispersion shown for the exocyclic C−C bond cleavage in the whole studied range (Figure 4-3b), it is reasonable to speculate that this cleavage mode has a large ensemble size requirement [32]. Indeed, a larger ensemble size requirement would lead to a stronger suppression of activity by an increase in the site occupation by adsorbed H-atoms, as evidenced in Figure 4-16b. Accordingly, at H_2 pressure of 0.2 MPa, the rate of endocyclic C−C bond cleavage still increases with H_2 pressure, while the exocyclic cleavage rate has already started to decline (Figure 4-11). As to the possible reactive state for the exocyclic C−C bond cleavage, we propose the 1,3-species (e.g., αγ-diadsorbed, ααγ-triadsorbed or even ααγγ-tetraadsorbed) to be the most likely candidates, as they apparently require a larger space than the 1,2-species. The intervention of these species was postulated first by Anderson [35] and later invoked by Leclercq et al. [36], both on Pt catalysts. The latter authors proposed that the C−C bond close to the more dehydrogenated carbon is more readily broken, contrary to Anderson’s mechanism. As the naphthenic C−H bonds (similar to normal secondary C−H bonds) are weaker than the primary C−H bonds [37], the methylene (–CH_2–) in the cyclohexyl ring that is involved in 1,3-adsorption is likely to be more dehydrogenated than the methyl group. Hence, our results obtained on Ir catalysts, showing prevalent cleavage of the C_{III}–C_I bond instead of the C_{II}–C_I bond, are in favor of Anderson’s proposal [35].

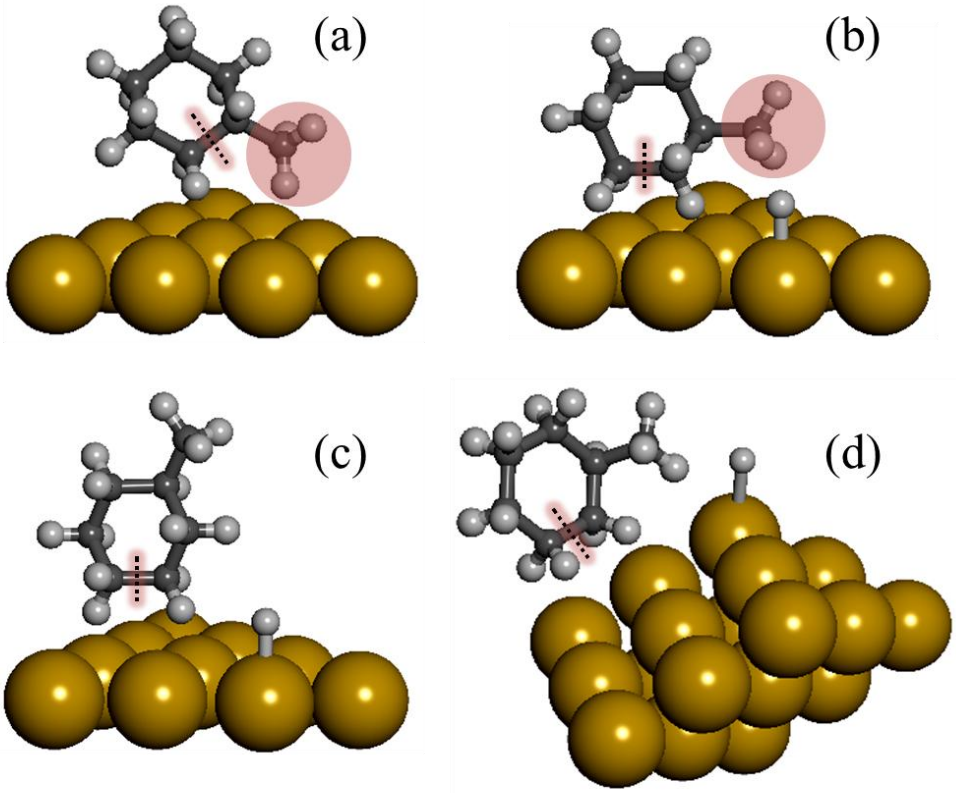

Scheme 4-1. Schematic representation of the steric effects originating from the methyl group, crowded surfaces (large clusters) and the co-adsorbed H-atoms: (a) steric hindrance that the methyl group feels on crowded low-index planes (ring opening to nHp); (b) repulsive interaction between the methyl group and co-adsorbed H-atoms (ring opening to 2MH); (c) no interaction between the methyl group and the surface or the co-adsorbed H-atoms (ring opening to 3MH); (d) little repulsive interaction between the methyl group and the surface or co-adsorbed H-atoms on small clusters (ring opening to 2MH).

4.4.4. Apparent and intrinsic energetics of endocyclic C−C bond activation

In the previous chapter, we have successfully shown that the effect of H_2 pressure on the measured energies of activation can be readily explained by the Temkin relation [38], from which the intrinsic activation barriers can be estimated at appropriate conditions where both reactants have nearly zero reaction orders. In the present work, similar trends as in CH hydrogenolysis have been shown concerning most of the C−C bond cleavage products, i.e., 2MH, 3MH and multiple-cleavage products, but not with those formed via cleavage at substituted positions, i.e. nHp and CH (Table 4-2). For catalysts that contain primarily small Ir clusters ($D > 0.50$), the reaction order in H_2 goes more negative at higher H_2 pressures, while the reaction order in MCH stays always positive and increases with H_2 pressures, both factors weighing on the increase of apparent activation energies (Table 4-2). By contrast, the slightly changed $E_{a,app}$ (not with nHp and CH) with increasing H_2 pressure, over large Ir clusters ($D < 0.20$), can be qualitatively interpreted in terms of the lower sensitivity of H_2 reaction order to H_2 pressure in the studied range. In addition, the markedly lower apparent activation barriers (90−110 kJ mol^{-1}) for ring opening (except for nHp) over the low-dispersion catalysts are attributed to the much smaller reaction orders in H_2 (-0.7~0.2) and in MCH (0.1~0.4) than those (-2.5~-1.0 and 0.4~0.7, respectively) featured by high-dispersion catalysts. Remarkably, the intrinsic activation barrier averaged for all the endocyclic C−C bond cleavages in MCH was estimated to be 83 ± 12 kJ mol^{-1} on large clusters, by applying the Temkin relation at conditions where reaction orders in H_2 and MCH are both close to zero (e.g., at 523 K, 1.2 kPa MCH, 0.6 MPa H_2). This value is very similar to that estimated in CH hydrogenolysis on Ir/Al_2O_3 catalysts, indicating that the methyl substitution does not influence the average reaction barrier of the endocyclic C−C bond cleavage to a discernible extent. However, the intrinsic rate constant decreases significantly after introducing the methyl (Table 4-3), compared to that in CH hydrogenolysis over the same catalyst (Chapter 3), indicating that the change in the intrinsic reactivity of the endocyclic C−C bond cleavage stems predominantly from the pre-exponential factor that contains steric and entropic contributions differing between unsubstituted and substituted C_6-naphthenes.

Estimated intrinsic activation barriers (70−90 kJ mol^{-1}) of the endocyclic C−C bonds (mostly as secondary-secondary) in relatively unstrained CH and MCH (with ring-strain energy of only ca. 6 kJ mol^{-1} [39]) over Ir/Al_2O_3 catalysts resemble that reported for C−C bond cleavage in CH on Ir(111) (E_a = ca. 80 kJ mol^{-1}) and is larger than that for n-butane

(E_a = ca. 70 kJ mol^{-1}), i.e., the unstrained standard with a similar backbone around the central C−C bond to be cleaved [39]. The barrier for the C−C bond cleavage of cyclopropane and cyclobutane (ca. 60 kJ mol^{-1}) is even lower than that for the unstrained butane [39]. It has been noted that the C−C bond strength is not the decisive factor in affecting the activation barrier, as this parameter does not correlate with the barrier for C−C bond cleavage [39,40]. Siegbahn and Blomberg suggested that the ring-strain energy difference between the initial state (reactant) and the transition state for C−C bond activation lowers or raises its barrier, depending on whether the transition state is less or more strained than the initial state [40]. The transition state structures that form as insertion products for the cycloalkanes are typically accepted as metallacycles that contain at least one metal atom and hence expand the initial ring structure [41]. Consequently, in the case of cyclopropane and cyclobutane, some ring-strain is released upon formation of transition states because of the ring expansion to less strained structures, leading to their lowered barriers than that of n-butane. Moreover, since the electron density maxima of the C−C σ bonds in strained cyclobutane lie outside of the C−C internuclear axis [42], interaction of the C−C bond orbitals with the Ir orbitals in the transition state for C−C bond cleavage is sterically more favorable than for an unstrained alkane. However, in the case of CH, the initial state contains little strain, whereas the transition state is similar to a metallacycloheptane or -octane that possesses a higher ring-strain than the initial state. In addition, the increased energy cost due to the perturbation of the initial cycloalkane conformation would cause the increase in the transition-state energy to be larger for CH than for the smaller rings [39]. Both factors conduce to the measured higher activation barriers for the C−C bond cleavage (endocyclic) in cyclohexanes than in n-butane and smaller cycloalkanes.

4.5. Conclusions

This chapter is the continuation of the previous one by using the same series of monofunctional Ir catalysts with varying dispersions. But this chapter focuses on understanding the different kinetics and structure sensitivities of endo- and exocyclic

C−C bond cleavages of methylcyclohexane. Several conclusions can be drawn after in-depth assessments of the reaction kinetics:

(1) In line with our previous finding in CH hydrogenolysis, the TOFs for the endocyclic C–C bond scission in MCH feature dual-branch sensitivity to Ir dispersion ($D = 0.035-0.65$). The sympathetic structure sensitivity ($D > 0.46$) originates from the decrease in the intrinsic rate constant due to declining population of low-coordination atoms. The increasing TOFs with further decreasing dispersion ($D < 0.40$) are attributed to the increased ensemble size requirement and reactivities of the catalytically relevant intermediates on atoms of less coordinative unsaturation.

(2) The structural requirement and pressure dependence of demethylation have been for the first time reported in substituted naphthenes over supported metal clusters. Exocyclic C−C bond cleavage is shown to be favored at lower H_2 pressures and over large Ir clusters, exhibiting monotonically higher TOFs with increasing cluster size. The optimum H_2 pressure is much lower than that for the endocyclic C−C bond cleavage. The strong suppression of exocyclic C−C bond cleavage by increasing H_2 pressure (both on small and large clusters) and by decreasing cluster size suggests that the adsorption mode for the exocyclic C−C bond cleavage is more spatially demanding than the 1,2-dicarbene mode proposed for ring opening.

(3) Endocyclic C−C bond cleavage at the substituted position is the least favored ring opening route at all cluster sizes, apparently due to larger repulsive interaction with the methyl group and surface metal atoms. This primary steric effect becomes smaller when the methyl group is farther away and the surface becomes less crowded. At the same conditions (H_2 partial pressure and temperature), the selectivity to n-heptane increases first with decreasing Ir cluster size, and levels off when the average cluster size becomes 1−2 nm, because the surface atom density is remarkably lower on 1−2 nm clusters than on larger ones. On large clusters, the already low tendency to cleave the substituted C−C bond is also exacerbated by secondary repulsive interaction arising from the methyl group and adsorbed H-atoms nearby. In comparison, adsorbed H-atoms do not impose additional steric effects on the accessibility of the secondary-tertiary C−C bond in the vicinal MCH to the catalytic center on small Ir clusters, at least in a considerable H_2

pressure range studied in this work. This secondary steric effect is operative even when the methyl group is not in the closest proximity to the breaking C−C bond.

4.6. Acknowledgements

Hui Shi thanks the Elitenetzwerk Bayern NanoCat for a Ph.D. grant and financial support. Prof. Dr. Xuebing Li is gratefully acknowledged for his help in technical aspects. The authors are indebted to Dipl.-Ing. Xaver Hecht for the help with construction of the reactor setup and for conducting N_2 physisorption and H_2 chemisorption measurements.

4.7. Appendix

A1. Differential equations for derivation of apparent pseudo-first-order rate constants

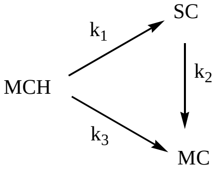

MCH: methylcyclohexane;
SC: single-cleavage products;
MC: multiple-cleavage products

Considering the simplified reaction network shown above, the following differential equations can be obtained by assuming the reaction orders in every compound is first order in each pathway:

$$\frac{dP_{MCH}}{dt} = -k_1 P_{MCH} - k_3 P_{MCH}$$

$$\frac{dP_{SC}}{dt} = k_1 P_{MCH} - k_2 P_{SC}$$

$$\frac{dP_{MC}}{dt} = k_2 P_{SC} + k_3 P_{MCH}$$

After data fitting, applying the Runge–Kutta integration method, apparent rate constants were obtained in $\mathrm{mol_{MCH}}$ $\mathrm{mol\text{-}Ir_s^{-1}}$ $\mathrm{min^{-1}}$. Figure 4A-1 shows the measured and modeled selectivities to single-cleavage products as a function of conversion over typical small and large Ir clusters. The goodness of fit (R^2) is better than 0.98 in any case.

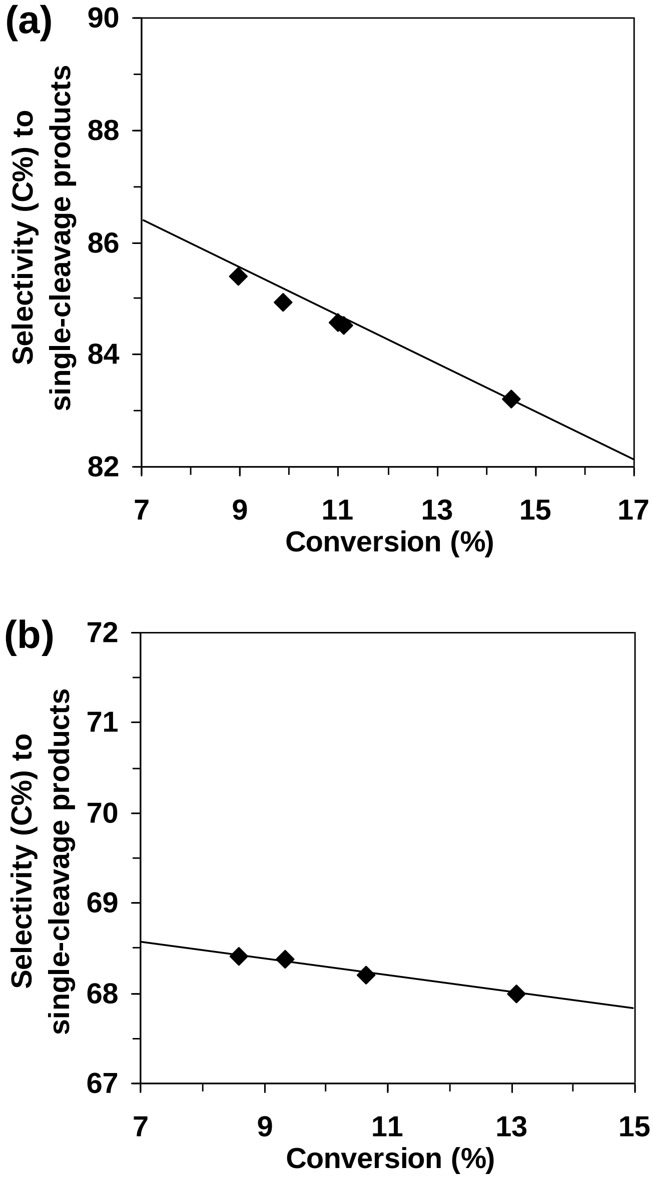

Figure 4A-1. Measured (solid symbols) and modeled (solid lines) selectivities (C%) to products formed via a single cleavage of C–C bond (C_7-ROPs and the demethylation product, CH) as a function of MCH conversion over (a) 0.50%Ir(0.61)-1/Al_2O_3 and (b) 0.50%Ir(0.16)-1/Al_2O_3 at 523 K, 1.2 kPa MCH and 0.37 MPa H_2.

4.8. References

1. G.B. McVicker, M. Daage, M.S. Touvelle, C.W. Hudson, D.P. Klein, W.C. Baird Jr., B.R. Cook, J.G. Chen, S. Hantzer, D.E.W. Vaughan, E.S. Ellis, O.C. Feeley, J. Catal. 210 (2002) 137.
2. A. Corma, V. González-Alfaro, A.V. Orchillés, J. Catal. 200 (2001) 34.
3. H. Du, C. Fairbridge, H. Yang, Z. Ring, Appl. Catal. A 294 (2005) 1.
4. G.C. Bond, Metal-Catalysed Reactions of Hydrocarbons, Springer, Berlin, 2005.
5. F.G. Gault, Adv. Catal. 30 (1981) 1.
6. M. Chow, G.B. McVicker, J. Catal. 112 (1988) 290.
7. Y. Zhuang, A. Frennet, Appl. Catal. A 134 (1996) 37.
8. D. Teschner, K. Matusek, Z. Paál, J. Catal. 192 (2000) 335.
9. M. Vaarkamp, P. Dijkstra, J. van Grondelle, J.T. Miller, F.S. Modica, D.C. Koningsberger, R.A. van Santen, J. Catal. 151 (1995) 330.
10. W.E. Alvarez, D.E. Resasco, J. Catal. 164 (1996) 467.
11. M. Chow, S.H. Park, W.M.H. Sachtler, Appl. Catal. 19 (1985) 349.
12. R. Kramer, H. Zuegg, J. Catal. 80 (1983) 446.
13. H. Glassl, K. Hayek, R. Kramer, J. Catal. 68 (1981) 397.
14. P. Samoila, M. Boutzeloit, C. Especel, F. Epron, P. Marécot, App. Catal. A 369 (2009) 104.
15. P. Samoila, M. Boutzeloit, C. Especel, F. Epron, P. Marécot, J. Catal. 276 (2010) 237.
16. K. Hayek, R. Kramer, Z. Paál, Appl. Catal. A 162 (1997) 1.
17. D. Kubicka, N. Kumar, P. Mäki-Arvela, M. Tiitta, V. Niemi, H. Karhu, T. Salmi, D.Y. Murzin, J. Catal. 227 (2004) 313.
18. M. Santikunaporn, J.E. Herrera, S. Jongpatiwut, D.E. Resasco, W.E. Alvarez, E.L. Sughrue, J. Catal. 228 (2004) 100.
19. K.C. Mouli, V. Sundaramurthy, A.K. Dalai, Z. Ring, Appl. Catal. A 321 (2007) 17.
20. U. Nylén, L. Sassu, S. Melis, S. Järås, M. Boutonnet, Appl. Catal. A 299 (2006) 1.
21. P.T. Do, W.E. Alvarez, D.E. Resasco, J. Catal. 238 (2006) 477.
22. S. Lecarpentier, J. van Gestel, K. Thomas, J.-P. Gilson, M. Houalla, J. Catal. 254 (2008) 49.

23. S. Nassreddine, L. Massin, M. Aouine, C. Geantet, L. Piccolo, J. Catal. 278 (2011) 253.
24. S. Rabl, A. Haas, D. Santi, C. Flego, M. Ferrari, V. Calemma, J. Weitkamp, Appl. Catal. A 400 (2011) 131.
25. R. Moraes, K. Thomas, S. Thomas, S. van Donk, G. Grasso, J.-P. Gilson, M. Houalla, J. Catal. 286 (2012) 62.
26. J.-W. Park, K. Thomas, J. van Gestel, J.-P. Gilson, C. Collet, J.-P. Dath, M. Houalla, Appl. Catal. A 388 (2010) 37.
27. B.J. Kip, F.B.M. Duivenvoorden, D.C. Koningsberger, R. Prins, J. Catal. 105 (1987) 26.
28. K. Foger, J.R. Anderson, J. Catal. 59 (1979) 325.
29. J.H. Sinfelt, J.L. Carter, D.J.C. Yates, J. Catal. 24 (1972) 283.
30. R. van Hardeveld, F. Hartog, Surf. Sci. 15 (1969) 189.
31. J.R. Engstrom, D.W. Goodman, W.H. Weinberg, J. Am. Chem. Soc. 110 (1988) 8305.
32. R.A. van Santen, M. Neurock, S.G. Shetty, Chem. Rev. 110 (2010) 2005.
33. R.N. Rao, N. You, S. Yoon, D.P. Upare, Y.K. Park, C.W. Lee, Catal. Lett. 141 (2011) 1047.
34. T. Sugii, Y. Kamiya, T. Okuhara, Appl. Catal. A 312 (2006) 45.
35. J.R. Anderson, Adv. Catal. 23 (1973) 1.
36. G. Leclercq, L. Leclercq, R. Maurel, J. Catal. 50 (1977) 87.
37. D.F. McMillen, D.M. Golden, Ann. Rev. Phys. Chem. 33 (1982) 493.
38. M. Temkin, Acta Phsiocochim. URSS 3 (1935) 312.
39. C.J. Hagedorn, M.J. Weiss, T.W. Kim, W.H. Weinberg, J. Am. Chem. Soc. 123 (2001) 929.
40. P.E.M. Siegbahn, M.R.A. Blomberg, J. Am. Chem. Soc. 114 (1992) 10548.
41. J.P. Collman, L.S. Hegedus, J.R. Norton, R.G. Finke, Principles and Applications of Organotransition Metal Chemistry, University Science Books, Mill Valley, CA, 1987.
42. A. Stein, C.W. Lehmann, P. Luger, J. Am. Chem. Soc. 114 (1992) 7684.

Chapter 5

Mechanistic implications from deuterium isotope effects

In hydrogen-involving reactions, replacing protium with deuterium typically gives rise to certain responses in reaction rates due to the isotope effect arising primarily from the mass difference between the two isotopes. This chapter is dedicated to revealing the mechanistic information about the identity and kinetic relevance of H/D-involving species in the C−C bond cleavage of methylcyclohexane over supported Ir clusters. It was shown that the measured H/D isotope effects showed normal values (>1) for all product formation rates on small Ir clusters, but depended on different reaction pathways on large clusters. These values increased, in general, with increasing H_2 *pressures. These trends reflect complex origins, both thermodynamics and kinetics in nature, of the effect of isotope identity on the kinetically significant surface steps.*

5.1. Introduction

The difficulty of devising a simple rate expression to embrace all the experimental observations has been discussed by Bond and Cunningham [1]. Nonetheless, following the criteria for the selection of the most satisfactory and reliable rate expression(s) [1,2], plenty of possibilities could be discarded, and the reaction data can be fitted with kinetic equations derived from proper mechanistic considerations (for instance, see previous chapters). In spite of some simplifications having been made, a great variety of plausible mechanisms still remain. The exclusion of some potential proposals, based on the fitting quality of kinetic modeling, might also be regarded as non-rigorous.

It is well accepted that the dissociative chemisorption of dihydrogen, as well as that of hydrocarbon, proceeds much faster than C–C cleavages and therefore both remain quasi-equilibrated in the time scale of hydrogenolysis turnovers [3−8]. Strictly speaking, the question as to whether the two reactants compete for the same sort of adsorption sites has been left open, though the sites, where H* resides, and those to which the reactive intermediate is bound, are usually treated as kinetically equivalent [3]. Transient evidence in methylcyclopentane ring opening and ethane hydrogenolysis over Pt and Ru catalysts, respectively, is in favor of the competitive adsorption for the two reactants [6,9]. Adsorption-limited kinetics is generally thought to be unlikely in alkane hydrogenolysis, but no compelling evidence for this speculation has been presented. Moreover, rehydrogenative desorption steps could also be rate-limiting, as the H-addition to carbon atoms requires lower binding energies of hydrogen on the surface sites. Typically, binding energies of reactants decrease with increasing coordination number of the surface metal atoms. The higher turnover rates of CH and MCH hydrogenolysis on very large Ir particles seem, at least, not to contradict this assumption (rate-limiting rehydrogenation).

Although the majority of mechanistic models for alkane hydrogenolysis assume an irreversible C–C bond cleavage as the rate-determining step (RDS), with all the preceding reactant activation steps quasi-equilibrated, the molecularity of the RDS and the identity of splitting agent (i.e., species other than the active intermediate that appears in the rate-limiting step) have remained, in a rigorous sense, largely elusive in metal-catalyzed hydrogenolytic reactions. In conflict with most mechanistic proposals containing a rate-limiting, irreversible C–C bond-rupture step assisted by a vacant site, a H-adatom or a dihydrogen molecule [1,6−8], a unimolecular, non-assisted C–C bond breaking as the RDS was found to describe most adequately the hydrogenolysis of a variety of lower alkanes over (111) and (110)-(1×2) surfaces of iridium [10].

To further discriminate among these candidate mechanisms, we have examined the H/D isotope effects by comparing the hydrogenolysis rates of deuterated and protiated reactants (MCH and dihydrogen) on supported Ir clusters. Protium/deuterium (H/D) kinetic and thermodynamic isotope effects can probe the involvement of hydrogen atoms in specific elementary steps within catalytic sequences, because rate and equilibrium constants for these elementary steps depend on isotopic identity. To avoid the complications by isotope exchange reactions between H- and D-containing species, both reactants contain the same type of hydrogen isotope, i.e., in non-deuterated and perdeuterated forms. These measured isotope effects, depending on the cluster size and reaction conditions, reflect complex thermodynamic and kinetic effects from the bond activation and cleavage which directly or indirectly involves hydrogen-derived species. After each of the contributions separately treated, we are able to infer the most plausible nature of the elementary step as a H*-assisted C−C bond cleavage with a relatively late transition state.

5.2. Theoretical background

5.2.1. H/D isotope effects

The incorporation of deuterium into selected positions of a molecule provides a powerful means to probe both molecular structure and reaction mechanism [11]. For a more detailed description of all the necessary theoretical knowledge relevant to isotope effects, the interested readers are referred to two books [12,13] and two excellent reviews/essays [11,14]. This section concisely introduces the useful principles in studying H/D isotope effects on heterogeneous catalysts.

For multistep reactions, the kinetic isotope effect (KIE) is a composite of the isotope effects for all forward and reverse steps up to and including the rate-determining step

(RDS). Quasi-equilibrated steps preceding the RDS exhibit equilibrium (or thermodynamic) isotope effects (EIEs). As a consequence, a knowledge of EIEs is essential for the proper interpretation of KIEs. In this regard, primary deuterium isotope effects are often interpreted by using the two simple guidelines illustrated in Schemes 5-1 and -2: (i) KIEs for an elementary bond breaking reaction are normal ($k_H/k_D > 1$) and (ii) EIEs are dictated by deuterium preferring to be located in the site corresponding to the highest frequency oscillator and, as such, may be either normal ($K_H/K_D > 1$) or inverse ($K_H/K_D < 1$).

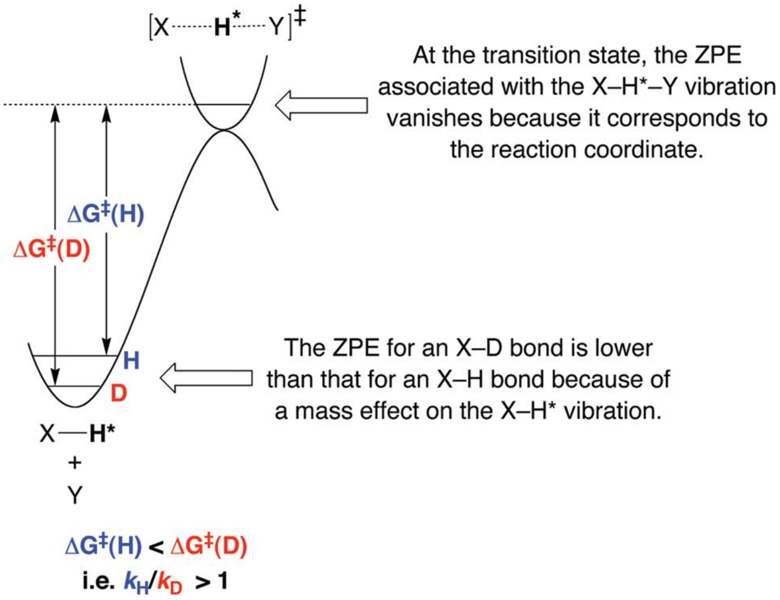
[X-----H*-----Y]‡
At the transition state, the ZPE associated with the X–H*–Y vibration vanishes because it corresponds to the reaction coordinate.
ΔG‡(H)
ΔG‡(D)
H
D
The ZPE for an X–D bond is lower than that for an X–H bond because of a mass effect on the X–H* vibration.
X—H*
+
Y
ΔG‡(H) < ΔG‡(D)
i.e. kH/kD > 1

Scheme 5-1. Simple rationalization of a normal primary KIE (i.e. $k_H/k_D > 1$) for cleaving X-H and X-D bonds (adapted from Ref [11]).

The KIE (Scheme 5-1) reflects the zero-point energy (ZPE) difference (or, free energy difference in Scheme 5-1) between reactants and transition states when they contain H or D. In a specific elementary step, since D sits at a lower position of the energy well than H, the activation barrier is higher if the bond containing H or D dissociates in the transition state, resulting in a larger-than-unity (‘normal’) ratio of rate constants for H- and D-containing species. On the other hand, the EIE reflects the ZPE difference between reactants and products in an elementary step. An important rule is that the higher frequency of the vibrational oscillator is, the larger than ZPE difference will be between H- and D-containing species. Therefore, as is shown in Scheme 5-2, the change of vibrational frequency from low to high is accompanied with an inverse equilibrium isotope effect. Whether the value is normal or inverse does not depend on the energetics (i.e., endothermic or exothermic) of this equilibrated step. It only depends on the relative magnitude of the vibrational frequencies in the H-containing oscillators with reactant (X−H) and with product (Y−H).

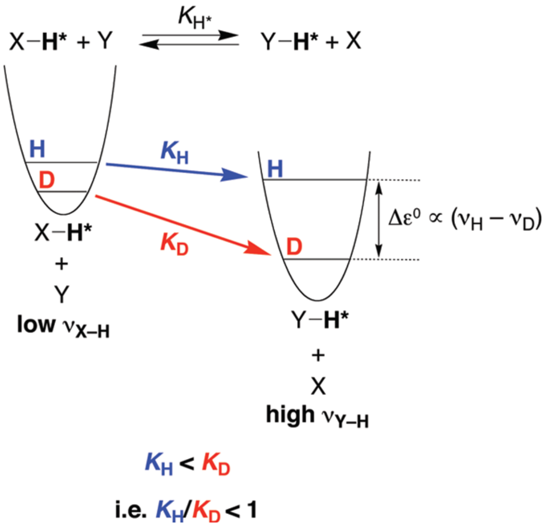

Scheme 5-2. Simple illustration that deuterium prefers to reside in the site that corresponds to the highest stretching frequency (i.e., Y-H* versus X-H*; H* = H, D) (adapted from Ref [11]).

However, keep in mind that we are here only talking about activation barriers and heat of adsorption, but so far not concerned with the entropy factors from translational, rotational and vibrational movements of the species. In a more rigorous treatment, these entropic factors must be taken into account as they have a good chance of overweighing the enthalpic factors at increasing temperatures. Moreover, unlike homogeneous reactions where coverage effects are not present, the isotope effects from the heterogeneous catalysis is more intricate, because not only kinetic and thermodynamic constants of the elementary steps but also coverages of reactive species might be influenced by isotopic substitution. For reactions showing fractional orders in the reactants, the evaluation of isotope effects typically becomes very difficult due to the coverage effects, as there is not a single species dominating the site coverage that would simplify the rate equation.

Even without the complication from coverage effects, it represents a grand challenge to predict the isotope effect within a reasonable precision. This is mainly due to the non-availability of thermodynamic data for the surface species, for some of which we do not even know structures. Making the situation worse, essential data (such as vibrational frequencies and bond strengths) for gas-phase molecules are often lacking. Despite all the difficulties, successful examples exist to show that predicting the isotope effect is not entirely impossible, at least for simpler reactions and specific conditions. Au-Yeung et al. applied a statistical thermodynamics approach to theoretically assessing the kinetic isotope effect (in a general context, KIE refers to the ratio of rate constants, or even more arbitrarily, rates for H- and D-containing species) for the overall reaction [15]. Figure 5-1 shows, with this literature example, how excellent the measured H/D isotope effect and the one predicted from a certain mechanism could be in agreement with each other. In this light, statistical thermodynamics could be very helpful to the theoretical evaluation of isotope effects, and thus to the elucidation of the elementary steps.

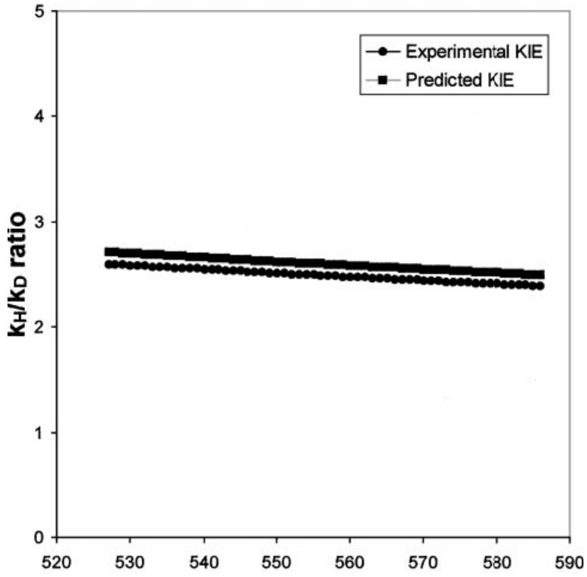

Figure 5-1. Measured and predicted H/D isotope effects in methane (CH_4/CD_4) oxidation rates over PdO clusters [15].

5.2.2. Statistical thermodynamics approach: evaluation of partition functions

The evaluation of all four types of partition functions is the core of this statistical thermodynamics approach. These four types of partition functions are, namely, translational, rotational, vibrational and electronic partition functions. The first three terms are typically lumped as entropic factors and the last one is dictated by the ZPE-corrected activation barrier.

$$k = \frac{k_B T}{h} \frac{(Q/V)_{TS}'}{\prod_{i=1}^{M} (Q/V)_i} \exp\left(\frac{-E_a}{RT}\right)$$

$$\mathrm{K}_{\mathrm{eq}} = \frac{\prod_{\mathrm{j}=1}^{\mathrm{N}} (\mathrm{Q}/\mathrm{V})_{\mathrm{j}}}{\prod_{\mathrm{i}=1}^{\mathrm{M}} (\mathrm{Q}/\mathrm{V})_{\mathrm{i}}} \exp\left(\frac{-\Delta \mathrm{E}_{\mathrm{rxn}}}{\mathrm{RT}}\right)$$

$$\frac{Q_{trans}}{V} = \frac{(2\pi m k_B T)^{3/2}}{h^3}$$

$$Q_{rot,i} = \frac{k_B T}{hcB_i}$$

$$Q_{vib,i} = \frac{1}{1 - \exp\left(\frac{-h\nu_i}{k_B T}\right)}$$

$$\mathrm{Q}_{\mathrm{elec,i}} = \exp\left(\frac{-\varepsilon_o}{\mathrm{k_B T}}\right)$$

Scheme 5-3. The statistical thermodynamics representations of rate and equilibrium constants and the four categories of partition functions.

Apparently from the representations in Scheme 5-3, upon replacing a H atom with a D atom, the mass difference will cause the translational partition function to increase. Since the moment of inertia increases, and the vibrational frequency decreases, with the reduced mass, rotational and vibrational partition functions also grow with displacement of H with D. The vibrational partition function is close to unity (< 1.01) for wavenumbers larger than 1600 cm^{-1} (e.g., both gaseous H_2, D_2) at practical temperatures (e.g., $T < 1000$ K). As a result, the isotope substitution only effectively affects the translations and rotations of gas-phase molecules which do not contain low-frequency vibrational modes. For molecules such as cyclohexane, however, the vibrational term still plays a role in affecting the H/D isotope effects. In summary, to evaluate the isotope effect by a statistical thermodynamics means, one would invoke the equations in Scheme 5-3, and above all, need to have all the necessary information (e.g., the moment of inertia, frequencies of specific vibrations, etc.) not only for the gas phase molecules, but also for the surface species and even transition states! In this context, it appears evident that certain assumptions (e.g., similar vibrational frequencies for the same type of bond in a free hydrocarbon and adsorbed intermediate) have to be made during the estimation of isotope effect in a proposed mechanistic sequence. Theoretical calculations would be particularly useful for providing estimates of vibrational frequencies for surface species, which are essential for the accuracy of predicted isotope effects.

5.3. Experimental

5.3.1. Catalyst preparation and characterization

The Ir/Al_2O_3 catalysts studied in this chapter were the same as those in Chapters 3 and 4, where the details of catalyst characterization could also be found.

5.3.2. Switch experiments between MCH-d_0–H_2 and MCH-d_{14}–D_2 mixtures

Kinetic isotope effects were measured in MCH hydrogenolysis, over Ir/Al_2O_3 catalysts with different dispersions, in a stainless packed bed reactor with plug-flow hydrodynamics. Two reaction mixtures were prepared by mixing a MCH/He mixture (from two saturators containing non-deuterated and perdeuterated liquid MCH) with H_2 or D_2, respectively. The flow configuration, the catalyst activation procedure and the typical reaction conditions were reported in Chapters 3 and 4. The switch experiments were typically performed first in a mixture containing no D-isotope until the steady-state was reached. Then the catalyst was exposed to a mixture containing no H-isotope, and the reactor outlet gas was analyzed after 30 minutes following the instant switching. Steady-state rates were measured for each mixture at low conversions (5−10%), while maintaining other reaction parameters unaltered. Space velocity experiments were also conducted to probe the isotope effects on secondary reaction pathways. The reaction rates and product selectivities were analyzed only by gas chromatography, without using a MS function, as each mixture contains only one type of hydrogen isotope. In the presence of D_2, the gas chromatograms were always shifted 3-6% toward shorter retention times as compared to the retention times that were measured in H_2.

5.4. Results and discussion

5.4.1. Measurements of isotope effects on conversion rates

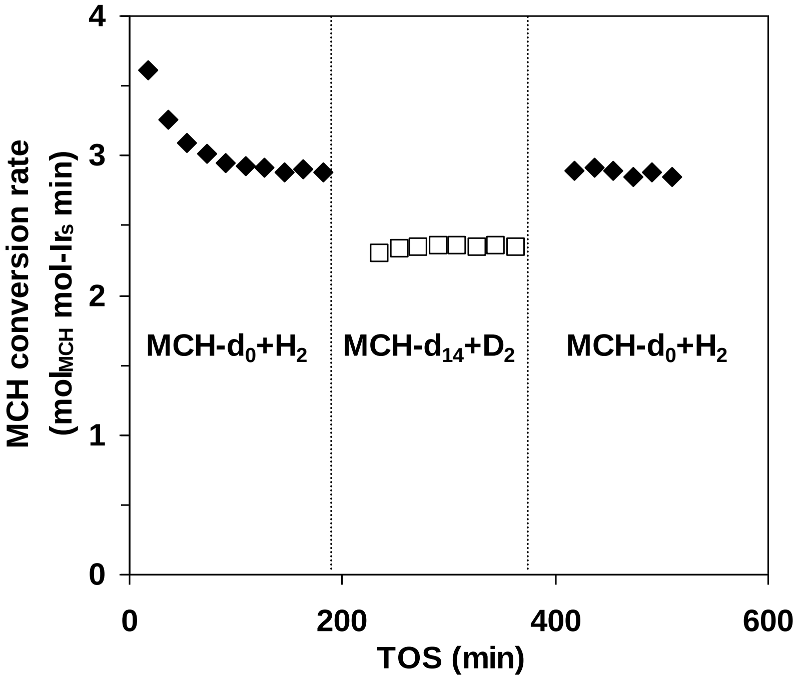

Figure 5-2. Exemplary **s**witch experiment for studying H/D isotope effects (ratios of MCH hydrogenolysis rates in MCH-d_0−H_2 and MCH-d_{14}−D_2 mixtures at 523 K, 1.2 kPa MCH, 0.63 MPa H_2). Catalyst: 1.96%Ir/Al_2O_3 (D_{Ir} = 0.11).

The typical time-on-stream behavior in switch experiments was shown in Figure 5-2, for a low-dispersion Ir/Al_2O_3 catalyst. The rates of MCH hydrogenolysis in the two mixtures were compared, and the ratio was defined as the isotope effect (IE). Note that the rates (and also selectivities shown later in Table 5-1) reported here were obtained by extrapolation of measured values to zero contact time, thus precluding the effect of secondary reactions. The IE was, in a majority of cases, reported as the averaged value of the ratios obtained at switching between different feeds. The hydrogenolysis rate decreased in the reactant mixture of perdeuterated MCH and D_2, suggesting a normal IE at the indicated conditions. Starting the reaction on the activated catalyst in a D-containing feed (an inverse sequence to that shown in Figure 5-2) caused little difference to the measured IEs (not shown).

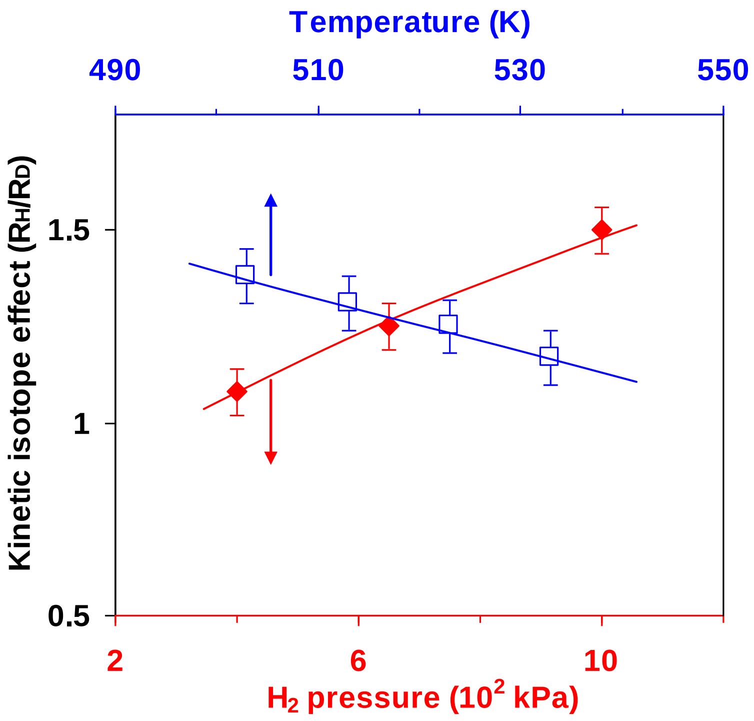

Figure 5-3. Measured effects of isotopic substitution on MCH hydrogenolysis (including endocyclic and exocyclic) rates at different H_2 pressures and reaction temperatures. Catalyst: 1.96%Ir/Al_2O_3 (D_{Ir} = 0.11). MCH partial pressure: 1.2 kPa.

Temperature and pressure variations lead to changes in the magnitude of isotope effect, as illustrated in Figure 5-3. Similar to this exemplified case, the IE increases modestly with increasing H_2 pressure and decreasing temperature on all studied catalysts. For instance, an increase of H_2 pressure from 0.37 to 1.0 MPa (a factor of 2.7) induced a 1.4-time increase in the IE on the 1.96%Ir/Al_2O_3 catalyst with Ir dispersion of 0.11 (Figure 5-3). The temperature effect indicated that the apparent activation barrier for MCH hydrogenolysis was higher in the D-containing reaction mixture. Although the IE remained normal (>1) under the prevalent conditions, the trend pointed to inverse IEs at lower H_2 pressures and higher temperatures. While the inversion of IE at lower H_2 pressures needs a specific analysis of the surface coverages for different species, the inversion of IE with reaction temperature is quite common, as in the isotope studies of homogeneous reactions [11], and is thought to stem primarily from the greater contribution of entropic factors than the enthalpic one (ZPE-corrected barrier) at higher temperatures.

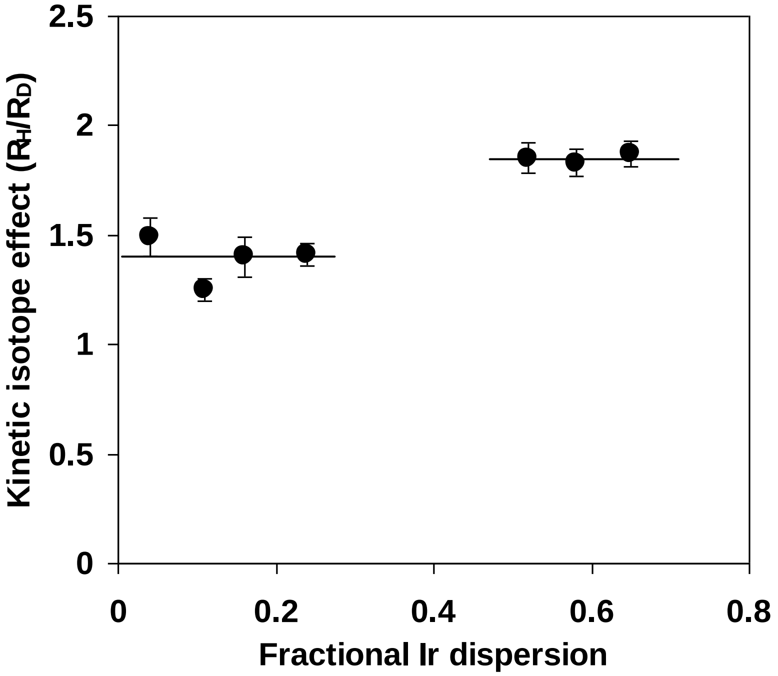

Figure 5-4. Measured isotope effects as a function of Ir dispersion at 1.2 kPa MCH, 0.64 MPa H_2 and 523 K on 0.50%Ir(D)-1/Al_2O_3 catalysts.

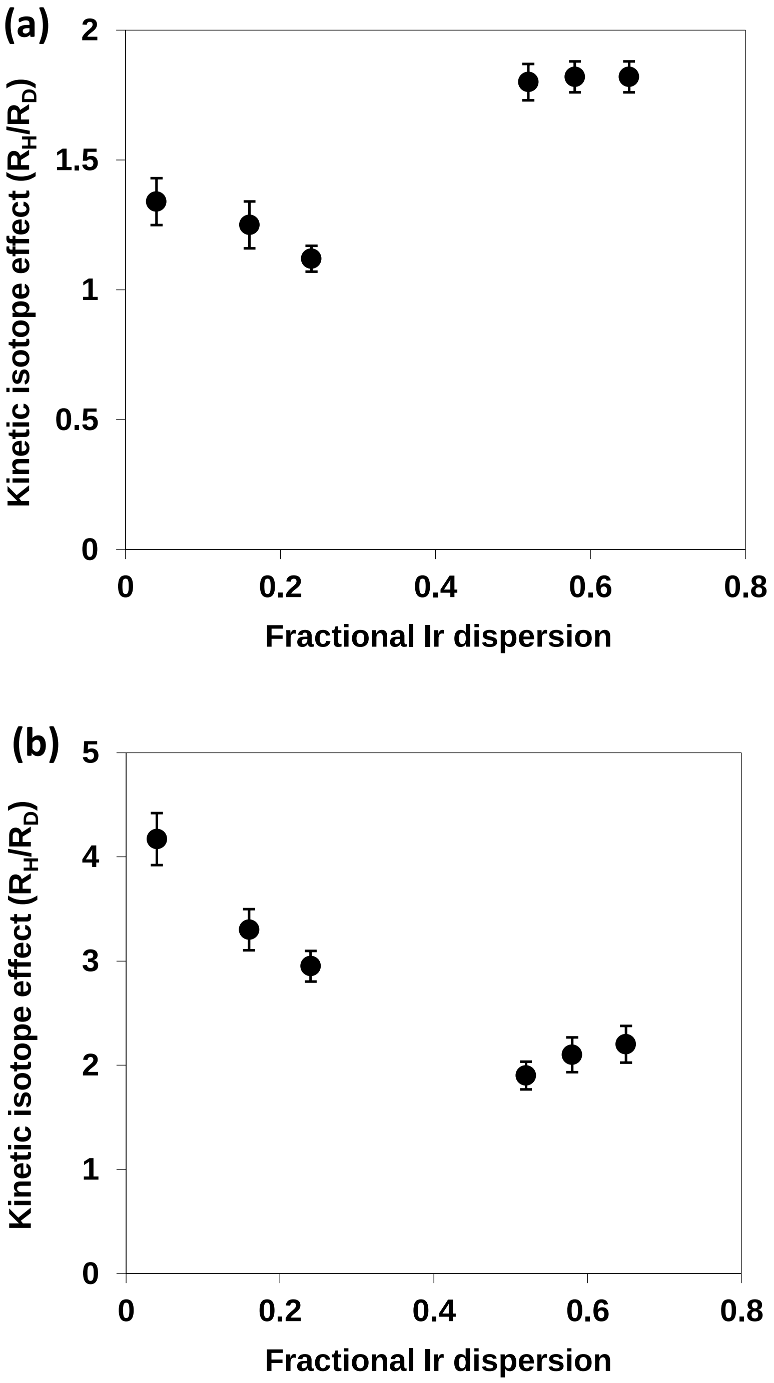

Figure 5-5. Measured isotope effects for (a) endocyclic C−C bond cleavage and (b) exocyclic C−C bond cleavage as a function of Ir dispersion at 1.2 kPa MCH, 0.64 MPa H_2 and 523 K on 0.50%Ir(D)-1/Al_2O_3 catalysts.

Typically, the entropic factor is such that gives rise to inverse isotope effects as a result of larger values of partition functions in the case of D-containing isotopmers or species. The ZPE-corrected barrier, on the other hand, is generally higher in the case of D-containing species. At higher temperatures, the enthalpic component of the IE, exp(-$\Delta E_{act}/RT_{rxn}$), becomes smaller relative to the entropic term, exp($\Delta S/R$), leading the overall IE to decrease (Figure 5-3). Of course, the magnitude of this decrease in IE with reaction temperature was further influenced by the surface coverages.

The isotope effects were explored on the Ir/Al_2O_3 catalysts with varying dispersions at the same reaction conditions. Higher IE values (ca. 1.8) were shown on small Ir clusters of D = 0.5−0.7, while the IEs were somewhat smaller on large Ir particles, in terms of both total hydrogenolysis and endocyclic C−C bond cleavage rates (Figures 5-4 and 5-5a). On the contrary, the IEs for exocyclic C−C bond cleavage rates were much greater on large Ir particles than on small ones (Figure 5-5b).

Table 5-1. Ring opening selectivity and ROP distribution in MCH-d_0–H_2 (denoted as 'H-feed') and MCH-d_{14}–D_2 (denoted as 'D-feed') reactions at 523 K and 1.2 kPa MCH, 0.64 MPa H_2.

Fractional Ir dispersion	RO selectivity (%)		ROP distribution (2MH:3MH:nHp)	
	H-feed	D-feed	H-feed	D-feed
0.65	87	90	42:48:10	44:47:9
0.52	84	85	41:48:11	42:47:11
0.24	47	55	37:57:6	35:61:4
0.11(Cl)	53	57	34:62:4	35:63:3
0.04	38	49	35:61:4	33:66:1

On small clusters, all the hydrogenolytic pathways exhibited lower rates in the fully D-containing reactant mixture than in the fully H-containing feed (not shown). The rates along these pathways, however, feature different isotope effects. Upon changing the feed to MCH-d_{14} and D_2, multiple hydrogenolysis was suppressed to a greater extent than single endocyclic C−C bond cleavage. Accordingly, the ring opening selectivity was slightly enhanced in the D-containing feed on small Ir clusters (Table 5-1). On large particles, the RO selectivity was also higher in the D-involving reactant, due mainly to the considerably decreased rates along the exocyclic C−C bond cleavage pathway. The product distribution with C_7-alkanes, on small clusters, was not appreciably altered upon isotopic substitution of reactants. In contrast, the nHp fraction within the C_7-ROPs on large particles decreased further in the ‘D-feed’ compared to that in the ‘H-feed’. On both small and large Ir particles, the ratio between 2MH and 3MH remained essentially unchanged between two feeds (Table 5-1).

5.4.2. Some postulated mechanisms and relevant IE predictions

Due to the large number of potential intermediates and the unknown reversibility of each elementary step, application of the pseudo-steady-state hypothesis (PSSH) would lead to a series of equations containing a great number of unknown parameters (rate constants in forward and reverse directions and equilibrium constants). De Donder relations and knowledge about the energetics of the specific kinetically significant steps are required to define the boundary conditions and to simplify the matrix of formula. In this work, we adopted an alternative, while also commonly used, approach via assuming a unique rate-determining step (RDS), quasi-equilibrated pre-steps and kinetically irrelevant post-steps [16]. The rate of the whole reaction is dictated by that of the RDS. The mechanisms to be discussed below are preliminarily grouped into three kinds, differing between each other in the nature of the RDS. In the first group of mechanisms, the RDS is assumed to be the C−H bond dissociation at a certain stage; in the second group (most widely accepted), the RDS is assumed to be the C−C bond cleavage; in the last group, the RDS is assumed to be the C−H bond formation. Variations exist within each group of mechanisms, as we discuss shortly afterwards.

The proposed sequences of steps (lumped or elementary), and the rate expressions, for the three groups of mechanisms are presented in the Appendix of this chapter. Next, we discuss the various mechanistic proposals by comparing the experimentally derived values (e.g., 1.8 at 523 K and 0.64 MPa H_2 on small clusters) with the theoretical (statistical thermodynamics) estimates of isotope effect in each mechanism.

5.4.2.1. C−H(D) bond dissociation

As long as the average dehydrogenation depth of the cyclic hydrocarbon does not change with the isotope identity, the predicted IE would be dependent on the ratio of the intrinsic rate constants ($k_{rds,H}/k_{rds,D}$) and that of the chemisorption equilibrium constants for both reactants. We detail below a separation of these entangled factors.

For H_2 activation, the partition functions are estimated (see Scheme 5-3 for the equation of the respective partition function, and Table 5-2 for all the vibrational frequencies and ZPE-differences adopted for calculation):

$$(\frac{Q_H}{Q_D})_{trans} = \frac{1}{(0.5)^{3/2}} = 2.83$$

$$(\frac{Q_H}{Q_D})_{rot} = \frac{1}{(0.5)^{1}} = 2$$

$$(\frac{Q_H}{Q_D})_{vib} = \frac{[(\frac{1-\exp(-h\nu_{D,A}/k_BT)}{1-\exp(-h\nu_{H,A}/k_BT)})(\frac{1-\exp(-h\nu_{D,E}/k_BT)}{1-\exp(-h\nu_{H,E}/k_BT)})^2]^2}{((\frac{1-\exp(-h\nu_{D_2}/k_BT)}{1-\exp(-h\nu_{H_2}/k_BT)})} = 0.6\,(\mathrm{T = 523\ K})$$

$$(\frac{Q_H}{Q_D})_{elec} = \exp([-2(ZPE_{Ir-H} - ZPE_{Ir-D}) + (ZPE_{H_2} - ZPE_{D_2})]/RT) = 0.54\,(\mathrm{T = 523\ K})$$

The denominator in the ratio of vibrational partition functions was close to 1, as both vibrational frequencies for gas-phase H_2 and D_2 are larger than 2000 cm^{-1}. For the vibrational frequencies of surface Ir−H(D) bonds and ZPEs, we assumed the same values for the Pt−H(D) [12,17] and Ir−H(D) bonds, while acknowledging that they should be different, due to the lack of experimental data or theoretical estimates on either Ir surfaces or supported catalysts. The product of the above partition functions lead to the equilibrium constant for H_2 activation at 523 K to be 1.7 as an upper boundary (smaller vibrational frequencies might be associated with modes such as scissoring, twisting and bending for H−Ir−H). This value (K_H/K_D) was larger than 2 on Ni film at 573 K [18], and was also estimated to be a normal isotope effect in two previous reports on Pt and Ru [17,19]. In contrast, it was reported to be 0.7 on Pt/Al_2O_3 by calorimetric measurements [20]. Inverse isotope effects (around 0.7) were also obtained by theoretical calculations on CO-saturated Fe and Co model surfaces [21]. In summary, the IE for H_2 activation seems to be in the range of 0.7−1.7.

Table 5-2. Vibrational frequencies and ZPE-differences between H- and D-containing species.

Species	Wavenumber (cm^{-1})[a]	ZPE-difference (kJ mol^{-1})[b]	References
Ir−H[c]	1230 (E), 550 (A)	~ 4.9	[17]
Ir−D[c]	900 (E), 400 (A)		
H_2	4160	> 7.0	[12,17]
D_2	2990		
C−H	2930 (A), 1465 (A), 1266 (E), … [d]	~ 7.6	[12,17,22]
C−D	2152 (A), 1117 (A), 937 (E), … [d]		

[a] There could be more vibrational modes than the considered A and E.

[b] ZPE(H-containing species) − ZPE(D-containing species), where ZPE = ½ hν.

[c] Ir−H and Ir−D were assumed to be identical with Pt−H and Pt−D, respectively.

[d] More modes exist for the C−H (and C−D) bond vibrations in cyclohexane(-d^0 and -d^{12}), the wavenumbers of which were reported in Ref [22].

For the dehydrogenative activation of the cyclic hydrocarbon (see Appendix for the chemical formula), the following ratios of partition functions are obtained when x = 2 for both H- and D-feeds:

$$\left(\frac{Q_{c,H}}{Q_{c,D}}\right)_{trans} = \frac{1\times[(\frac{2}{4})^{3/2}]^2}{(\frac{98}{112})^{3/2}} = 0.153$$

$$\left(\frac{Q_{c,H}}{Q_{c,D}}\right)_{rot} < \frac{(\frac{2}{4})^2}{(\frac{2}{4}\times\frac{2}{4}\times\frac{2}{4})^{1/2}} = 0.71$$

$$1 < \left(\frac{Q_{c,H}}{Q_{c,D}}\right)_{vib} < 3$$

$$\left(\frac{Q_{c,H}}{Q_{c,D}}\right)_{elec} = \exp([4(ZPE_{C-H} - ZPE_{C-D}) - 2(ZPE_{H-H} - ZPE_{D-D})]/RT) > 30 \text{ (T = 523 K)}$$

Some comments are required for the above equations. In non-symmetric molecules, the ratio of inertia of moments is not proportional to the ratio of masses between H and D in all the three dimensions, thereby causing 0.71 to be the upper boundary for the ratio of rotational partition functions.

The change of vibrational partition function must be larger for C−D bond breaking (prior to the rate-limiting C−D bond dissociation), because the frequency is always lower with C−D bond than with C−H bond for a specific vibrational mode, resulting in larger partition functions of the former (C−D bond). Consequently, C−H(D) bond dissociation means greater losses of vibrational entropies in the case of deuterated hydrocarbon. The upper boundary of 3 is less certain, as it is estimated from the vibrational frequencies of gas-phase molecules of cyclohexane and cyclohexane-d_{12} [22]. Since not all the H(D)-atoms are detached, not all the vibrational entropies are lost, meaning that the difference in the vibrational partition functions between gas-phase H- and D-isotopmers represents the upper boundary for that between the partly deprotiated and dedeuterated surface intermediates.

The ZPE difference between C−H and C−D bond is approximately 7.6 kJ mol^{-1} [12], and may become larger if other vibrational modes are taken into account. As a result, the last term is predicted to be larger than 30, using the literature estimates. The product of the above partition functions lead to the equilibrium constant for C−H(D) bond breaking (not rate-limiting) at 523 K to be in the range of 2−4.

We assumed at the beginning that the dehydrogenation depth before the RDS is such that four C−H bonds are cleaved. While this (x = 2) is in line with the kinetic modeling results in a mechanism where the RDS is the C−C bond cleavage (see Chapters 3 and 4), this stoichiometry is not guaranteed to be true for the current type of mechanisms. Different pre-set values of x from 0.5 to 2.5 have been tried, and it is surprising that the final product of $K_{cyc,H}/K_{cyc,D}$ is not very sensitive to the value of x and remains above 2.

For the RDS which is cleavage of a certain C−H bond, the lateness of transition state (i.e., the extent of C−H bond dissociation and Ir−H/Ir−C bond formation) determines the magnitude of the IE ($k_{rds,H}/k_{rds,D}$) on the intrinsic rate constant.

$$(\frac{Q_{rds,H}}{Q_{rds,D}})_{trans} \approx 1$$

$$(\frac{Q_{rds,H}}{Q_{rds,D}})_{rot} \approx 1$$

$$(\frac{Q_{rds,H}}{Q_{rds,D}})_{vib} \approx 1$$

$$(\frac{Q_{rds,H}}{Q_{rds,D}})_{elec} > \exp([(ZPE_{C-H} - ZPE_{C-D}) - (ZPE_{Ir-H} - ZPE_{Ir-D})]/RT) = 1.9 \text{ (T = 523 K)}$$

$$(\frac{Q_{rds,H}}{Q_{rds,D}})_{elec} < \exp([(ZPE_{C-H} - ZPE_{C-D})]/RT) = 5 \text{ (T = 523 K)}$$

The first two terms are very close to unity because surface adsorbed species are sometimes assumed to possess no translational and rotational freedoms. The third term ought to be slightly larger than unity, because of the differences in vibrational frequency between H- and D-containing species. It should be small (at most 2 at 523 K), however, because the RDS only involves the breaking and forming of one bond. The lower and upper boundaries of the electronic partition function ratio represent a very early and very late transition state, respectively.

Replacing these estimated values or range of values into the rate expression for this type of mechanism (see the Appendix) leads to a large IE (> 4), which is not supported by the measured values (1.8 on small clusters and <1.5 on large ones). Therefore, we reject such type of mechanistic proposals as responsible for the ring opening catalysis on supported Ir clusters at the studied reaction conditions.

5.4.2.2. C−C bond cleavage

The foregoing analyses for partition function ratios in the H_2/D_2 activation (Q_H/Q_D) and cyclics dehydrogenation ($Q_{c,H}/Q_{c,D}$) steps basically apply in this section, while the ratio of intrinsic rate constants ($k_{C-C,H}/k_{C-C,D}$) is totally different from that in the C−H(D) bond dissociation RDS.

For the RDS which is cleavage of the C−C bond, the species that is involved in the C−C bond cleavage (i.e., an empty site, a H-adatom, a gas-phase H_2 molecule or simply unassisted) as well as the lateness of transition state (i.e., the extent of C−C and/or Ir−H bond dissociation and Ir−C and/or C−H bond formation) determines the magnitude of the

IE ($k_{rds,H}/k_{rds,D}$) on the intrinsic rate constant. We first discuss the RDS involving a H-adatom. The assistance by H-adatom might induce kinetic coupling of C−H bond formation with the C−C bond cleavage, bringing down the activation barrier.

The translational and rotational partition functions, again, do not differ for surface species with H- and D-isotopes. The vibrational term is slightly larger than unity, because the entropy loss in cleaving the Ir−D bond is larger than the gain in forming the C−D bond, the difference being smaller in the case of cleaving an Ir−H bond and forming a C−H bond. The following would result from these considerations:

$$(\frac{Q_{rds,H}}{Q_{rds,D}})_{trans} \approx 1;\ (\frac{Q_{rds,H}}{Q_{rds,D}})_{rot} \approx 1;\ (\frac{Q_{rds,H}}{Q_{rds,D}})_{vib} \approx 1.0 - 1.2$$

For a relatively late transition state:

$$(\frac{Q_{rds,H}}{Q_{rds,D}})_{elec} = \exp([-(ZPE_{C-H} - ZPE_{C-D}) + (ZPE_{Ir-H} - ZPE_{Ir-D})]/RT) \approx 0.5 (\mathrm{T} = 523\ \mathrm{K})$$

The smaller-than-unity value is interpreted by the fact that C−H bond is a higher-frequency oscillator than Ir−H bond, causing the ZPE difference larger between C−H and C−D bond than between Ir−H and Ir−D bond.

Replacing these estimated values or range of values into the rate expression for this type of mechanism (see the Appendix), as well as inputting the reactant pressures and the modeled value of K_H (Tables 3-4, 3-6, 4-3 and 4-4), gives rise to a range of 1−2 for the IE, a range comprising the measured values.

The last term (ZPE factor) will become larger than 3 if no C−H(D) bond is formed in the transition state. This would lead to a large IE inconsistent with the measured values. In consequence, the 'H*-assisted C−C bond cleavage RDS' mechanism is likely to involve a late transition state.

Along similar lines, the isotope effects for other proposals of Group II mechanisms can also be evaluated. Without providing the calculation details, we note that H_2-assisted C−C bond cleavage as the RDS leads to a larger-than-3 isotope effect, slightly above the error of estimation. The 'unassisted C−C bond cleavage RDS' mechanism, which was brought forth by Engstrom et al. [10], gives a theoretical IE of larger than 2 at the reaction condition (1.2 kPa MCH, 0.64 MPa H_2 and 523 K). Unfortunately, this slight difference between this predicted value and the measured one is within the error of estimation. As a result, we are not able to reject the contribution of this mechanism.

5.4.2.3. C−H(D) bond formation

The RDS for this type of mechanisms is the addition of a H-adatom to one of the originally surface-bound C-atoms in the ring-opened intermediate. Without specifying the details, we note a larger-than-unity IE in this case. As a result, the question as to whether this type of mechanism is operative or not cannot be answered at this stage, simply by judging the magnitude of the IE.

5.5. Conclusions

This chapter serves as an outlook for future research on the mechanistic aspects of the ring opening of six-membered naphthenes, and more generally, hydrogenolysis reactions of hydrocarbons.

A few mechanistic proposals have been rejected by a preliminary evaluation of isotope effects in MCH hydrogenolysis on Ir clusters. It is concluded that none of the dehydrogenation steps could be rate determining in catalytic turnovers of the C−C bond cleavage, even on large Ir particles with lower reactivities towards C−H bond dissociation.

Although D-containing species sit at lower positions of the potential well than H-containing species do, the isotope effect arising from surface coverage is estimated to be a normal one for cyclics-derived intermediates ($\theta_{cyc,H}/\theta_{cyc,D} > 1$).

H_2-assisted C−C bond cleavage lead to larger predicted isotope effects than observed values, from which we argue that this mechanism is not principally responsible for the hydrogenolysis reaction. If the reaction proceeds via H*-assisted C−C bond cleavage, the relevant transition state is inferred as late, i.e., involving H-addition to one carbon atom of the cleaved bond, by comparing the observed and predicted isotope effects.

5.6. Appendix

Group I mechanisms (kinetically irrelevant steps not shown):

(i) H_2 chemisorption:

$$H_2\,(g) + 2^* \rightleftarrows 2H^* \qquad K_H = \frac{{\theta_H}^2}{P_{H2}{\theta_v}^2}$$

(where θ_V, θ_H are the vacancy coverage and H*-coverage, respectively)

(ii) Hydrocarbon activation (lumped with recombination of H^* into gas phase H_2):

$$c\text{-}C_7H_{14}\,(g) + n^* \rightleftarrows (c\text{-}C_7H_{14\text{-}2x})_n^{\#} + xH_2\,(g) \qquad K_{cyc} = \frac{\theta_{cyc}{P_{H2}}^x}{P_{cyc}{\theta_v}^n}$$

(where θ_{cyc}, n and x are the coverage by the most abundant CH-derived surface intermediates, the number of free surface atoms and the depth of dehydrogenation)

(iii) C–H bond dissociation (rate determining)

$$(c\text{-}C_7H_{14\text{-}2x})_n^{\#} + {}^* \longrightarrow (c\text{-}C_7H_{13\text{-}2x})_n^{\#} + H^* \qquad R_{rds} = k_{rds}\,\theta_{cyc}\,\theta_v$$

(where x is the depth of dehydrogenation)

General rate expression (when n = 1) for Group I mechanisms:

$$r = \frac{k_{rds}K_{cyc}{P_H}^{-x}P_{cyc}}{(1 + {K_H}^{0.5}{P_H}^{0.5} + \frac{K_{cyc}P_{cyc}}{{P_H}^x})^2}$$

Group II mechanisms (kinetically irrelevant steps not shown):

(i) H_2 chemisorption:

$$H_2\ (g) + 2^{*} \rightleftarrows 2H^{*} \qquad K_H = \frac{\theta_H{}^2}{P_{H2}\theta_v{}^2}$$

(where θ_V, θ_H are the vacancy coverage and H*-coverage, respectively)

(ii) Hydrocarbon activation (lumped with recombination of H^* into gas phase H_2):

$$c\text{-}C_7H_{14}\ (g) + n^{*} \rightleftarrows (c\text{-}C_7H_{14\text{-}2x})_n{}^{\#} + xH_2\ (g) \qquad K_{cyc} = \frac{\theta_{cyc}P_{H2}{}^{x}}{P_{cyc}\theta_v{}^{n}}$$

(where θ_{cyc}, *n* and *x* are the coverage by the most abundant CH-derived surface intermediates, the number of free surface atoms and the depth of dehydrogenation)

(iii) C–C bond cleavage (rate determining)

$$(c\text{-}C_7H_{14\text{-}2x})_n{}^{\#} + \text{‘}\mathbf{S}\text{’} \longrightarrow (C_7H_{14\text{-}2x})_n{}^{\#} \qquad R_{rds} = k_{rds}\ \theta_{cyc}\,[\text{'s'}]$$

(where ‘**S**’ can be an empty site (*), an adsorbed hydrogen (H^*), molecular H_2, and so forth, or even non-existent for non-assisted C–C bond scission)

General rate expression (when n = 1) for Group II mechanisms:

$$r = \frac{k_{rds}K_{cyc}P_H{}^{-x+1}P_{cyc}}{(1 + K_H{}^{0.5}P_H{}^{0.5} + \dfrac{K_{cyc}P_{cyc}}{P_H{}^{x}})} \quad (\text{‘S’} = H_2)$$

$$r = \frac{k_{rds}K_{cyc}K_H{}^{0.5}P_H{}^{-2.5}P_{cyc}}{(1 + K_H{}^{0.5}P_H{}^{0.5} + \dfrac{K_{cyc}P_{cyc}}{P_H{}^{2}})^2} \quad (\text{‘S’} = H^*,\ x \approx 2 \text{ from kinetic modeling results})$$

$$r = \frac{k_{rds}K_{cyc}P_H{}^{-x}P_{cyc}}{(1 + K_H{}^{0.5}P_H{}^{0.5} + \dfrac{K_{cyc}P_{cyc}}{P_H{}^{x}})} \quad (\text{no ‘S’})$$

Group III mechanisms (kinetically irrelevant steps not shown):

(i) H_2 chemisorption:

$$H_2\,(g) + 2^* \rightleftarrows 2H^* \qquad K_H = \frac{\theta_H{}^2}{P_{H2}\theta_v{}^2}$$

(where θ_V, θ_H are the vacancy coverage and H*-coverage, respectively)

(ii) Lumped equilibrated steps before the RDS (hydrocarbon dehydrogenation lumped with the C−C bond cleavage step and recombination of H^* into gas phase H_2):

$$c\text{-}C_7H_{14}\,(g) + n^* \rightleftarrows (C_7H_{14\text{-}2y})_n{}^{\#} + yH_2\,(g) \qquad K_{cyc} = \frac{\theta_{cyc}P_{H2}{}^y}{P_{cyc}\theta_v{}^n}$$

(where θ_{cyc}, *n* and *y* are the coverage by the most abundant CH-derived surface intermediates, the number of free surface atoms and the overall extent of dehydrogenation in the MASI appearing in the RDS)

(iii) C–H bond formation (rate determining)

$$(C_7H_{14\text{-}2x})_n{}^{\#} + H^* \longrightarrow (C_7H_{15\text{-}2x})_n{}^{\#} + {}^* \qquad R_{rds} = k_{rds}\,\theta_{cyc}\,\theta_H$$

General rate expression (when n = 1) for Group III mechanisms:

$$r = \frac{k_{rds}K_H{}^{0.5}K_{cyc}P_H{}^{0.5-y}P_{cyc}}{(1 + K_H{}^{0.5}P_H{}^{0.5} + \frac{K_{cyc}P_{cyc}}{P_H{}^y})^2}$$

5.7. References

1. G.C. Bond, R.H. Cunningham, J. Catal. 166 (1997) 172.
2. M.A. Vannice, Kinetics of Catalytic Reactions, Springer-Kluwer, New York, 2005.
3. G.C. Bond, Metal-Catalysed Reactions of Hydrocarbons, Springer, Berlin, 2005.
4. J.H. Sinfelt, D.J.C. Yates, J. Catal. 8 (1967) 82.
5. J.H. Sinfelt, Catal. Rev.-Sci. Eng. 9 (1974) 147.
6. S.B. Shang, C.N. Kenney, J. Catal. 134 (1992) 134.
7. S.A. Goddard, M.D. Amiridis, J.E. Rekoske, N. Cardona-Martinez, J.A. Dumesic, J. Catal. 117 (1989) 155.
8. A. Cimino, M. Boudart, H. Taylor, J. Phys. Chem. 58 (1954) 796.
9. Y. Zhuang, A. Frennet, Appl. Catal. A 134 (1996) 37.
10. J.R. Engstrom, D.W. Goodman, W.H. Weinberg, J. Am. Chem. Soc. 110 (1988) 8305.
11. G. Parkin, Acc. Chem. Res. 42 (2009) 315.
12. A. Ozaki, Isotopic Studies of Heterogeneous Catalysis, Academic Press, New York, 1977.
13. J.S.J. Hargreaves, S.D. Jackson, G. Webb, Isotopic Studies of Heterogeneous Catalysis, Imperial College Press, London, 2008.
14. E.M. Simmons, J.F. Hartwig, 51 (2012) 3066.
15. J. Au-Yeung, K.D. Chen, A.T. Bell, E. Iglesia, J. Catal. 188 (1999) 132.
16. M. Boudart, G. Djéga-Mariadassou, Kinetics of Heterogeneous Catalytic Reactions, Princeton University Press, Princeton, NJ, 1984.
17. S.M. Davis, F. Zaera, G.A. Somorjai, J. Catal. 85 (1984) 206.
18. G. Wedler, F.J. Broker, G. Fisch, G. Schroll, Z. Phys. Chem. N.F. 76 (1971) 212.
19. C.S. Kellner, A.T. Bell, J. Catal. 67 (1981) 175.
20. H. Wang, E. Iglesia, ChemCatChem. 3 (2011) 1166.
21. M. Ojeda, A.-W. Li, R. Nabar, A.U. Niekar, M. Mavrikakis, E. Iglesia, J. Phys. Chem. C 114 (2010) 19761.
22. T. Shimanouchi, Tables of Molecular Vibrational Frequencies Consolidated Vol. I, National Bureau of Standards, 1972, 1−160.

Chapter 6

Summary and conclusions

The incentive of this dissertation is dual: practically, the six-membered naphthenes, which are abundant molecular structures after deep hydrogenation of aromatic-rich feeds and after oxygen removal of phenolic bio-oils, can be upgraded to meet surging demands for diesel-range fuels; fundamentally, far from sufficient knowledge has been available on the structure-performance relation, in regard to the metal component, either in the complex bifunctional or the simpler metal catalytic systems where acid-mediated elementary steps are absent. To explore the nature of active sites and intermediates in the monofunctional metal-catalyzed C−C bond cleavage of naphthenes, metal nanoparticles with different surface coordination environments were prepared by controlling the thermal treatment severity. Two most important catalytic metals, Pt and Ir, were studied in the ring opening of five-membered and six-membered naphthenes, respectively.

Compared to the well-known particle size dependence of regioselectivity in methylcyclopentane ring opening, the question concerning the identity of active surface entities remains far less addressed. In the current thesis work, an antipathetic structure sensitivity has been observed in the whole range of Pt dispersion studied (D = 0.07−0.98) for ring opening of cyclopentane, suggesting that the terrace planes are more catalytically active than the low-coordination atoms. Moreover, a promotional effect of chlorine on the TOF was noticed, which we relate to a slightly decreased electron density and a lower concentration of H-adatoms on the surface Pt atoms by retaining a certain level of Cl in the Pt catalysts. In this light, incorporation of an appropriate level of Cl in the catalyst may be a useful strategy to enhancing the activity towards the hydrogenolytic reactions on Pt catalysts, while suppressing hydrogenation of some co-present unsaturated bonds whose reactivities are usually inhibited by halogens.

Although monofunctional Pt catalysts show the highest preference, among all potential catalysts of choice, to cleaving the substituted C−C bonds in a cyclic molecule, they are generally less active than metals such as Ir, Rh and Ru, and are not suitable for six-membered naphthene ring opening due to the prevailing dehydrogenation and isomerization tendencies. In this work, the ring opening reactions of cyclohexane and methylcyclohexane were studied on Ir catalysts of varying dispersions. Endocyclic C−C bond cleavages exhibit in both reactions a dual-branch dependence of TOFs to Ir dispersion (D = 0.035−0.65). The sympathetic structure sensitivity (D > 0.46) originates from the decrease in the intrinsic rate constant due to declining population of low-coordination atoms. The increasing TOFs with further decreasing dispersion (D < 0.40) are attributed to the increased ensemble size requirement and reactivities of the catalytically relevant intermediates on atoms of less coordinative unsaturation. In contrast, exocyclic C−C bond cleavage is shown to exhibit monotonically higher TOFs with increasing particle size. The strong suppression of exocyclic C−C bond cleavage by increasing H_2 pressure (both on small and large particles) and by decreasing cluster size suggests that the adsorption mode for the exocyclic C−C bond cleavage is more spatially demanding than the 1,2-dicarbene mode proposed for ring opening.

Repulsive forces between the methyl group and the surface metal atoms exert a significant impact on the effect of cluster size on the endocyclic C−C bond cleavage at the substituted position. This steric effect becomes smaller when the methyl group is farther away and the surface becomes less crowded. On large particles, the already low tendency to cleave the substituted C−C bond is even more exacerbated by secondary repulsive interaction arising from the methyl group and adsorbed H-atoms nearby. This secondary steric effect is operative even when the methyl group is not in the closest proximity to the breaking C−C bond, as evidenced by the progressively higher selectivity to 3MH with increasing H_2 pressure. In comparison, on small Ir clusters, adsorbed H-atoms do not impose additional steric effects, in a considerable H_2 pressure range, on the accessibility of the secondary-tertiary C−C bond to the catalytic center.

By replacing all the H atoms in the reactants with D atoms, the C−C bond cleavage rates decreased at all Ir particle sizes, being more pronounced on small clusters. These isotope effects provide important insights into the reaction mechanism of the ring opening reactions of six-membered naphthenes on the surface of Ir particles. The rate determining step is unlikely to be dissociation of a certain C−H bond, as this would lead to a very large isotope effect inconsistent with the measured values. One of the possible mechanisms involves a H*-assisted C−C bond cleavage with a late transition state as the rate-determining step.

Curriculum vitae

Hui Shi was born on January 29th, 1983 in Jiangsu, China. After completing his high-school education in 2001, he was matriculated into the Department of Chemistry at Tsinghua University (Beijing, China), where he received his bachelor's degree in Science in July 2005. His education as a master student continued at Tsinghua University, under the supervision of Prof. Bo-Qing Xu. In July 2008, he earned his master's degree in Science, with the thesis titled "*Chemselective hydrogenation of α,β-unsaturated aldehydes on supported gold catalysts* ". In September of the same year, he joined the research group of Prof. Johannes A. Lercher and started his Ph.D. study at Technical Chemistry II at Technische Universität München, Germany. Recent research of his focuses on the fundamental understanding of the C−C bond cleavage in cyclic hydrocarbons over supported noble metal domains, the results of which constitute the current dissertation.

List of publications

1. **Active sites and reactive intermediates in the hydrogenolytic cleavage of C–C bonds in cyclohexane over supported iridium.** Hui Shi, Xuebing Li, Gary L. Haller, Oliver Y. Gutiérrez, Johannes A. Lercher, Journal of Catalysis 295 (2012) 133-145.

2. **Structure sensitivity of hydrogenolytic cleavage of endocyclic and exocyclic C–C bonds in methylcyclohexane over supported iridium particles.** Hui Shi, Oliver Y. Gutiérrez, Gary L. Haller, Donghai Mei, Roger Rousseau, Johannes A. Lercher, Journal of Catalysis 297 (2013) 70-78.

3. **Catalytic consequences of particle size and chloride promotion in the ring opening of cyclopentane on Pt/Al_2O_3.** Hui Shi, Oliver Y. Gutiérrez, Gary L. Haller, Johannes A. Lercher, ACS catalysis, submitted.

4. **Mechanistic implications of protium/deuterium (H/D) isotope effects in methylcyclohexane hydrogenolysis on supported Ir catalysts.** Hui Shi, Oliver Y. Gutiérrez, Gary L. Haller, Johannes A. Lercher, in preparation.

5. **Controlled synthesis of platinum loaded hierarchic silica spheres.** Sabine Scholz, Hui Shi, Johannes A. Lercher, Topics in Catalysis 55 (2012) 800-810.

6. **Vital roles of hydroxyl groups and gold oxidation states in Au/ZrO_2 catalysts for 1,3-butadiene hydrogenation.** Xin Zhang, Hui Shi, Bo-Qing Xu, Journal of Catalysis 279 (2011) 75-87.

7. **Immobilized PVA-stabilized gold nanoparticles on silica show an unusual selectivity in the hydrogenation of cinnamaldehyde.** Hui Shi, Na Xu, Dan Zhao, Bo-Qing Xu, Catalysis Communications 9 (2008) 1949-1954.

8. **Synthesis of chloroanilines: selective hydrogenation of the nitro in chloronitrobenzenes over zirconia-supported gold catalyst.** Daiping He, Hui Shi, Bo-Qing Xu, Green Chemistry 9 (2007) 849-851.

9. **Comparative study of Au/ZrO_2 catalysts in CO oxidation and 1,3-butadiene hydrogenation.** Xin Zhang, Hui Shi, Bo-Qing Xu, Catalysis Today 122 (2007) 330-337.

10. Performance control of hydrogenation catalysis by regulating the percentage of cationic gold in Au/ZrO$_2$ catalysts. Xin Zhang, Hui Shi, Bo-Qing Xu, Studies in Surface Science and Catalysis 172 (2007) 481-484.

11. Catalysis by gold: Isolated surface Au^{3+} ions are active sites for selective hydrogenation of 1,3-butadiene over Au/ZrO$_2$ catalysts. Xin Zhang, Hui Shi, Bo-Qing Xu, Angewandte Chemie International Edition 44 (2005) 7132-7135.

List of presentations

Influence of surface modified mesoporous silica on the stability and reactivity of platinum nanoparticles (poster). Sabine Scholz, Beatriz Blas Molinos, Hui Shi, Johannes A. Lercher, 43. Jahrestreffen Deutscher Katalytiker, 2010, Weimar, Germany.

A detailed kinetic study of the direct ring opening of cyclohexane and methylcyclohexane over monofunctional Ir/Al_2O_3 catalysts (poster). Hui Shi, Oliver Y. Gutiérrez, Johannes A. Lercher, Deutsche Wissenschaftliche Gesellschaft (DGMK) Annual Conference, 2011, Dresden, Germany.

Structural requirements of direct ring opening of cyclohexane over supported Ir clusters (poster). Hui Shi, Oliver Y. Gutiérrez, Johannes A. Lercher, 45. Jahrestreffen Deutscher Katalytiker, 2012, Weimar, Germany.

Active site requirements and mechanism of hydrogenolysis of six-membered naphthenes over Ir/Al_2O_3 catalysts (poster). Hui Shi, Oliver Y. Gutiérrez, Johannes A. Lercher, SynFuel 2012 Symposium, 2012, Munich, Germany.

On the apparent and intrinsic structure sensitivities of hydrogenolytic C−C bond cleavages of C_6-naphthenics over supported Ir clusters (poster). Hui Shi, Oliver Y. Gutiérrez, Johannes A. Lercher, 15th International Congress on Catalysis, 2012, Munich, Germany.

Supported Ir nanoclusters in catalysis: particle size effect on the direct ring opening of cyclohexane (poster). Hui Shi, Oliver Y. Gutiérrez, Johannes A. Lercher, 5. Joint Nanoworkshop NanoDay, 2012, Lyngby, Denmark.